Naval Research Laboratory
Washington, DC 20375-5320

NRL/6120/MR—2024/4

Insulation Aging Behaviors Characterized with Dielectric Thermal Analysis

DR. RICCARDO CASALINI

Polymer Physics Group
Chemistry Division

DR. ALETA T. WILDER

Center for Energy & Environmental Resources
Cockrell School of Engineering
The University of Texas at Austin
Austin, TX

July 1, 2024

DISTRIBUTION STATEMENT A: Approved for public release; distribution is unlimited.

REPORT DOCUMENTATION PAGE

PLEASE DO NOT RETURN YOUR FORM TO THE ABOVE ORGANIZATION

1. REPORT DATE	2. REPORT TYPE	3. DATES COVERED	
01-07-2024	NRL Memorandum Report	START DATE 01/01/2020	END DATE 01/01/2023

4. TITLE AND SUBTITLE
Insulation Aging Behaviors Characterized with Dielectric Thermal Analysis

5a. CONTRACT NUMBER	5b. GRANT NUMBER	5c. PROGRAM ELEMENT NUMBER
N00014-18-2586		
5d. PROJECT NUMBER	**5e. TASK NUMBER**	**5f. WORK UNIT NUMBER**
		991L91

6. AUTHOR(S)
Dr. Riccardo Casalini and Dr. Aleta T. Wilder*

7. PERFORMING ORGANIZATION / AFFILIATION NAME(S) AND ADDRESS(ES)	8. PERFORMING ORGANIZATION REPORT NUMBER
Naval Research Laboratory 4555 Overlook Ave SW Washington, DC 20375-5320	NRL/6120/MR-2024/4

9. SPONSORING / MONITORING AGENCY NAME(S) AND ADDRESS(ES)	10. SPONSOR / MONITOR'S ACRONYM(S) NUMBER	11. SPONSOR / MONITOR'S REPORT NUMBER(S)
Office of Naval Research 331 875 North Randolph Street Arlington, VA 22217	ONR	

12. DISTRIBUTION / AVAILABILITY STATEMENT
DISTRIBUTION STATEMENT A: Approved for public release; distribution is unlimited.

13. SUPPLEMENTAL NOTES
*The University of Texas at Austin, 2515 Speedway, Austin, TX 78712

14. ABSTRACT
This is the final report on the study of aging in dielectric insulators under high electric fields and high temperatures. The aging was characterized mainly using broadband dielectric spectroscopy to monitor the change of dynamics in the relaxation processes and the diffusion of charged impuritiries. This investigation involved a large number of commercially available dielectric materials.

15. SUBJECT TERMS
Electric insulation, Aging, Broadband dielectric spectroscopy, polymers

16. SECURITY CLASSIFICATION OF:			17. LIMITATION OF ABSTRACT	18. NUMBER OF PAGES
a. REPORT	b. ABSTRACT	c. THIS PAGE		
U	U	U	SAR	173

19a. NAME OF RESPONSIBLE PERSON	19b. PHONE NUMBER *(Include area code)*
Dr. Riccardo Casalini	(202) 404-8042

This page intentionally left blank.

Table of Contents

	Page
1. Project Summary	4
2. *Characterization:* Dielectric Loss of Commercial VPI Resins	
2.1. Dielectric Heating of Nine Commercial VPI Resins	10
2.2. DETA & DMA for Nine VPI Resins	12
2.3. DETA of a Polyester-Epoxy Copolymer	17
2.4. Summary of Dielectric Loss of VPI Resins	18
3. *Review:* Physical Aging	20
4. *Characterization:* DETA & DMA of Thermally Aged Commercial Polymer Composites	
4.1. Comparison of PTFE Materials	25
4.2. Comparison of PI Materials	28
4.3. Comparison of PEEK Materials	31
4.4. Comparison of Structural Laminate Materials	34
4.5. Summary of Thermal Aging of Commercial Polymer Composite Materials	37
5. *Review:* Kinetic Models of Aging	
5.1. Nature of Aging	39
5.2. Lifetime Prediction	40
5.3. Molecular Dynamics and Aging	41
5.4 Kinetic Models based on Dynamic Behavior	44
6. *Characterization:* Mechanical, Electrical & Thermal Aging of Resins & Laminates	
6.1. Molecular Dynamics Characterization with DETA & DMA	47
6.2. Thermal, Mechanical, and Electrical Aging Studies	47
6.2.1. Epoxy (Permafil 74050)	
6.2.2. Silicone (Silres H62c)	
6.2.3. Epoxy+Fiberglass Laminate (FR5)	
6.2.4. Silicone+Fiberglass Laminate (G7)	
6.3. Complimentary Characterization	78
6.4. Dynamic Field Aging vs. Thermal Aging	82
6.5. Aging in Proximity to the Glass Transition	92
6.6. DETA & DMA Correlation	92

7. *Review:* DETA and Aging of Polymer Matrix Composite (PMC) Dielectrics
7.1. Introduction 95
7.1.1. Overview
7.1.2. Selection of Literature
7.1.3. Relaxation Processes
7.2. DETA of Polymer Matrix Composites: Specific Interest Areas 99
7.2.1. DETA of Polymer Matrix Composites: "Interphase Design"
7.2.2. DETA of Polymer Matrix Composites" "Charge Distribution"
7.2.3. DETA of Polymer Matrix Composites: "Absorbed Water"
7.2.4. DETA of Polymer Matrix Composites: "Mica"
7.2.5. DETA of Polymer Matrix Composites: "Laminated Composites"
7.3. Polymer Matrix Composites: Insulation Aging & DETA 109
7.3.1. Thermal Aging of PMC
7.3.2. Mechanical Aging of PMC
7.3.3. Electrical Aging of PMC
7.4. Recommendations from Literature Survey 128

8. *Characterization:* DETA and Aging - PMC Dielectrics
8.1. Sequential Aging 130
8.2. DETA of Polymer Matrix Composites: Nanosilica Modified 134
8.3. DETA of Polymer Matrix Composites: Mica-filled 138
8.4. DETA of Polymer Matrix Composites: Fiberglass Laminate 142
8.5. DETA of Multilayer Epoxy-Mica-Fiberglass Tape 148

9. *Characterization:* Relaxation Modes and Activation Energies
9.1. Activation Energies from Imaginary Electric Moduli 152
9.2. DETA of Polymer Matrix Composites: Nanosilica Modified 158

Appendix 1: Useful Relationships 173
Appendix 2: *Characterization:* DETA & DMA for Commercial VPI Resins, as cured 175
Appendix 3: *Characterization:* DETA & DMA for Commercial Engineered Plastics 194
Appendix 4: *Review & Characterization:* Aging Mechanisms for Five Insulation Materials 234

1. PROJECT SUMMARY

This compendium provides novel information on aging of electrical insulation containing polymers. The science described will both enable improved insulation lifetimes and guide prediction of insulation lifetimes in service. The characterization methodology displayed will encourage systematic tracking of insulation condition. The information on aging was generated using Dielectric Thermal Analysis (DETA) and Dynamic Mechanical Analysis (DMA). Both material characterizations are shown to be sensitive to changes in the polymer microstructure and meso-structure with aging. DETA also provides information for calculating dielectric heating. DMA is included for a more complete examination of rheological behavior. Predicting insulation lifetimes in service will require development of a new kinetic model that synthesizes the type of phenomenological data reported here.

The project combines:
(i.) dielectric property survey of representative insulation materials;
(ii.) application of individual aging regimen representative of electric machinery environments;
(iii.) examination and differentiation of specific aging behaviors; and
(iv.) review of literature for improved interpretation of results.

More aggressive environmental exposures will be used in subsequent studies on endurance behaviors and accelerated aging techniques, so the studies reported here establish baseline information. This compendium is structured to provide access to the developed information. Sections of explanation ("review") are followed by sections largely comprised of graphical data to illustrate behaviors and summary points ("characterization"). The sections of explanation are considered critical to reduce confusion due to varying terminology. Significant data has been placed in Appendices for future reference.

The theory for quantifying dielectric and mechanical response in both time and frequency domains is already well developed. Use of the information gathered from DETA and DMA for condition assessment of insulation materials is making progress in the research community. Some care is needed in the analyses as many insulation materials must be formed into appropriate samples and forming processes may alter the sample material. Techniques relevant to high moduli materials are also required for DMA. Due to the importance of the resulting information in making design decisions, information from DETA and DMA is recommended for wide availability and utilization by the electric machine industry.

Key Findings:

1.) A survey of nine commercial thermoset polymer resins gave a wide range of permittivity. Whereas the real permittivity was found to change up to a factor of 2x between 10^{-3} – 10^{6} Hz at 50°C, the change was an order of magnitude for several cured resins at 150°C. Likewise, the imaginary permittivity varied up to an order of magnitude at 50°C and up to 3 orders of magnitude at 150°C. (No aging treatments were applied for this survey.) The results highlight the importance of DETA and DMA data in choosing insulation materials for electric machinery with variable frequency and/or variable speed power drives (i.e., a few datapoints at room temperature are not acceptable characterizations of dielectric behavior).

Manuscript approved June 28, 2024.

2.) A survey of thermal aging of commercial materials included polyimide, PTFE, and PEEK, representing the primary insulation layer. (PTFE and PEEK are thermoplastic polymers.) A few semiconductive composites with these materials as matrices (polymer matrix composites or "PMC") were included in the survey. Composites where the dynamic elastic ("mechanical") moduli and dynamic electric moduli changed dramatically after thermal aging were found. This suggests that thermal exposure can permanently change properties of insulation in machinery well below the "maximum continuous use temperature".

3.) Electrical insulation systems for power-dense applications utilize layered PMC materials that age under thermal, mechanical, and electrical stresses. Aging is documented without accelerated aging techniques. Eventually, accelerated aging techniques may be unnecessary to rank material lifetimes. The pertinent dielectric behaviors of PMCs and insulation systems remain empirical and must be measured (e.g., ac breakdown stress). Few hard rules have been found for measured behaviors. To change this, the materials studied must be reproducible from lab to lab (i.e., processing sensitivities must be understood) and characterization methods must be adequate for analysis.

4.) It was discovered that one of the physical manifestations of dielectric aging in thermoset polymers is a measurable density change. The meso-structure of the cured thermoset changes with aging. For the thermoset polymers studied, the density change due to thermal aging is different from that of dynamic field aging. Furthermore, density change due to dynamic field aging appears to be independent of the temperature of field exposure. This is a critical finding. It clearly illustrates that aging in electric fields and/or pressure waves is not the same mechanism as thermal aging. Kinematic models for aging prediction should differentiate these aging phenomena. This is particularly important for insulation in power-dense environments. As expected from established dielectric theory, the measured real permittivity is sensitive to these density changes.

5.) Further studies concentrated on DETA characterization of polymer matrix composites (PMC) and their aging behaviors. Due to the complexity of multicomponent PMC insulation, studies first analyzed neat and two-component composites. This was then followed by a study of a three-component system (layered epoxy-mica-fiberglass tape). The strategy for choosing the PMC reported here is to examine the aging behaviors of the composite components to then assess aging of the layered insulation system consisting of multiple PMC components. This approach is novel and successful to the extent of effort reported at this time.

6.) Variation in the molecular dynamics of the polymer matrix *can* provide comparative information on aging behaviors. Characterization of the molecular dynamics using DETA & DMA is adopted and a consistent technique has been demonstrated. A more complete representation of the molecular dynamics behavior of a PMC is gleaned with a broader frequency range *and* temperature range using *both* techniques. Synthesis of this information is of particular urgency for layered insulation systems.

7.) "Interphase" behaviors in PMC are accepted as largely responsible for property deviations from neat polymers. Interface charge models, once used to explain such deviations, have been shown to be inadequate. As with most complex material systems, there are property & behavior trade-offs that need to be addressed for each application's requirements to effectively exploit PMC advantages in electrical insulation system design.

8.) Nano-silica is often added at ~1 wt% to VPI resins to increase thixotropy. Nano-silica modification of an epoxy thermoset and a silicone thermoset had opposite effects on the molecular dynamics. Where the modified silicone increased in dynamic stiffness and upper glass transition temperature (T_g), the modified epoxy showed a decrease in dynamic stiffness and T_g. Modification by nano-silica had only minor effects on the dielectric spectra. Aging trends were similar to those for the neat polymer matrix.

9.) The DETA of mica-filled PMC was studied at 1 wt% and 90 wt% mica. The concentration of mica in the epoxy matrix or silicone matrix has a large impact on the DETA spectra. At 1 wt% and low temperatures, the mica-filled epoxy and mica-filled silicone composite materials have increased real permittivity over the neat polymer. The same general spectral trends in permittivity are observed for the 1 wt% mica in epoxy with various aging treatments. Thermal aging has minimal impact on the real permittivity magnitude. Both mechanical aging and electrical aging of mica-filled epoxy cause increases in permittivity across the spectrum. A newly active, secondary relaxation (γ-relaxation) is only observed at high temperatures with 1 wt% mica. (This high temperature behavior was also observed for 1 wt% nano-silica modified PMC.) The permittivity spectra of 90 wt% mica PMC with an epoxy or silicone matrix are remarkably similar and demonstrate pronounced differences from the spectra of the low concentration PMC. The real permittivities are very high at low frequency trending to lower values as frequency increases. Following thermal aging, the electrical aging treatment reduced the real permittivity of the epoxy PMC. The MWS-relaxation was observed at all temperatures for all 90 wt% mica PMC.

10.) The matrix polymer's molecular dynamics dominate the DETA behavior when the second phase is at low concentration (~1 wt%). A secondary polarization (referred to as a γ-relaxation) was only observed at elevated temperatures for low concentration PMC materials. The MWS-relaxation was found to be temperature and concentration dependent in PMC, in contrast with prevailing understanding. Dynamic field aging changed the molecular dynamics of the polymer in PMC similar to its effect in the neat polymer.

11.) Fiberglass laminate PMC (with either epoxy or silicone matrix) also respond similarly to aging treatments. At room temperature, the spectra of the real and imaginary electric moduli resemble those of neat matrix polymers. However, a strong relaxation is observed at high temperatures that is probably due to thermally activated charge mobility in the fiberglass-polymer interphase. This produced unacceptably high imaginary permittivities for insulation materials. Dynamic field aging caused an increase in real permittivity for both fiberglass laminate PMC. MWS-relaxation was not identified for the fiberglass laminate PMC conditions examined.

12.) The DETA of cured Calmicaglas®, a commercial epoxy-mica-fiberglass tape used as a wound ground-wall insulation, was examined. Thermal aging had a different effect on the composite meso-structure than dynamic field aging. At 50°C, the relaxation processes between the epoxy-mica dominated the dielectric spectrum. At 150°C, the relaxation processes between the epoxy-fiberglass dominated the dielectric spectrum. The change in aging mechanisms with temperature and with aging treatment precludes the accurate use of kinetic models based solely on a simple Arrhenius relationship. A new approach to kinetic modeling is warranted. Furthermore, accelerated aging regimes based on simple Arrhenius models are unlikely to give accurate predictions of aging lifetimes.

13.) Of special note is the measurable effects of dynamic field aging that persist after subsequent thermal aging. Additional dynamic field aging treatments at the original treatment frequency and power had minimal effect on the DETA spectra.

14.) Activation energies for molecular dynamics were determined for representative materials after aging treatments. Only the activation energies of the α-relaxation were affected by the aging treatments. This means that aging modifies the cooperative molecular dynamics of the polymer network. The α-relaxation mode was examined by cooling the fiberglass-epoxy laminate. The activation energy was found to be 2.02×10^5 J/mol with thermal aging and 1.46×10^5 to 1.60×10^5 J/mol for dynamic field aged samples. The activation energies of the β-relaxation and MWS-relaxation were not affected by the aging treatments used here. The MWS-relaxation mode was examined for the 90 wt% mica-filled epoxy PMC. A slight progression to higher temperature was found, leading to an activation energy of 1.2×10^4 J/mol. The β-relaxation was examined at high temperatures for neat, 1 wt% nano-silica modified epoxy, and 1 wt% mica-filled epoxy. The activation energies for this mode are 6.4×10^4 to 6.5×10^4 J/mol regardless of the composition or dynamic field aging.

Science Advances:

1.) Aging can occur over time with micro-structural and meso-structural changes of the polymer that do not include measurable chemical change (e.g., oxidation or decomposition). Thermal aging has a different impact on the structural changes as compared with dynamic field aging (mechanical or electrical). The structural changes can be examined by comparing the molecular dynamics.

2.) Some correlation was discerned between dynamic elastic moduli and dynamic electric moduli. This is a valid reason to display dynamic electric moduli as well as permittivity.

3.) Dynamic field aging is accomplished by applied cyclic mechanical stress and/or cyclic electrical stress. Dynamic field aging is non-Arrhenius (unlike thermal aging). Dynamic field aging appears similar in effectiveness at and below the glass transition temperature of the thermoset polymer. This aging is hypothesized to be caused by acoustic phonons and/or optical phonons moving through the material. The mechanical aging treatment applied here would produce mostly acoustic phonons and the electrical aging treatment would produce optical phonons.

4.) Dynamic field aging impacts the meso-structure differently than thermal aging, thus leading to different properties (behavior) that we have shown can be characterized for thermoset polymers. Thermal aging at or above the glass transition (but well below the upper temperature limit where thermo-oxidation typically occurs) causes:

i. Lowered density, maintaining a higher temperature network structure and perhaps more brittle behavior;
ii. Higher stiffness (perhaps due to lessened coordination of network molecular dynamics at room temperature); and
iii. Possible thermally-induced phase separation or crystal growth.

Dynamic field aging typically causes:

iv. Increased density;
v. Lowered stiffness (perhaps due to increased molecular dynamics coordination);
vi. No observed phase separation;
vii. Possible adhesion issues at some interfaces only with dynamic mechanical aging; and
viii. Reduced "charge accumulation" and more rapid "charge relaxation" with DC voltage application and removal, respectively.

5.) Activation energies derived from DETA of thermoset polymers indicate:

i. β-relaxations exhibit classic Arrhenius behavior. Activation energies are consistent and not affected by aging treatments. β-relaxations are minimally affected by thermal or dynamic field aging, i.e., low frequency motions of side groups are not affected by our aging treatments (i.e., by minor volume changes or minor network elasticity changes).

ii. MWS-relaxations have an Arrhenius dependence leading to low activation energy. Secondary relaxations, here labeled γ-relaxations, were observed for some materials in the same frequency region as anticipated for MWS-relaxations. The γ-relaxations corresponded with phase separation due to thermal aging, delamination or weakening of adhesion at boundaries due to dynamic mechanical aging, and dynamic electrical aging.

iii. α-relaxations exhibit a nonlinear dependence on inverse temperature. Activation energies vary with the aging treatment. With respect to unaged material, thermal aging increases activation energy. Dynamic field aging decreases activation energy. The Cole-Cole plot of the electric modulus clearly differentiates the effects of aging on the relaxation.

Comments:

1.) Any aging or lifetime studies, particularly those including breakdown or voltage endurance, should consider the condition of the sample material w.r.t. the dynamic motion of the molecular structure. These studies suggest that variability in behaviors may be due to variability in the meso-structure of the sample materials. DETA and DMA are appropriate tools to study the molecular dynamics.

2.) To be informative, thermal aging treatments must relate the proximity of the aging temperature to both the thermoset polymer's glass transition and the temperature where chemical reactions (e.g., oxidation and/or decomposition) can be detected. (The latter is best accomplished by Thermogravimetric Analysis (TGA) measurements rather than other methods used with insulation materials for identifying "maximum continuous use temperatures".) The cooling rate from the aging temperature is also important information.

3.) Although other characterization tools provide complimentary information for improved interpretation of DETA and DMA trends, these two characterization tools continue to be the most sensitive for examining aging (via molecular dynamics).

4.) Controlled dynamic mechanical aging treatments with DETA characterization may improve interfacial bonding (adhesion). Treatments could be particularly successful with surface modifications of mica or fiberglass fillers. Improved interfacial bonding would positively improve integrity and longevity of PMC.

5.) Applying a controlled dynamic field aging treatment (after processing of insulation) to stabilize the polymer structure(s) prior to operation with extended thermal aging and/or thermal cycling is recommended.

6.) Several concepts for improvements of commercial insulation materials arose during this project:

- DETA may be used to examine phase separation.
- Debonding of fiberglass and the polymer matrix may be observed using DETA, suggesting that delamination in layered insulation systems may also be observed. This finding might be utilized to monitor the viability of surface-active agents for chemically modifying interphases.
- It is possible that the very high permittivities observed for 90 wt% mica PMC and fiberglass laminate PMC may be reduced by chemically modifying the interphases. If properly designed, the modification would improve the insulation's properties, including stronger interphase adhesion. (Use of DETA to help guide process choices would be especially efficient.)
- FR5/G11 fiberglass laminate may be improved by substituting S-glass cloth for the traditional e-glass cloth. S-glass cloth is reported to have ~40% higher tensile strength and ~20% higher modulus. S-glass also contains less alkali (no Li_2O vs. ~7 wt% Li_2O for e-glass). Dielectric heating may be reduced and the stiffness-to-weight ratio could be increased with the same substitution. These improvements might be successful with a silicone matrix in G7, also. The caveat is appropriate surface modification of the fiberglass cloth for good adhesion with the polymer matrix.

2. *Characterization:* DIELECTRIC LOSS OF COMMERCIAL VPI RESINS.

Material behaviors of nine commercial vacuum pressure impregnation (VPI) resins are compared in this chapter using Dielectric Thermal Analysis (DETA) and Dynamic Mechanical Analysis (DMA). All nine resins have temperature ratings of class H or higher and are designed for electric machinery applications to 15 kV. The results indicate large variations in dielectric loss with temperature and frequency between resins. A phase transition was detected for each of the resins within the temperature range measured (20°C-180°C). With this baseline behavior established and combined with a literature review, two resins were chosen for subsequent aging studies. The literature review (see Appendix 4) was useful to identify possible aging mechanisms and guide design of aging protocols. Appendix 1 is a list of terms and relationships.

Assessment of dielectric loss is discussed in section 2.1, the results of the DETA and DMA analyses for the nine cured VPI resins are described in section 2.2, and the findings and recommendations from this effort are summarized in section 2.3. Complete datasets for the nine materials are in Appendix 2.

2.1. Dielectric Heating Calculated for Nine Commercial VPI Resins

Characteristic material parameters are discerned from DETA and DMA that are sensitive to small changes in the ability of the molecular structure to move in response to an external stimulus. The analyses techniques used here are well established. For DETA, an electric field is applied at varying frequency and a constant temperature. Complex permittivity is quantified, where the imaginary permittivity is related to dielectric loss. Complex electric moduli can be calculated. For DMA, a periodical mechanical strain is applied and the required stress is measured as temperature increases. Complex dynamic elastic moduli are quantified, where the loss moduli are related to viscoelastic losses (for these polymer materials). Both permittivity and elastic moduli are dependent on frequency and temperature. Viscoelastic losses contribute to heating in rotating electric machinery, although the contribution may be minor. Because of the complexity of coupling mechanical and electrical behaviors in calculations, viscoelastic losses are usually studied separately to gauge the variation in response of the material to mechanical stresses as temperature changes.[1] It is the dielectric loss that is of interest in assessing heating of insulation at higher power frequencies.

Finite Element Analysis (FEA) is now routinely used for calculating thermal runaway conditions in electric machinery. Beyond Joule heating in conductors, heating in magnetic cores is directly relatable to magnetic switching frequencies.[1] Dielectric heating is often assumed negligible in comparison. Dielectric heating in a stator's insulation as a function of switching frequency is examined in Figure 2.1. The information shows that dielectric heating increases with frequency and that inverter-fed machinery should be anticipated to have higher dielectric loss than machinery with analog power supplies. The thermal runaway threshold will be lowered as dielectric losses increase. Dielectric losses should not be ignored in thermal condition modeling & simulations.

[1] Separation of electrical and mechanical response in insulation materials is a first estimate. The electrical and mechanical responses are related.

This behavior is extremely important in considering insulation aging in machinery as higher switching frequencies are explored.

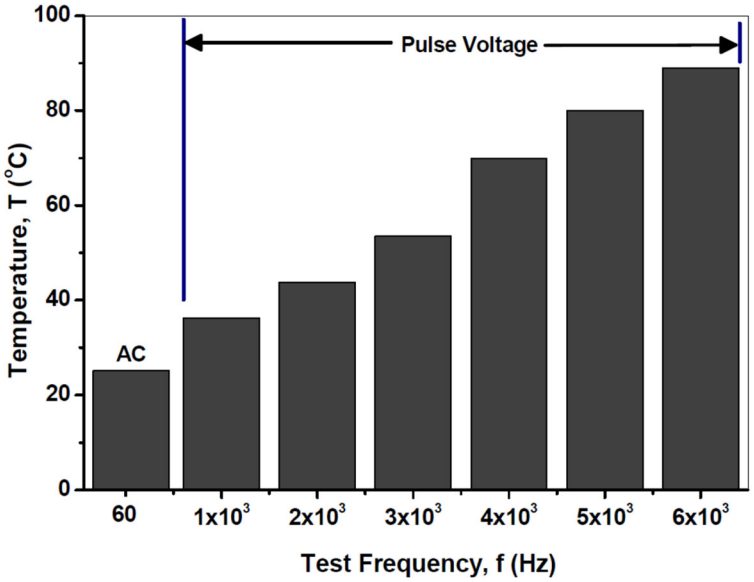


Figure 2.1. Temperature rise in groundwall insulation of stator bar samples (peak voltage 5 kV) with an increase in switching frequencies (IR camera): Figure 3.23 in [2].

The calculation of heating and temperature rise with pulsed (e.g., pulse-width modulated) waveforms is difficult. A quantitative calculation should take into account harmonics and voltage spikes.[3] Several approaches have been suggested.[3,4,5] Unfortunately, these calculations are beyond the scope of this project as there is no known rigorously reviewed or vetted approach. A computer simulation of heat flow in a stator coil due to dielectric heating comparing different materials is presented in [6]. Here the losses can be ranked based on sinewave voltage at a designated frequency and/or temperature.

The imaginary permittivity, ϵ'', is the critical materials parameter in determining dielectric loss. Imaginary permittivity is a nonlinear function of frequency in all the DETA spectra reported here. A ranking is only a reasonable first effort as loss calculations with voltage spikes and harmonics are also highly nonlinear. Equation 1 indicates ϵ'' is directly related to power loss and all power loss is assumed to result in dielectric heating. This equation also shows a linear relationship between power loss and frequency. $\frac{A}{d}$ is the geometric factor for a parallel plate capacitor configuration. The dielectric heating figure-of-merit (DH_{fom}), given by equation 2, is directly proportional to the power loss assuming a steady sinewave excitation at a constant peak voltage, V, for a given geometry. (These equations and other relationships are listed in Appendix 1.) DH_{fom} is considered a reasonable parameter for ranking at a given temperature.

$$P_{Diel} = \left(2\pi f V^2 \frac{A}{d}\right) \cdot \epsilon'' \quad (1)$$

$$DH_{fom} = 2\pi f \epsilon'' \quad (2)$$

Temperature scans of dynamic extensional moduli derived using DMA are included in this study for each material. An embedded model of the single cantilever technique was used to calculate complex dynamic extensional moduli.[2] Here sinusoidal force is applied at a constant frequency of 1 Hz to achieve a constant peak strain. Although examining viscoelastic behaviors, the results are analogous to DETA. The temperature scans may indicate phase changes in the material. DETA and DMA are considered the most sensitive techniques available to distinguish phase changes in materials.

2.2. DETA & DMA for Nine VPI Resins.

The nine VPI resins listed in Table 2.1 are all rated for at least 180°C (Class H) and 15 kV operation. These commercial resins include epoxy-, polyester-, and silicone-based products. Three of the resins were prepared in both "neat" (no filler) and "thixo" versions. The thixo versions contain ~1% of a fumed silica filler. This nanoparticulate is used in the industry to control viscosity and promote thixotropic behavior in the uncured resin. Recent evidence suggests that the addition of a silica filler may reduce localized space charge development and thereby improve erosion resistance when partial discharge is present.[7] However, the explanation may be more involved (see section 7.3.3).

Table 2.1. Nine commercial VPI resins.

Material	Manufacturer	Material Type	Insulation Class	Filler	T_g (°C)*
Conapoxy FR 1080 "Neat"	Conap	Epoxy (2-part)	Class H VPI resin	No Filler	119
Permafil 74050 "Neat"	Von Roll	Epoxy (1-part)	Class H VPI resin	No Filler	83
Permafil 74050T "Thixo"	Von Roll	Epoxy (1-part)	Class H VPI resin	Silica	52 (& 90?)
RanVar R2003 VTC "Neat"	Elantas	Polyester-Epoxy Copolymer	Class H VPI resin	No Filler	42
RanVar R2003 VTC "Thixo"	Elantas	Polyester-Epoxy Copolymer	Class H VPI resin	Silica	42
Pedigree 70VTC "Neat"	Elantas	Polyester	Class H VPI resin	No Filler	40
Silres H62c "Neat"	Wacker	Silicone	Class 220 VPI resin	No Filler	<20 & 62
Silres H62c T "Thixo"	Wacker /Wilder Innov.	Silicone	Class 220 VPI resin	Fumed Silica	<20 & 57
Damisol 3551 "Neat"	Von Roll	Silicone	Class 220 VPI resin	No Filler	<20 & 79

**Glass transition temperatures were determined from the peak dynamic loss modulus using single cantilever Dynamic Mechanical Analysis (DMA) at 1 Hz, see Appendix 2.*

[2] The model embedded in the TA Instrument's Q800 DMA instrument has been thoroughly vetted.[8]

DETA and DMA results are displayed graphically in Appendix 2. The following Figures summarize these results. Figures 2.2 and 2.3 show the real permittivity (ϵ') as a function of frequency at 50°C and 150°C. Similarly, Figures 2.4 and 2.5 show the imaginary permittivity (ϵ'') as a function of frequency at 50°C and 150°C.

The largest differences in dielectric behaviors of unaged commercial VPI resins are between the types of polymer materials. The silicone materials have consistently low real permittivity, and the polyester-containing materials have the highest real permittivity (greatly increased at low frequencies and 150ºC). The permittivities of the 1-part epoxies are improved over the traditional 2-part anhydride epoxy at the higher temperature. The large increase of dielectric loss at low frequency for all nine cured resin materials can be ascribed to an increase of conduction losses due the presence of polarizable constituents (space charges or ions) in the samples and increased charge migration on heating above the glass transition of the polymers. The presence of a silica filler appears to have a limited effect on the dielectric behavior. However, both the real and imaginary permittivities of the polyester-epoxy copolymer were reduced in the filled material.

Calculated DH_{fom} values are charted on a log scale in Figures 2.6 and 2.7 for three frequencies: 60 Hz, 10 kHz, and 100 kHz. Both an increase in frequency and an increase in temperature lead to increased DH_{fom} (i.e., higher dielectric heating). At high temperature, the Silres and Permafil materials perform the best of the five matrix resins. It is noteworthy to point out that the ordinate is a log-scale, thus the increases of these parameters is large (orders of magnitude in some cases).

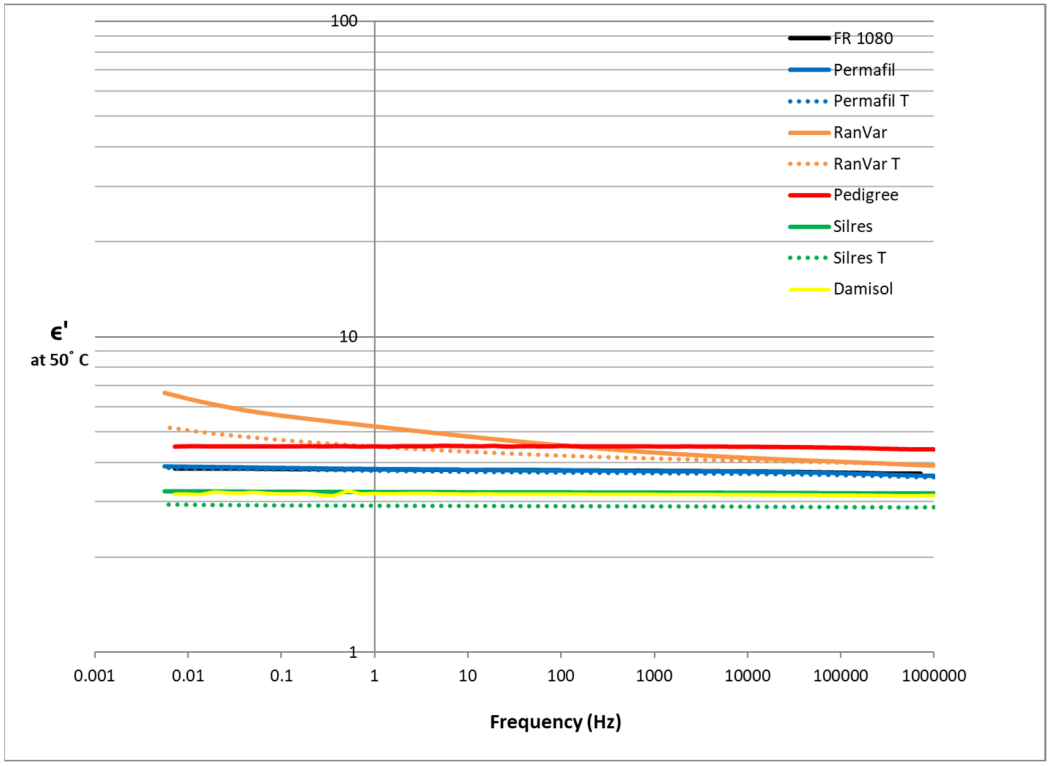


Figure 2.2. Real permittivity vs. frequency for nine VPI resins at 50°C.

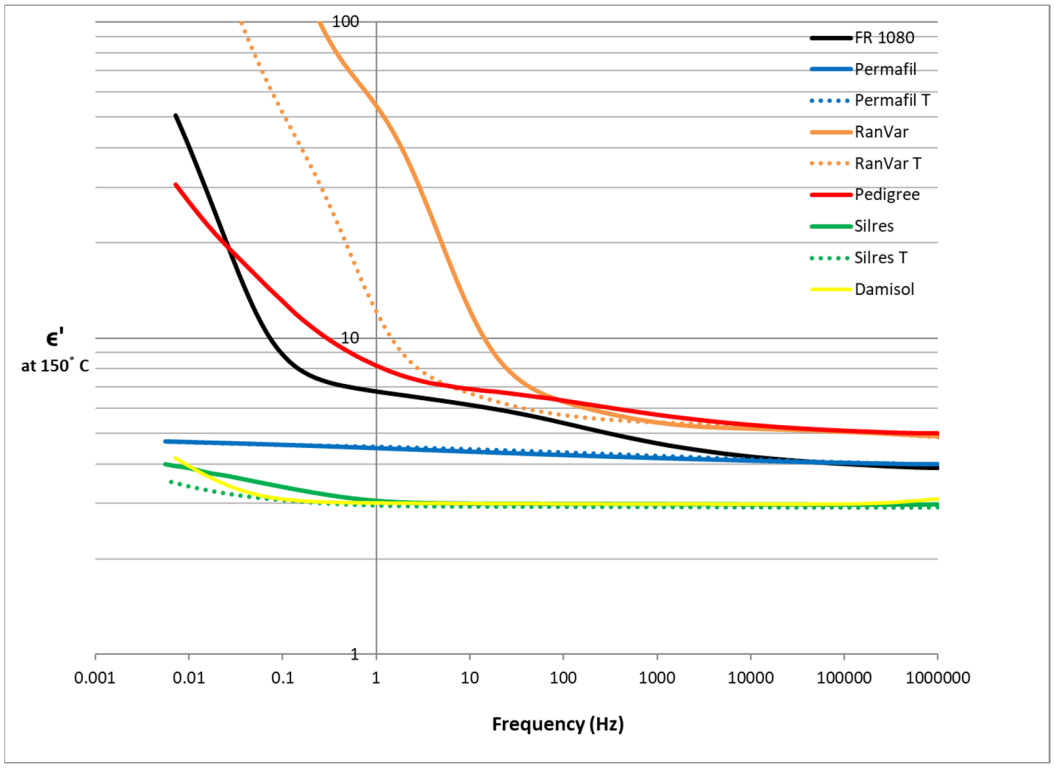


Figure 2.3. Real permittivity vs. frequency for nine VPI resins at 150°C.

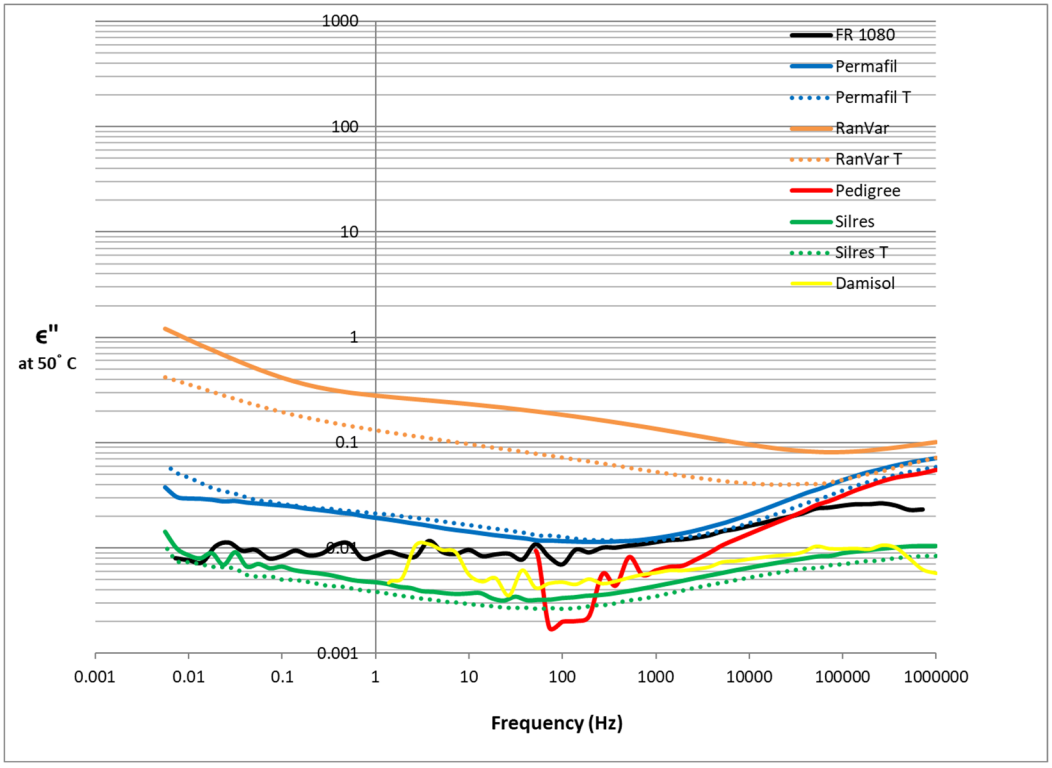


Figure 2.4. Loss permittivity vs. frequency for nine VPI resins at 50°C.

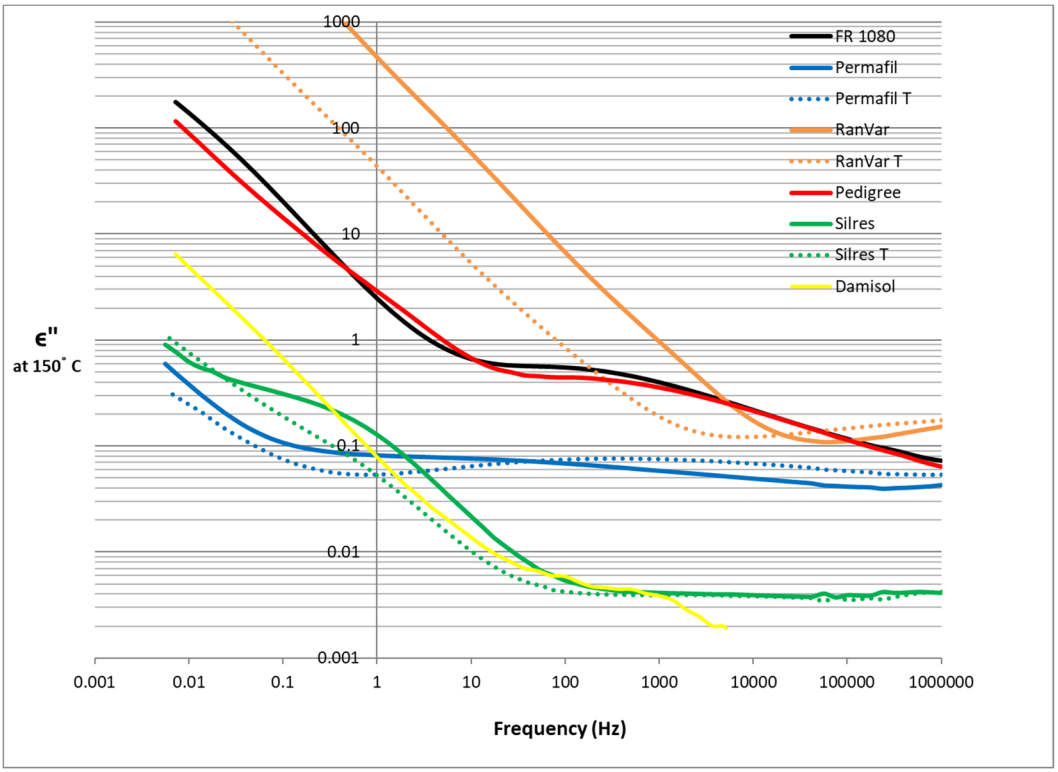


Figure 2.5. Loss permittivity vs. frequency for nine VPI resins at 150°C.

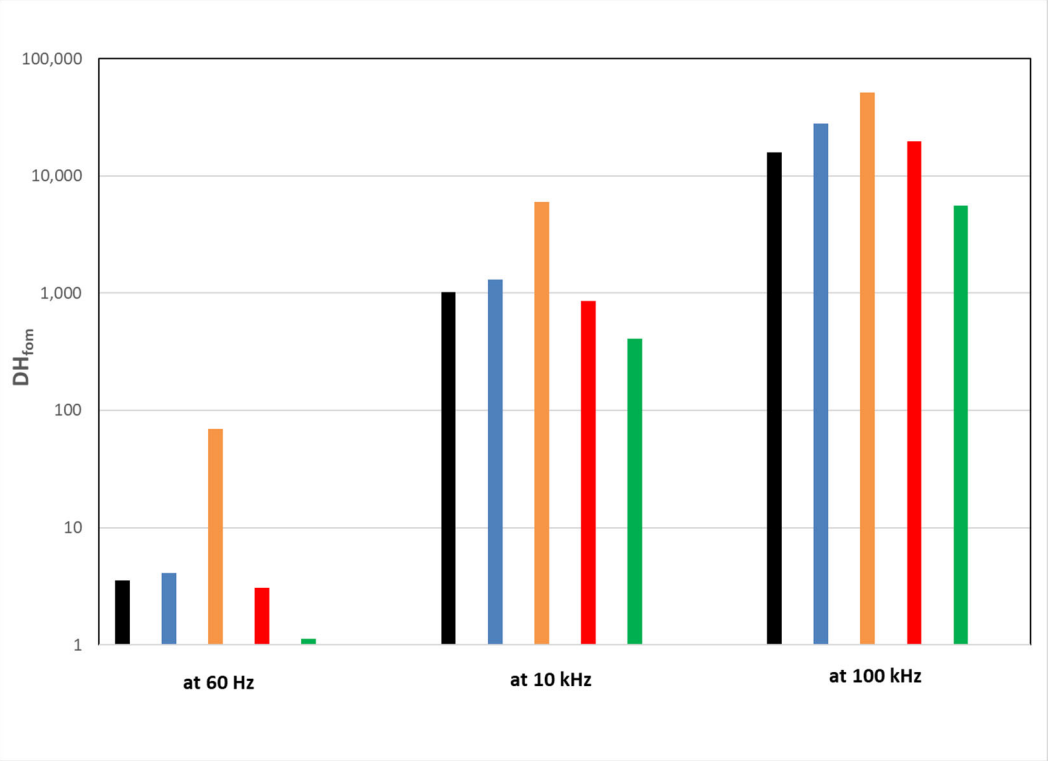


Figure 2.6. DH_{fom} for five unfilled resins at 3 frequencies: all at 50°C; (FR 1080-black, Permafil-blue, RanVar-orange, Pedigree-red, & Silres-green).

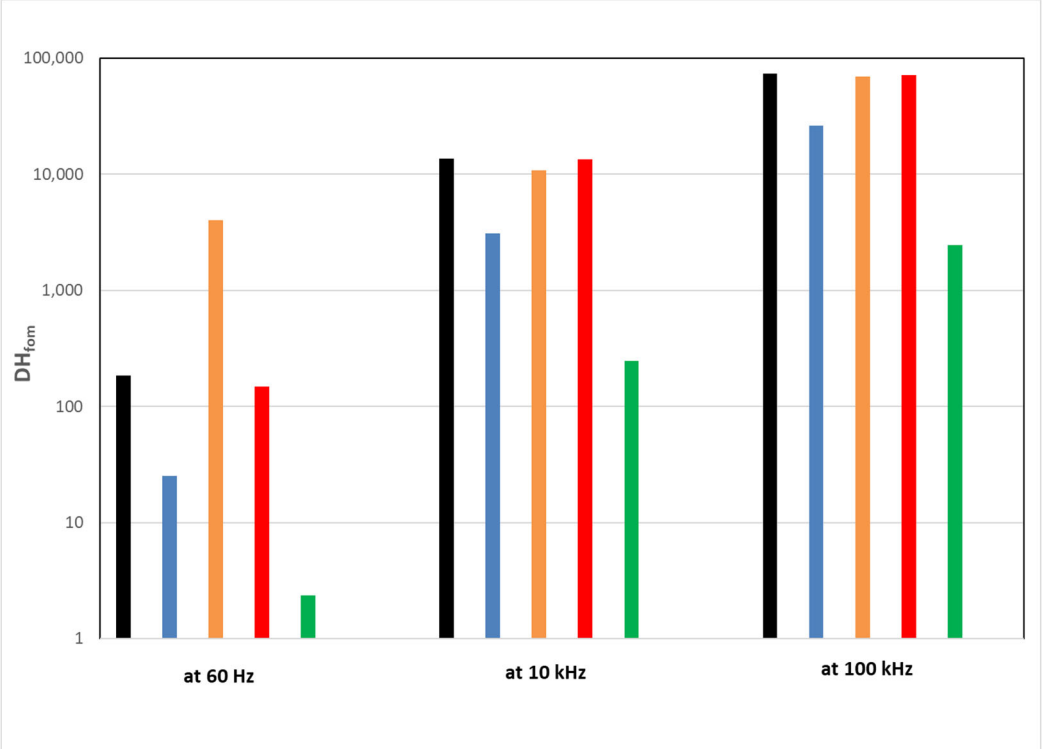


Figure 2.7. DH_{fom} for five unfilled resins at 3 frequencies: all at 150°C; (FR 1080-black, Permafil-blue, RanVar-orange, Pedigree-red, & Silres-green).

2.3. DETA of a Polyester-Epoxy Copolymer

Copolymers are materials that combine functional groups of two polymer chemistries within the polymer network. The resulting material is designed to combine properties of the two polymers without forming interfaces. Some DETA information for copolymer RanVar R2003 VTC (neat and Thixo) was included in section 2.2. In this section, the DETA and DMA of this polyester-epoxy copolymer is compared to a cured polyester resin. The copolymer is cured from a commercial resin specified for VPI processing. It is rated for 15 kV applications with temperature class H. The polyester resin by the same manufacturer is included for reference.[3] Aging studies for this resin were not pursued. The as-cured materials are designated here as:

- Rn0 – RanVar R2003 VTC, polyester-epoxy copolymer
- Rt0 – RanVar R2003 VTC Thixo, polyester-epoxy copolymer containing nano-silica
- Poly – Pedigree V70, crosslinking polyester

DETA for the copolymer is summarized in Figure 2.8. At 50°C, real permittivities of the copolymer are higher than that of the polyester and the epoxy (Pn0). At 150°C, significant low frequency charge dynamics are observed. The imaginary permittivities indicate high loss at frequencies to well above 1 Hz at this elevated temperature. The losses are significantly higher than for the polyester material (and for the epoxy materials in Figures 2.4 and 2.5). The presence of nano-silica appears to slightly reduce the charge dynamics.

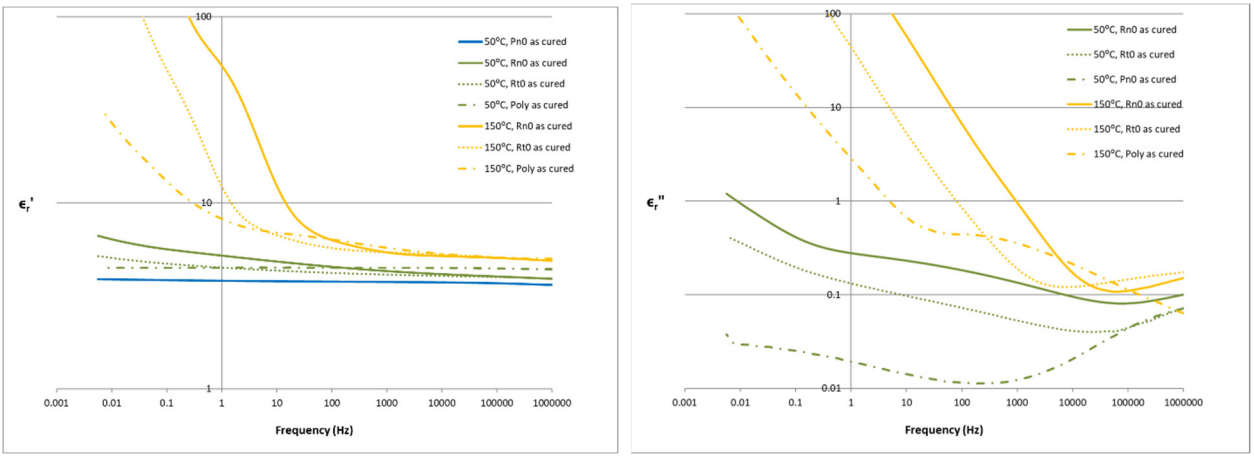


Figure 2.8. Real permittivity (left) and imaginary permittivity (right) for Rn0 (polyester-epoxy copolymer), Rt0 (with nano-silica), and Poly (polyester) at 50°C and 150°C.

Results of DMA are shown in Figure 2.9. The glass transition (T_g observed as the temperature of peak loss moduli) is higher than the T_g for polyester and lower than the T_g for epoxy Pn0. Although the dynamic storage modulus is quite high at room temperature, it falls rapidly through the glass transition. The nano-silica addition appears to increase the dynamic mechanical storage modulus and reduce the loss modulus for the cured copolymer.

[3] DETA of this polyester resin, as cured, was reported in [114].

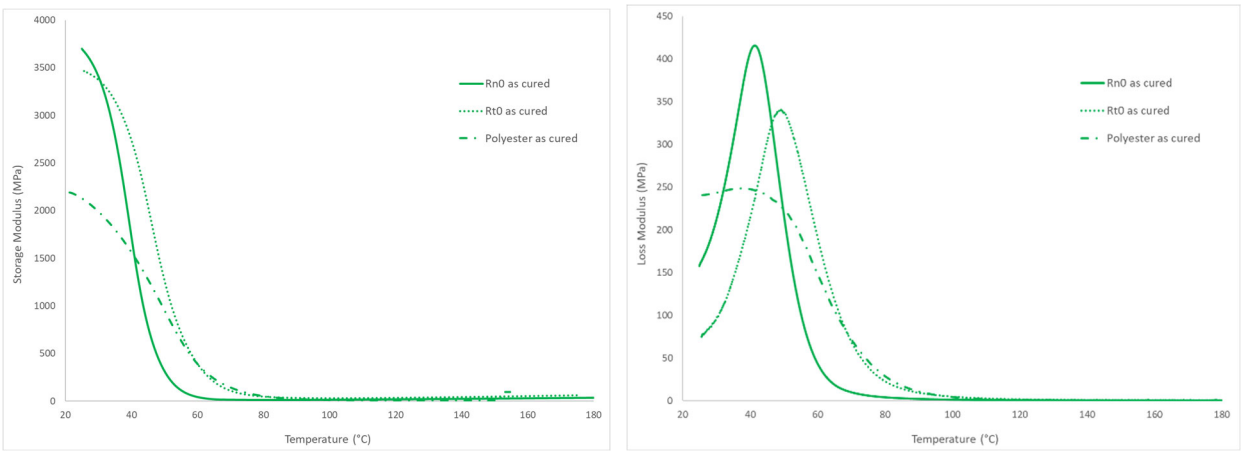


Figure 2.9. Dynamic elastic storage modulus (left) and loss modulus (right) for Rn0 (polyester-epoxy copolymer), Rt0 (with nano-silica), and Poly (polyester) at 1 Hz.

The combination of a low glass transition temperature, very high real permittivity, and high imaginary permittivity at high temperatures may be representative of copolymers and polymer blends. This is supported by a published DETA study of copolymers.[9] These are not desirable properties for power-dense machine insulation. The additional degrees of freedom in the copolymer network structure and lower glass transition appear to have moved the α-relaxation to higher frequencies than for either the epoxy or the polyester materials. The results underscore the need to include this type of DETA and DMA in any resin selection program.

2.4. Summary of Dielectric Loss Comparison for VPI resins

1. Large differences in dielectric behavior are observed between cured VPI resins as temperature and frequency are varied. This indicates that there will be large differences in dielectric heating and thermal loads in machines where these resins are used. Considering this type of data when choosing a VPI resin could reduce the dielectric heating and thermal load in electric machinery.

2. Specifying a resin based on one or two real permittivity and tan(δ)[4] values is inadequate for machines using variable speed drives (vsd) or variable frequency drives (vfd). We recommend DETA as shown here when qualifying a VPI insulation for a machine design. The DMA temperature scan at a reference frequency (e.g., 1 Hz) is sensitive for identifying phase changes and their characteristic temperatures. Monitoring the change in DMA information with aging is an important tool. The "time zero condition" or unaged condition of the cured resin is needed to monitor how the molecular structure or the thermodynamic phase (i.e., crystal or glass phase) changes in use. DMA is an important tool for planning condition-based maintenance of insulation materials.

[4] tan(δ) is the ratio of the imaginary permittivity to the real permittivity. One value at a specified frequency is often used to gauge dielectric loss in electrical insulation.

3. Permafil 74050 (a 1-part epoxy product of Von Roll) and Silres H62c (a silicone product of Wacker), both unfilled, were chosen for the aging studies reported in Chapter 6. Permafil was ranked second in high temperature permittivity and has excellent mechanical properties. Silres was ranked best for all-round permittivity and has excellent thermal properties.

4. The epoxy-polyester copolymer investigated showed dramatically increased real permittivity and loss permittivity compared with either an epoxy or a polyester material. Due to the modified network structure, this behavior may be typical of copolymers and resin blends. The results underscore the need to include this type of DETA and DMA in any resin selection program.

Appendix 2 contains DETA and DMA datasets for each of the seven resins. The real permittivity and loss permittivity spectra at six temperatures are plotted along with the extensional storage and loss moduli as a function of temperature.

3. *Review:* PHYSICAL AGING

Aging of polymer materials in service is difficult to categorize as many different forces may act at any given time and those forces can change over time. There are numerous potential paths that engender aging and the path can influence the behavioral change. Aging of polymer materials has been studied for decades.[10] Laboratory studies usually provide insight as to singular aging mechanisms for model materials. It is difficult to extrapolate these mechanisms to composite materials in more complicated environments. A brief guide on physical aging is provided here to help categorize aging treatments, mechanisms, and resulting behavior changes. An in-depth discussion of aging can be found in Chapter 7. Figure 3.1 depicts six main categories of polymer aging. The categories are physical, thermal, mechanical, electrical, ionizing radiation, and ambient.

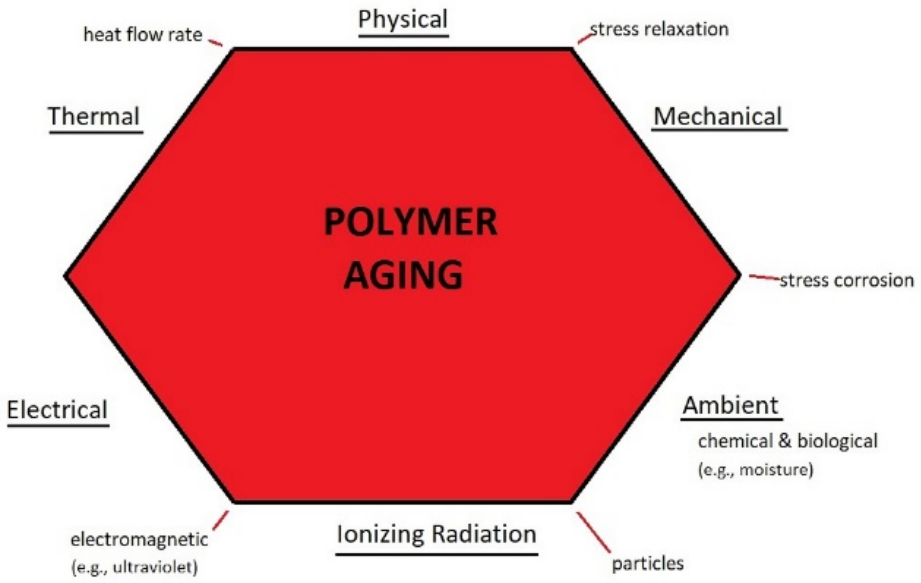


Figure 3.1. Six categories of polymer aging.

Physical aging has been limited to refer to shift in a material's glass transition (due to varied cooling rate through the transition, for example). A traditional diagram of paths leading to this effect is shown in Figure 3.2. As a material experiences physical aging, the total density is expected to change. Shift in the glass transition is directly related to free volume change in the molecular structure. A change in free volume, in turn, may vary the dynamic behavior at the molecular level. Rheological behavior is observed based on macro-scale properties. As the rheological behavior varies, a change in response to electromagnetic and/or mechanical fields can be anticipated. The term "molecular dynamics" is preferred for motions on the scale of the microstructure and meso-structure. Chain reorientations, crystal nucleation, and crystal growth may be encouraged. With composites, it is particularly important to remember that the dimension of polymer matrix between filler particles or crystals of the polymer, itself, may be on the order of a micron. Interfacial interactions are also important. A discussion of interface concepts can be found in section 7.2.

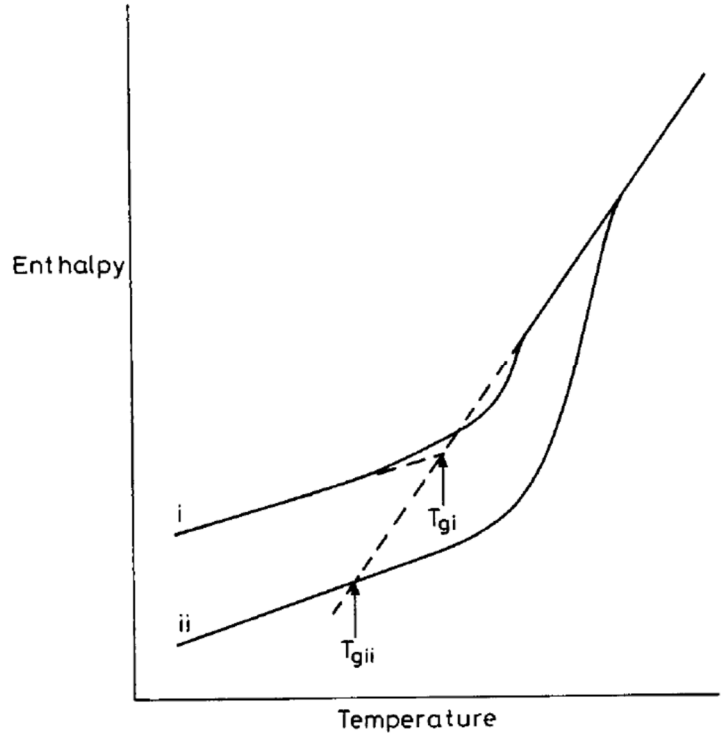


Figure 3.2. Schematic of enthalpy vs. temperature paths for (i) quenched glass and (ii) well-annealed glass demonstrating physical aging.[11]

The mechanisms involved in the limited definition of physical aging are considered reversible. David and LaMarre[12] stated that "physical aging, involving free volume relaxation, also occurs in the absence of any significant external stress, being related only to the fact that a given material might not be at thermodynamic equilibrium at a given temperature". Crystal growth and changes in crystal structure may also be reversible under many conditions.[13] A recent schematic (shown in Figure 3.3) is useful for visualizing a variety of possible morphological phases in polymeric microstructures (c and d). Associated phase changes do not require change in chemical composition such as oxidation, hydration, and/or decomposition. Here, the materials studied are known to be stable to oxidation and/or decomposition to avoid ambient aging during heat treatment. (This is discussed in Appendix 4). For thermal aging, temperatures were chosen well below the maximum continuous use temperatures. More in-depth studies could be pursued to confirm exact aging mechanisms. Our goal is to survey materials and point to possible changes occurring in polymeric insulation with moderate heating over time as might be experienced in service.

The heat treatments used had a cooling rate of <1°C/min. The results indicate that the high temperature (lower volume) structure established at the dwell temperature is largely maintained even with this low cooling rate. Although physical aging occurs, the maintenance of the high temperature (low density) structure dominates. Because the cumulative effect is important, and due to the accompanying possibility of phases changes (e.g., phase separation, crystallization, crystal growth), the term "thermal aging" will refer to extended exposure to temperatures above room temperature. The resulting structure is best characterized by a combination of DETA and DMA.

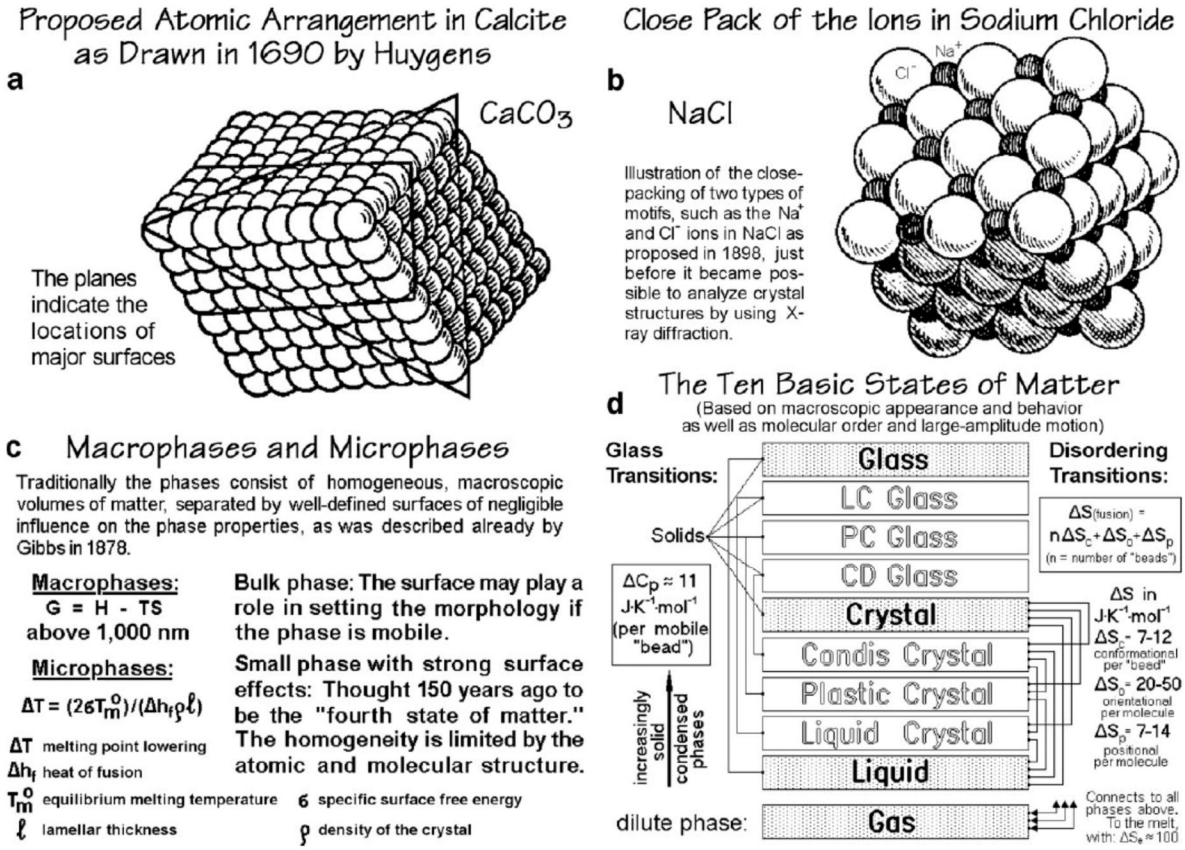


Figure 3.3. Diagram: a and b- development of the knowledge of crystal structure, c- phase property and size, and d- the 10 basic states of matter.[14]

4. *Characterization:* DETA & DMA of THERMAL AGED COMMERCIAL POLYMER COMPOSITES

Thirteen commercial engineered composite materials were characterized before and after a thermal heat treatment. The materials were chosen to survey four groups of polymer matrix materials, all well known for their high temperature properties. The temperature of the heat treatment (120°C or 160°C) was below the maximum continuous use temperature reported by each manufacturer. (In later studies, heat treatment was changed to a uniform exposure of 100 hours at 155°C, but keeping the same sample designation of "HT".) The cooling rate was <1°C/min. Table 4.1 provides information on each of the materials.

The three matrix polymer materials examined are used as a primary insulation layer on copper wires. These polymers are polytetrafluoroethylene (PTFE), polyimide (PI), and polyetheretherketone (PEEK). The polymers are also manufactured with fillers. Fillers are of interest as it has become popular to add a nanodielectric filler to a polymer matrix to improve erosion resistance in the presence of surface partial discharge (see section 7.3.3 for some published information). The filler sizes in the composites studied here are in the range of microns and some of the fillers are proprietary. Fillers of this size can improve stiffness and thermal conductivity, as well as improve erosion resistance to partial discharge. Two of the materials are specifically designed and marketed for static charge reduction. One of the materials is filled with graphite. This latter material is considered analogous to a graphite based, semiconductive tape often used on medium voltage windings. Fiberglass laminate polymer matrix composites are commonly specified in electrical equipment represented here by FR5, G7, and GPO3 designations.

The anticipation is that commercial engineered composite materials *will change* when exposed to temperature, even below the maximum continuous use temperature. This is important to consider prior to examining specific aging of electrical insulation in more depth. As the twelve materials are all commercial products and only limited knowledge of the manufacturing processes is available, interpretation of the data is also limited. The information provided here should be considered a survey. Further work could be pursued to explain changes observed after the heat treatment. Both DETA and DMA techniques utilize relatively large, flat samples. Coatings on wire are difficult to analyze, so differences in processing between primary layer materials and the materials analyzed here are to be expected. The summary points are made keeping this fact in mind. It is important to all subsequent aging studies that DETA and DMA are shown to identify complimentary information as to changes in behavior with a relatively minor thermal aging regimen (as compared with many years in service).

A summary of the DETA and DMA data is provided in the following four sections. Each section describes the effect of the 48 hour heat treatment on materials of one of the groups: PTFE, PI, PEEK, or fiberglass laminates. A more complete set of plots for each material is provided in Appendix 3. The findings and recommendations regarding thermal aging are summarized in section 4.5.

Table 4.1. Thirteen commercial materials surveyed.

Material	General Info	Material Condition	Max Cont. Use Temp. (°C)*	Aging Temp. (°C)
Polytetrafluoroethylene (PTFE) Matrix				
PTFE	low dielectric constant primary layer candidate	semicrystalline	260	120
PTFE + 25% glass		semicrystalline, filled	260	120
Fluorosint 500 PTFE + mica	machined	semicrystalline, filled	260	120
Semitron ESD 500hr PTFE + synthetic mica	machined static dissipative product	semicrystalline, filled	260	120
Polyimide (PI) Matrix				
PI XP-131 Polyimide	machined primary layer candidate	amorphous	260	120
PI XP-130 Polyimide + 30% PTFE	machined	amorphous, filled	260	120
PI XP-132 Polyimide + 15% graphite	machined	amorphous, filled	260	120
Polyetheretherketone (PEEK) Matrix				
Ketron 1000 virgin PEEK	primary layer candidate	semicrystalline	250	160
Ketron PEEK GF30 PEEK + 30% glass	machined	filled	250	160
Semitron ESD 520hr PEEK + proprietary filler	machined static dissipative	filled	260	160
Structural Insulation Products				
FR5 (epoxy matrix)	2D cloth in molded sheet	nonisotropic fiberglass laminate	180	160
G7 (silicone matrix)	2D cloth in molded sheet	nonisotropic fiberglass laminate	221	160
GPO3 (polyester matrix)	fiber mat in molded sheet	nonisotropic fiberglass laminate	160	120

**Maximum Continuous Use Temperature as reported by manufacturer on material datasheet.*

4.1. Comparison of PTFE Materials.

PTFE is a common dielectric insulation material due to a high breakdown strength, small dielectric loss, ease in forming to very thin coatings and superior reliability. PTFE coated wire products are inexpensive and widely available throughout the electronics industry. PTFE film is also used in capacitors. PTFE exhibits good durability at both high and low temperatures, resistance to many industrial chemicals and moisture, and fire resistance. Wire with PTFE insulation has become widely used in automotive and downhole drilling applications.

Four materials with a matrix of polytetrafluoroethylene (PTFE) were included in this survey. Material PTFE is pure with no filler, PTFE+25GF contains 25% glass filler, Fluorosint 500 is a mica filled PTFE, and Semitron ESD 500hr is another mica filled PTFE. The real permittivities for the PTFE materials at 50°C are shown in Figure 4.1 and at 150°C in Figure 4.2. The imaginary permittivities at 50°C and 150°C are shown in Figures 4.3 and 4.4.

The unfilled PTFE exhibited the lowest and most temperature stable complex permittivity of all materials studied. Heat treatment has limited effect on the real permittivities of the materials in the PTFE group. All PTFE matrix composites showed a small decrease in both real and imaginary permittivity across the frequency range. The two mica filled materials showed a decrease in imaginary permittivity below 1000 Hz at high temperature. Filling with glass caused a significant increase in imaginary permittivity.

The addition of fillers dramatically increases the dynamic storage modulus of PTFE. The heat treatment had some minor effects, notably a slight increase in a phase transition at ~45°C with a slight decrease in a phase transition at ~60°C. Only Semitron ESD 500hr became notably stiffer with heat treatment.

DETA spectra at six temperatures were plotted for each material. These are accompanied by DMA temperature scans at 1 Hz in Appendix 3.

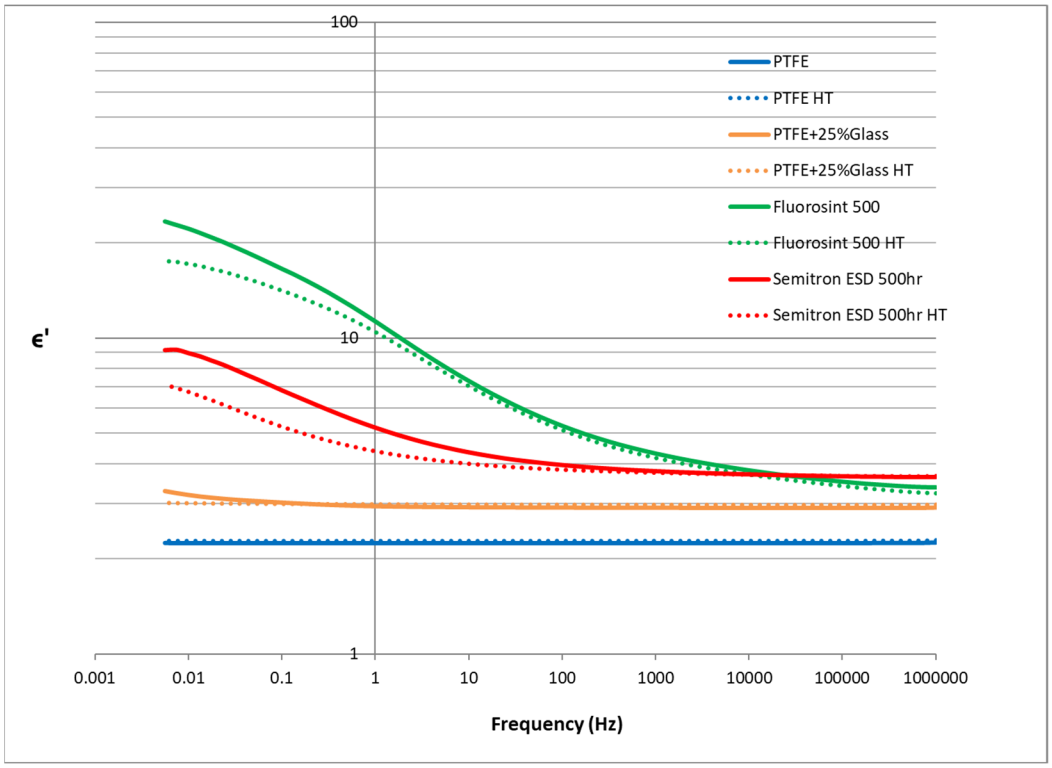


Figure 4.1. Real permittivity vs. frequency for PTFE matrix materials at 50°C.

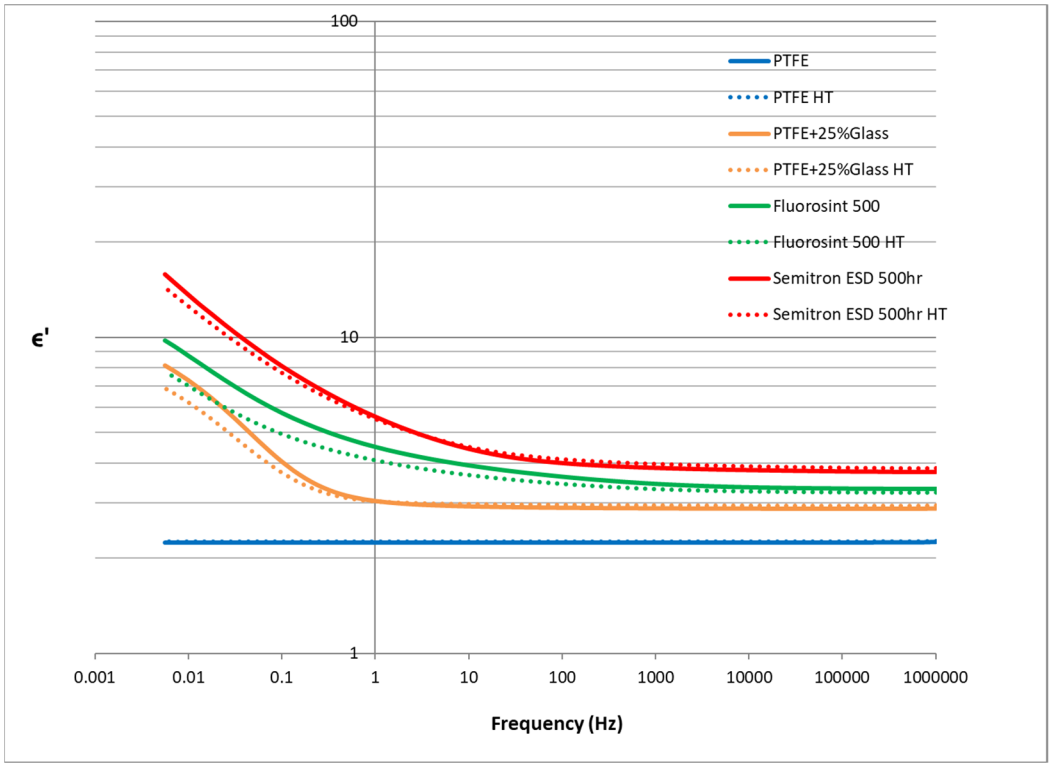


Figure 4.2. Real permittivity vs. frequency for PTFE matrix materials at 150°C.

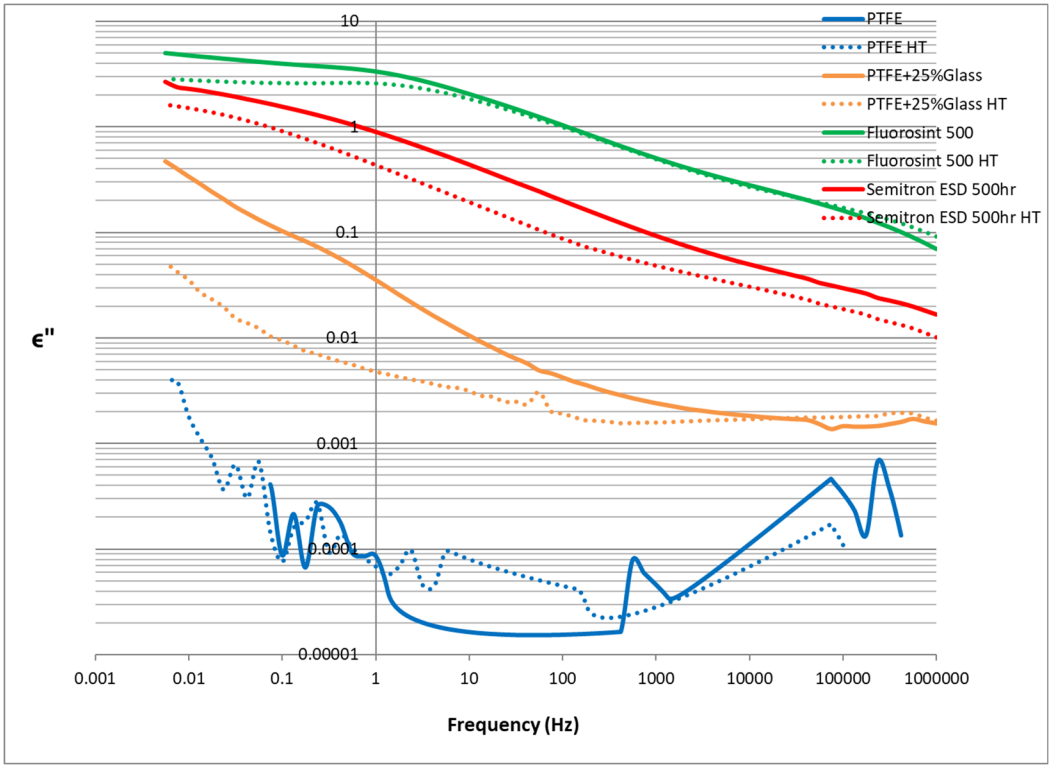


Figure 4.3. Imaginary permittivity vs. frequency for PTFE matrix materials at 50°C.

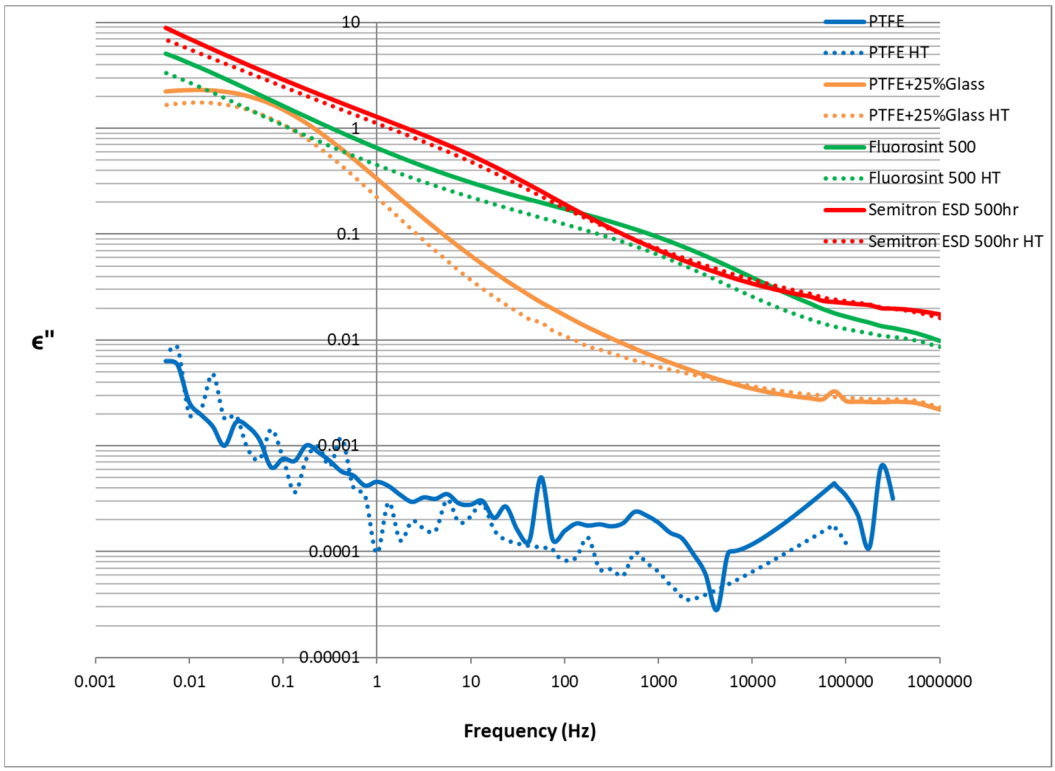


Figure 4.4. Imaginary permittivity vs. frequency for PTFE matrix materials at 150°C.

4.2. Comparison of PI Materials.

Polyimide (PI) coatings have been used as electrical insulation since the early 1970's. The wide temperature range for use and extremely high breakdown strength both encourage the widespread application of PI. This material is specified as a primary layer in several medium voltage insulation systems due to its compatibility with VPI resins. The low density of PI has encouraged its use in aircraft wiring. However, there have been concerns regarding low resistance to mechanical wear. When used as a primary layer, PI insulation material can be protected by a secondary layer (e.g., a VPI resin). This also mitigates concerns regarding combustibility.

Three materials with a matrix of polyimide (PI) were included in this survey. Material XP-131 is pure with no filler, XP-130 contains 30% PTFE filler, and XP-132 contains 15% graphite filler. The real permittivities for the PI materials at 50°C are shown in Figure 4.5 and at 150°C in Figure 4.6. The imaginary permittivities at 50°C and 150°C are shown in Figures 4.7 and 4.8.

Both the unfilled PI and the 30% PTFE filled polyimide exhibited excellent permittivities across the frequency range. With heat treatment, these two materials exhibited a slight decrease in both real permittivity across the frequency range and imaginary permittivity at frequencies below 1 Hz. The polyimide filled with 15% graphite was very sensitive to the heat treatment. Both real permittivity and imaginary permittivity decreased dramatically after heat treatment, particularly at frequencies below 1000 Hz.

The dynamic elastic moduli of these materials are very different. Where the unfilled and 15% graphite filled polyimide show a decrease in storage modulus after heat treatment, the 30% PTFE filled polyimide shows an increase in storage modulus. The unfilled polyimide has a distinct glass transition near 65°C that diminished with heat treatment. A second glass transition was not observed for unfilled PI. The two filled materials initially also have glass transitions near 65°C. With heat treatment, a glass transition at lower temperature was favored and the loss modulus near 65°C decreased.

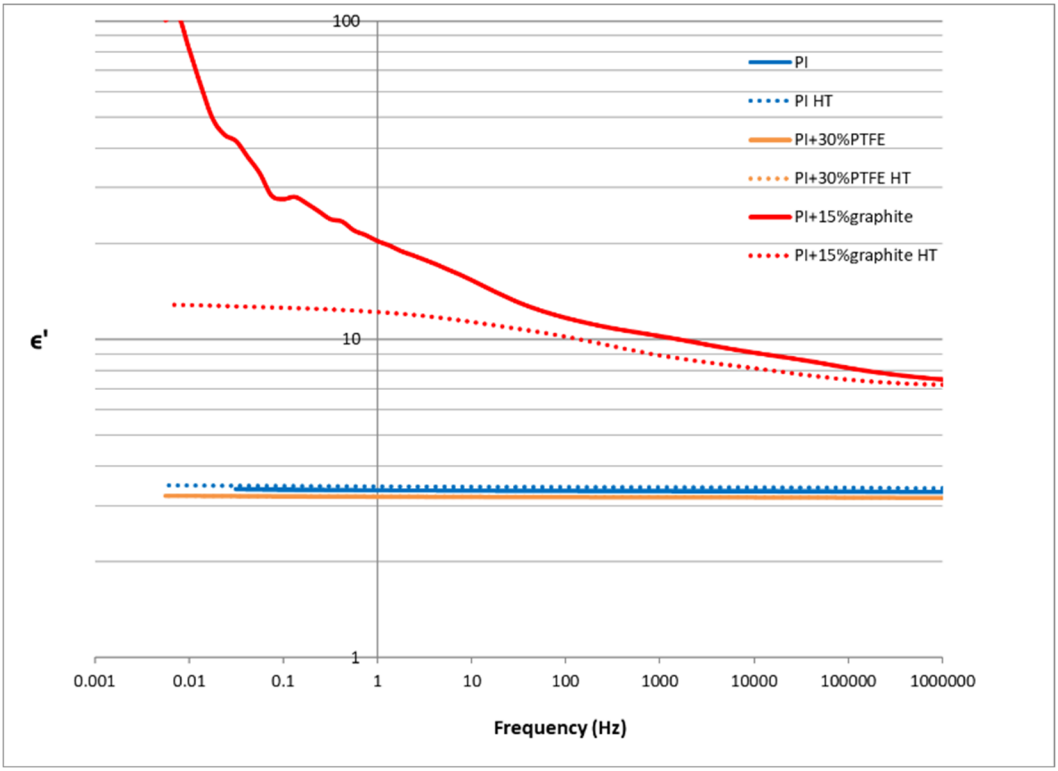


Figure 4.5. Real permittivity vs. frequency for PI matrix materials at 50°C.

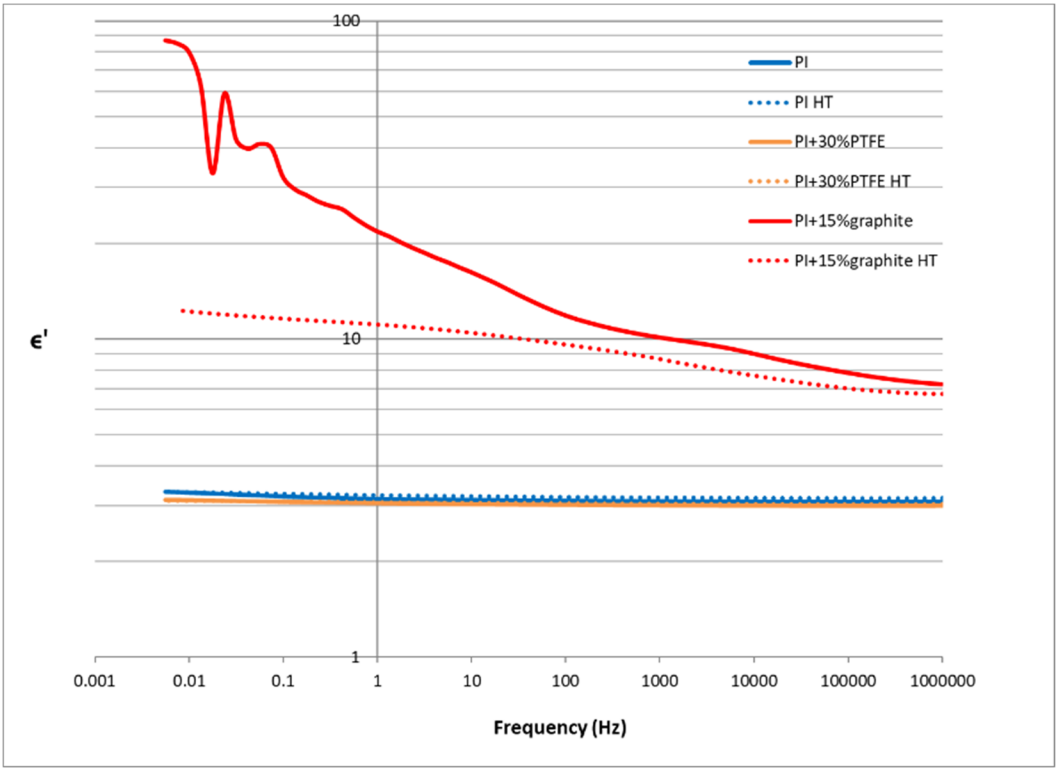


Figure 4.6. Real permittivity vs. frequency for PI matrix materials at 150°C.

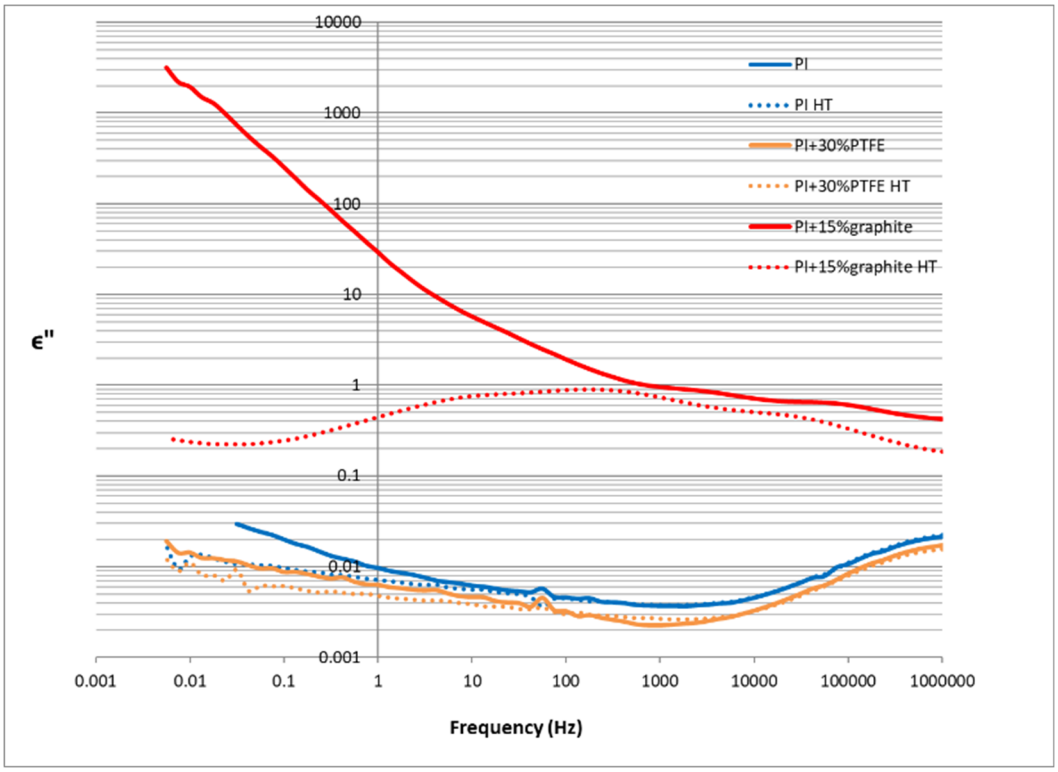


Figure 4.7. Imaginary permittivity vs. frequency for PI matrix materials at 50°C.

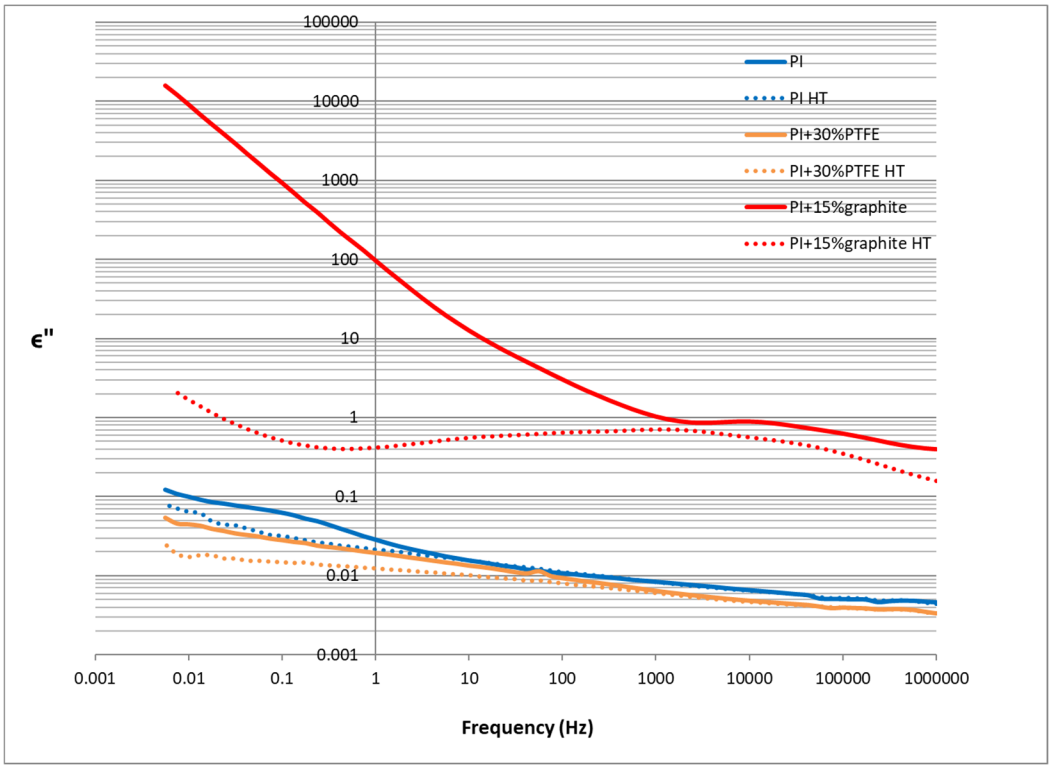


Figure 4.8. Imaginary permittivity vs. frequency for PI matrix materials at 150°C.

4.3. Comparison of PEEK Materials.

Polyetheretherketone (PEEK) has a very high strength-to-weight ratio and maintains a high tensile strength over a wide temperature range. It is particularly useful in abrasive environments, where the primary insulation layer cannot be protected. PEEK has a good resistance to harsh chemicals and moisture. There are also reports of high resistance to some forms of radiation. As a relatively new insulation for wires, PEEK coatings are more expensive and less available than PTFE and PI. Experience with this material is now being gained in the electric machine industry.

Three materials with a matrix of PEEK were included in this survey. Material PEEK0 is pure with no filler, PEEK30GF contains 30% glass filler, and ESD 520hr contains a proprietary dielectric filler. The real permittivities for the PEEK materials at 50°C are shown in Figure 4.9 and at 150° C in Figure 4.10. The imaginary permittivities at 50°C and 150°C are shown in Figures 4.11 and 4.12.

Decreases in real permittivity and imaginary permittivity are observed after heat treatment in all three materials of the PEEK group. The permittivity values are good at and below 125°C. At 150 °C, the losses are much higher. As a consequence, the use of PEEK materials as electrical insulation above 125°C should be carefully considered. The Semitron ESD 520hr material has higher complex permittivity at all frequencies.

All three materials exhibit a strong glass transition near 65°C. The response of this transition to heat treatment varied. For unfilled PEEK, the dynamic storage modulus increased and the glass transition decreased (as evidenced by a decrease in the loss peak at 65°C). The 30% glass filled PEEK had a high dynamic elastic modulus which decreased slightly with heat treatment. The Semitron ESD 520hr also exhibited a reduction in loss modulus at 65°C with a better defined and narrower loss peak after heat treatment.

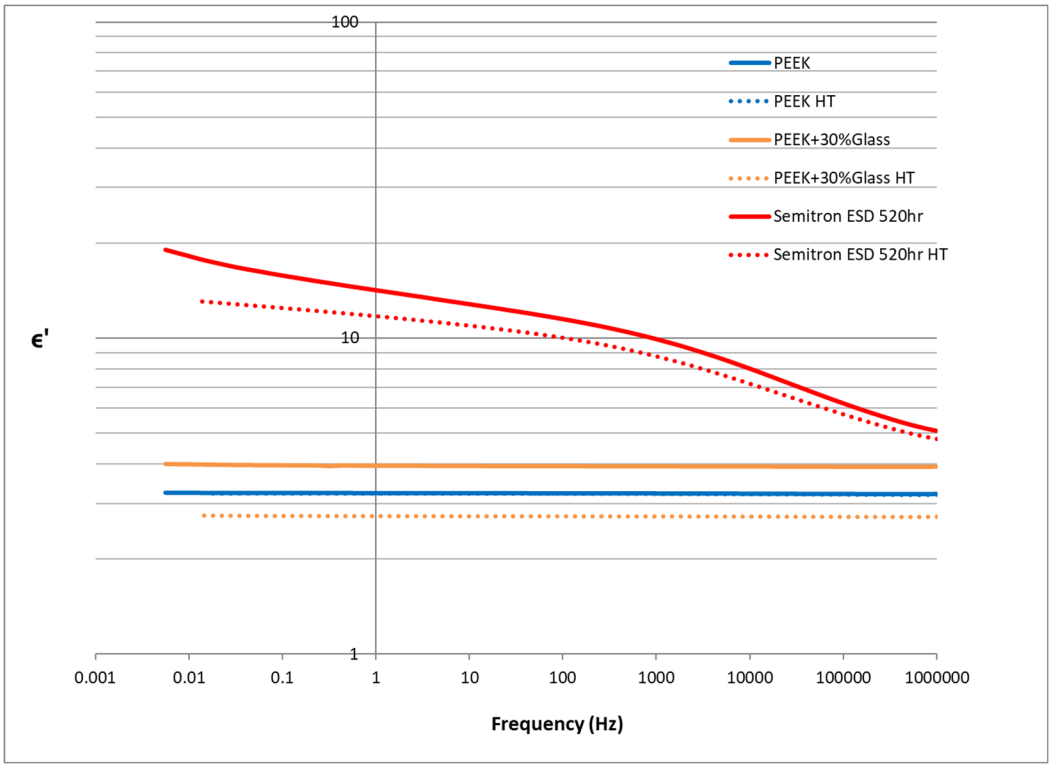


Figure 4.9. Real permittivity vs. frequency for PEEK matrix materials at 50°C.

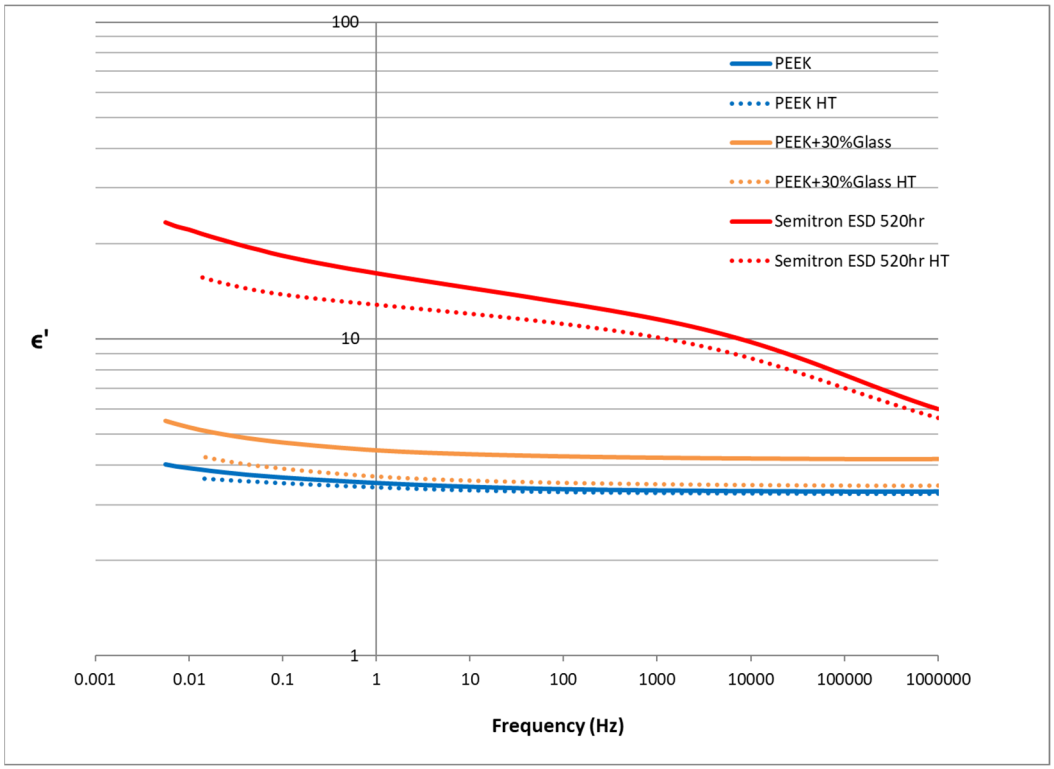


Figure 4.10. Real permittivity vs. frequency for PEEK matrix materials at 150°C.

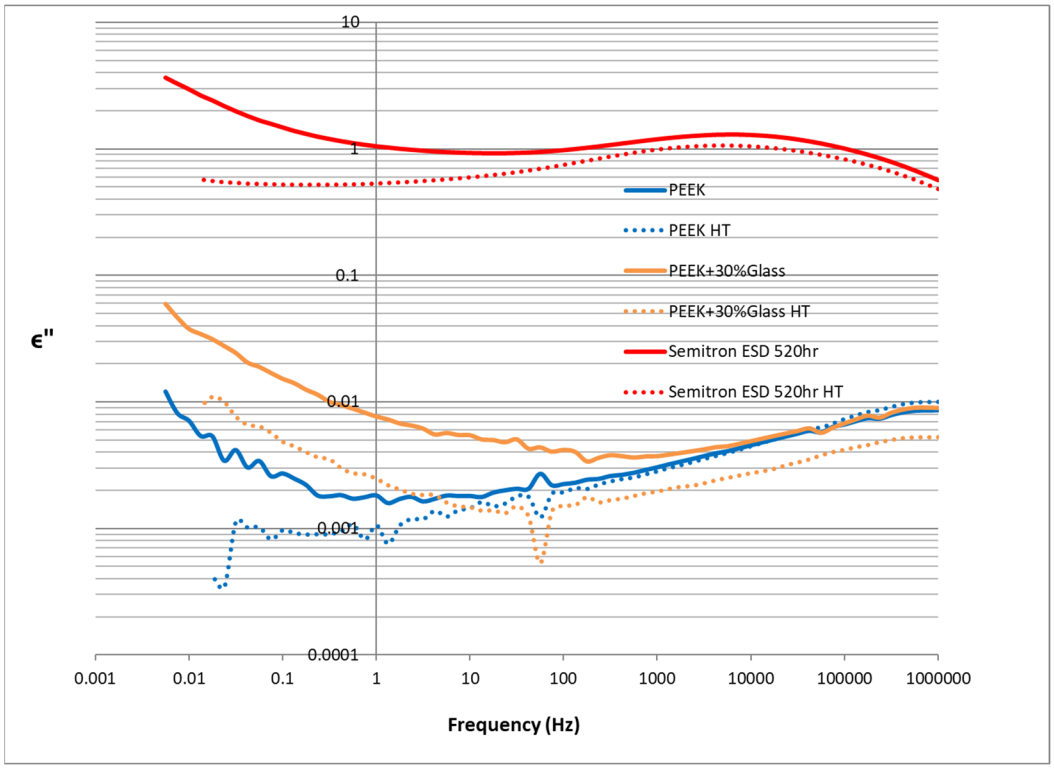


Figure 4.11. Imaginary permittivity vs. frequency for PEEK matrix materials at 50°C.

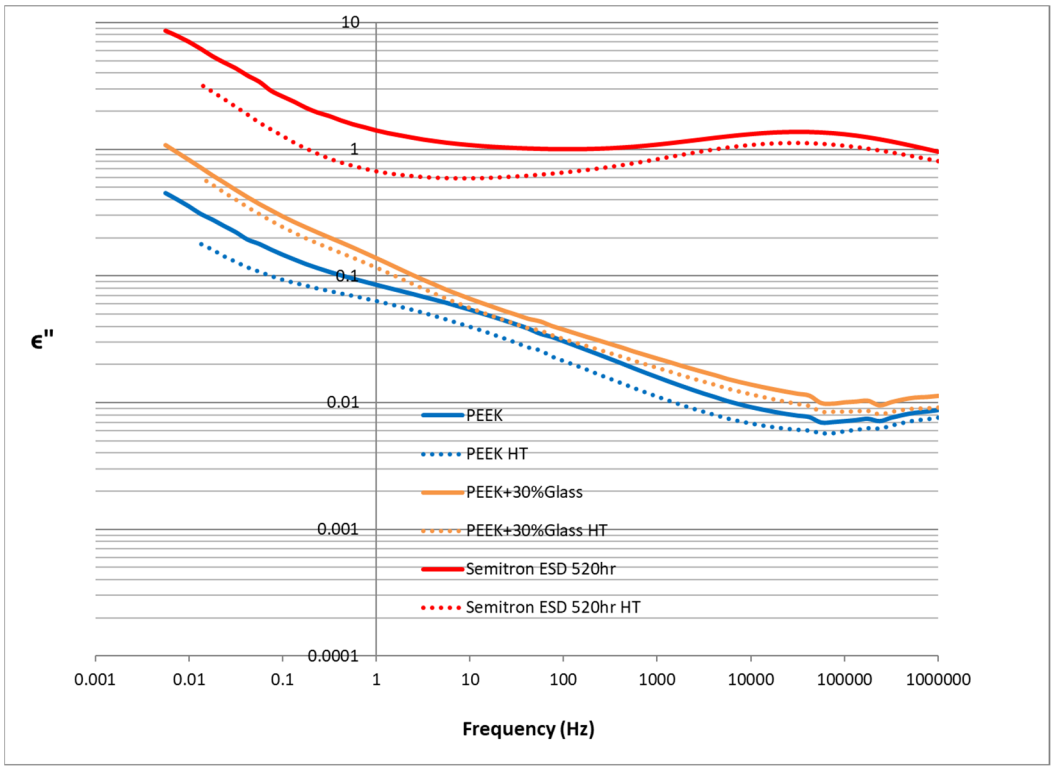


Figure 4.12. Imaginary permittivity vs. frequency for PEEK matrix materials at 150°C.

4.4. Comparison of Structural Laminate Materials.

Structural laminate materials can be purchased in several formulations and in a variety of shapes and sizes. Flat insulating laminate materials are used as a base for printed circuit boards. These laminates are typically a woven e-glass cloth compression molded in a polymer matrix. The e-glass has a low sodium content to reduce space charge accumulation. The embedded textile increases stiffness and provides high toughness. The materials are machined to size and used as spacers, slot covers, end plates, and other electric machine components.

Three structural laminate materials containing fiberglass cloth were included in this survey. Laminate G7 has a cured silicone resin matrix. Laminate FR5 is a fire-resistant version of G11 with a cured epoxy resin matrix. Laminate GPO3 has a cured polyester resin matrix and is noted for surface arc resistance. The real permittivities for the fiberglass laminate materials at 50ºC are shown in Figure 4.13 and at 150ºC in Figure 4.14. The imaginary permittivities at 50ºC and 150º C are shown in Figures 4.15 and 4.16.

The G7 material exhibited a constant and low real permittivity at temperatures of 100ºC and below. The imaginary permittivity was also very low at these temperatures. Almost no change was indicated in the complex permittivity of FR5 with heat treatment. FR5 exhibited high losses above 100ºC. GPO3 exhibited high losses for all conditions.

Both fiberglass laminates have extremely high dynamic mechanical storage moduli at room temperature (~4x that of the unfilled resin). The dynamic storage modulus of G7 diminishes at lower temperatures after heat treatment. A glass transition near 65ºC becomes much better defined and a broad loss peak at higher temperatures is greatly reduced after heat treatment. The dynamic storage modulus of FR5 decreased with the heat treatment. The glass transition at 120ºC shifted to higher temperatures and a new glass transition was detected near 68ºC. The dynamic storage modulus of GPO3 was lower than that of either G7 or FR5 at all temperatures. A glass transition centered at 55°C expanded towards 80°C with heat treatment at 120°C. The broad band observed in the dynamic loss modulus could be indicative of a second, higher temperature glass transition.

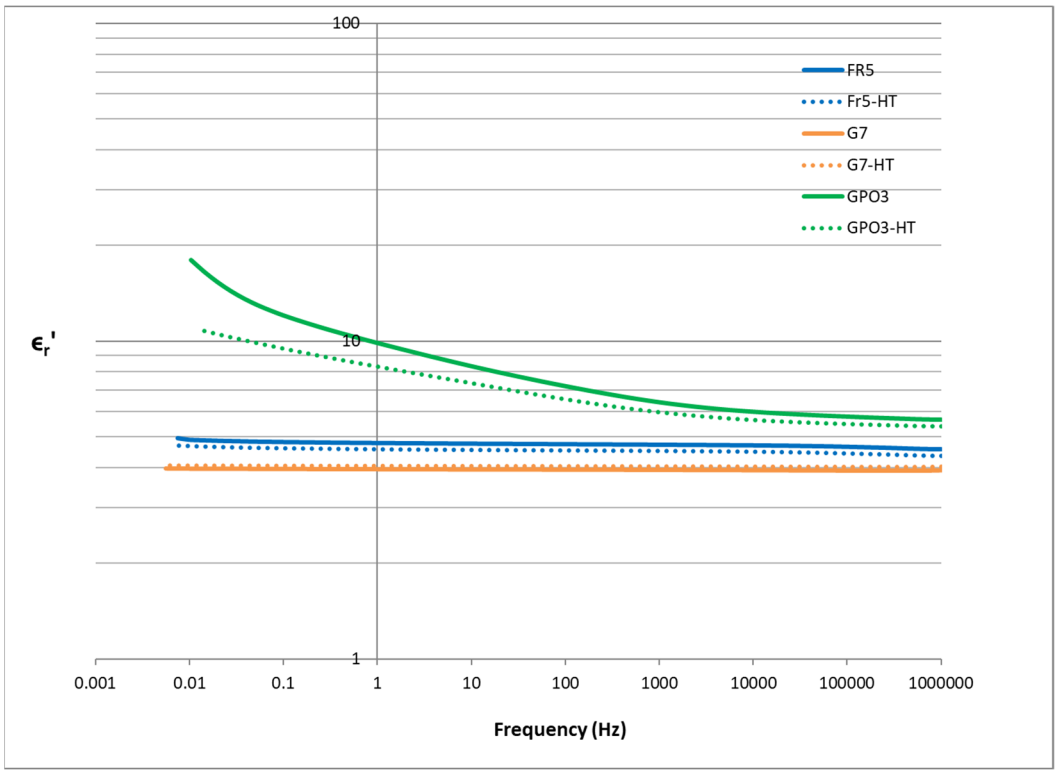


Figure 4.13. Real permittivity vs. frequency for fiberglass laminates at 50°C.

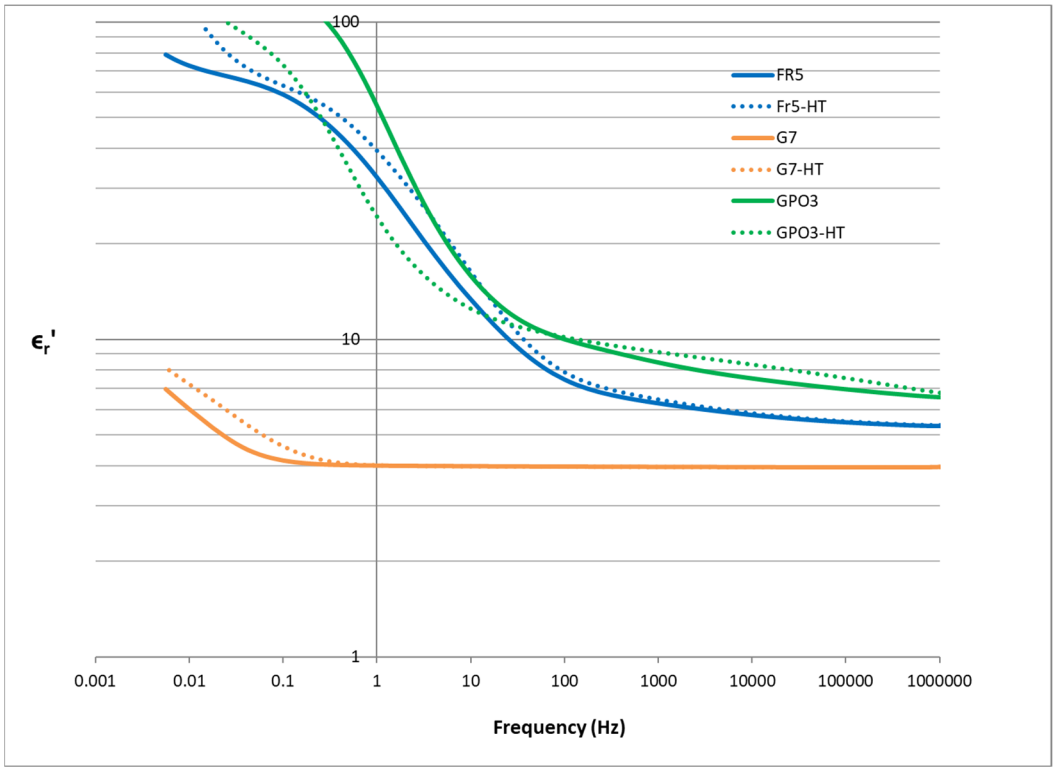


Figure 4.14. Real permittivity vs. frequency for fiberglass laminates at 150°C and at 125°C for GPO3 and GPO3-HT.

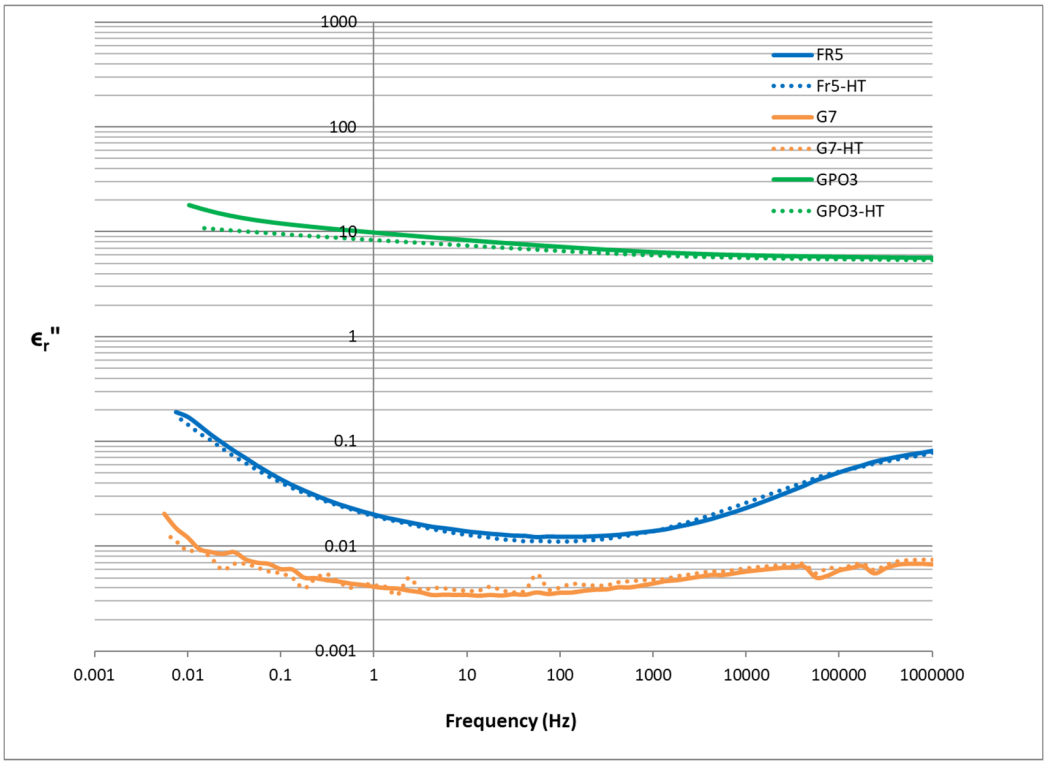


Figure 4.15. Imaginary permittivity vs. frequency for fiberglass laminates at 50°C.

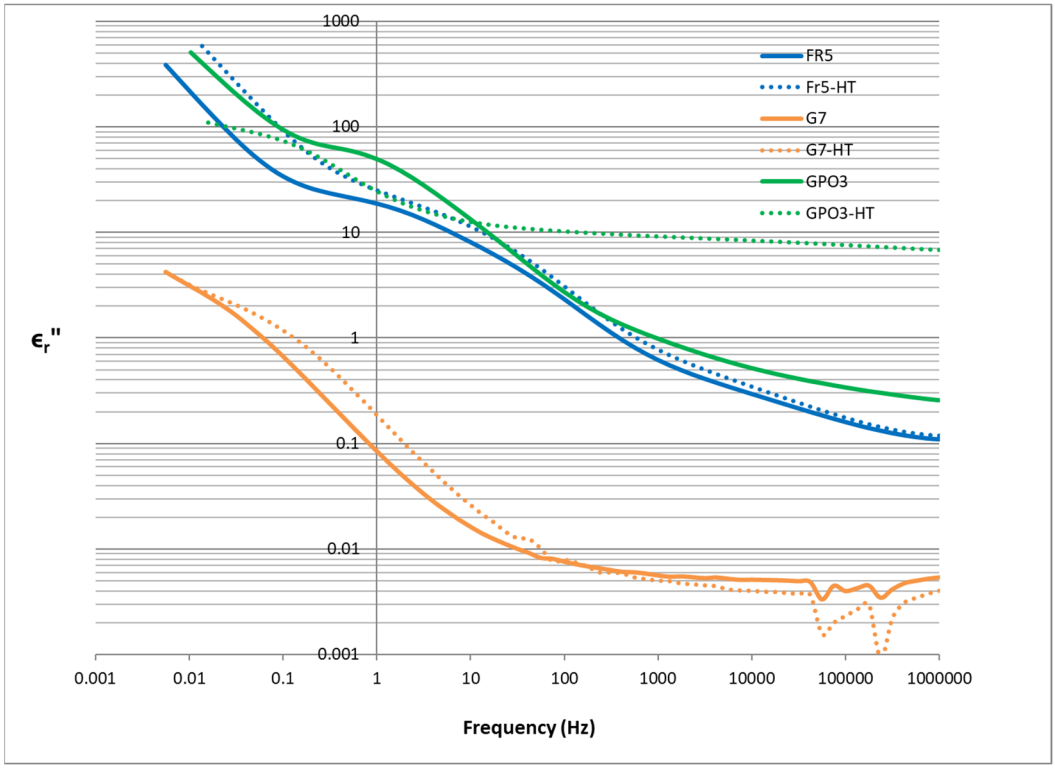


Figure 4.16. Imaginary permittivity vs. frequency for fiberglass laminates at 150°C and at 125°C for GPO3 and GPO3-HT.

4.5. Summary of Thermal Aging of Commercial Polymer Composite Materials.

The spectra reported in this section show that polymeric materials thermally age to different degrees when exposed to a relatively minor heat treatment for 48 hours. After an extended period in service where elevated temperatures are experienced, the behavior of polymer insulation is anticipated to change. If the change is potentially reversible (i.e., a morphological rearrangement of the molecular structure), this change is considered "Physical Aging". The life history is important in gauging a material's subsequent response to more critical or extreme aging environments. The life history is built into the evolving molecular structure and can be described by examining molecular dynamics (i.e., rheological response to stimuli on the meso-scale) using DETA and DMA.

The behavioral changes reported here varied widely. Our current approach to this issue is to document the propensity for *thermal aging* of each material on a laboratory sample. The variability can then be considered when examining statistical behavior for more extreme aging environments (e.g., via Weibull analysis). To clarify, we would anticipate the PTFE filled polyimide material (XP-130) to exhibit a much lower standard deviation "in service" to an appropriate condition-based maintenance model than the static dissipative filled PEEK material (Semitron ESD 520hr) using the information gathered in this effort. The following four points summarize other findings.

Effect of heat treatment: Nine of the twelve materials exhibit decreases in both real and imaginary permittivity across the frequency range after heat treatment. The extent of change can be seen more clearly with the expanded axes in Appendix 3. Two fiberglass laminate materials both exhibit slight increases in real and imaginary permittivities across the frequency range. A notable exception is the graphite-filled polyimide material (XP-132), which exhibited a very large reduction in real and imaginary permittivities at frequencies below 100 Hz. This dielectric response to heat treatment was consistent for all temperatures studied.

More varied behavior was observed for dynamic elastic moduli as a function of temperature after heat treatment. Change in the dynamic storage modulus is minor for the PTFE group materials and dramatic for the PI group materials. The dynamic loss modulus tends to decrease with heat treatment. A notable exception is the synthetic mica-filled PTFE (ESD 500hr), which exhibited increased loss at temperatures above 70°C. The composites with thermoplastic matrices exhibit a shift of glass transition region to lower temperatures. After heat treatment, a second glass transition at a higher temperature was indicated for two thermoset matrix composites.

Primary layer materials: The three unfilled polymer materials are representative of polymers used as a primary insulation layer on copper wires. PTFE exhibits the least change in complex permittivity and complex dynamic storage moduli with heat treatment. Although the complex permittivity of PI (XP-131) remained relatively unchanged, both the dynamic storage moduli and the loss moduli showed significant decrease. PEEK exhibited an increase in dynamic storage moduli at temperatures above 45°C. Although the imaginary permittivity decreased with heat treatment, it remained much higher at 150°C. PEEK may not be the best choice for primary layer insulation at temperatures above 125°C.

Effect of fillers: The presence of fillers increased both the real and imaginary permittivities. A notable exception is the PTFE-filled PI material (XP-130). Both of the static dissipative materials and the graphite-filled PI have large increases in imaginary permittivity. The two mica-filled PTFE materials also exhibited large increases in imaginary permittivity, particularly at higher temperatures. This finding is also investigated for mica tape products which are used routinely in insulation systems for medium voltage machinery (see section 8.5).

Comparison of fiberglass laminate materials: The G7 and FR5 fiberglass laminate materials are also routinely used in medium voltage machinery. The G7 material has low real and imaginary permittivities across the spectrum with little change after heat treatment. This is particularly dramatic at elevated temperatures. The reduction in dynamic mechanical storage modulus for G7 after heat treatment should be considered as a trade-off with predicted lower dielectric heating in comparison to FR5. The very high variations in complex permittivities and dynamic elastic moduli for GPO3 laminate indicate inferior temperature stability and lower thermal aging resistance.

Simulations of dielectric heating and effect on local temperature: Two separate studies utilizing the loss data reported here present (i.) adiabatic heating calculations due to dielectric losses [15]; and (ii.) heat transfer simulations for dielectric heating at 100 kHz switching frequency for a stator bar in a non-adiabatic environment [6]. These publications demonstrate further utility of the reported data.

Using DETA and DMA techniques, thermal aging has been documented with relatively modest heat treatments for thirteen commercial polymer composite materials. The twelve materials are analogous to materials used in insulation systems. Polymers representing three primary layer insulation materials, filled versions of these materials, a material representing semiconducting grading tape, and fiberglass laminates were included. The materials showed varying degrees of changed behavior with heat treatment. Recommendations are that DETA and DMA should be utilized as demonstrated for qualifying insulation materials. These analysis techniques also provide data that should prove useful in establishing condition-based maintenance for insulation systems in electrical machinery.

5. *Review:* KINETIC MODELS OF AGING.

Dielectric materials include polymers, ionic salts (e.g., NaCl), and ceramics (e.g., $BaTiO_3$). Electrical insulation is often a composite system of several dielectric materials. The manufacturability, low permittivity, and ductility of some polymers makes them valuable in electrical insulation systems. Of the materials used in common insulation systems, it is the polymers that dominate aging. This Chapter summarizes information on aging phenomena in polymer materials pertinent to this report.

5.1. Nature of Aging

The properties of polymer materials will change over time. We define this progressive change as aging.[16] The property changes (i.e., aging) may sometimes be beneficial. The rates of such property changes are generally hard to characterize as they can be very small and due to multiple different underlying phenomena. Because of the importance to engineering, aging is currently extensively studied and modeled. Dielectric breakdown, itself, is not considered an aging process. Properties of the material along a breakdown path will change. However, dielectric breakdown is usually extremely rapid. Rapid changes can be separated and referred to as catastrophic degradation.

Aging Mechanisms: There are two outcomes of aging:

1. Reversible aging: including both "physical aging" and "healing" schemes; and
2. Irreversible aging: including forms of structural changes on multiple size scales.

Various mechanisms are used to examine and differentiate between specific aging behaviors in polymers. A listing of some possible outcomes of aging mechanisms is shown in Table 5.1.

Table 5.1. List of some possible outcomes of aging mechanisms for insulation materials.

"Chemical or Ambient Aging"	"Thermal Aging"	"Field Intensity"
Volatilization	Crystallization	Fatigue
Carbon Formation	Zone Melting	Creep /Stress Relaxation /Annealing
Oxidation	Chain Scission / New Crosslinks	Crack Growth
Hydration	Free Volume or Density Changes	Environmental Stress Cracking
Contaminant Diffusion	Phase Separation	Interfacial Debonding /Delamination
		Void Formation
		Space Charge Concentration

Along with aging rate, the dominant aging mechanism is dependent on the material, the condition of the material, and the environment (particularly ambient chemicals, pressure, temperature, and any other stress). Aging mechanisms are usually studied in single component (ideal) polymers.

Phase Changes: Phase changes can be reversible. Physical aging is typically studied in amorphous and semicrystalline polymers by monitoring specific volume, viscosity, or enthalpy with various cooling and heating rates. As polymer processing and heating methods have become more complex, the observation of physical aging has expanded. When physical aging coincides with other aging mechanisms, the property changes during phase transformation often become irreversible.

Dynamic Measurements: Dynamic measurements provide a macroscopic quantification of the character of "molecular dynamics" (i.e., the movements of polymer molecules in a controlled environment and under prescribed stresses). Molecular dynamics can be probed on nano-, meso- and micro-scales using various broadband experiments, including DETA. Significant and thorough theoretical information on molecular dynamics is available.[17] Rheology, the study of deformation and flow either in the time or frequency domain, gives property information that is highly sensitive to microstructural changes, including phase changes. DMA experiments provide complex rheological information. The application of dynamic measurements to aging will be further discussed in section 5.3.

5.2. Lifetime Prediction

The basis of lifetime prediction is to assess reliability. Aging is often studied to predict lifetime of a material exposed to a specific environment. "End of life criteria" may be chosen as a set of properties reaching pre-established values. For example, exposure to partial discharge will gradually lower the insulation breakdown strength to a quantifiable field level. The aging rate with exposure to partial discharge is critical information to gauge when an insulation's breakdown strength will be reached.

Accelerated Aging: Accelerated aging testing, where the conditions of laboratory aging are more extreme then in practice, adds additional uncertainty to lifetime prediction. Accelerated aging is generally successful with single component materials, when molecular dynamics only vary due to heating, and when phase changes do not occur in service. In these limited situations, Arrhenius models are valuable tools for examining kinetic behavior. With exceptions to these limits, semi-empirical modifications to Arrhenius models are required.[18] Arrhenius models are predicated on extracting activation energies to use in rate equations and probability statistics. One difficulty is that highly modified Arrhenius models rarely improve understanding of the aging behavior or active aging mechanisms. Electrical insulation systems are usually layered polymer matrix composite materials, rarely used in a temperature use range without phase change, and usually experience a multi-stress environment. Furthermore, the polymer microstructures, themselves, may be quite complex. Lifetime prediction testing methods continue to be improved.[19]

5.3. Molecular Dynamics and Aging

The use of dynamic measurements to study aging is making rapid progress. The connection between dynamic measurements and aging of polymers is foundational for developing lifetime predictions with complex environments. This compendium is providing information to help establish that connection. Dynamic behavior determines a polymer material's response to alternating fields in the range of 10^{-3} to 10^{6} Hz. Dipolar activity in this regime (i.e., polarizing motion) sensitizes the material to fields and stresses (e.g., chemical sensitivity, heat conduction, ultrasound transmission). As documented in section 6, aging changes the dynamic behavior of polymer materials. Four relevant topics in dynamic behavior are introduced in this section.

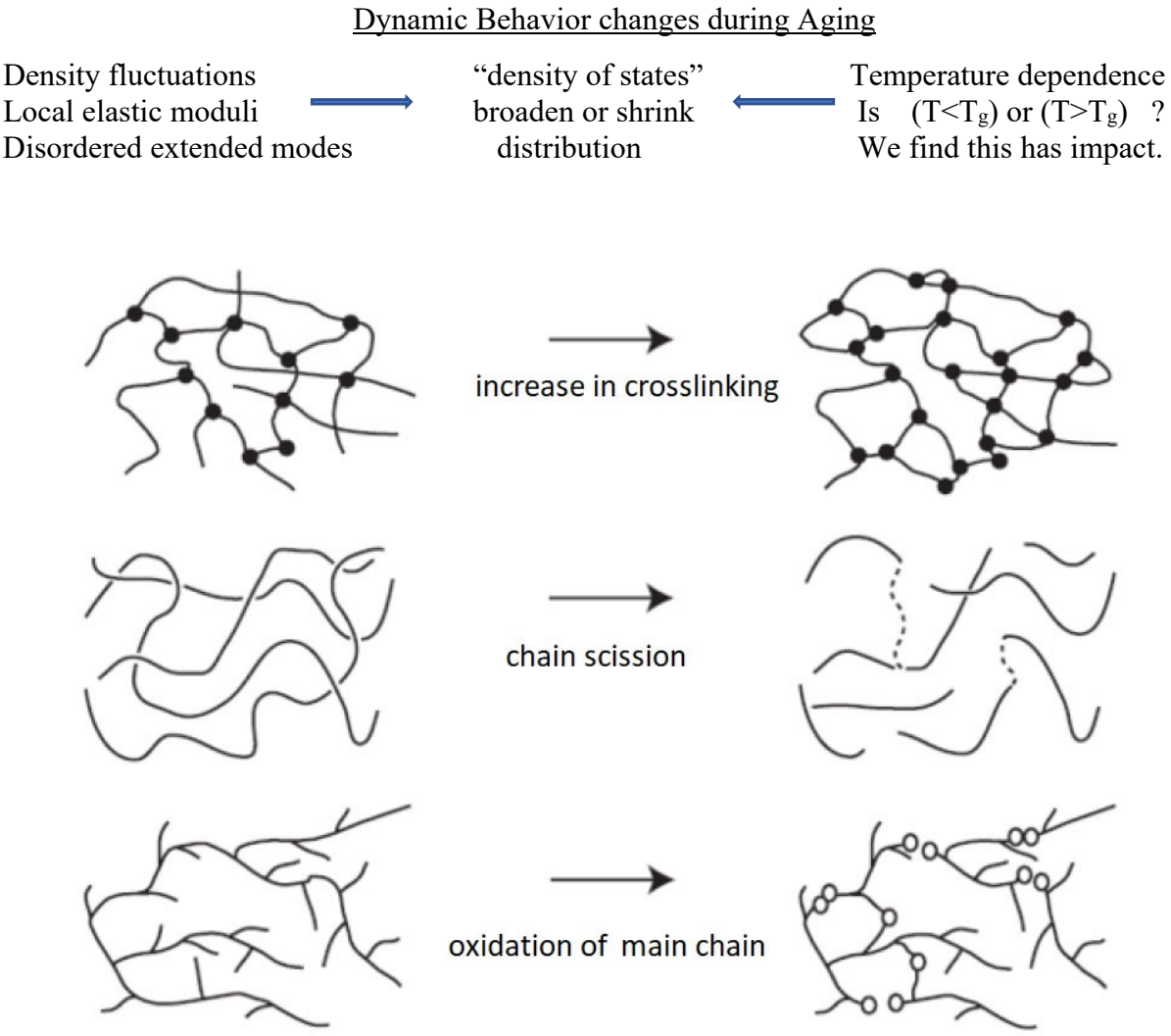


Figure 5.1. Schematics of structural changes that promote variation in dynamic behavior.[20]

Molecular Dynamics and Internal Friction: Where molecular dynamics examines the movement of features of the polymer's structure, "internal friction" gauges the resistance to that movement. Internal friction may be considered the loss component of molecular dynamics (e.g., damping). The mathematical frameworks for molecular dynamics are well-developed: the Linear Response Theory (for low electric field strengths) and the Fluctuation Dissipation Theorem (macroscopic response is related to microscopic fluctuations). Both theories are used to predict spectral densities as a function of frequency as electric dipoles polarize and move.[21]

Phase Changes: As the state of a material nears a phase change, the molecular dynamics change dramatically. An example is amorphous material undergoing a glass transition, which is currently studied in the context of "jamming" of regions of the material. Energy accommodation within the material structure also changes. Inhomogeneities, such as density fluctuations or phase separation, ensure that dynamic behavior is not uniform on the nanoscale, mesoscale, and microscale.

Dynamic losses expressed by both elastic and dielectric responses are intense during phase changes, resulting in highly nonlinear moduli. Consequently, resilience of the material is near a minimum. We postulated that the material could be more sensitive to aging when approaching a phase change.[5] Common phase changes in polymers are glass transitions, crystallization/melting, and recrystallization or crystal growth. Order-disorder and oriented-isotropic transitions may be considered phase changes. Figure 5.2 shows schematics of the polymer chains before and after such transitions.

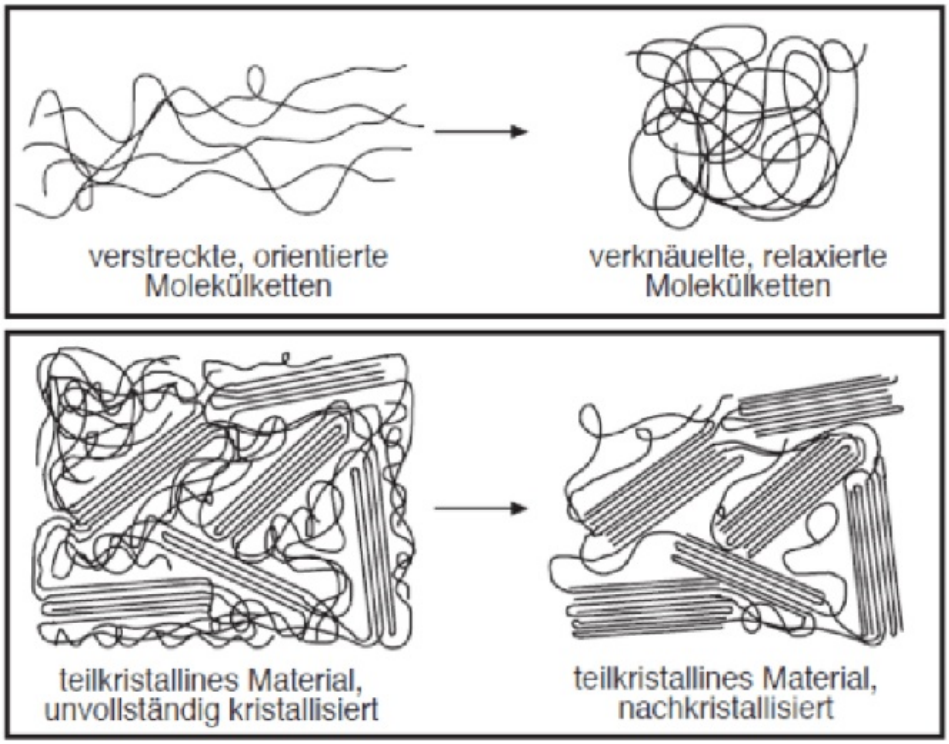


Figure 5.2. Schematics of some configurational changes possible with a phase change (top- oriented amorphous to isotropic amorphous structure, bottom- crystal growth).[20]

[5] This holds for physical aging by definition.

The molecular segments that contribute to a polymer's molecular dynamics (with oscillating fields below 10^6 Hz) are on the order of the size of nanoparticles (see Figure 5.3). A large effect of nanoparticulate on composite rheology occurs at very small weight percentage (<1%) additions. This behavior is normally explained by considering the larger ratio of interfacial area over volume in the composite.[22] For example, with spherical particles the ratio increases one order of magnitude for a magnitude decrease of particle radius. A similar fraction of a second phase (e.g., crystallites or supercooled liquid regions) are likely to produce a similar impact on the dynamic behavior.

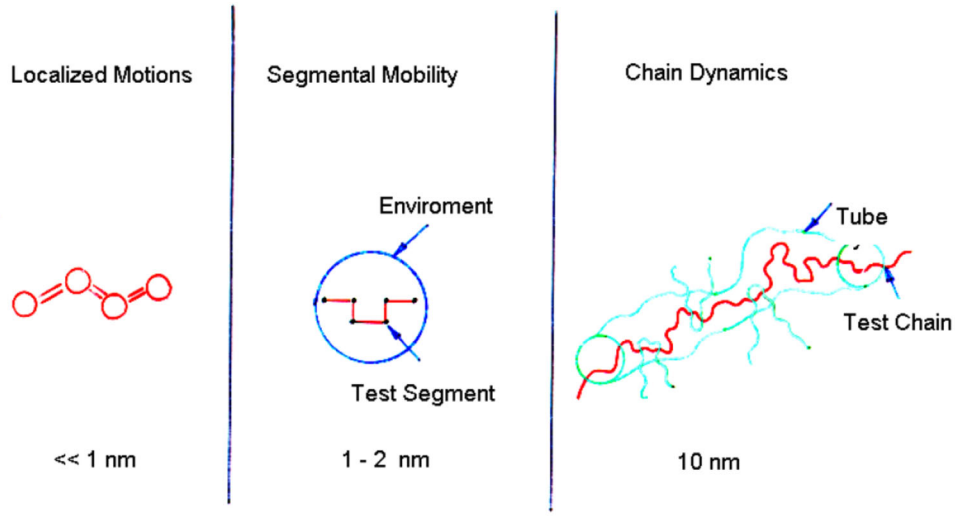


Figure 5.3. Some length scales and motional processes in polymeric systems.[23]

Interphase Behavior Dominates: With newly developed characterization techniques, recent work clearly indicates the dominance of interphase behavior in the dynamic response of semicrystalline and composite materials.[24] The interface between two phases can be considered as a third phase (i.e., "interphase"), as its properties are measurably different. The dimensional scale of the effective interphase is highly variable. Polymer chains interacting with particulate in the interphase can restrict or enhance the chain dynamics.[24] For some nanocomposites, the "association" of the polymer with the nanoparticles leads to a more ordered structure than would be expected, resulting in an elevated viscosity and higher elastic moduli.[26]

Suppression mechanisms of space charge at the interphase are thought to lead to local heating and possibly thermal aging in the interphase. Local heating would affect the rheological behaviors.[25] Explanations of the role of interfacial space charge in aging has often used an internal electric field concentration model. The two characterization techniques[6] most commonly used for space charge detection both require the propagation of an acoustic wave through the sample to detect localized space charge.[27] When the acoustic wave perturbs density fluctuations in the material structure, the wave is impeded or facilitated by these density fluctuations. The inhomogeneity inherent at interfaces results in an apparent space charge accumulation.[28] Density fluctuations also represent space charge rarefaction or accumulation. The space charge is measured with the material in a dynamic viscoelastic state. Space charge measurements of dielectrics with fields

[6] The two characterization techniques are Pulsed Electro-Acoustic (PEA) and Pressure Wave Propagation (PWP).

other than ideal DC should be considered as electrorheological behaviors. It follows that the aging behaviors ascribed to the presence of space charge with dynamic fields are actually an electro-mechanical aging behavior.[29]

Phonons and Non-phonons: Phonons (i.e., lattice excitations) can be used to probe rheological behaviors particularly in the elastic regime of liquids and crystals. Examples are Brillouin and Raman scattering. Well-behaved, effective models and measurement techniques exist for high frequency exploration. Dynamic elasticity changes with frequency. At lower frequencies, more time is available for molecular rearrangement and the complex viscosity usually decreases. Additional motions or degrees of freedom become active. The rheological models applicable to phonons in crystalline materials are not viable for glassy and semi-crystalline polymers at power frequencies[7]. Modeling of phonon behaviors in amorphous materials is an area of intense study due to anomalous thermal conductivity behaviors. Researchers have quantified surface phonon frequencies on a polymer surface by examining nanoparticle motion on that surface using Brillouin Spectroscopy.[29b] The science is important for enhancement of thermoelectric materials.[26] Recent studies emphasize that elastic heterogeneities in amorphous structures deform vibrational modes into non-phonons (i.e., "soft modes").[30] Ensuing models are anticipated to become useful in understanding changes in molecular dynamics with aging.

Phonons are considered as two types: acoustic phonons and optical phonons. Acoustic phonons require "collective" or coherent motion of mass. Acoustic phonons usually do not set up charge dipoles. Acoustic phonons may scatter light but do not absorb light. Spectra developed using Dynamic Mechanical Analysis (DMA) are related to acoustic phonons. Optical phonons operate by moving masses in opposition to each other. Optical phonons (due to oscillating dipoles) may absorb electromagnetic radiation. Spectra developed using Dielectric Thermal Analysis (DETA) may be related to optical phonons. At power frequencies, the dipole "masses" are not nearest neighbor bonds. The "range of influence" or "spatial scale" of these two types of phonon motions may correlate to some extent.[8]

Recent examinations of glasses at low frequencies have concluded that elastic heterogeneity is responsible for several anomalous behaviors. The phonon scattering due to the heterogeneities becomes dominant over phonon transmission at power frequencies. Vibrational excitations are not "wavelike"; they become "random-matrix type vibrational states".[31,32,33] This is a specific heterogeneity: the local elastic shear modulus fluctuates from location to location in the structure.[31] The "correlation length" of these regions (i.e., "locations") is thought to grow with aging.[34]

5.4. Kinetic models based on Dynamic Behavior

Many kinetic models based on changing polymer properties have been developed over the last seven decades. Kinetic models for predicting electrical insulation aging have traditionally been based on weight loss and fitted to Arrhenius equations for thermal aging [35,36] and power laws for electrical aging [18]. The statistical analyses of lifetime data are complex.[32] The scatter on

[7] Power frequencies achievable by switching power electronics building blocks (PEBBs) now range to 10^6 Hz.
[8] Phenomenological correlation between measured DETA and DMA spectra is described in section 6.6.

these lifetime predictions is high, even when defects are visible and known.[37] Many other kinetic models have been suggested.

Kinetic models for aging, which take into account Arrhenius behavior and also accommodate rheological behavior, are needed. Arrhenius models are inappropriate to gauge the complexity of structural changes during multifactorial aging in polymers. Semi-empirical models developed for polymers cannot be readily extended to complex composite materials. Furthermore, few aging models accept dynamic dielectric and mechanical data, the most sensitive characterizations of aging available.

Phenomenological models require life tests to fit parameters to mathematical forms that are accepted based on known behaviors. Physical models require a specific mechanism for behavior, where material characteristics are then used for prediction. Physical models are desirable in insulation research for two main reasons: validation of a mechanism promotes engineering, and time-consuming life testing for each material and each stress environment is avoided. There are several proposed kinetic aging models that are largely "physical models" that have begun to consider rheological changes related to aging. Four such models are summarized in the following.

Extended KAHR Model: This model has been used to investigate physical aging (i.e., reversible aging) by examining volume recovery using creep experiments.[38] The goal is to predict aging with time as temperature fluctuates (i.e., non-isothermal environment). The model is based on structural relaxations and utilizes Dynamic Mechanical Analysis (DMA).

Extended Space-Charge Model: The aging mechanism for this model suggests space charge lowers the energy barrier for permanent structural change.[39] The relationship between electric field and space charge is claimed to lead to electric aging. The ac component of the field is related to the mechanical energy of the polymer network oscillations at the ac field frequency. The extended model accommodates the effects of thermal, electrical, and mechanical stresses in forming microcavities. The extended model is designed for homogeneous, single component materials.

Electrostriction Model: The aging mechanism for this model recognizes applied electric stress as producing electrostriction (an electro-mechanical response) as well as accounting for phonon vibrations.[40] Here again, overcoming energy barriers for bond breakage accumulates until an "activation volume" is formed. Interestingly, a "strain activation volume" and a "stress activation volume" are two of the three main materials characteristics. The model's activation energy includes not only that for bond breakage, but also energies related to molecular relaxations (i.e., a phonon activation enthalpy and a configurational entropy change). These parameters may predict variations in aging near structural relaxations. This model is also designed for homogeneous, single component materials.

Mesoscale Vibration Model: The science of heterogeneous and glassy structures has developed new concepts and models that show promise of predicting rheology in composites. The anticipated fundamental benefit is correctly modeling the distorted energy barriers ascribed to a singular value in existing aging models. This quote summarizes the work:

> "In recent years, evidence has mounted that the dynamical slowing down of super-cooled liquids, colloids and granular media might indeed be related to the existence of genuine phase transitions, but of very peculiar nature. Contrasting with usual phase transitions, the dynamics of these materials dramatically slows down with nearly no changes in their conventional structural properties. One of the most interesting consequences of these ideas is the existence of dynamical heterogeneities, which have been discovered to be, in the space-time domain, the analog of critical fluctuations in standard phase transitions. Dynamic heterogeneity is now recognized to be a key feature of glassy dynamics."[17]

Dynamic heterogeneity accommodates a distribution of relaxation times due to heterogeneous structures. The heterogeneities are observed from (i.) the interaction of structural regions with the local environment; and (ii.) intrinsic mobility differences between regions.[41] Aging has been suggested to involve "growing length scales" (i.e., a characteristic length of each heterogeneity and/or its effect on the neighboring region is anticipated to increase with time).[34] Structural heterogeneities are hypothesized to extend to mesoscale structures in amorphous materials, necessitating a localized model (i.e., elasticity is not homogeneous).[42] The mesoscale structure models are a possible route for accommodating molecular dynamics behavior with nanoparticulate additions to an amorphous matrix.

A mesoscale structure model would need to predict relaxation or dynamic accommodation of the "next stress" from the environment. The three features would involve:

- History (meso-structure density of states);
- Proximity to T_g (as with an Arrhenius model or related to ductile-brittle transition); and
- "Next Stress": freq/temp/amplitude w.r.t. current state (for discontinuous stress states).

6. *Characterization:* MECHANICAL, ELECTRICAL, & THERMAL AGING OF RESINS & FIBERGLASS LAMINATES

6.1. Molecular Dynamics Characterization with DETA & DMA

The amount of specific phases present in materials is typically characterized by thermal analysis (e.g., differential scanning calorimetry- DSC and modulated DSC- MDSC) or by diffraction (e.g., small angle x-ray scattering- SAXS). Dynamic measurements, such as DETA and DMA, are more sensitive to changes in phase. The moduli discerned from DETA and DMA are sensitive to the ability of the molecular structure to move in response to an electric field or a mechanical field, respectively. In other words, DETA and DMA are ideal for examining changes in molecular dynamics.[43] Interpretation of results is aided by complimentary characterization tools. Dynamic mode frequency assignments may be made by experimentation that changes the structure in a known way (a structural trend) and then compares the results with an unknown. Frequency shifts can indicate changes in mass or free volume. The band intensity and shape also provide data as to variation or distortion within the dynamic motion.

6.2. Thermal, Mechanical, and Electrical Aging Studies

Aging studies have been pursued for general comparison of behaviors and to generate data that could be tested in future kinetic models. The thermal, mechanical, and electrical aging studies in this section emphasized comparison of cured neat resins and fiberglass laminates.

Experimental: The four dielectric materials chosen for aging studies are listed in Table 6.1. All four are rated to at least class H (maximum use temperature of 180°C) by their manufacturers. Although the matrix materials are not identical (i.e., the epoxy in FR5 is not Permafil 74050), the comparison of aging behaviors of neat materials with related composite materials is of interest, particularly in relationship to many published studies with micro-composites and nano-composites. The information gathered for the micro-composite materials was useful as aging of nano-composite materials was studied.

Table 6.1. Commercial materials examined with aging treatments.

Commercial Designation	Type	Form
Permafil 74050 (von Roll)	Epoxy	Cured Resin
Silres H62c (Wacker)	Silicone	Cured Resin
FR5 (Accurate Plastics)	Epoxy & Woven Fiberglass	Laminate Composite Board
G7 (Accurate Plastics)	Silicone & Woven Fiberglass	Laminate Composite Board

Methods for Thermal, Electrical, and Mechanical Aging: Samples were dimensioned prior to aging by machining and dry polishing with SiC paper (600 grit or finer). Thermal aging was carried out in a temperature-controlled oven in an air atmosphere. All thermal aging consisted of a heat treatment of 100 hours at 155°C with a cooling rate of <1°C/min.

Application of mechanical aging was achieved using an oscillating pressure from a wound electromagnetic actuator transmitted by direct contact through a fused silica column to the cross-section of each sample. A thin layer of silicone grease was applied to each side of the sample to facilitate wave transmission. The sample rested on a copper block with a thermocouple within 1 cm of the sample. An Agilent waveform generator produced the 9 kHz sine waveform and a Kepco Bipolar 36-120L amplifier produced the power to drive the actuator (V_{pk} = 42 V, I = 0.94 A). Images of the mechanical aging test chamber are shown in Figure 6.3a. The signal was applied continuously for 1 hour, at either room temperature or the glass transition temperature. The glass transition temperature at 9 kHz was determined using a standard time-temperature-transformation of DMA measurements on unaged samples.[44]

Application of electrical aging was achieved using an oscillating voltage from a fixed-frequency power supply transmitted with the sample in a parallel plate configuration between two circular copper electrodes. The specially machined copper electrodes were 1.0 inch in diameter and connected to Litz wire leads. The parallel plate arrangement rested on a fused silica tube containing the lead. A thermocouple was located within 1 cm of the sample. An AspenLabs Inc MF360A Electrosurgical RF power supply produced the 500 kHz sine waveform with a peak field of 0.3 kV/mm. Voltage and current were monitored using a Tektronix oscilloscope. The electrical aging test apparatus is shown in Figure 6.3b. The signal was applied for 1 hour at either room temperature or the glass transition temperature. The glass transition temperature at 500 kHz was determined using a standard temperature-time transformation of DMA measurements on unaged samples.[44]

Samples were characterized by Dynamic Mechanical Analysis (DMA) and Dielectric Thermal Analysis (DETA). All DMA thermal ramping measurements used 1 Hz. Procedures for these characterizations have been previously described.[45] For ease of discussion, only DETA spectra at 50°C and 150°C are shown in the following graphs, although spectra at 30°C, 75°C, 100°C, and 125°C were also collected and examined.

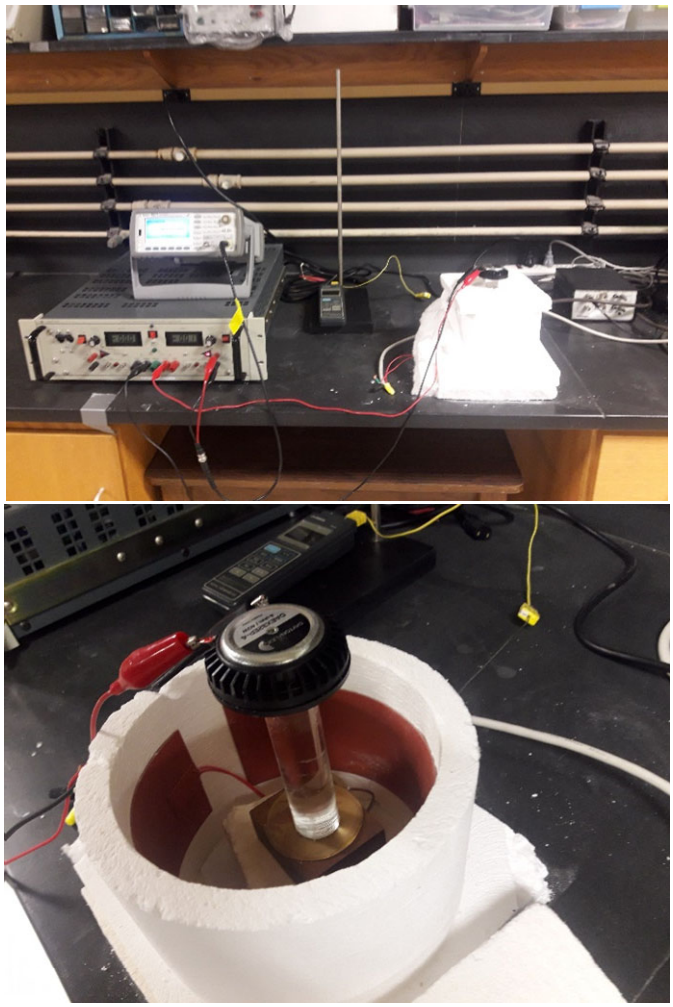


Figure 6.3a. Mechanical aging test chamber.

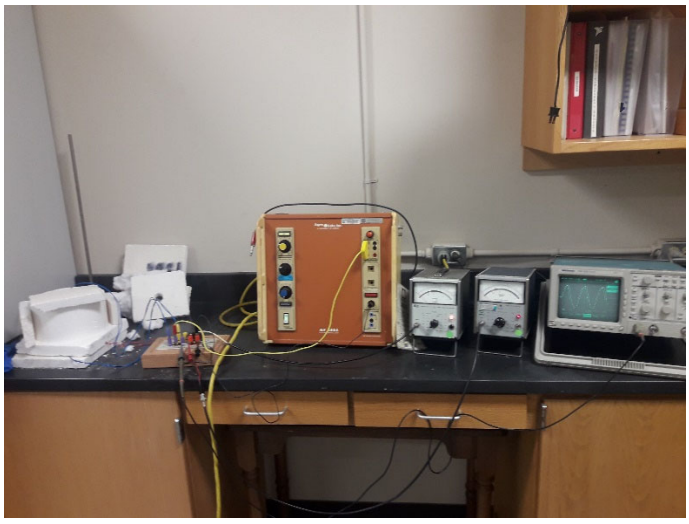


Figure 6.3b. Electrical aging test apparatus.

6.2.1. Epoxy (Permafil 74050)

Thermal aging of the Epoxy resulted in a slight decrease in loss permittivity at low frequency. A shift of the relaxation spectrum to lower frequency is suggested with thermal aging. The real permittivity increased significantly across the frequency spectrum for all temperatures (see Figure 6.4). The DMA graphs show that thermal aging reduced stiffness and increased the dominant glass transition temperature, T_g (see Figure 6.6). Although relaxation near the original glass transition temperature range (~80°C) may still be observed after thermal aging, a new relaxation (near 140°C) is shown (see Figure 6.7). This suggests phase separation during thermal aging.

Mechanical aging caused an increase in loss permittivity at lower frequencies. This increase was more pronounced for Epoxy when mechanically aged at T_g. The difference is also much more pronounced at 150°C than at 50°C (see Figure 6.9). These changes suggest a shift of the relaxation spectra to higher frequencies. As with thermal aging, the real permittivity of mechanically aged Epoxy increased across the spectrum. At 150°C, the real permittivity of the Epoxy mechanically aged at the T_g shows more change from the as cured Epoxy. Graphs of mechanical storage modulus for epoxy subjected to mechanical aging show a reduction in stiffness. The loss of stiffness decreases more rapidly with temperature when mechanically aged at room temperature as compared with material aged at the glass transition (see Figure 6.10). The mechanical loss modulus shows a small decrease in intensity with mechanical aging (see Figure 6.11). The relaxation band shifts (-11°C) to lower temperature with mechanical aging at room temperature and (-1°C) with mechanical aging at the glass transition.

The changes in the Epoxy behaviors after electrical aging follow the same trends as those of mechanical aging. Electrical aging near the glass transition caused more dramatic changes. The dynamic loss relaxation band shifts (-14°C) to lower temperature with electrical aging at room temperature and (-3°C) with electrical aging at the glass transition.

- *Epoxy (cured Permafil 74050 resin): Thermal Aging*

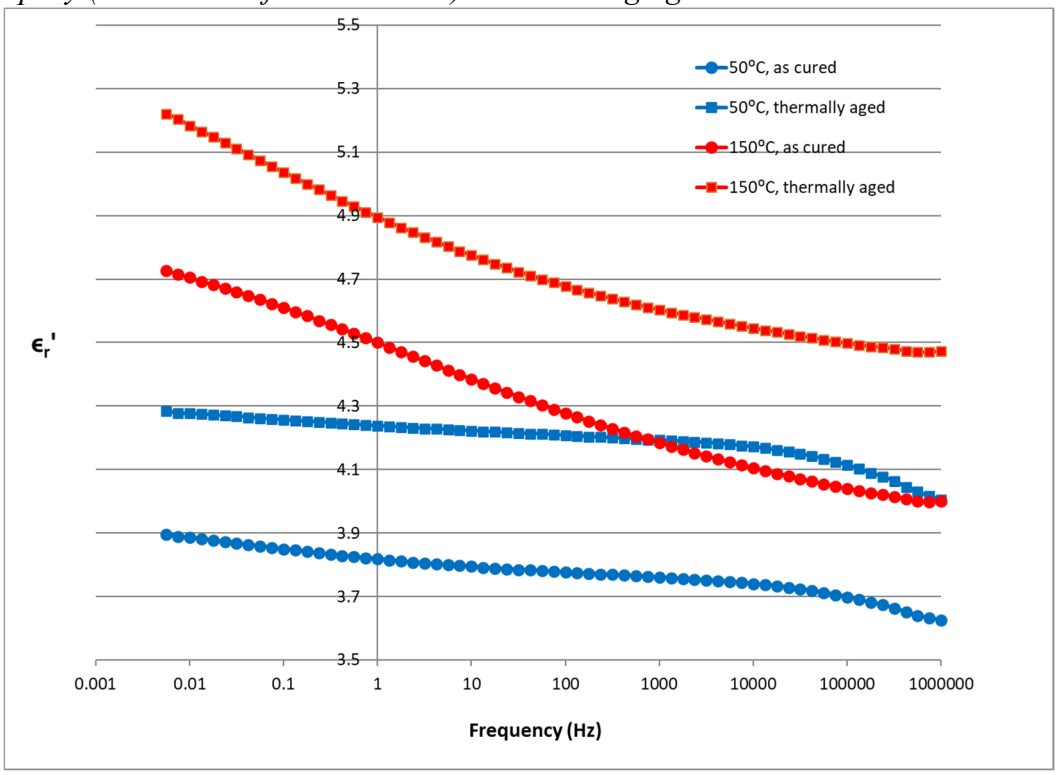


Figure 6.4. Real Permittivity vs. frequency for Permafil 74050 with thermal aging.

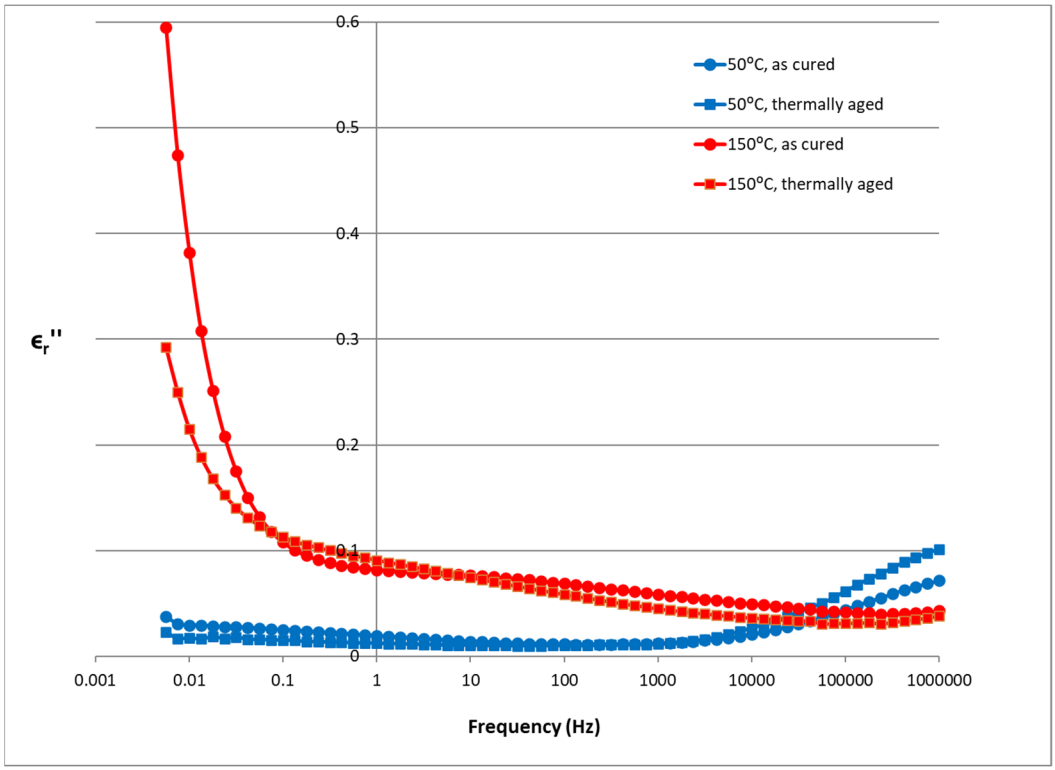


Figure 6.5. Imaginary Permittivity vs. frequency for Permafil 74050 with thermal aging.

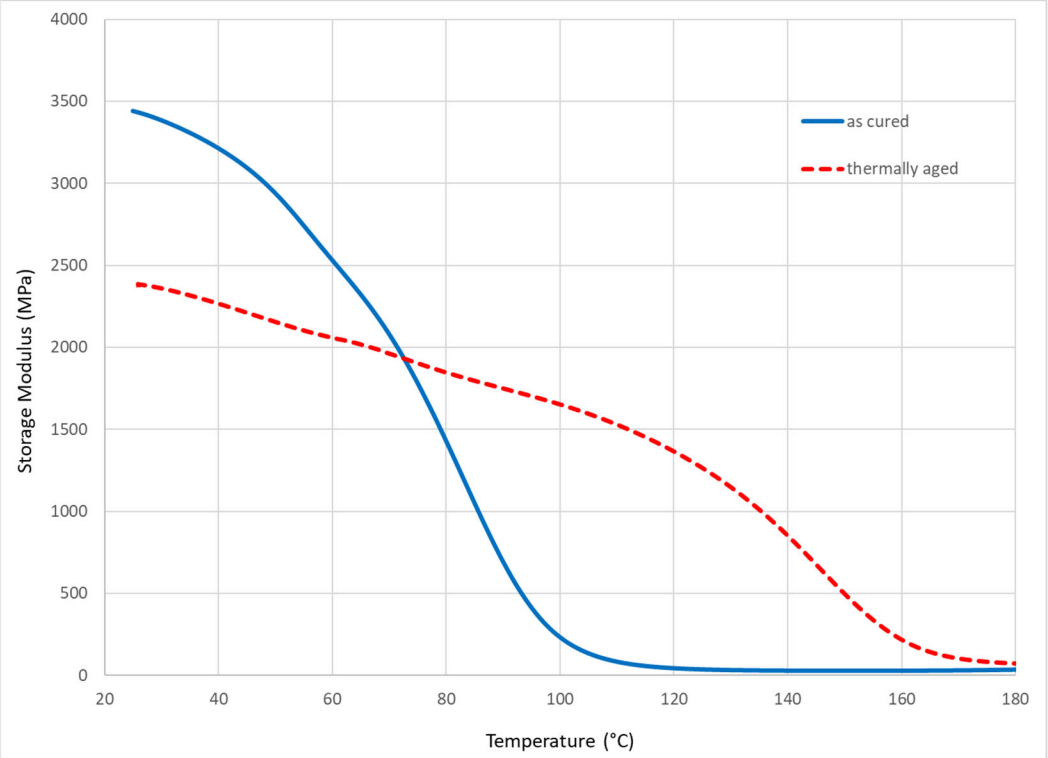


Figure 6.6. Dynamic Storage Modulus vs. temperature for Permafil 74050 with thermal aging.

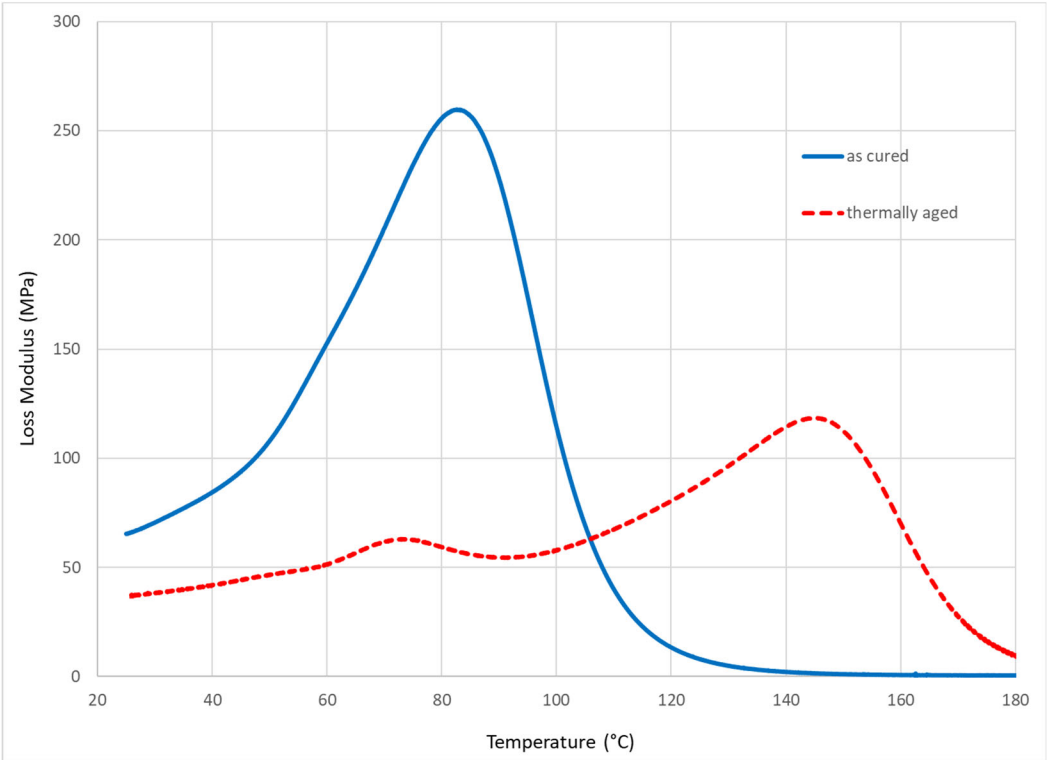


Figure 6.7. Dynamic Loss Modulus vs. temperature for Permafil 74050 with thermal aging.

- *Epoxy (cured Permafil 74050 resin): Mechanical Aging*

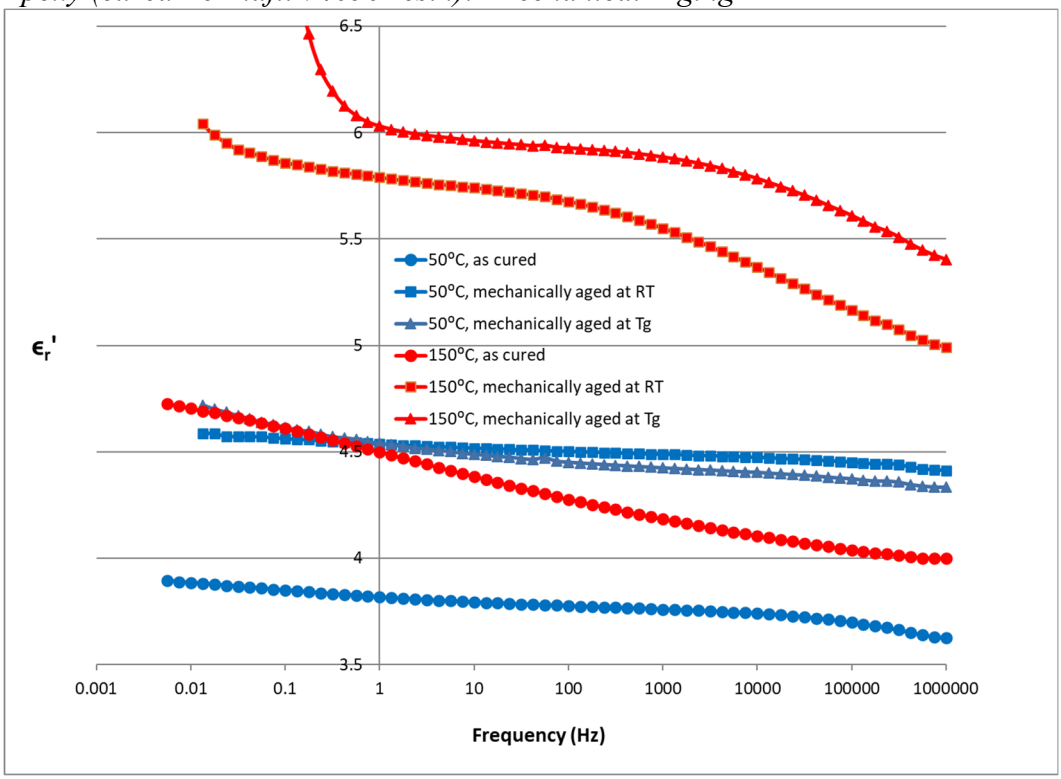


Figure 6.8. Real Permittivity vs. frequency for Permafil 74050 with mechanical aging.

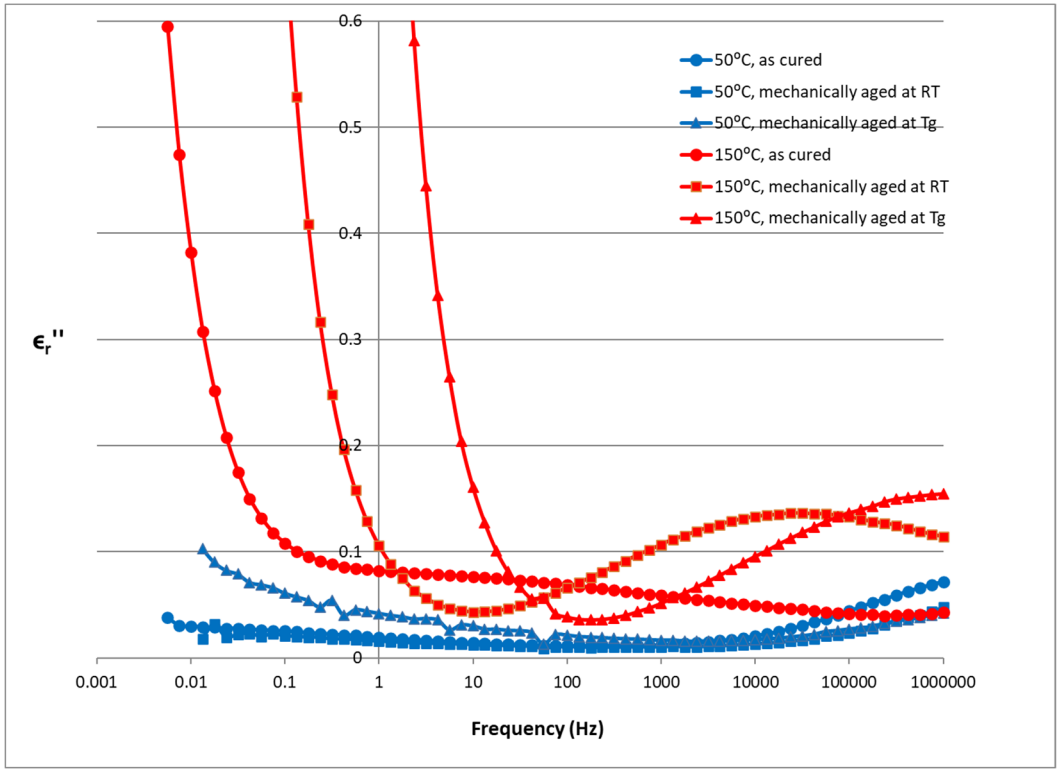


Figure 6.9. Imaginary Permittivity vs. frequency for Permafil 74050 with mechanical aging.

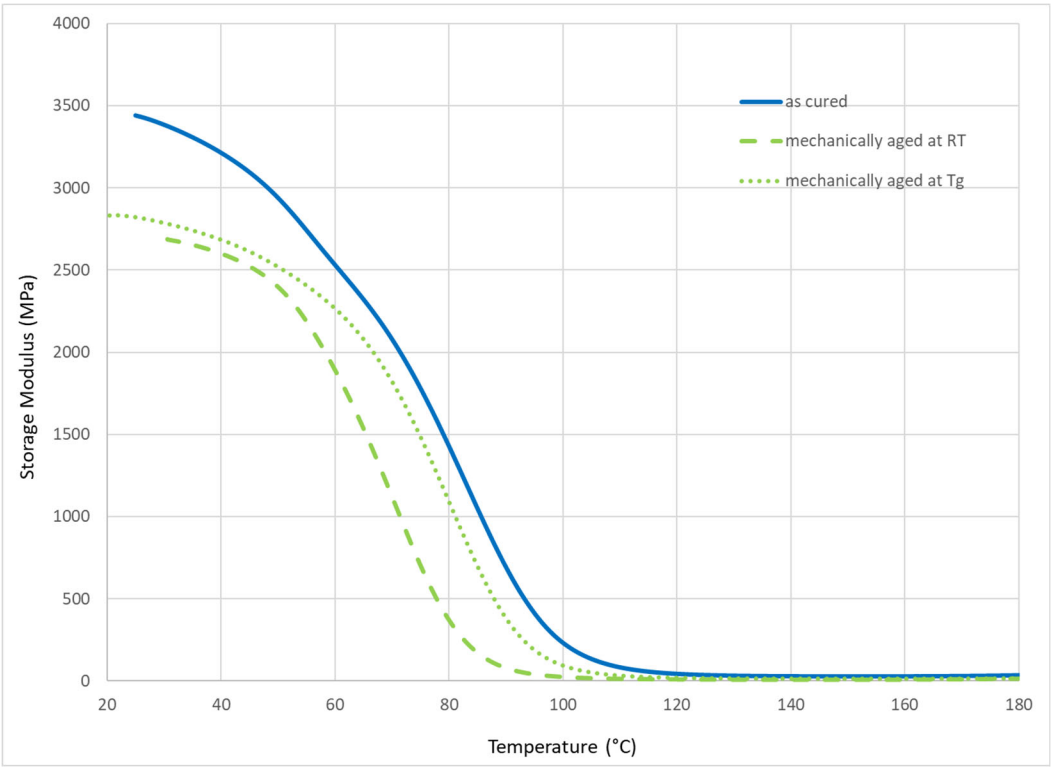


Figure 6.10. Dynamic Storage Modulus vs. temperature for Permafil 74050 with mechanical aging.

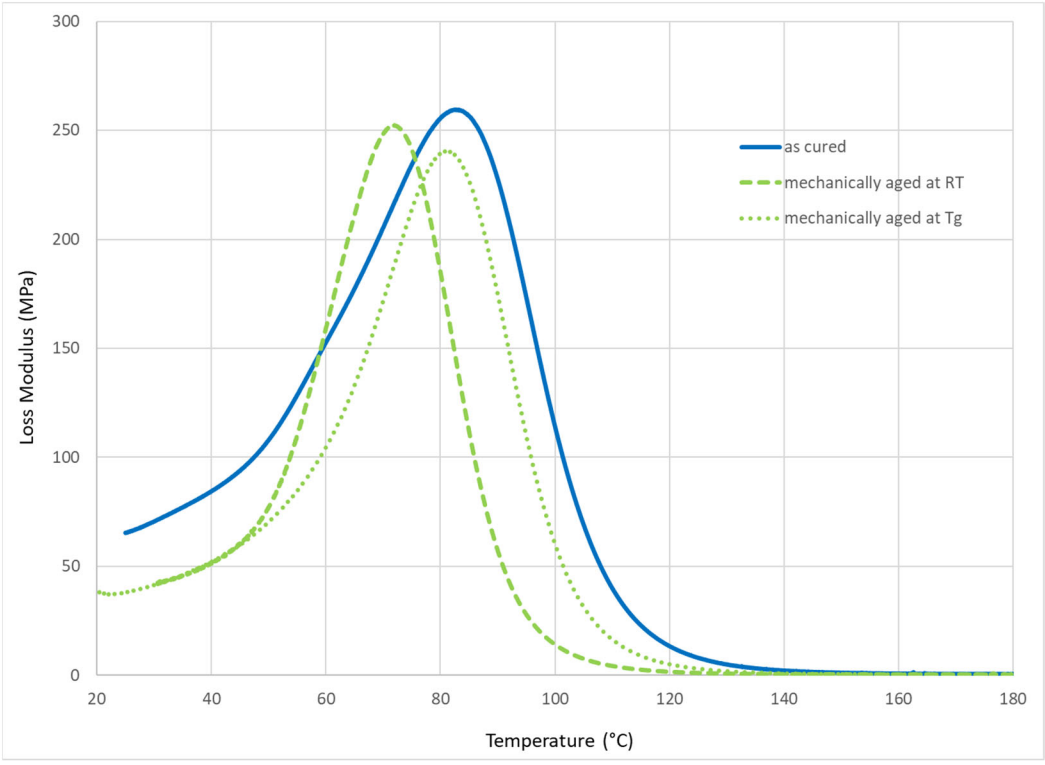


Figure 6.11. Dynamic Loss Modulus vs. temperature for Permafil 74050 with mechanical aging.

- *Epoxy (cured Permafil 74050 resin): Electrical Aging*

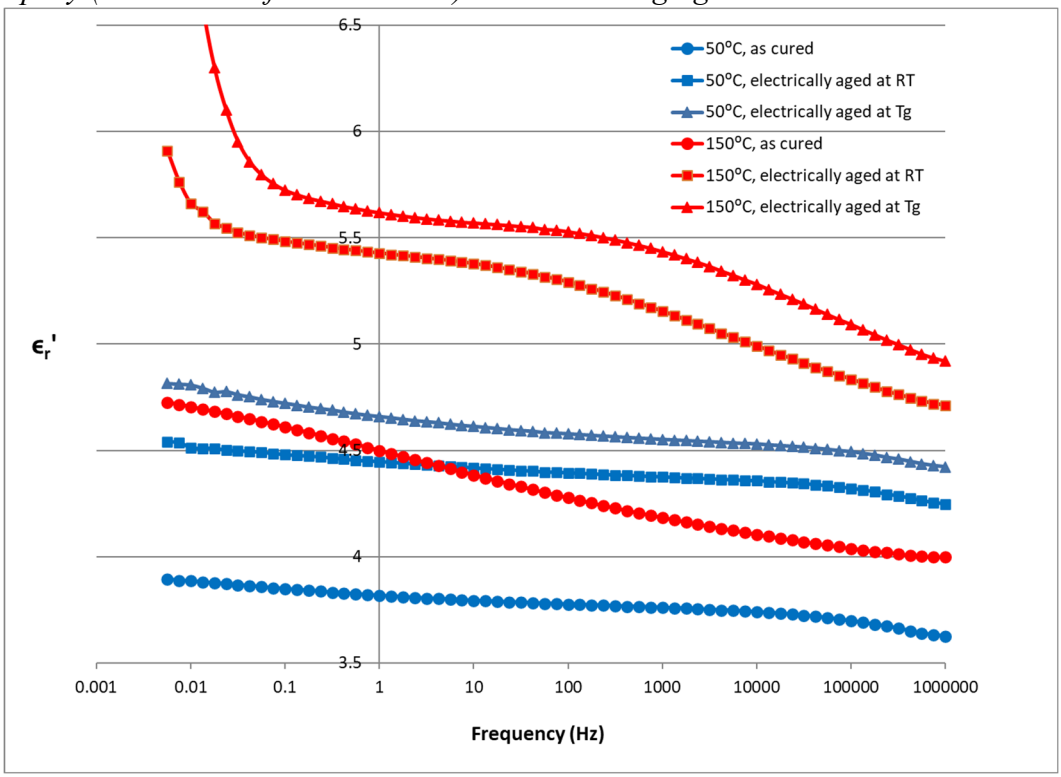


Figure 6.12. Real Permittivity vs. frequency for Permafil 74050 with electrical aging.

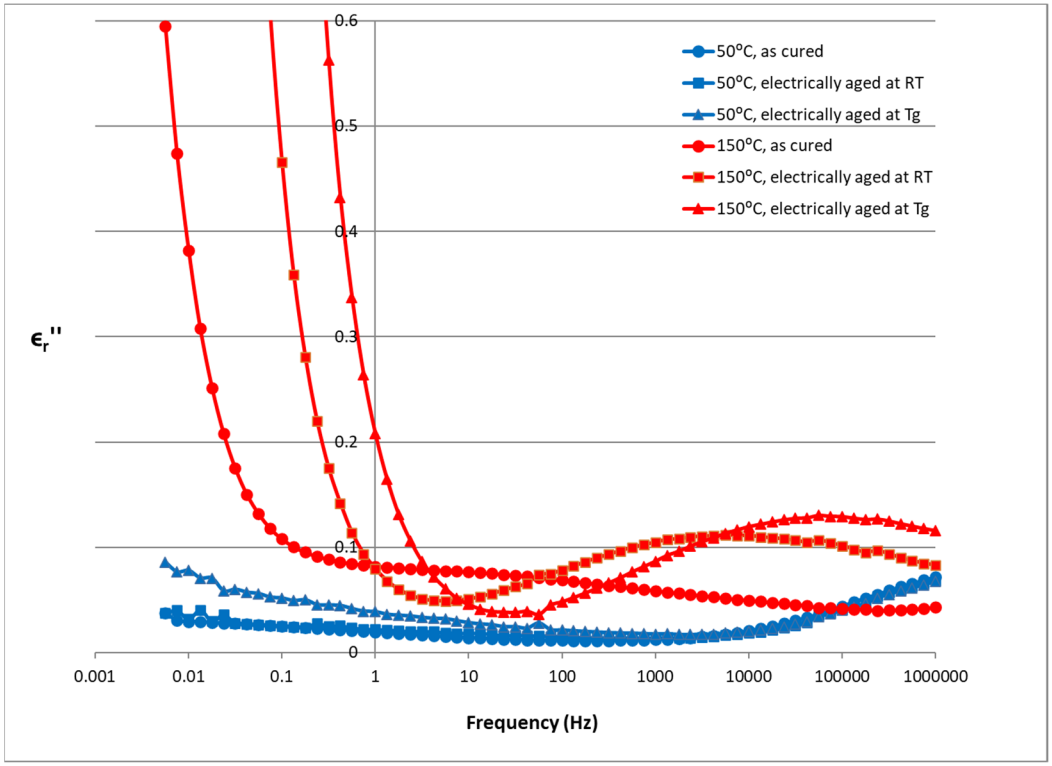


Figure 6.13. Imaginary Permittivity vs. frequency for Permafil 74050 with electrical aging.

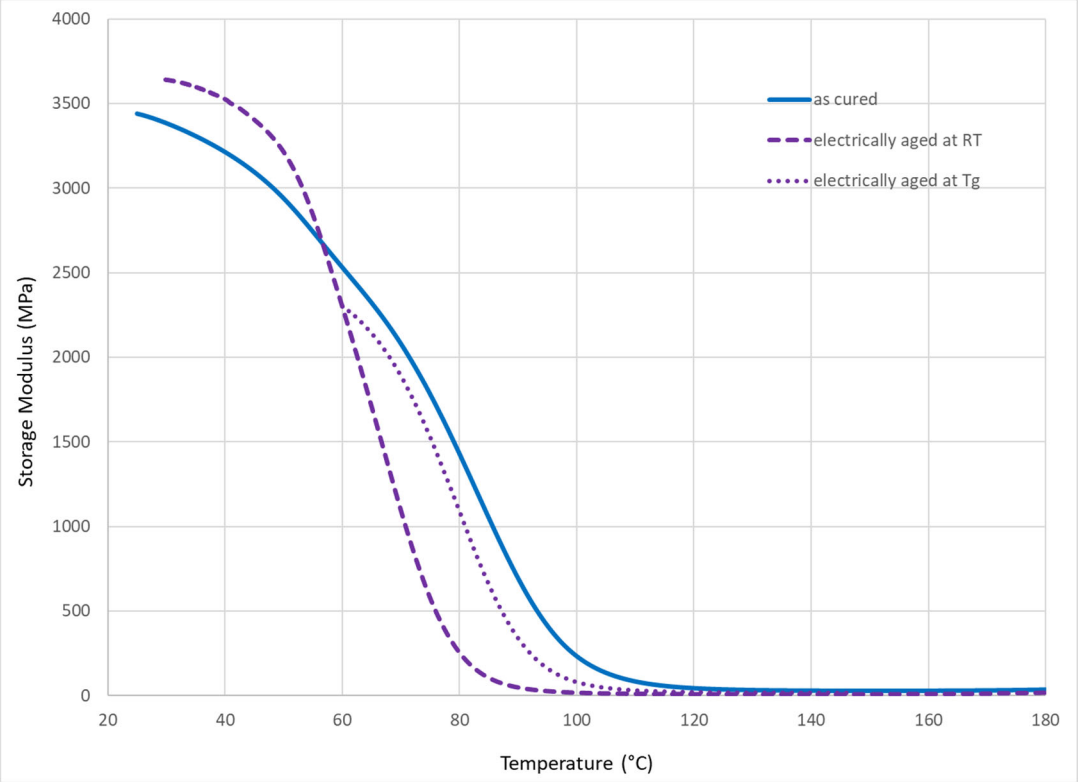


Figure 6.14. Dynamic Storage Modulus vs. temperature for Permafil 74050 with electrical aging.

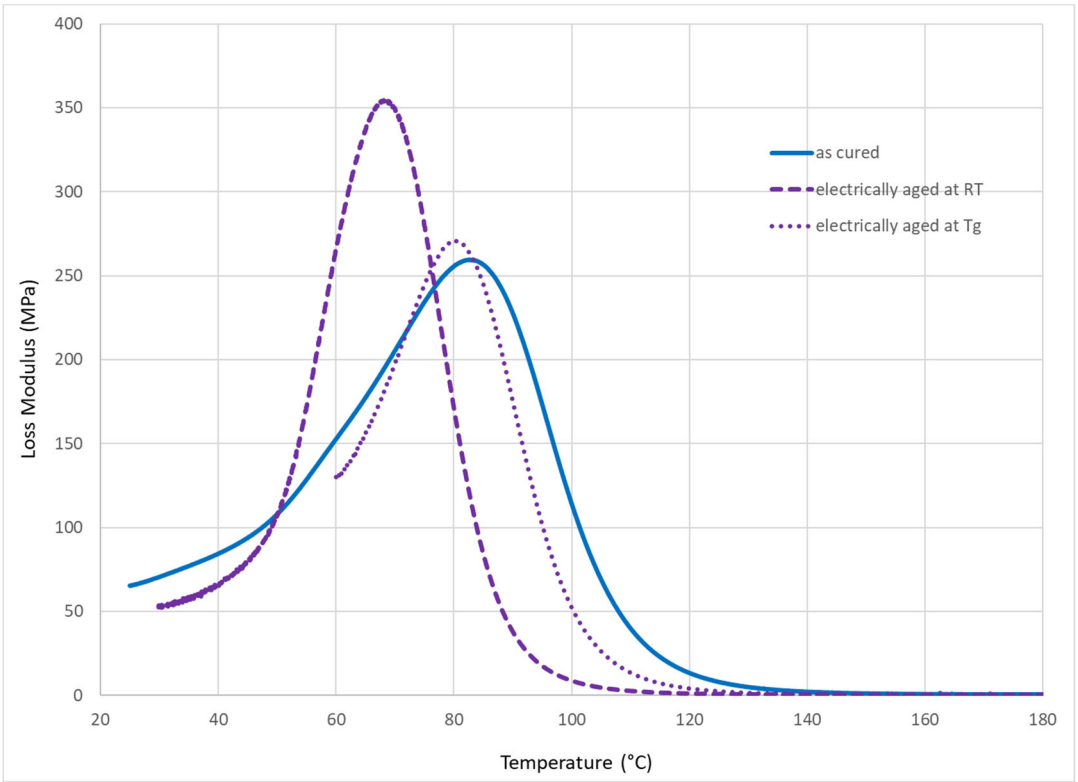


Figure 6.15. Dynamic Loss Modulus vs. temperature for Permafil 74050 with electrical aging.

6.2.2. Silicone (Silres H62c)

The real permittivity of the silicone material decreased with thermal aging (see Figure 6.16). This is especially pronounced for the thermally aged Silicone when probed at 150°C and low frequencies. Similarly, the loss permittivity is reduced with thermal aging (see Figure 6.17). A decrease in stiffness at temperatures below 60°C is observed in the DMA storage modulus after thermal aging (see Figure 6.18). Thermal aging further caused the relaxation peak to decrease in intensity and shift (+10°C) to higher temperatures (see Figure 6.19).

The Silicone's real permittivity increased with mechanical aging (see Figure 6.20). An exception is the low frequency (<0.1 Hz) behavior at 150°C. This change at elevated temperature is also observed in lowered permittivity loss (see Figure 6.21). Mechanical aging reduced the permittivity loss (now observable at frequencies below 100 Hz). The Silicone lost stiffness at low temperatures with mechanical aging (see Figure 6.22). Mechanical aging shifted (-10°C) the relaxation peak (see Figure 6.23). The temperature of the mechanical aging treatment appears to have only a minor effect.

The trends in real permittivity after electrical aging followed the same trends as observed for the Silicone after mechanical aging. The trends in dynamic moduli, however, were markedly different. Electrical aging resulted in increased stiffness and shifts (+10°C) in the relaxation peak to higher temperatures (see Figures 6.26 and 6.27). Only minor differences were found after aging at room temperature vs. aging near the high temperature transition.

- *Silicone (cured Silres H62c resin): Thermal Aging*

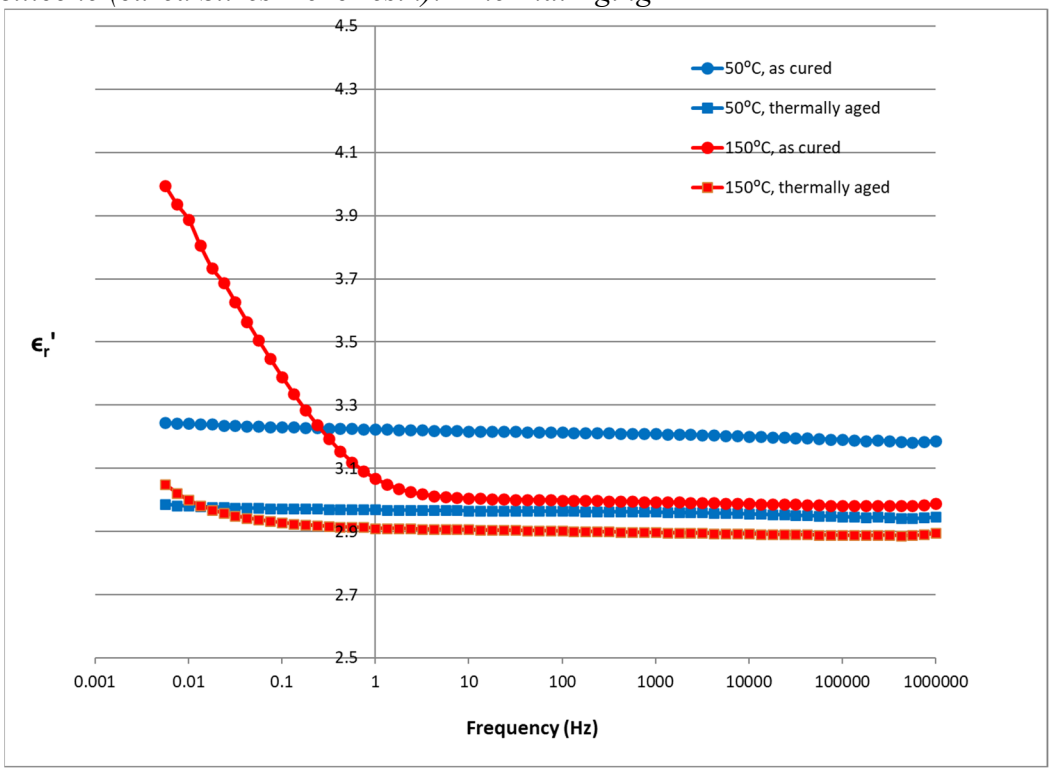


Figure 6.16. Real Permittivity vs. frequency for Silres H62c with thermal aging.

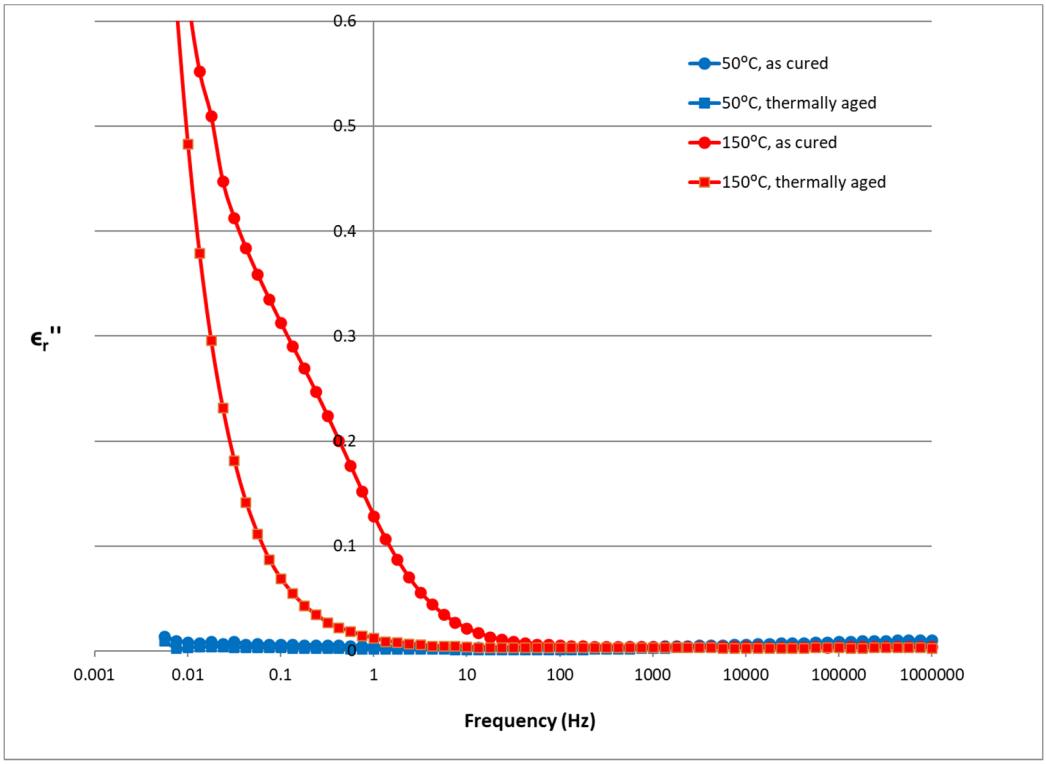


Figure 6.17. Imaginary Permittivity vs. frequency for Silres H62c with thermal aging.

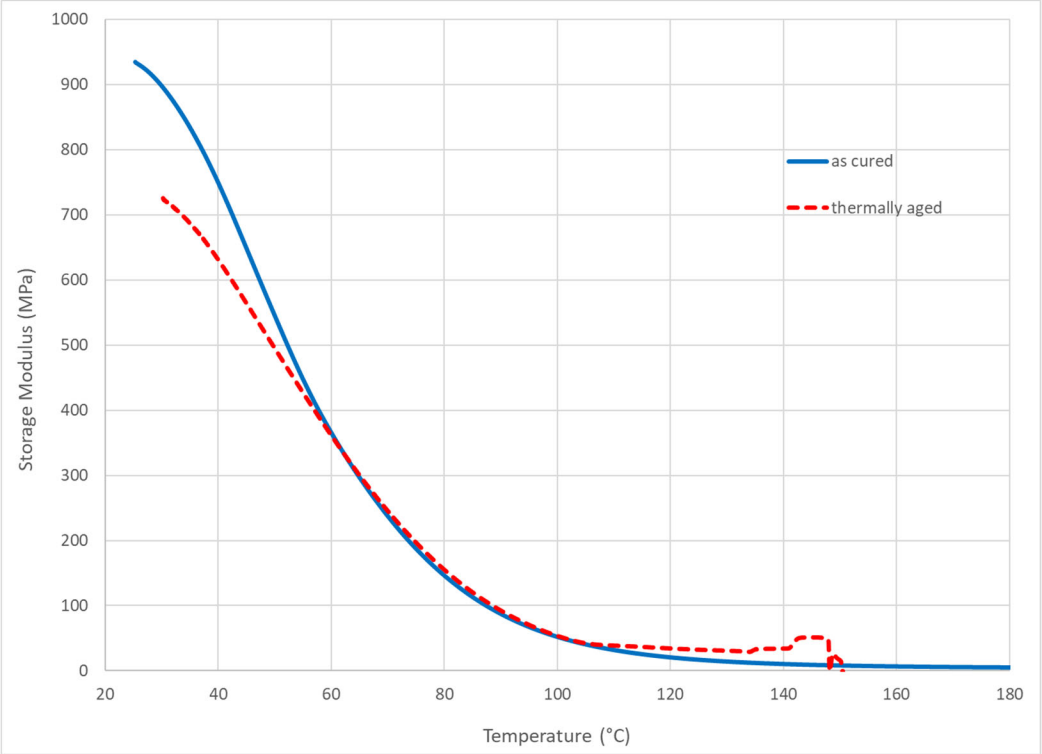


Figure 6.18. Dynamic Storage Modulus vs. temperature for Silres H62c with thermal aging.

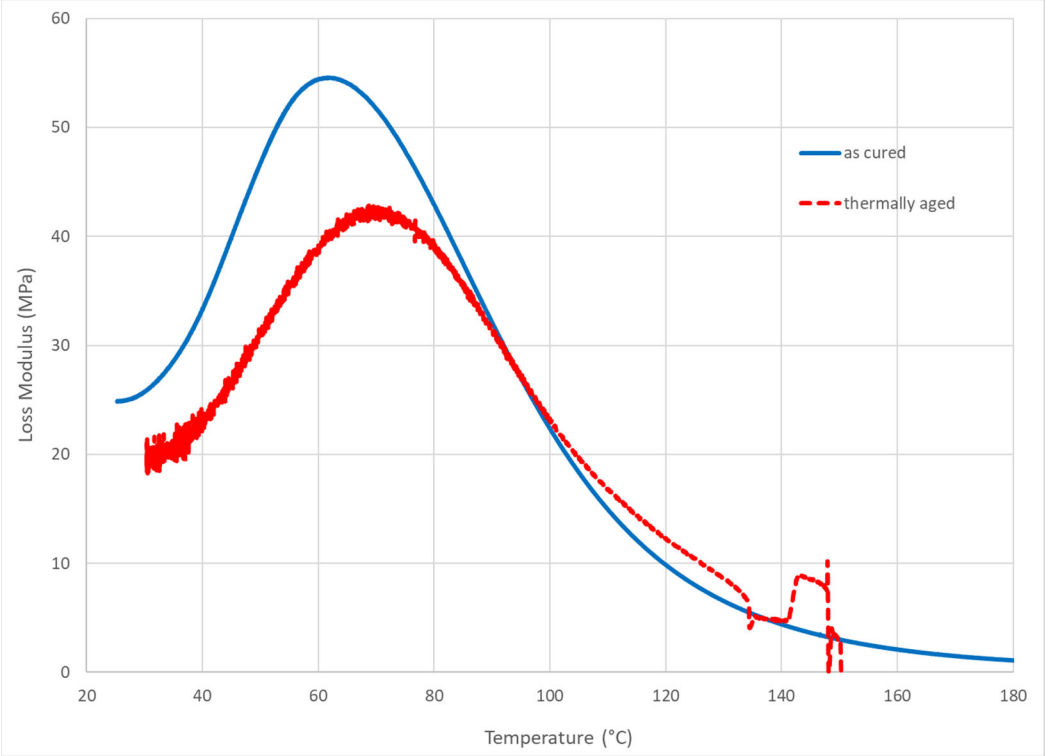


Figure 6.19. Dynamic Loss Modulus vs. temperature for Silres H62c with thermal aging.

- *Silicone (cured Silres H62c resin): Mechanical Aging*

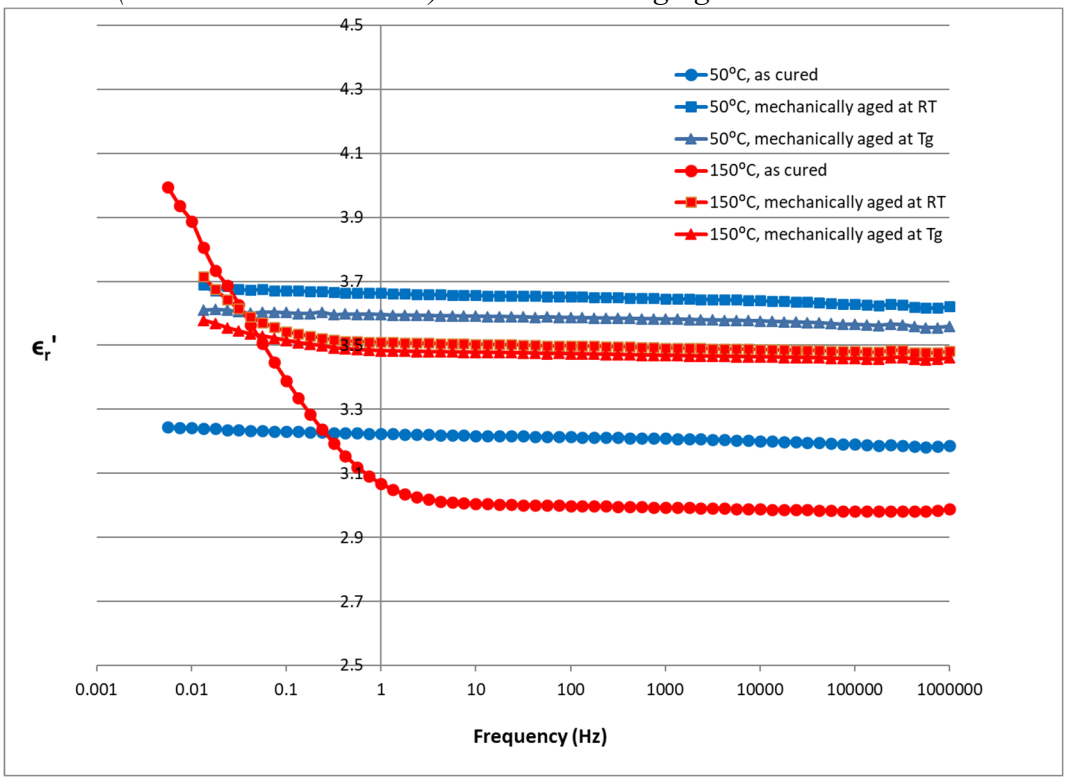


Figure 6.20. Real Permittivity vs. frequency for Silres H62c with mechanical aging.

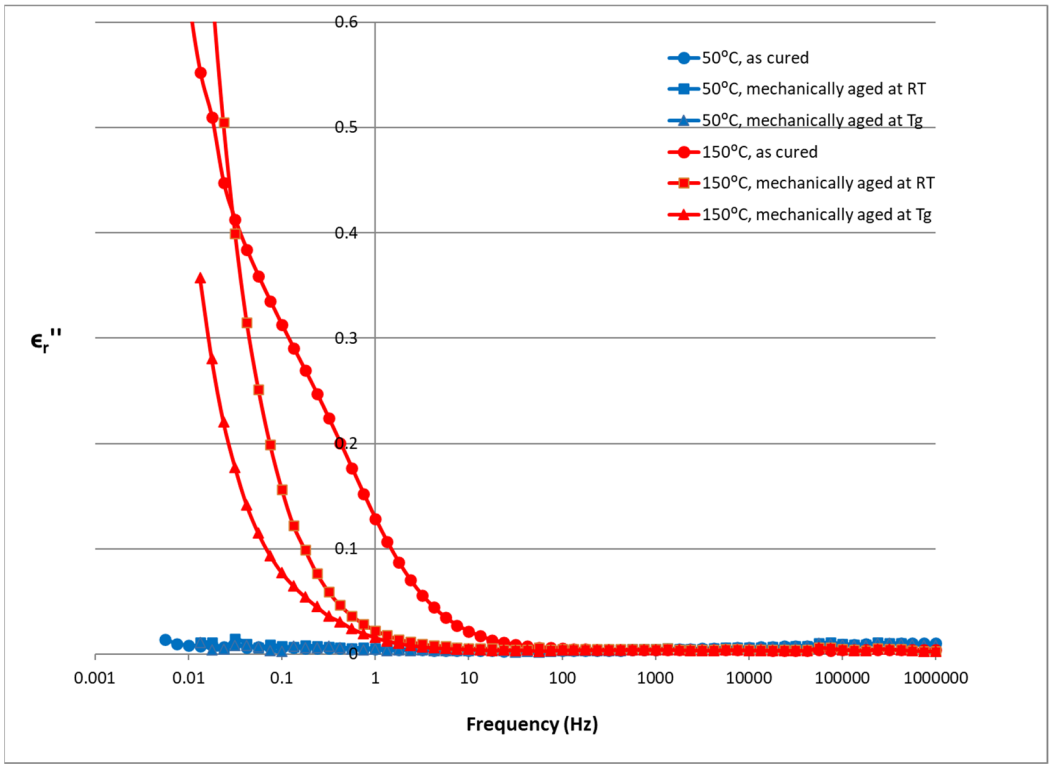


Figure 6.21. Imaginary Permittivity vs. frequency for Silres H62c with mechanical aging.

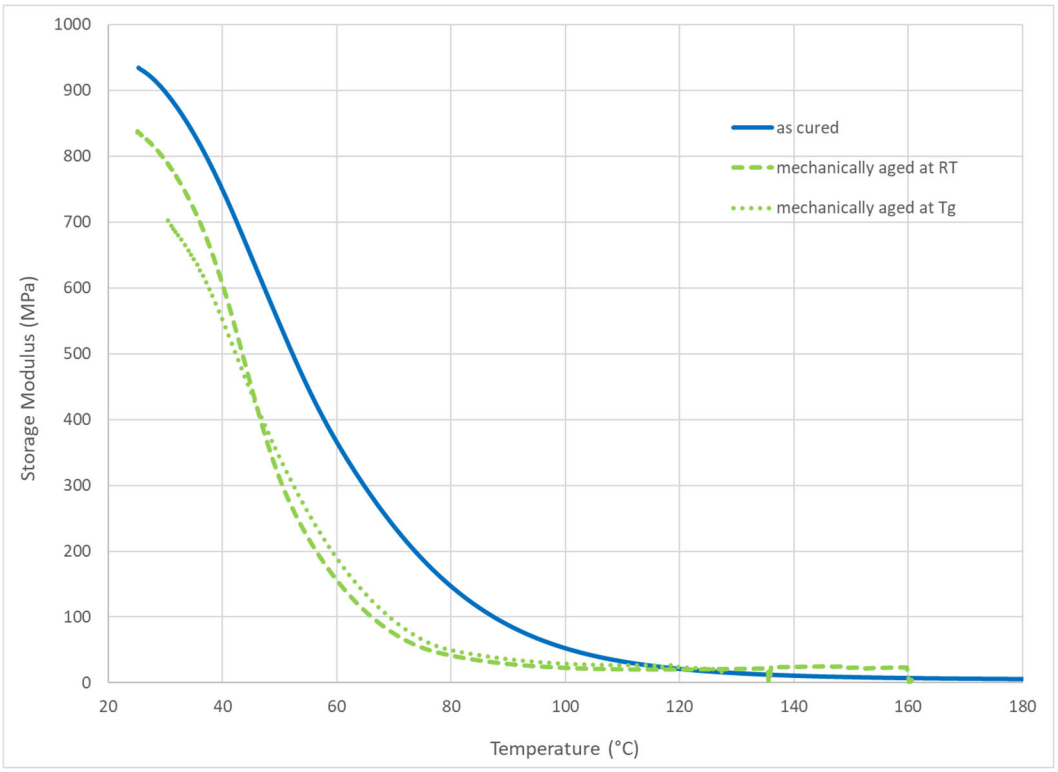


Figure 6.22. Dynamic Storage Modulus vs. temperature for Silres H62c with mechanical aging.

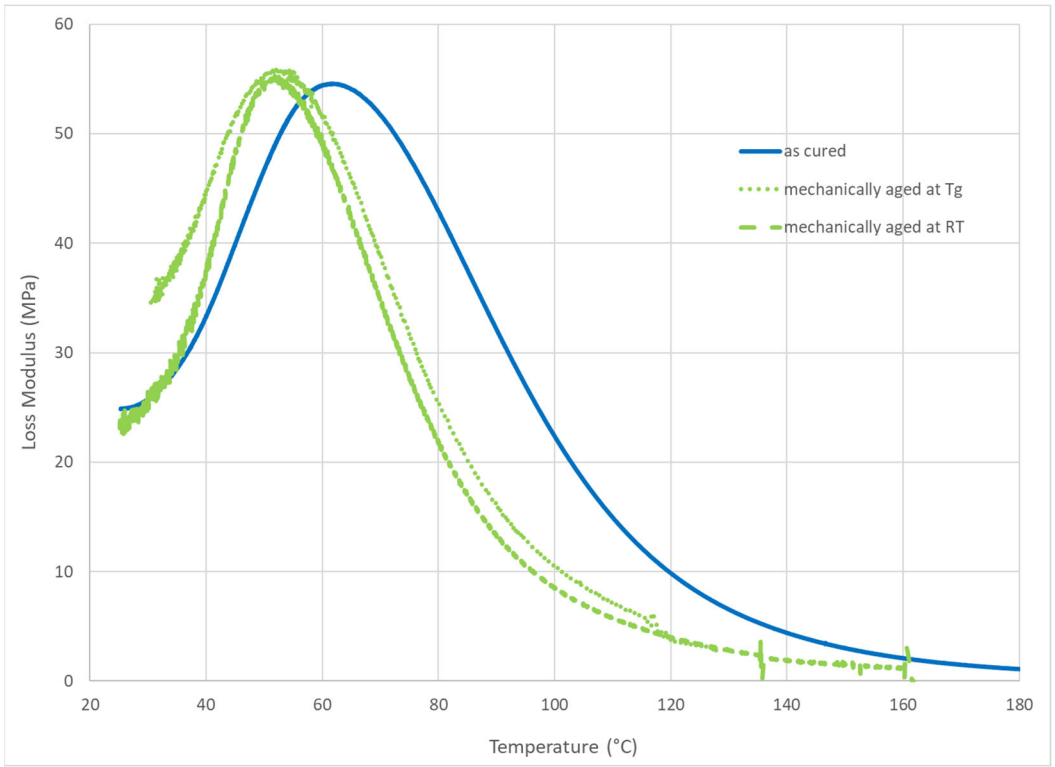


Figure 6.23. Dynamic Loss Modulus vs. temperature for Silres H62c with mechanical aging.

- *Silicone (cured Silres H62c resin): Electrical Aging*

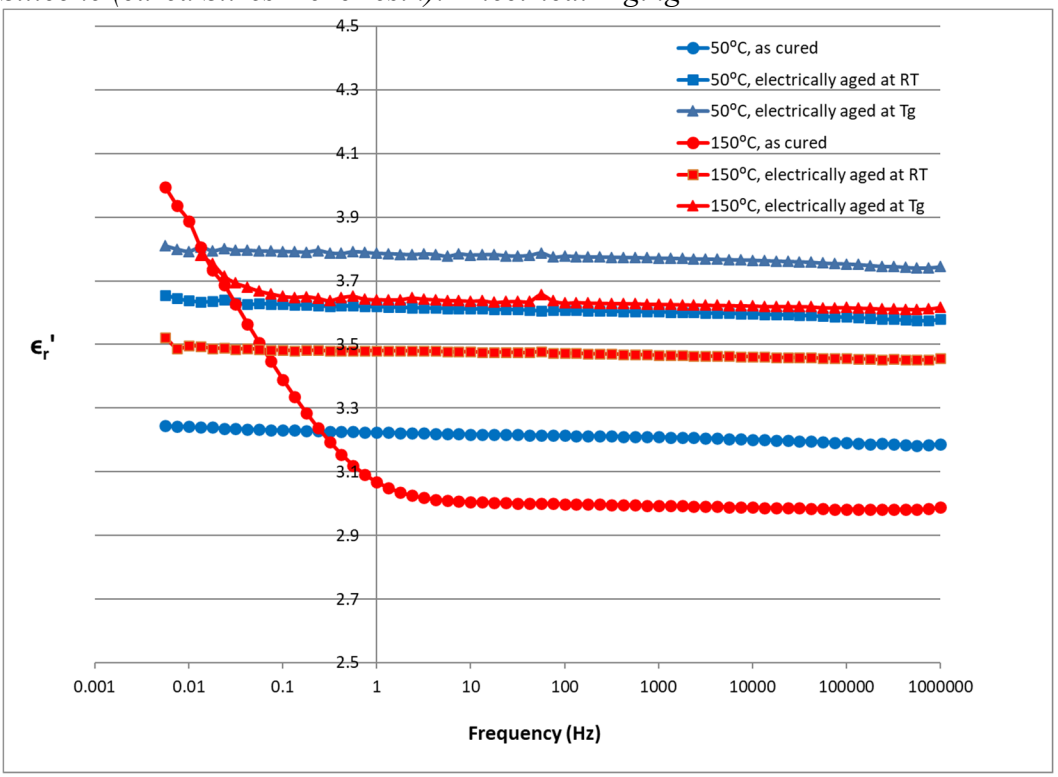


Figure 6.24. Real Permittivity vs. frequency for Silres H62c with electrical aging.

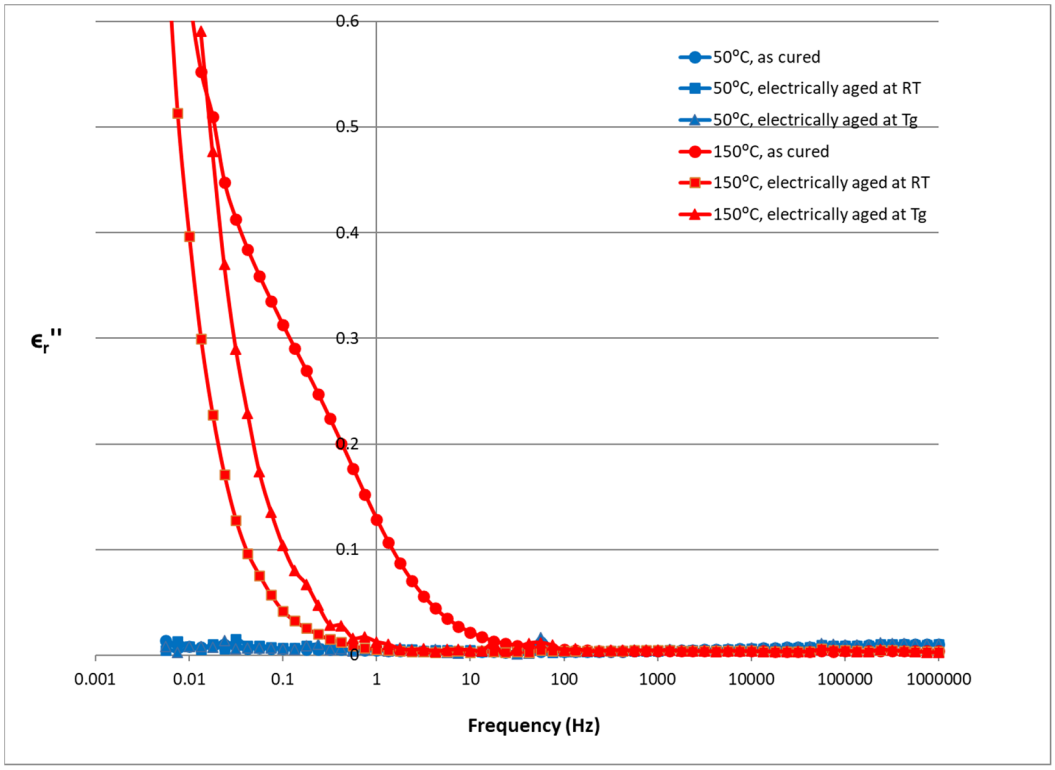


Figure 6.25. Imaginary Permittivity vs. frequency for Silres H62c with electrical aging.

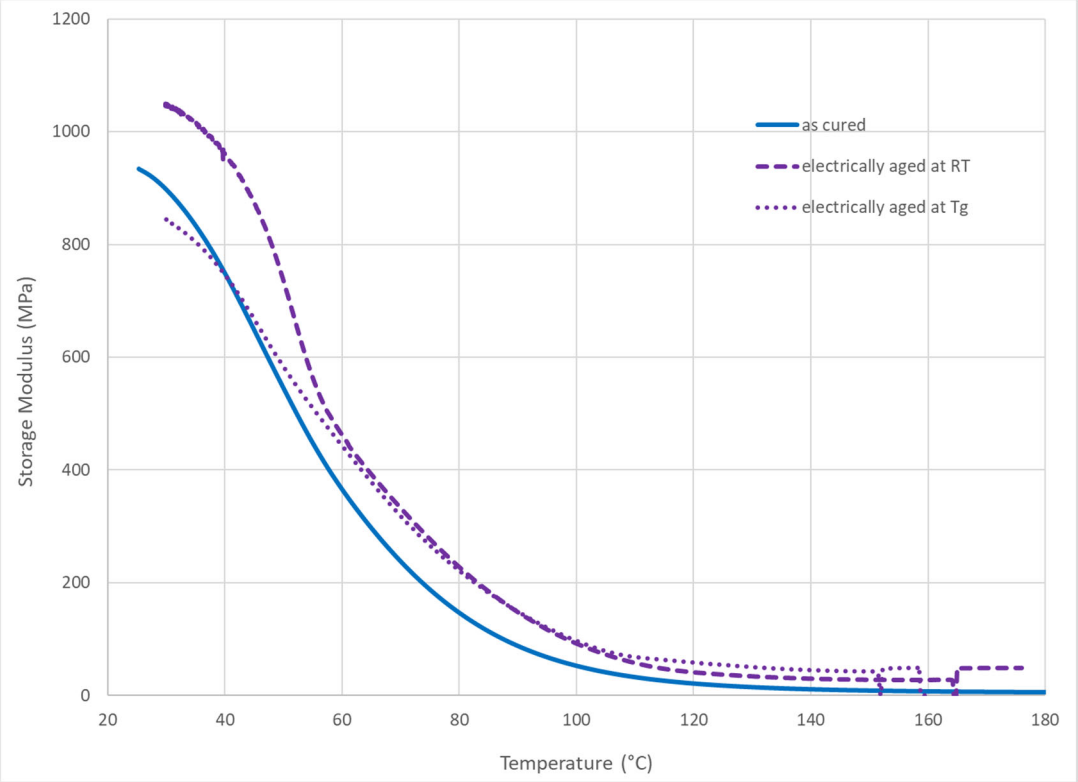


Figure 6.26. Dynamic Storage Modulus vs. temperature for Silres H62c with electrical aging.

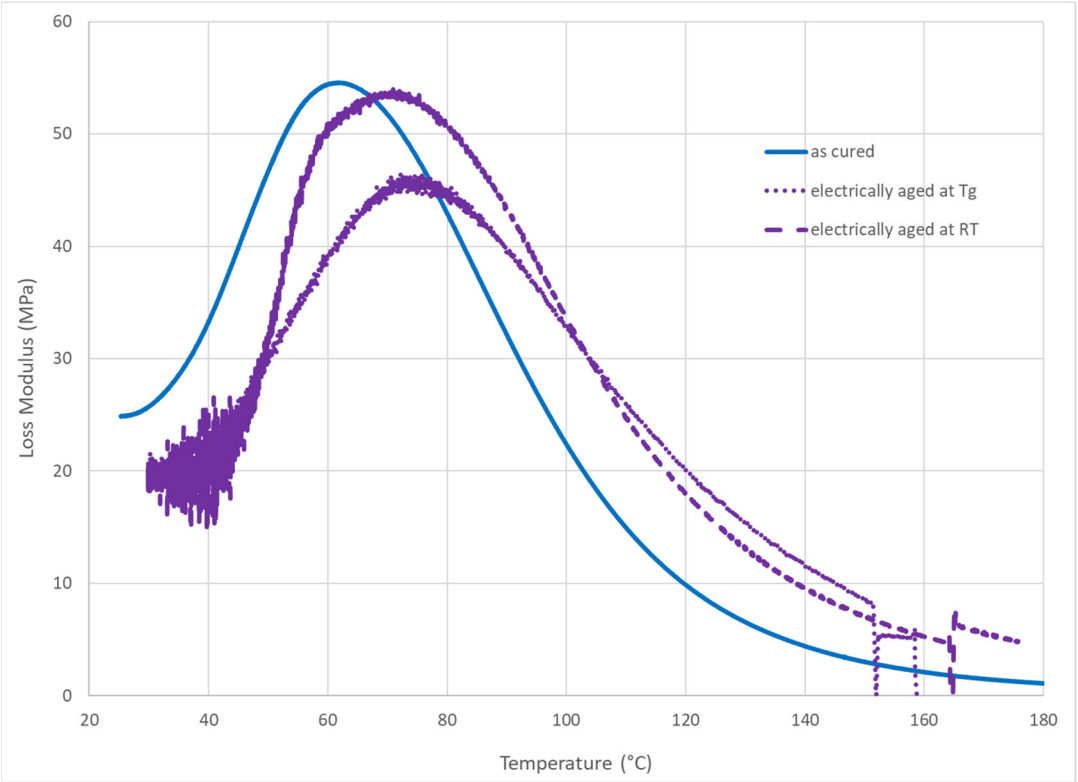


Figure 6.27. Dynamic Loss Modulus vs. temperature for Silres H62c with electrical aging.

6.2.3. Epoxy+Fiberglass Laminate (FR5)

Thermal aging of the Epoxy Laminate caused a small increase in both the real permittivity (see Figure 6.28) and the loss permittivity (see Figure 6.29). Very high permittivity loss at measurement temperature of 150°C is observed regardless of aging. This product should be used with caution in applications at and above 150°C. With thermal aging, the dynamic stiffness is observed to have decreased for temperatures below the glass transition (see Figure 6.30). Concurrently, the loss modulus peak is observed to decrease in intensity and shift (+10°C) to higher temperature. A second, minor relaxation is observed at 80°C after thermal aging. This behavior is similar to that observed with thermal aging of the neat epoxy.

Mechanical aging of the Epoxy Laminate increases both the real permittivity (see Figure 6.32) and the loss permittivity (see Figure 6.33) across the spectrum at both 50°C and 150°C. The temperature of the mechanical aging treatment (room temperature or glass transition temperature) has no effect. The storage modulus shows a decrease in stiffness with mechanical aging (see Figure 6.34). The loss modulus peak intensity decreased by almost the same amount with mechanical aging at both aging temperatures (see Figure 6.35). (The reduction is more pronounced at lower temperatures for the material aged at room temperature and at higher temperature for the material aged at the glass transition.) There is a possible minor relaxation observed near 80°C for both aged materials.

The effects of electrical aging on both the real and loss permittivities are the same as observed for mechanical aging. The real dynamic elastic moduli and loss moduli were unaffected by electrical aging (see Figures 6.38 and 6.39). The temperature at which electrical aging was applied had no discernable effect on the Epoxy Laminate.

- *FR5 (epoxy + fiberglass composite): Thermal Aging*

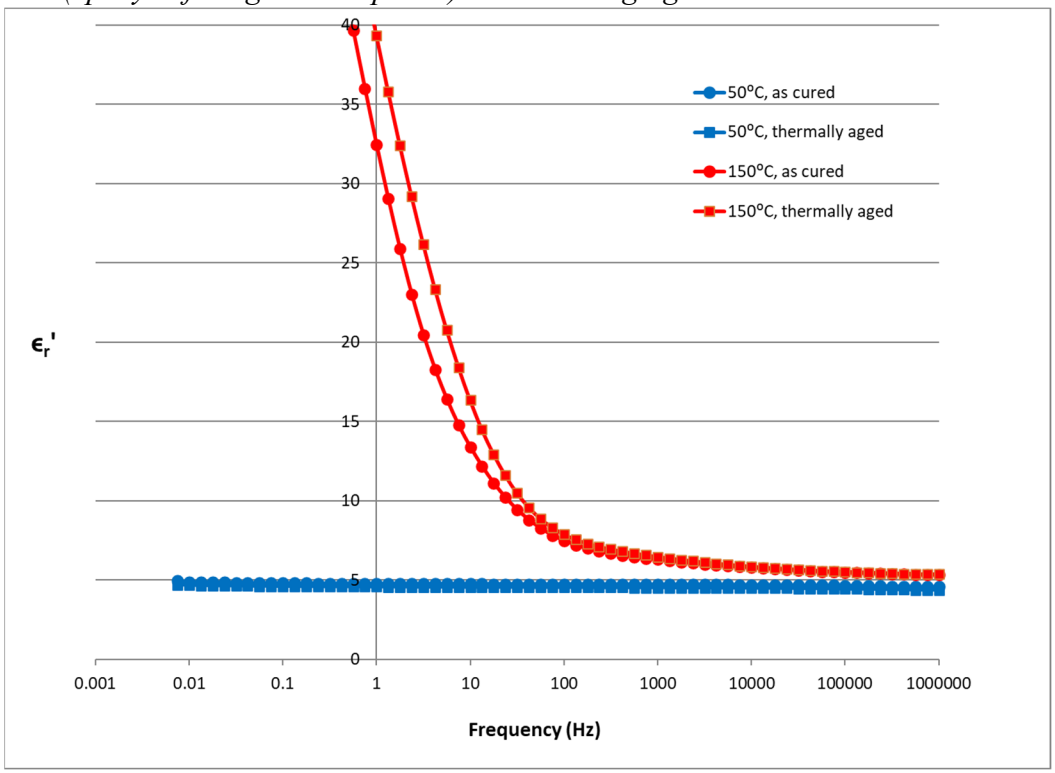


Figure 6.28. Real Permittivity vs. frequency for FR5 with thermal aging.

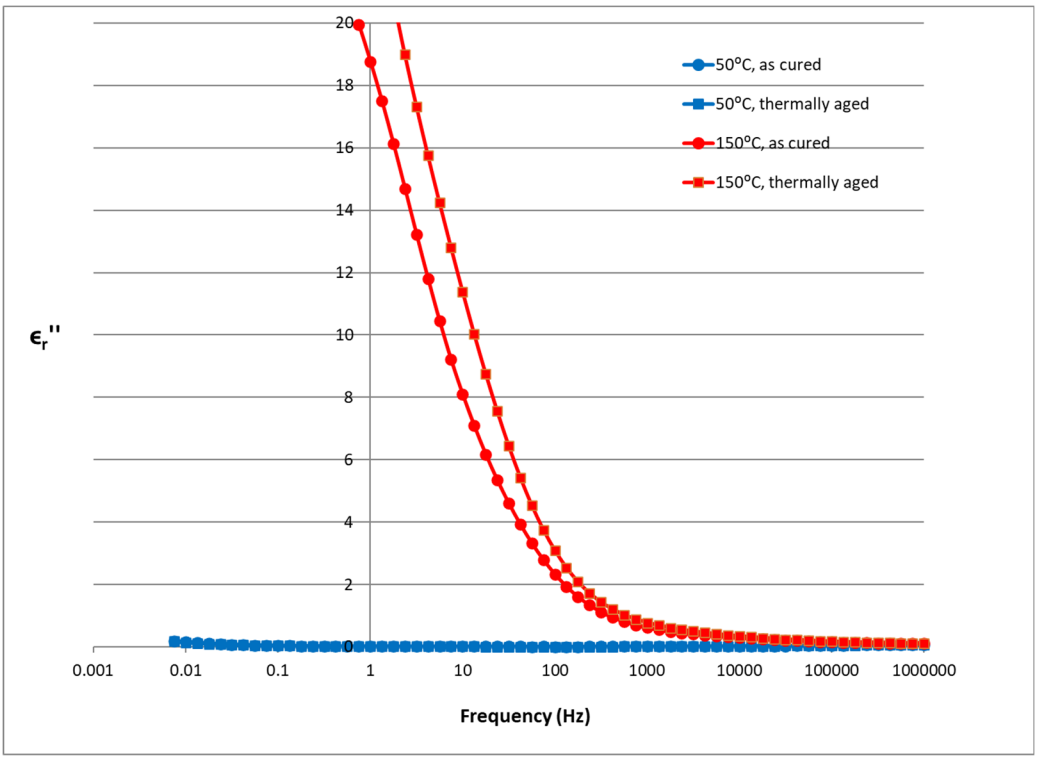


Figure 6.29. Imaginary Permittivity vs. frequency for FR5 with thermal aging.

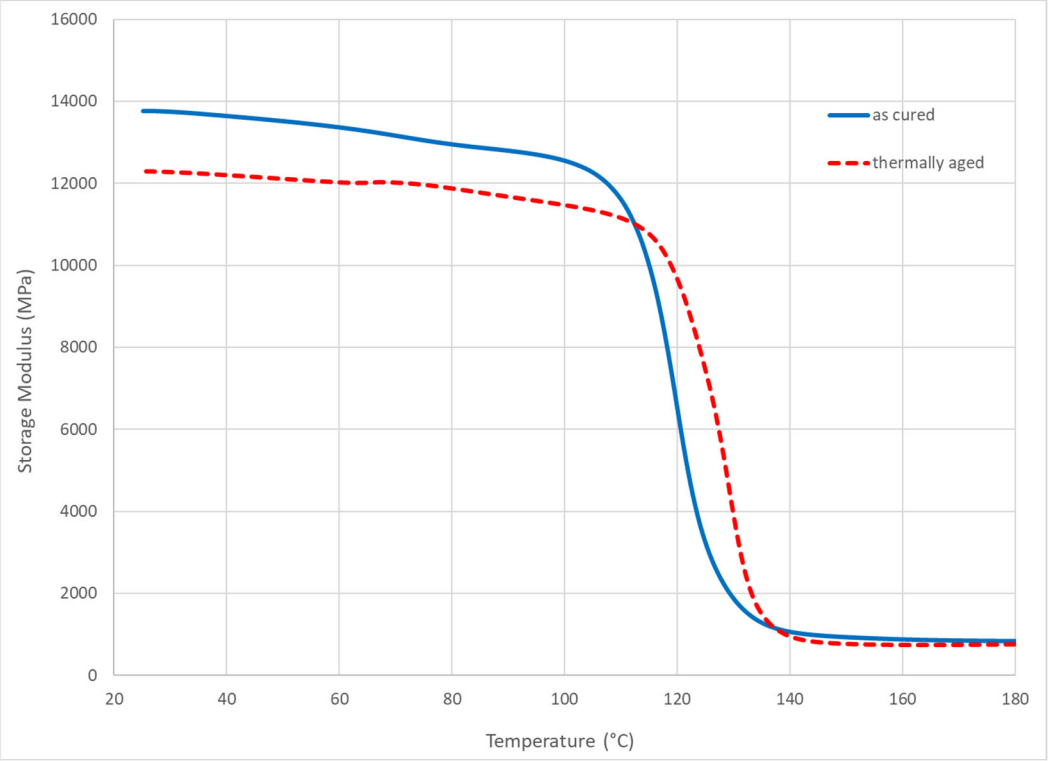


Figure 6.30. Dynamic Storage Modulus vs. temperature for FR5 with thermal aging.

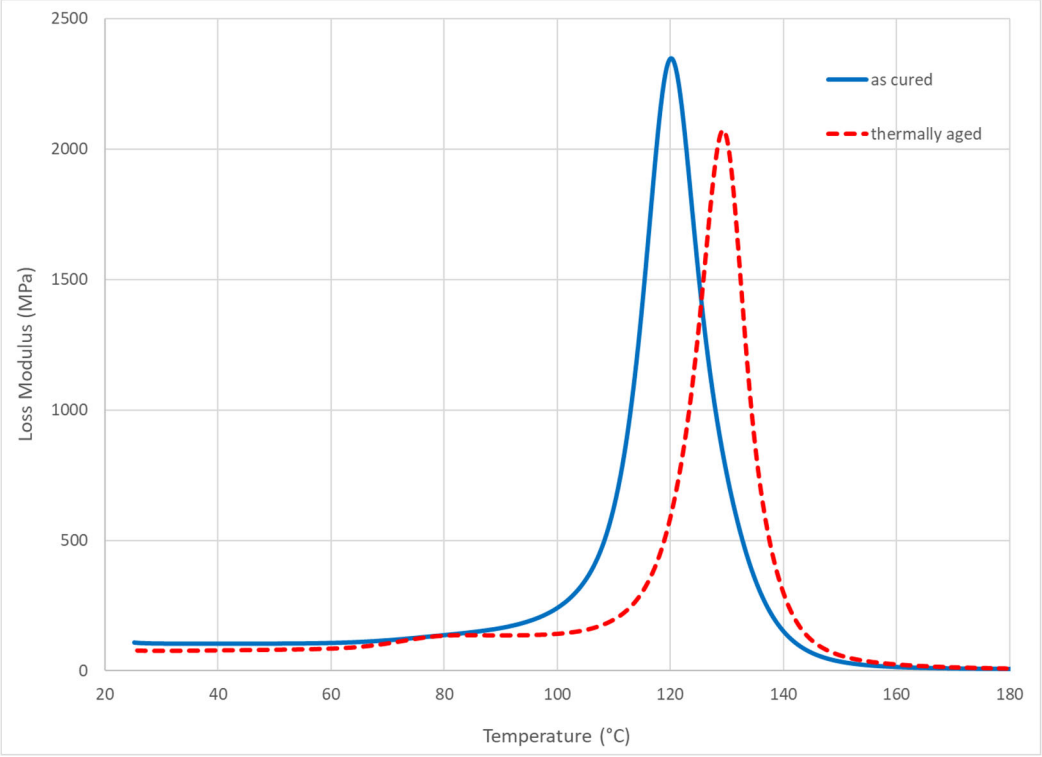


Figure 6.31. Dynamic Loss Modulus vs. temperature for FR5 with thermal aging.

- *FR5 (epoxy + fiberglass composite): Mechanical Aging*

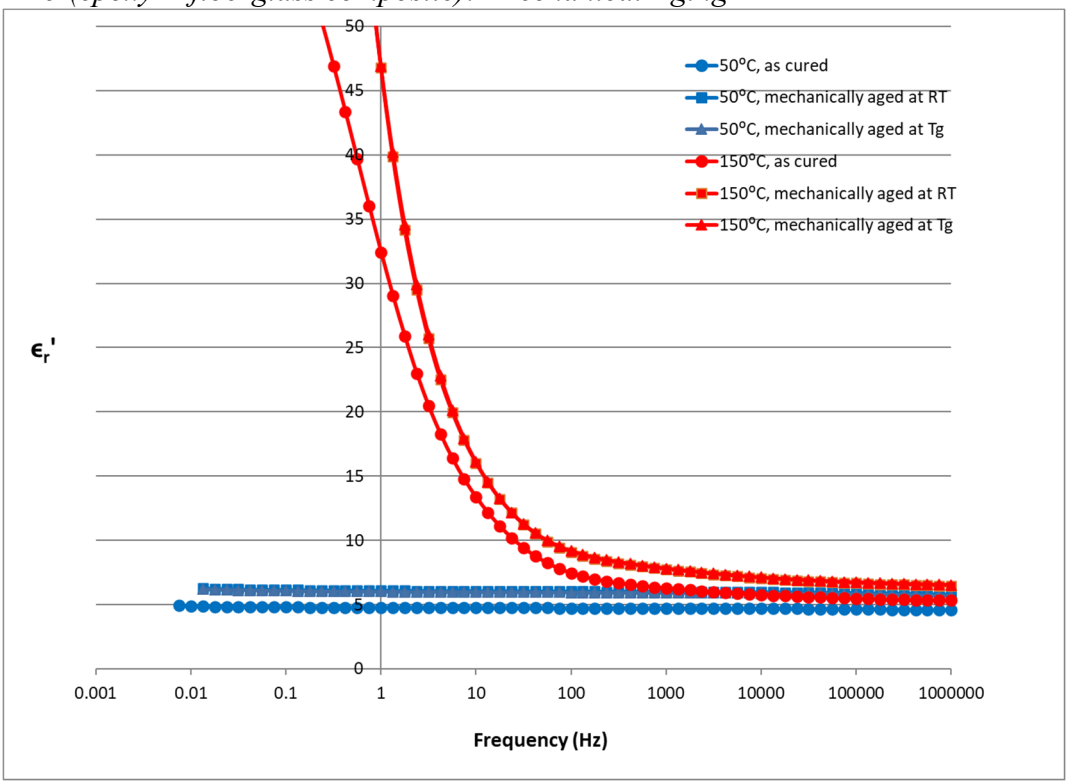


Figure 6.32. Real Permittivity vs. frequency for FR5 with mechanical aging.

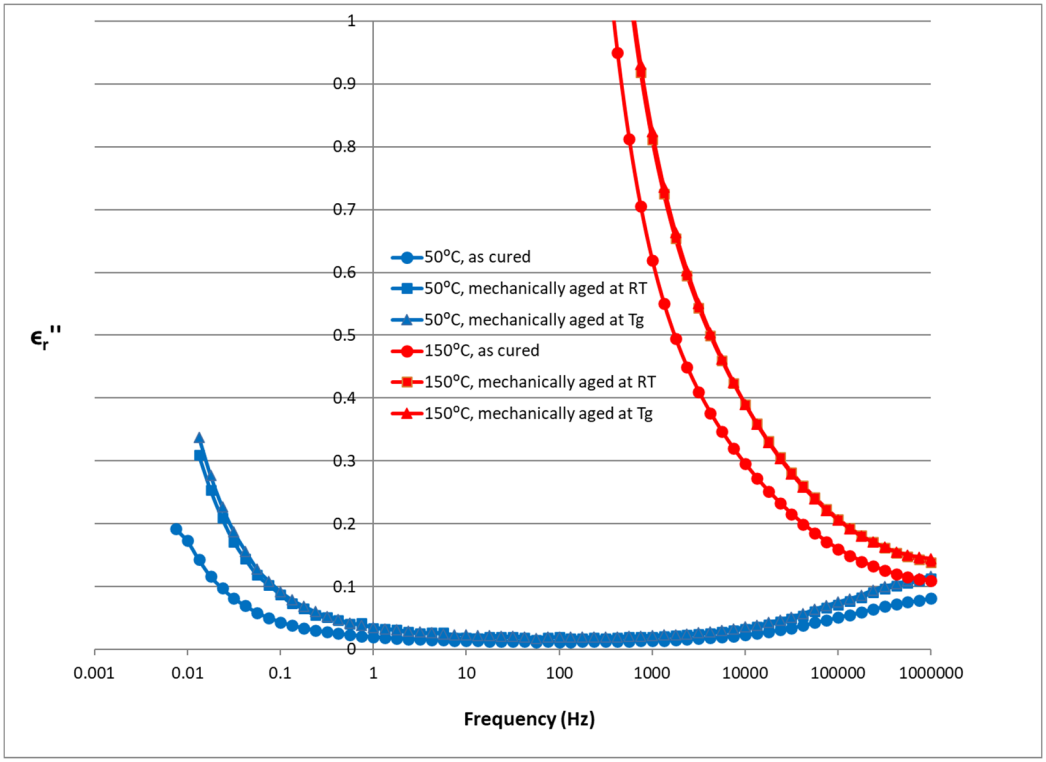


Figure 6.33. Imaginary Permittivity vs. frequency for FR5 with mechanical aging.

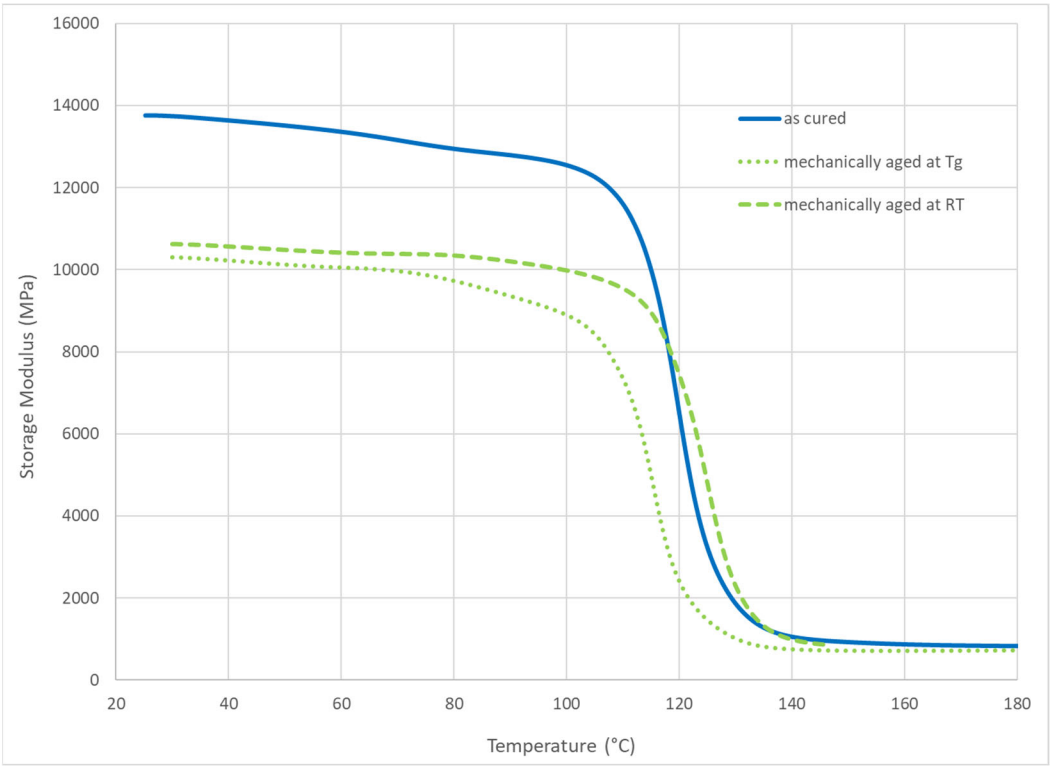


Figure 6.34. Dynamic Storage Modulus vs. temperature for FR5 with mechanical aging.

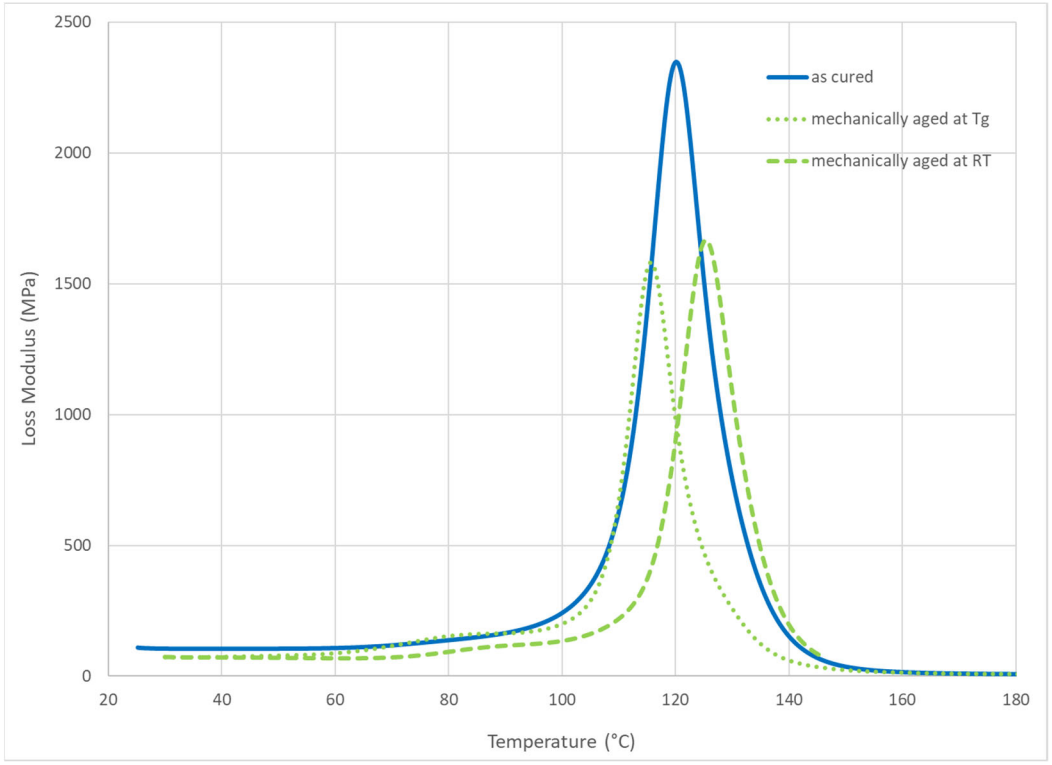


Figure 6.35. Dynamic Loss Modulus vs. temperature for FR5 with mechanical aging.

- *FR5 (epoxy + fiberglass composite): Electrical Aging*

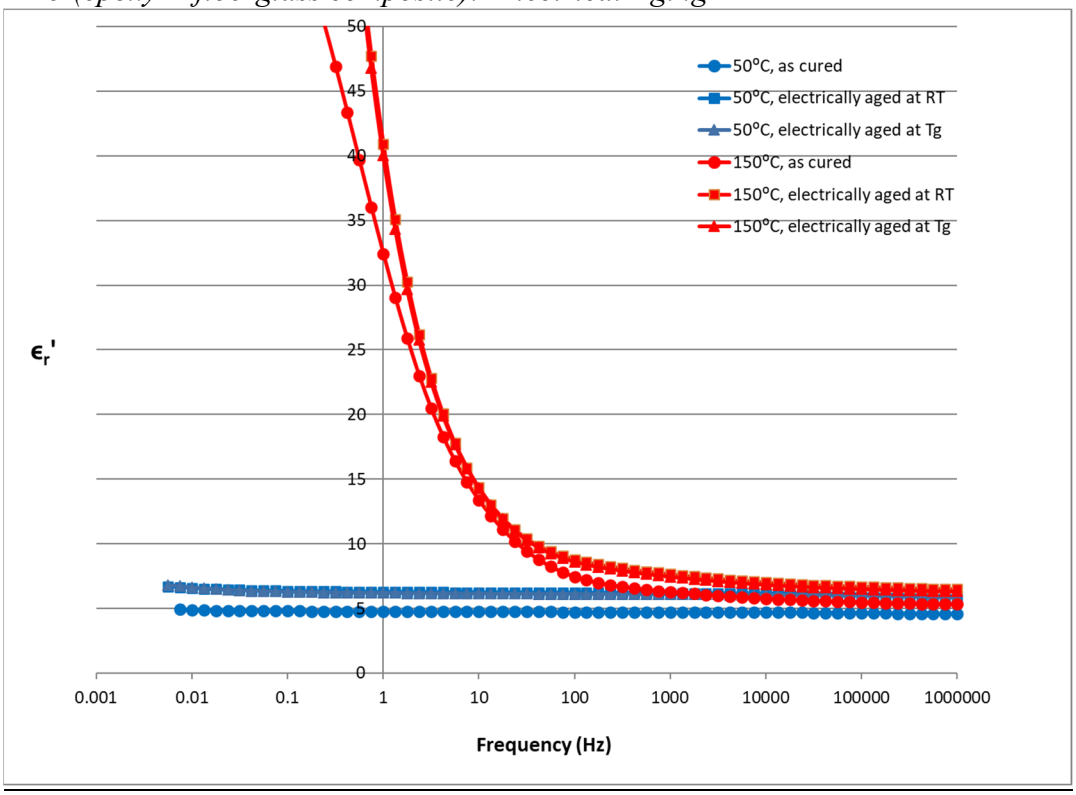


Figure 6.36. Real Permittivity vs. frequency for FR5 with electrical aging.

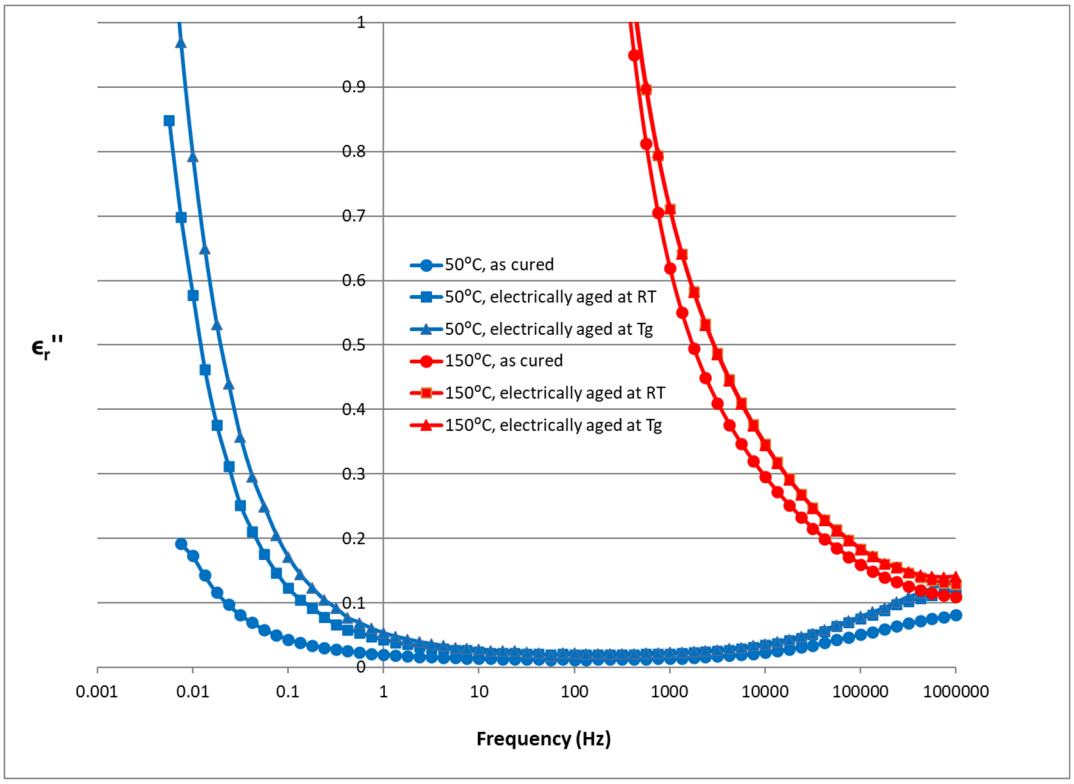


Figure 6.37. Imaginary Permittivity vs. frequency for FR5 with electrical aging.

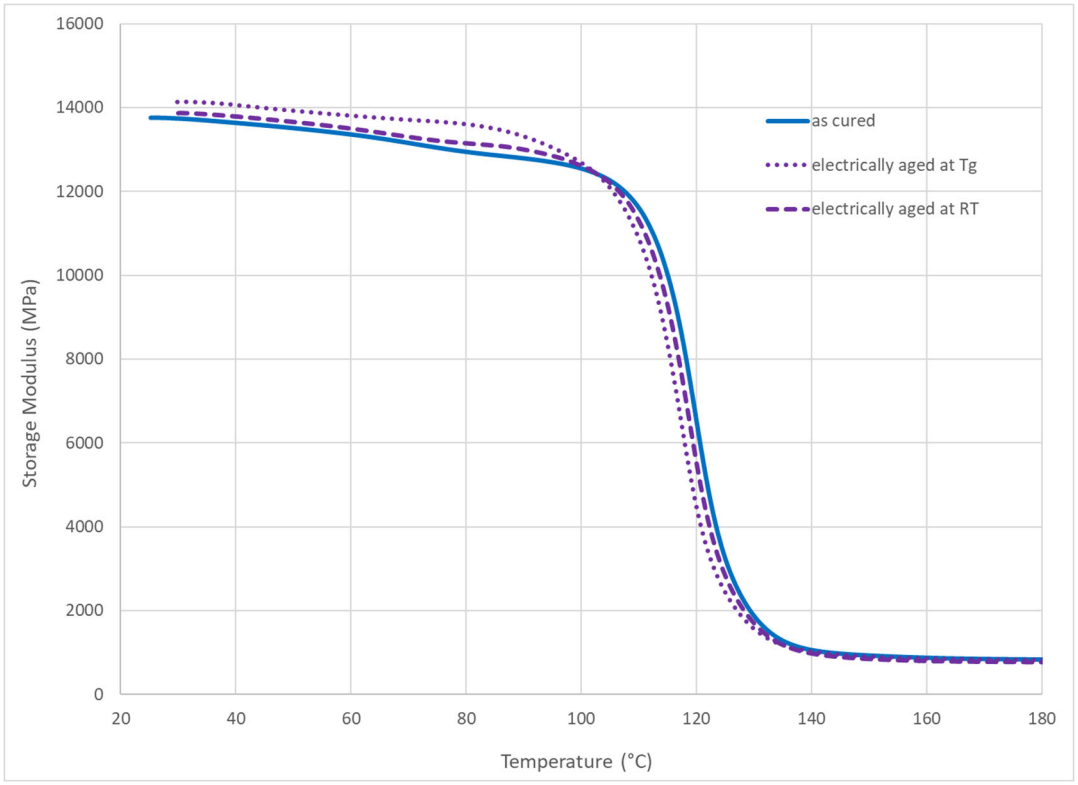


Figure 6.38. Dynamic Storage Modulus vs. temperature for FR5 with electrical aging.

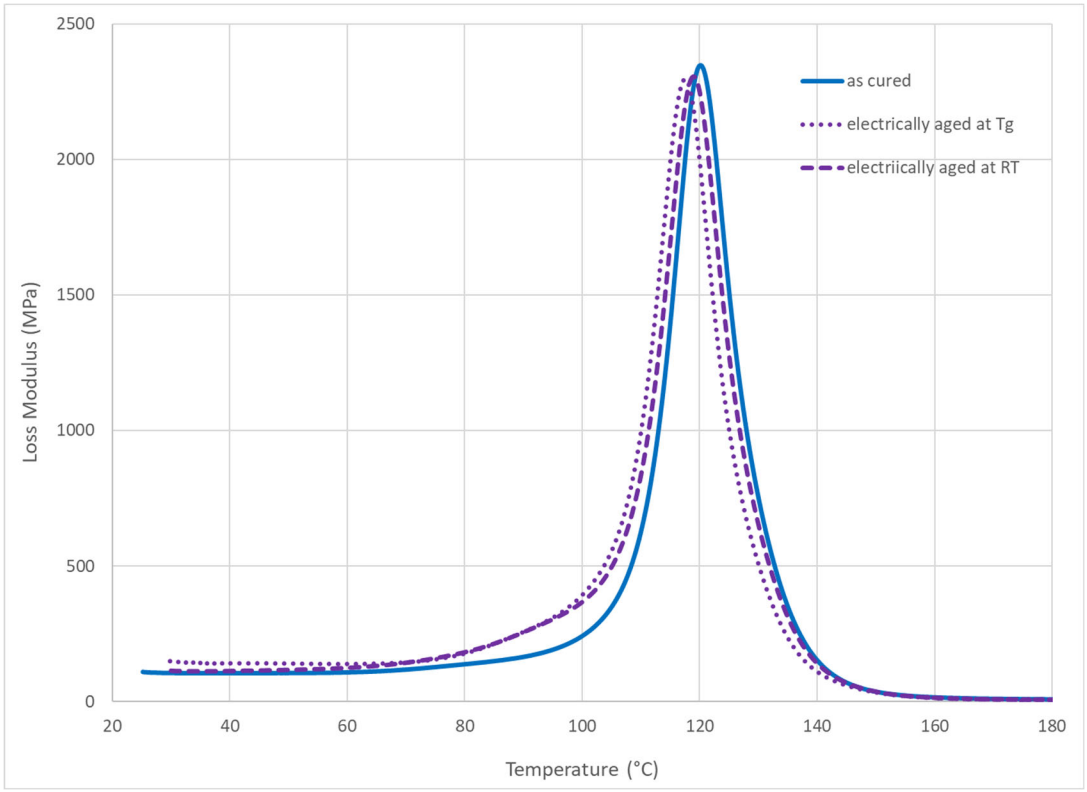


Figure 6.39. Dynamic Loss Modulus vs. temperature for FR5 with electrical aging.

6.2.4. Silicone+Fiberglass Laminate (G7)

The real permittivity of the thermally aged Silicone Laminate increased across the frequency range when measured at 50°C (see Figure 6.40). An increase in real permittivity at 150°C was only observed at frequencies below 1 Hz. An increase at 150°C was also observed in the permittivity loss of the thermally aged material (see Figure 6.41). Thermal aging appears to have essentially no effect for sample G7 when loss permittivity is measured at 50°C. Stiffness is reduced at temperatures below 120°C and increased above this temperature (see Figure 6.42). Also observed is a large reduction in the very broad loss modulus peak with thermal aging (see Figure 6.43).

Both mechanical aging treatments of the G7 laminate caused increases in real permittivity across the frequency spectrum (see Figure 6.44). The room temperature mechanical aging appears to have a slightly greater effect. This is true of the loss permittivity, as well, although the differences between the as cured laminate and the mechanically aged laminates are minor. Dynamic storage moduli decreased with mechanical aging across the temperature range measured. A decrease in the dynamic loss moduli is only observed above 100°C with both mechanical treatments (see Figure 6.47). The broad loss modulus peak is still apparent.

The effects of electrical aging are similar to those of mechanical aging. However, the temperature of electrical aging has no impact (see Figures 6.48-6.49). A slight decrease in dynamic storage moduli is observed over the temperature range. An increase in dynamic loss moduli was measurable over this same range.

- *G7 (silicone + fiberglass composite): Thermal Aging*

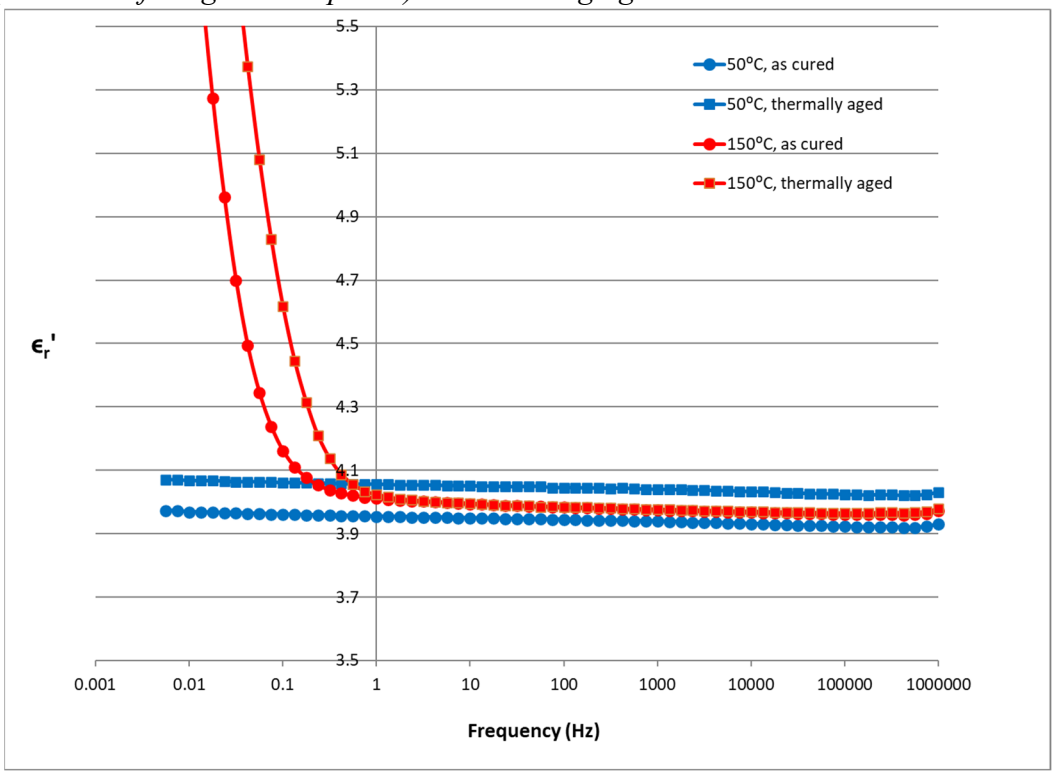


Figure 6.40. Real Permittivity vs. frequency for G7 with thermal aging.

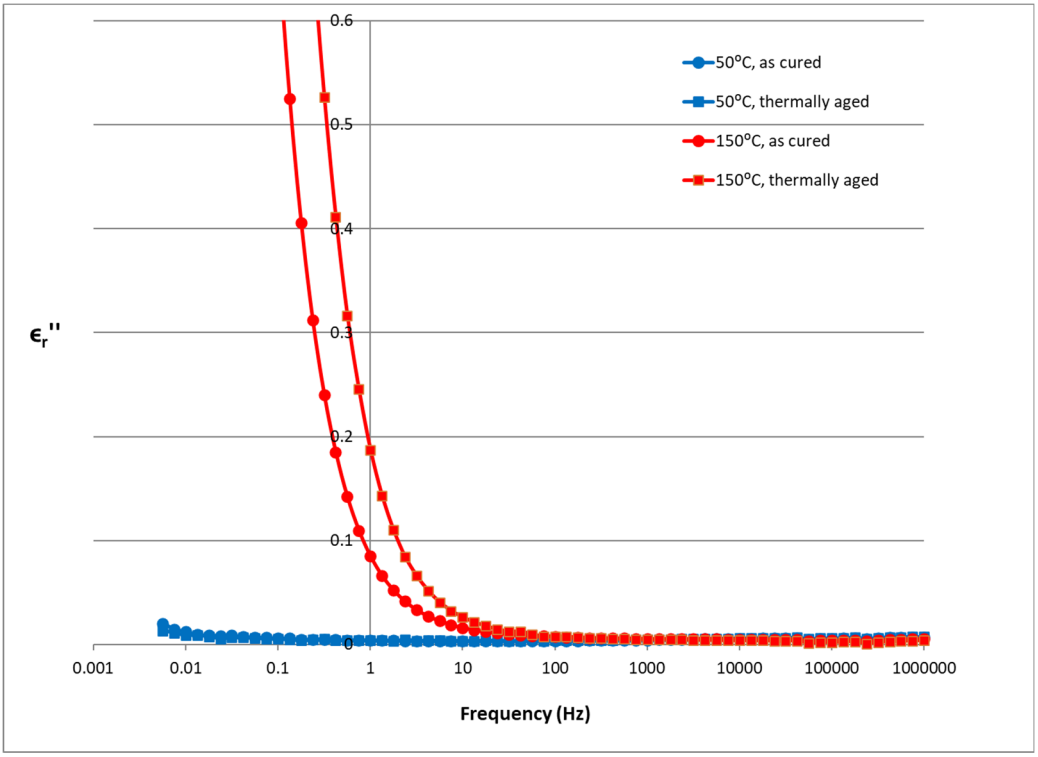


Figure 6.41. Imaginary Permittivity vs. frequency for G7 with thermal aging.

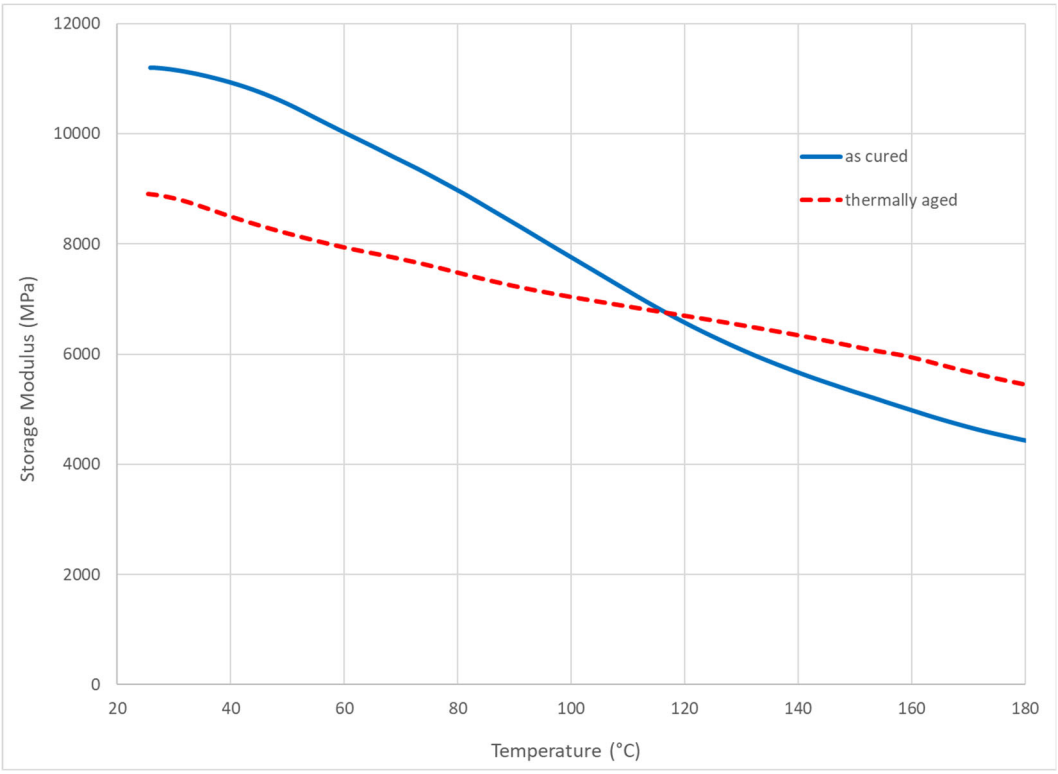


Figure 6.42. Dynamic Storage Modulus vs. temperature for G7 with thermal aging.

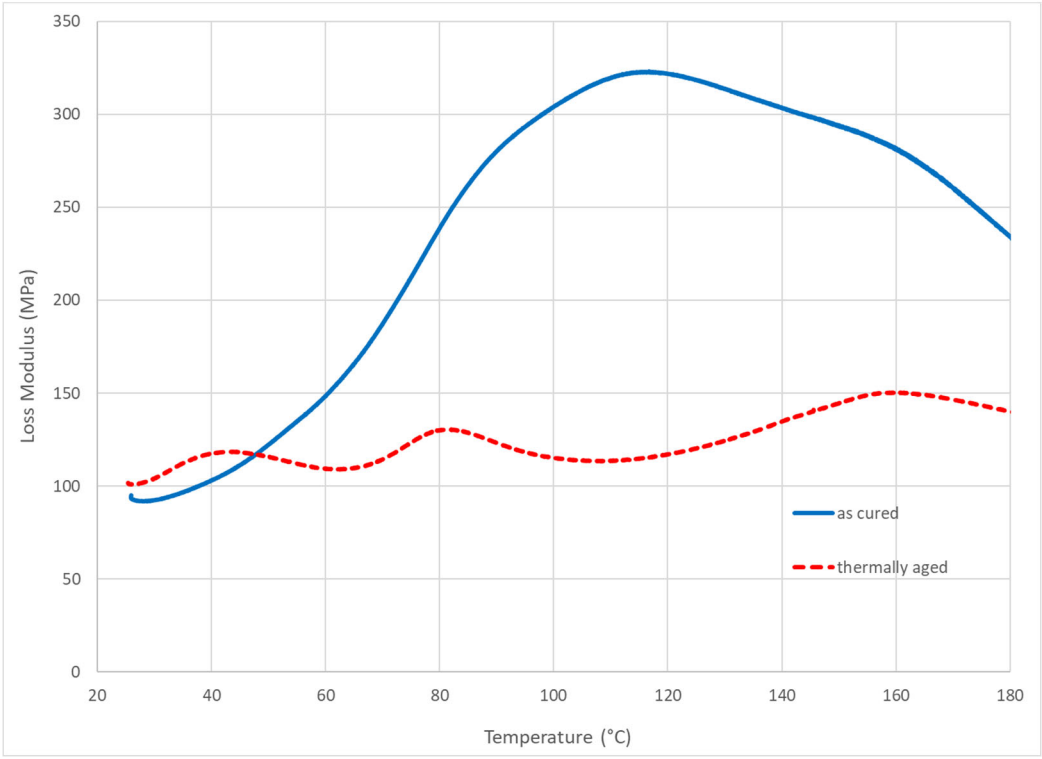


Figure 6.43. Dynamic Loss Modulus vs. temperature for G7 with thermal aging.

- *G7 (silicone + fiberglass composite): Mechanical Aging*

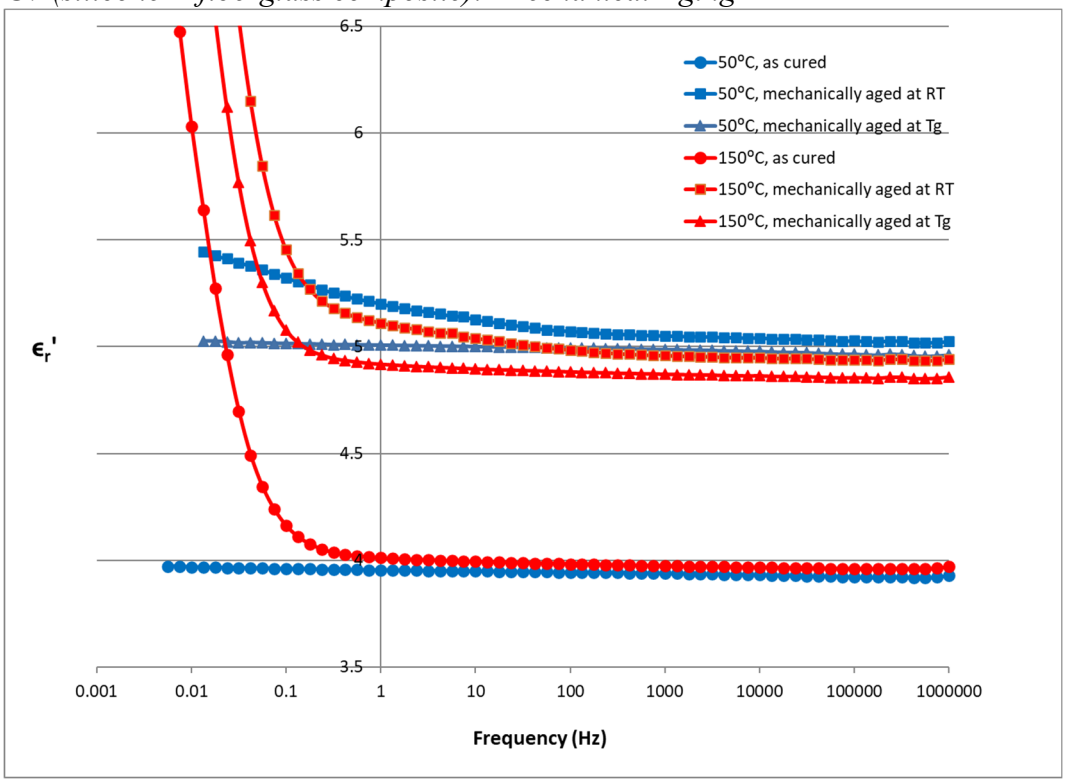


Figure 6.44. Real Permittivity vs. frequency for G7 with mechanical aging.

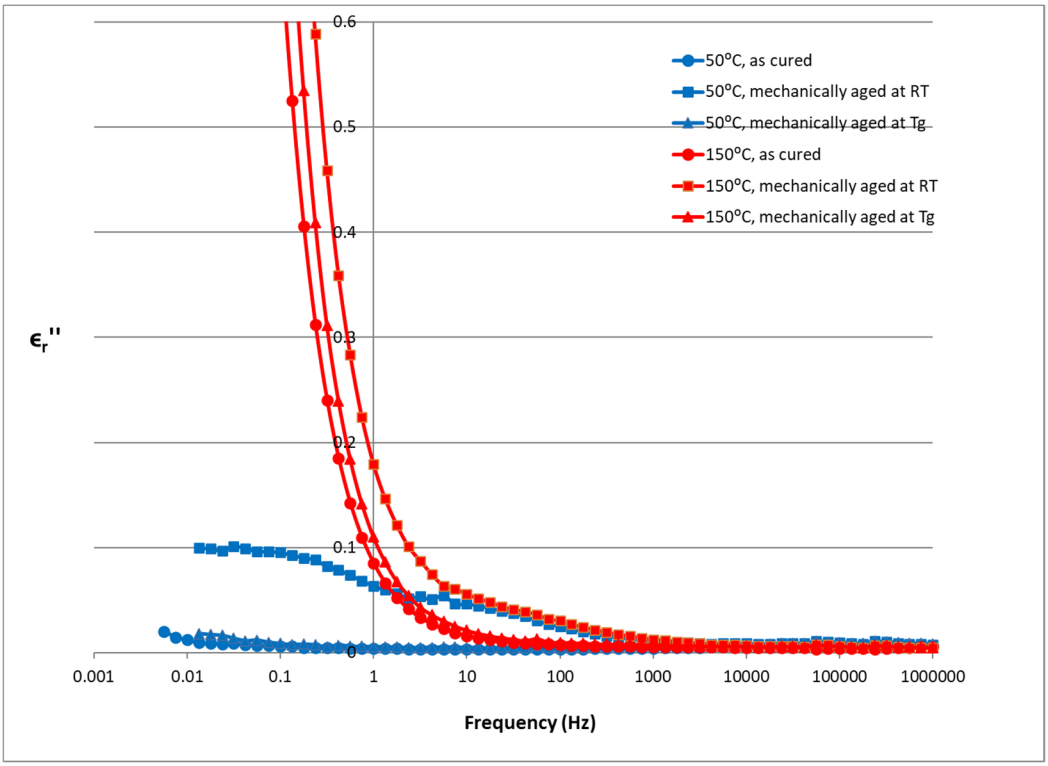


Figure 6.45. Imaginary Permittivity vs. frequency for G7 with mechanical aging.

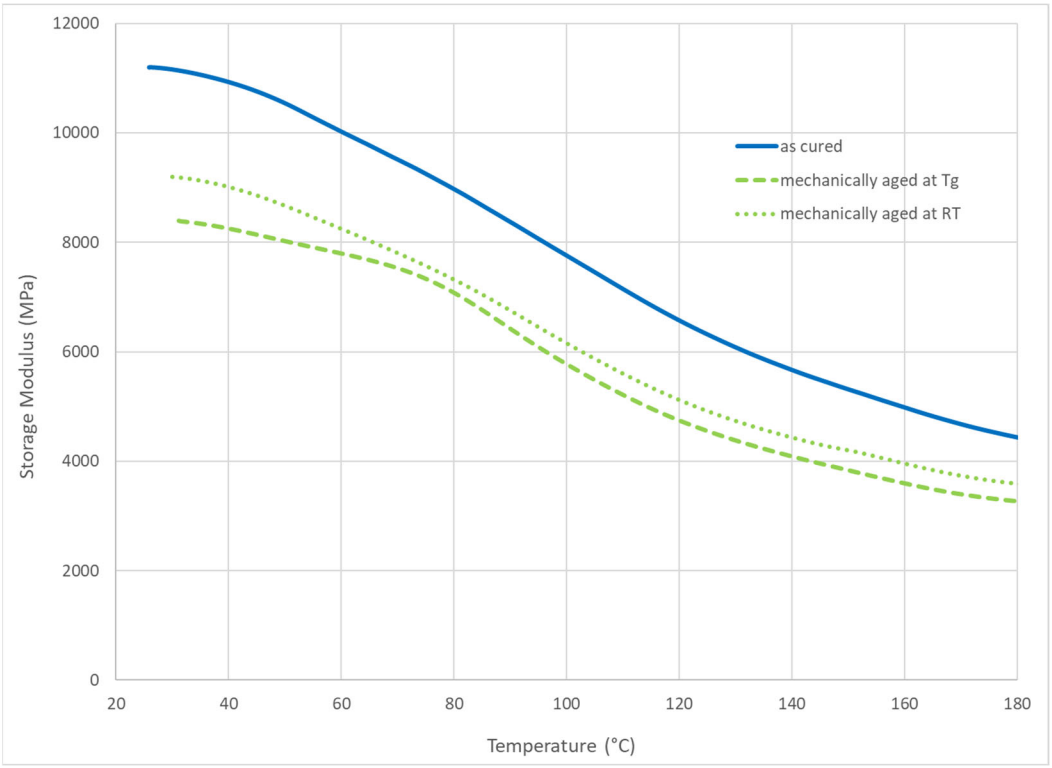


Figure 6.46. Dynamic Storage Modulus vs. temperature for G7 with mechanical aging.

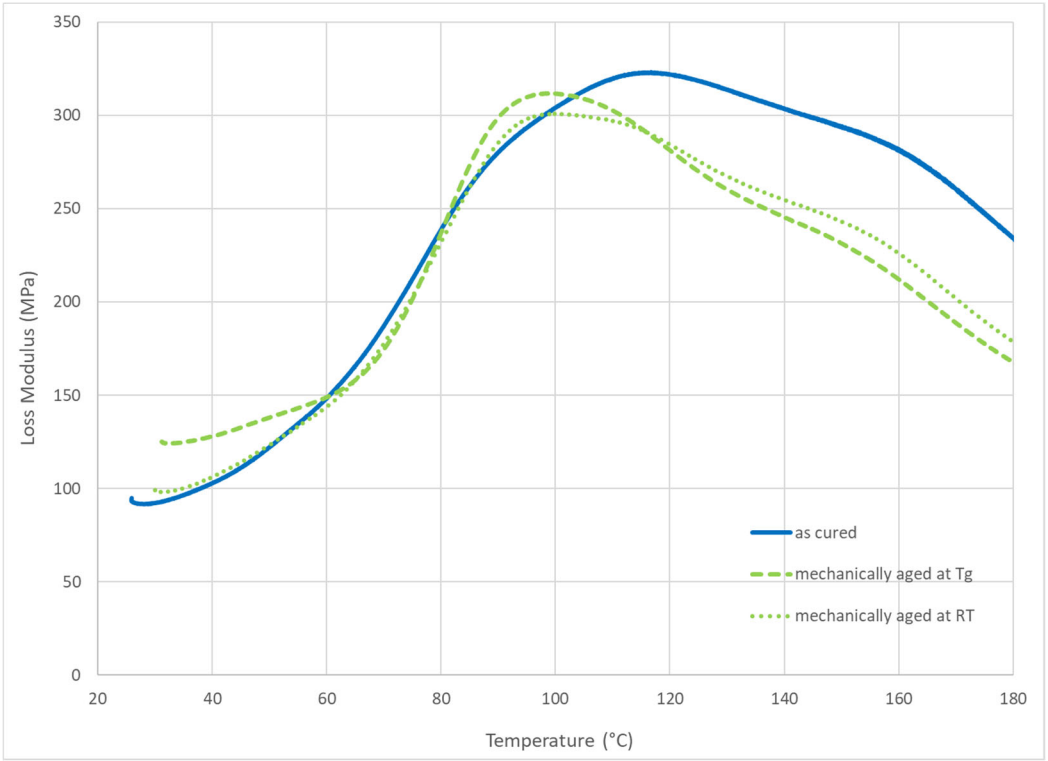


Figure 6.47. Dynamic Loss Modulus vs. temperature for G7 with mechanical aging.

- *G7 (silicone + fiberglass composite): Electrical Aging*

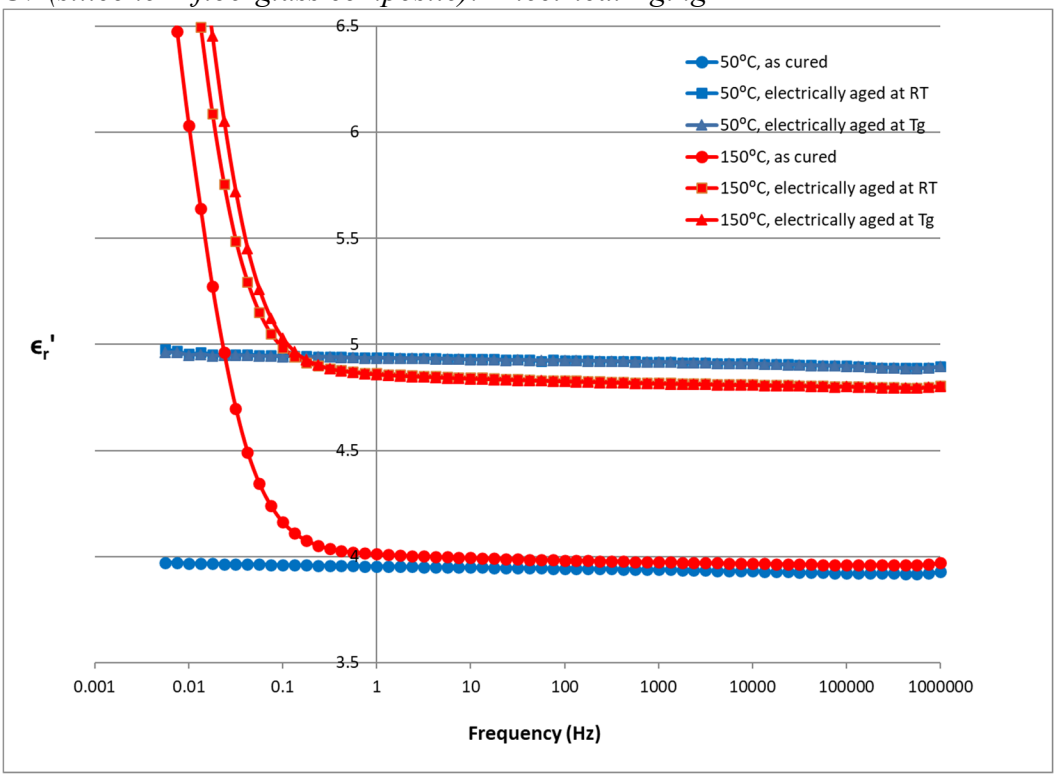


Figure 6.48. Real Permittivity vs. frequency for G7 with electrical aging.

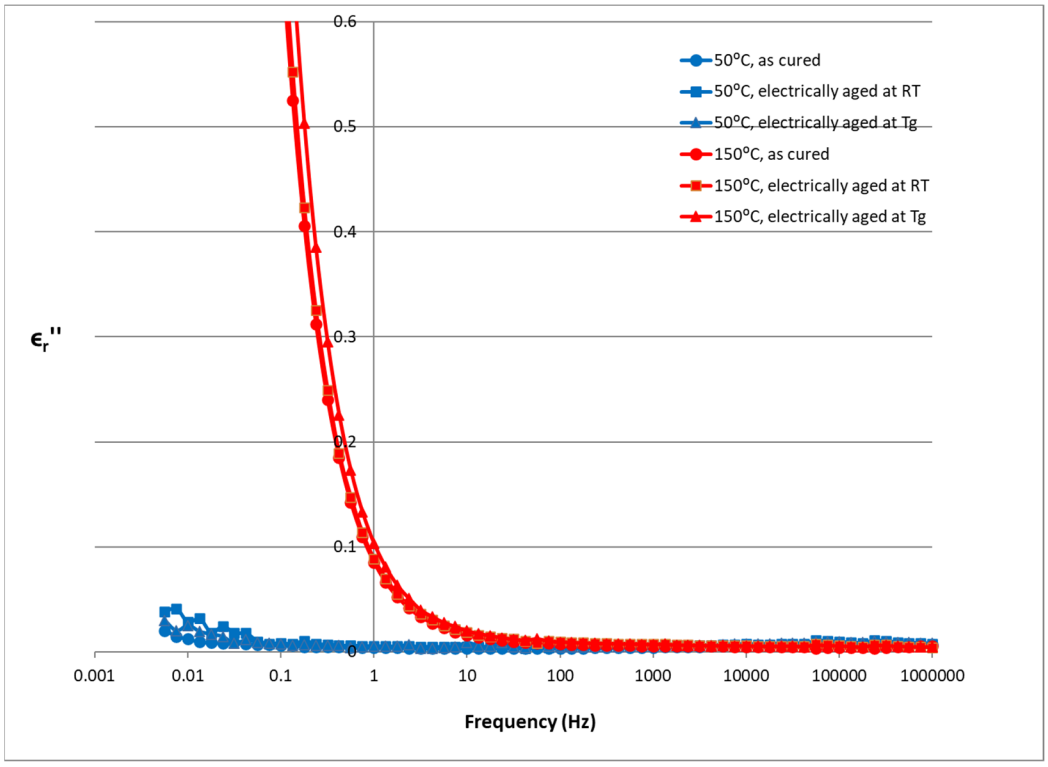


Figure 6.49. Imaginary Permittivity vs. frequency for G7 with electrical aging.

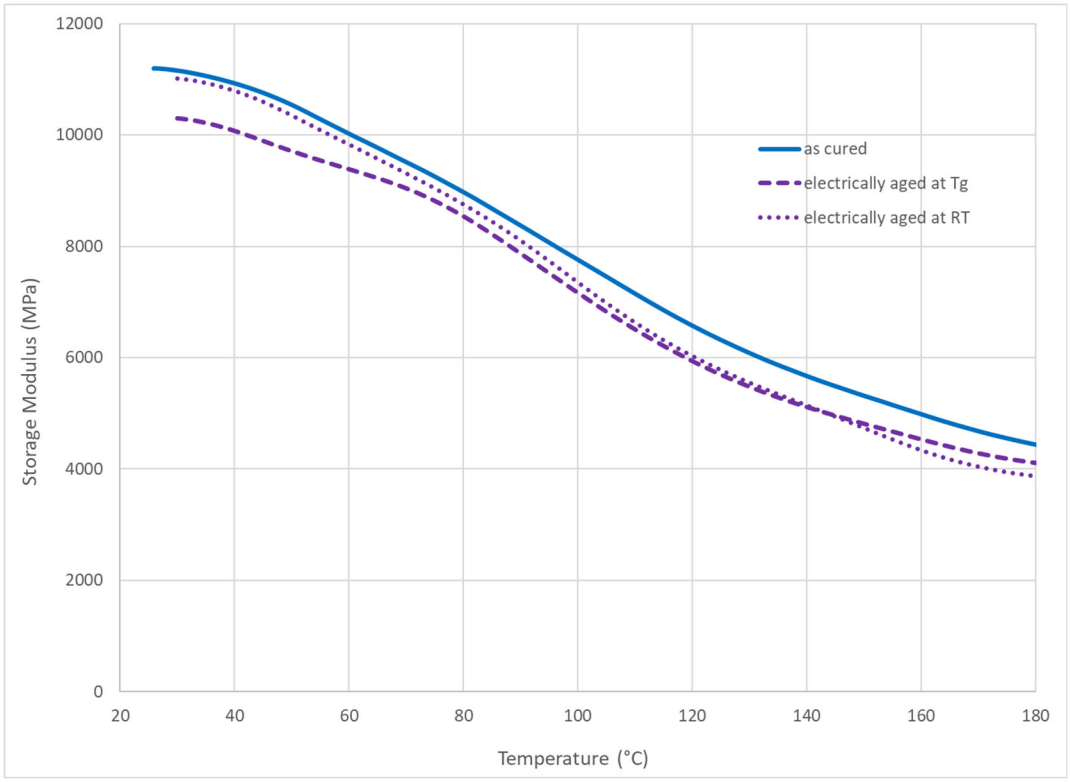


Figure 6.50. Dynamic Storage Modulus vs. temperature for G7 with electrical aging.

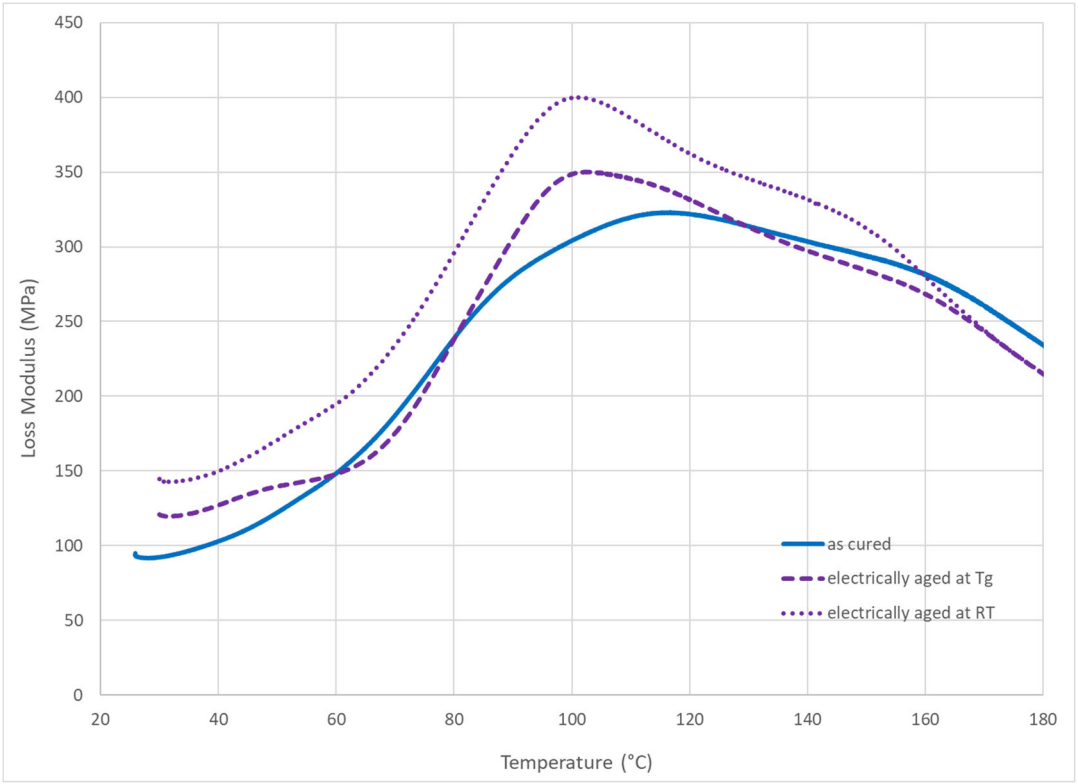


Figure 6.51. Dynamic Loss Modulus vs. temperature for G7 with electrical aging.

6.3. Complimentary Characterization

Three complimentary characterization techniques were evaluated on as-cured, thermally aged, mechanically aged, and electrically aged samples of the epoxy resin, Pn-0 (Permafil 74050) and the silicone resin, Sn-0 (Silres H62c). Prepared samples were sent to Particle Testing Authority (a service lab affiliated with Micrometrics Instrument Corporation) for pycnometry, N_2 porosimetry, and specific surface area (BETA). In the future, pycnometry, BETA with krypton, and mercury porosimetry are encouraged if resources are available. There are differences in the material microstructures observed after all three types of aging. Pulsed Electroacoustic Analysis (PEA) is also reported.

Pycnometry: The density values produced from pycnometry characterizations are listed in Table 6.2. Thermal aging reduced density for both the Epoxy (Pn-0) and the Silicone (Sn-0). Density increased with mechanical aging at room temperature and at the glass transition temperature. The density increase was only slightly greater with mechanical aging at the glass transition than at room temperature for the Epoxy. The converse was observed for the Silicone.

Electrical aging at room temperature also caused an increase in the density of the Epoxy. This increase was essentially the same as observed with mechanical aging. Electrical aging of the Silicone also resulted in an increased density. However, the density increase with electrical aging was significantly greater than for mechanical aging.

A density increase can indicate reduced free volume, which often accompanies structural ordering. The measured changes in density are commensurate with the changes observed in real permittivity trends with aging treatments.

Table 6.2. Pycnometry results for cured epoxy and silicone resin materials.

No.	Sample Description	Density	Std Dev	Ratio
		(g/cm^3)	(g/cm^3)	(/no aging)
2001837	Epoxy as cured	1.1899	0.0015	1.0000
2001838	Epoxy 100 hr at 155°C	1.1820	0.0045	0.9934
2001839	Epoxy Mechanically Aged at room temp.	1.2043	0.0003	1.0121
2001840	Epoxy Mechanically Aged at T_g	1.2058	0.0003	1.0134
2005006	Epoxy Electrically Aged at room temp.	1.2057	0.0007	1.0133
2001841	Silicone as cured	1.1681	0.0008	1.0000
2001842	Silicone 100 hr at 155°C	1.1575	0.0011	0.9909
2001843	Silicone Mechanically Aged at room temp.	1.1733	0.0011	1.0045
2001844	Silicone Mechanically Aged at T_g	1.1694	0.0014	1.0011
2005008	Silicone Electrically Aged at room temp.	1.1829	0.0045	1.0126

BET Surface Area: The BET surface area data is listed in Table 6.3. Thermal aging reduced total specific surface area for the Epoxy but increased the surface area for the Silicone. The reduction in specific surface area for the Epoxy is not anticipated from a reduced density. The thermally aged Silicone increased surface area with reduced density. The Silicone incurs the largest changes at elevated temperatures. All mechanically aged samples indicated large reductions in specific surface areas.

Although the trends appear valid, two factors discourage further interpretation of these surface area results. First, the amount of surface area accessible for measurement is very low, which affects confidence. Second, the technique requires access by pressurized krypton through the sample surface into the bulk of the sample. Variations in the sample surfaces could affect this access.

Table 6.3. Specific Surface Area (BET) results for cured epoxy and silicone resin materials.

No.	Sample Description	Single Point Surface Area	BET (Kr) Specific Surface Area	Ratio
		(m^2/g)	(m^2/g)	(/no aging)
2001837	Epoxy no aging	0.0115	0.0133	1.0000
2001838	Epoxy 100 hr at 155°C	0.0109	0.0124	0.9323
2001839	Epoxy Mechanically Aged at room temp.	0.0047	0.0051	0.3835
2001840	Epoxy Mechanically Aged at T_g	0.0076	0.0085	0.6391
2005005	Epoxy Electrically Aged at room temp.	0.0012	0.0017	0.1278
2001841	Silicone no aging	0.0081	0.0092	1.0000
2001842	Silicone 100 hr at 155°C	0.0095	0.0130	1.4130
2001843	Silicone Mechanically Aged at room temp.	0.0020	0.0030	0.3261
2001844	Silicone Mechanically Aged at T_g	0.0016	0.0017	0.1848
2005008	Silicone Electrically Aged at room temp.	0.0050	0.0098(?)	0.6173

Pulsed Electro-Acoustic (PEA): This characterization is used to examine charge injection and migration in dielectrics. (A brief discussion of PEA can be found in section 5.3.) The technique usually provides novel spatial information in one dimension by tracking the timed response of an acoustic signal. A cursory study comparing PEA results of FR5 (epoxy-fiberglass laminate) samples showed differentiation with aging treatments. FR5 samples of the same thickness were prepared as the other DETA samples investigated in this Compendium. The PEA characterizations were produced and analyzed by Dr. Tony Pearson of Box Elder Innovations.[9]

For one sample each of FR5-HT, FR5-ERT, and FR5-MRT, voltage was ramped across the sample thickness (1.6 mm) from 10 kV to 16 kV at 10 V/s. The maximum DC voltage was then held for 40 minutes. The voltage was set to zero ("grounded") and monitored for 10 additional minutes. PEA measurements were recorded during these three time periods. The calculated acoustic attenuation coefficients for the "hold" period were 7.31×10^{-6} s/m, 5.8×10^{-6} s/m, and 4.20×10^{-6} s/m for FR5-HT, FR5-ERT, and FR5-MRT, respectively. The acoustic attenuation is reduced with dynamic field aging suggesting improved homogeneity. Figure 6.5.2 shows the peak amplitude time traces at peak 1 (high voltage electrode), peak 2 (20% thickness from HV electrode), and peak 3 (low voltage electrode). The timed progressions indicate that the dynamic field aging treatments reduced polarization during voltage hold ("charge accumulation") and reduced polarization retention ("charge trapping") after grounding. While supporting the DETA results for dynamic field aging, these PEA observations warrant further investigation of PEA as a complimentary condition characterization for medium voltage applications of insulation.

[9] Box Elder Innovations LLC developed the PEA technology with support from AFRL STTR FA9453-13-C-0067. Please see www.boxelderinnovations.com/pulsed-electro-acoustic-systems.html for more information.

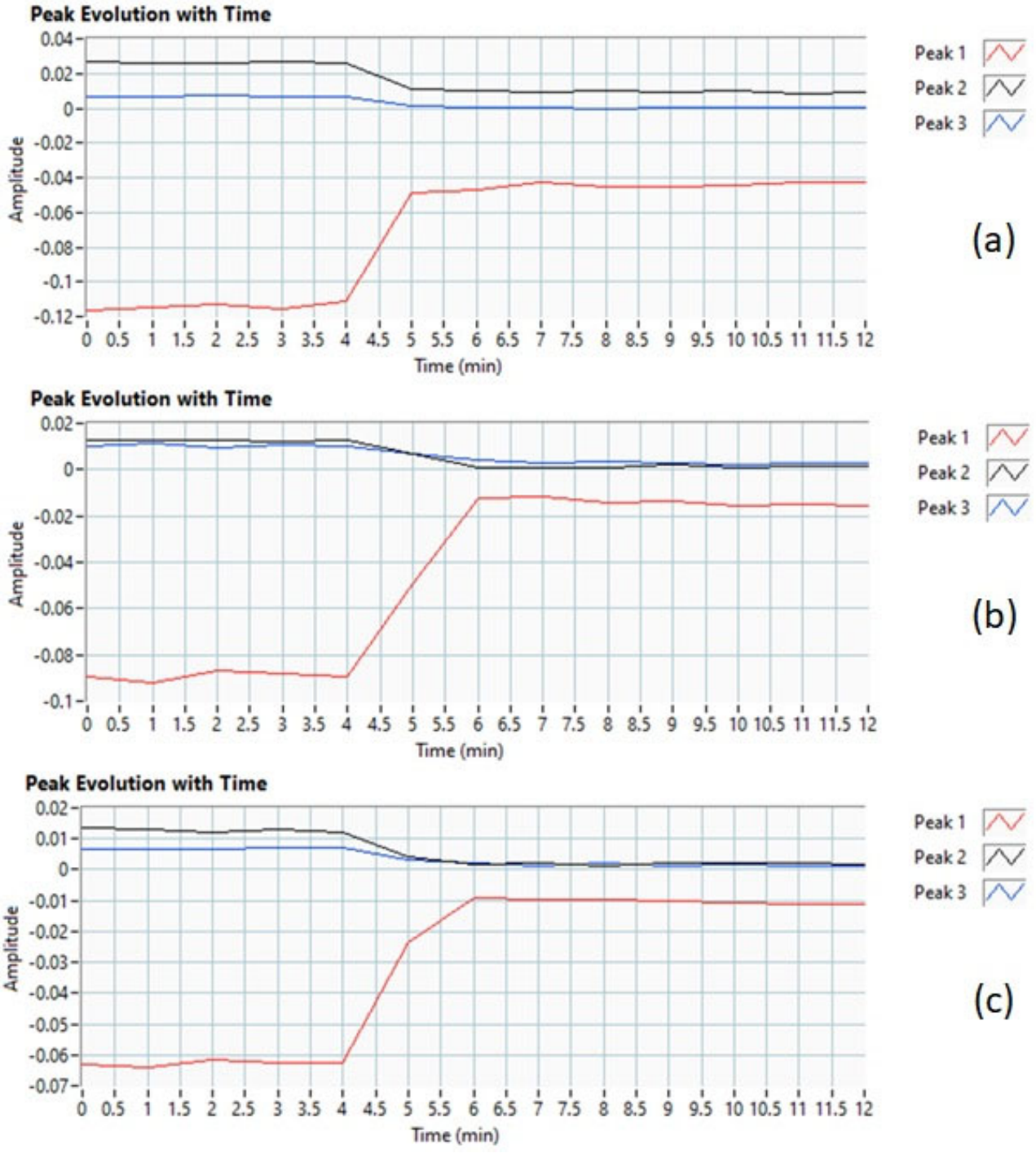


Figure 6.5.2. PEA peak signal decay after grounding: (a) FR5-HT, (b) FR5-ERT, and (c) FR5-MRT.

6.4. Dynamic Field Aging vs. Thermal Aging

The type of stress that produces aging has a pronounced effect on the aging behaviors for all four materials. For the controlled aging treatments used here, the molecular dynamics of the sample material after thermal aging are distinct from the molecular dynamics after mechanical or electrical aging. Thermal aging and mechanical or electrical aging produce differing structural changes. It follows that mechanical aging and electrical aging cannot be treated simply (e.g., as resulting from adding thermal energy, such as from friction, to a molecular structure). A representative kinetic model will need to accommodate this finding. The term "dynamic field aging" is used to refer to both mechanical aging and electrical aging as applied here.

The comparative graphs (see Figures 6.53-6.68) give evidence that mechanical or electrical aging is not due to a heating effect. The resulting behaviors do not imitate those observed after thermal aging. For brevity of this discussion, the data shown are limited to those measured at room temperature after aging. Dielectric moduli are graphed instead of permittivity. The pycnometry and BET data described in section 3.3 are used to help interpret the results.

The similarities of behaviors after mechanical aging and electrical aging illustrated by the dielectric moduli and elastic moduli of the Epoxy and Silicone are in agreement with changes in density. Density changes, however, do not provide a full explanation. An inverse proportionality is expected between the dielectric storage modulus and both the dipole concentration and the dipole moment. With no change in dipole moment, the dipole concentration should be proportional to density. The dielectric storage moduli for the Epoxy decrease with mechanical or electrical aging compared to Epoxy with no aging (see Figure 6.53). Increases in density are also observed. The dielectric storage modulus of the Epoxy Laminate similarly changed with mechanical or electrical aging (see Figure 6.57). For both mechanically aged Silicone materials, the dielectric moduli decrease almost the same amount across the spectrum (compared to the Silicone with no aging). Both exhibited increases in density. The thermally aged Silicone developed an increase in dielectric storage modulus. The density for the Silicone decreased with thermal aging. The dielectric loss moduli for both Epoxy and Silicone demonstrated essentially the same behaviors after thermal and mechanical aging as those of the unaged materials. At 155°C, the thermally aged Silicone is well above its sub-room temperature relaxation. During thermal aging at 155°C, nano- and microscopic regions of the Silicone may respond more actively to stress relaxation.

The density of the thermally aged Epoxy also decreased compared to the unaged density. However, the dielectric storage modulus of the thermally aged Epoxy decreased significantly. This suggests that the phase separation existing after thermal aging could increase the specific mean-squared dipole moment of the Epoxy material. Mechanical loss moduli as a function of temperature show evidence of phase separation in the Epoxy. After thermal aging, a new, higher temperature relaxation peak is present. This phase separation was not observed after the mechanical or electrical aging treatments (see Figure 6.56).

Phase separation of the Epoxy Laminate FR5 after thermal aging is also observed (see Figure 6.60). There is a suggestion of phase separation in the Epoxy Laminate after mechanical aging, as well (see the elastic loss modulus as a function of temperature in Figure 6.60). A peak at lower temperature appears after thermal and possibly mechanical aging. The high temperature relaxation is active in the elastic moduli of the as-received Epoxy Laminate.

The Epoxy Laminate's dielectric storage modulus is observed to decrease with mechanical aging in the same manner as for the Epoxy. However, thermal aging caused this modulus to increase slightly in comparison to the unaged Epoxy Laminate. The dielectric loss moduli appear unaffected by the five aging treatments. The Silicone Laminate's dielectric storage modulus was also observed to decrease with mechanical or electrical aging in the same manner as for the Silicone. However, thermal aging caused this modulus to decrease slightly in comparison to the as-received Silicone Laminate. Only the mechanical aging at room temperature caused the dielectric loss moduli to differentiate, resulting in increased losses at frequencies below 1000 Hz.

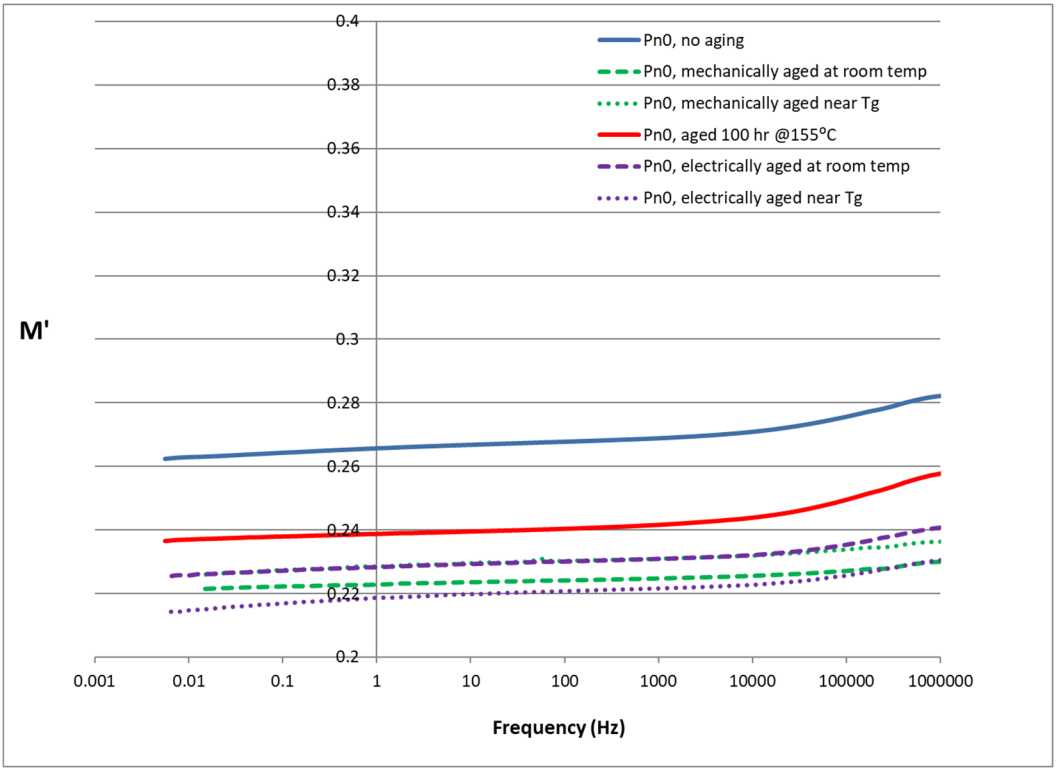


Figure 6.53. Dielectric storage modulus for Epoxy with aging treatment.

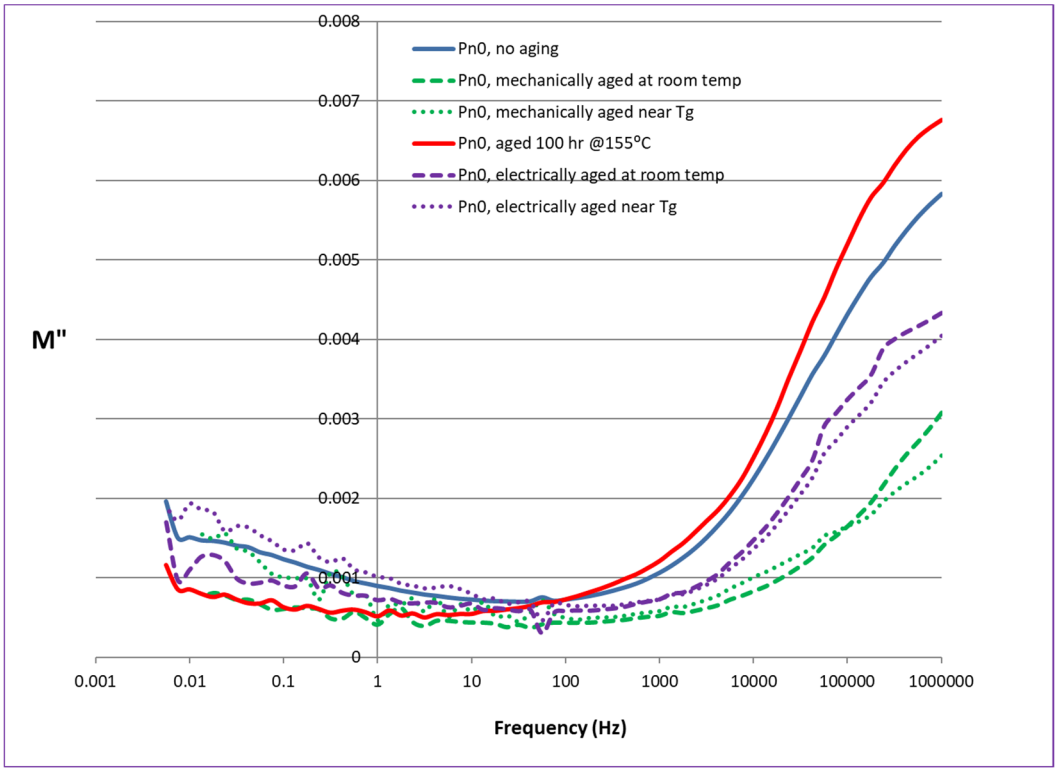


Figure 6.54. Dielectric loss modulus for Epoxy with aging treatment.

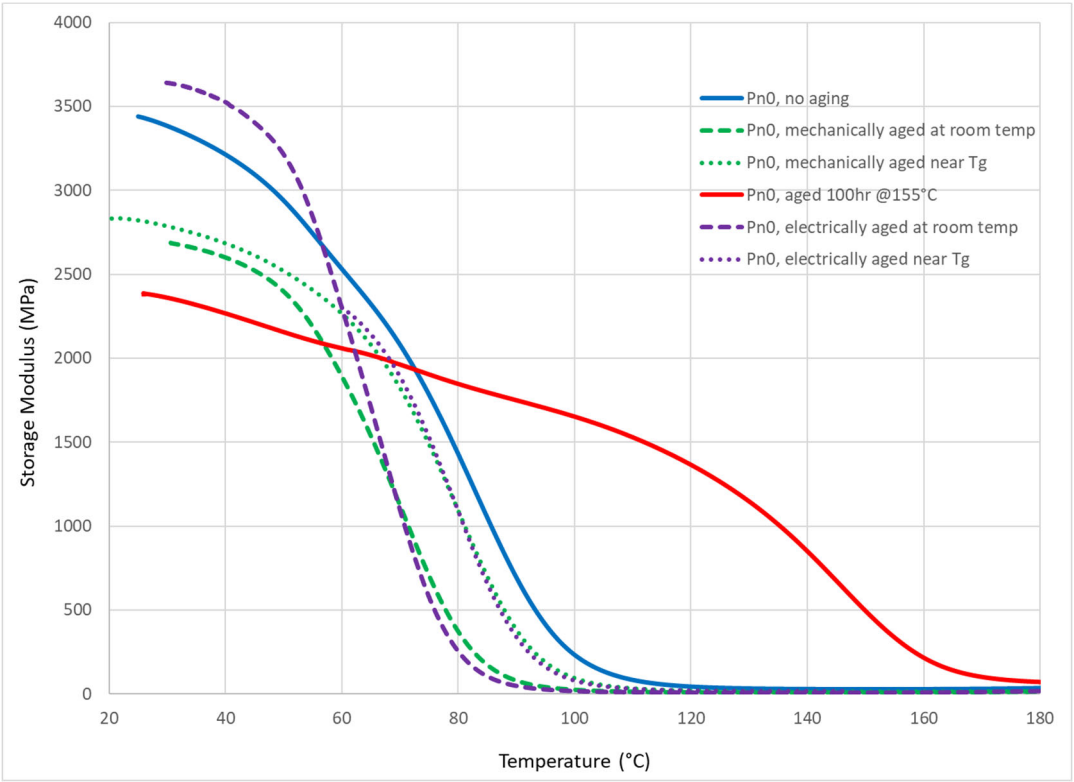


Figure 6.55. Mechanical storage modulus for Epoxy with aging treatment.

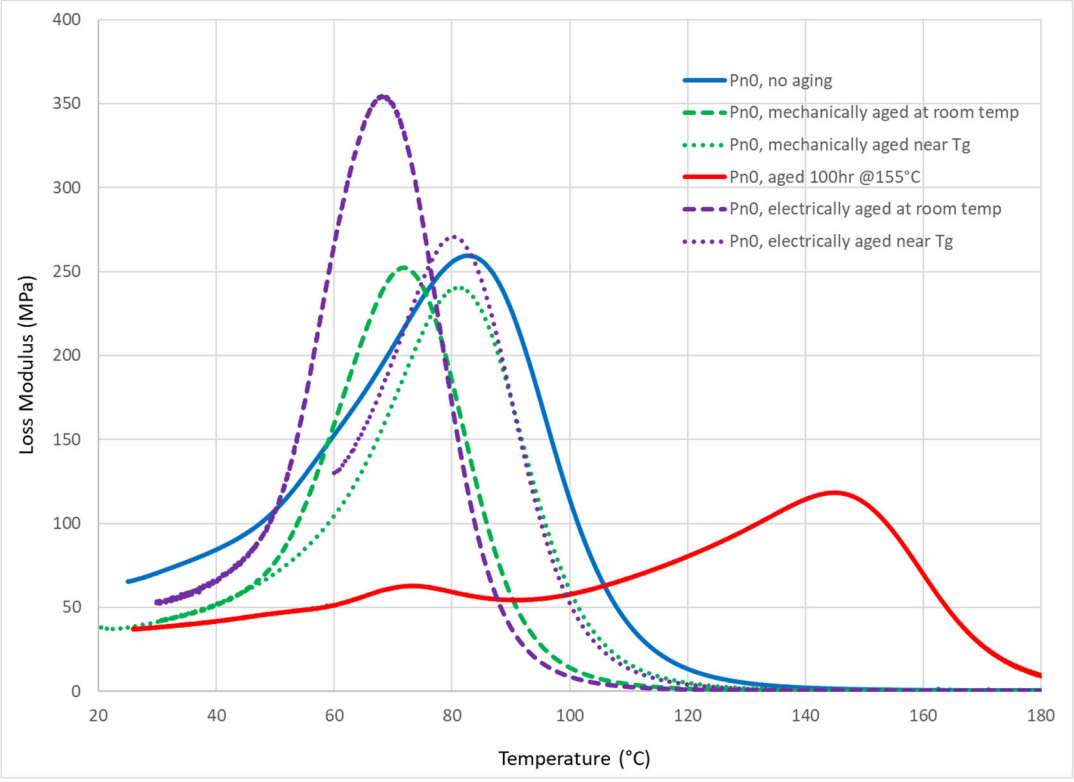


Figure 6.56. Mechanical loss modulus for Epoxy with aging treatment.

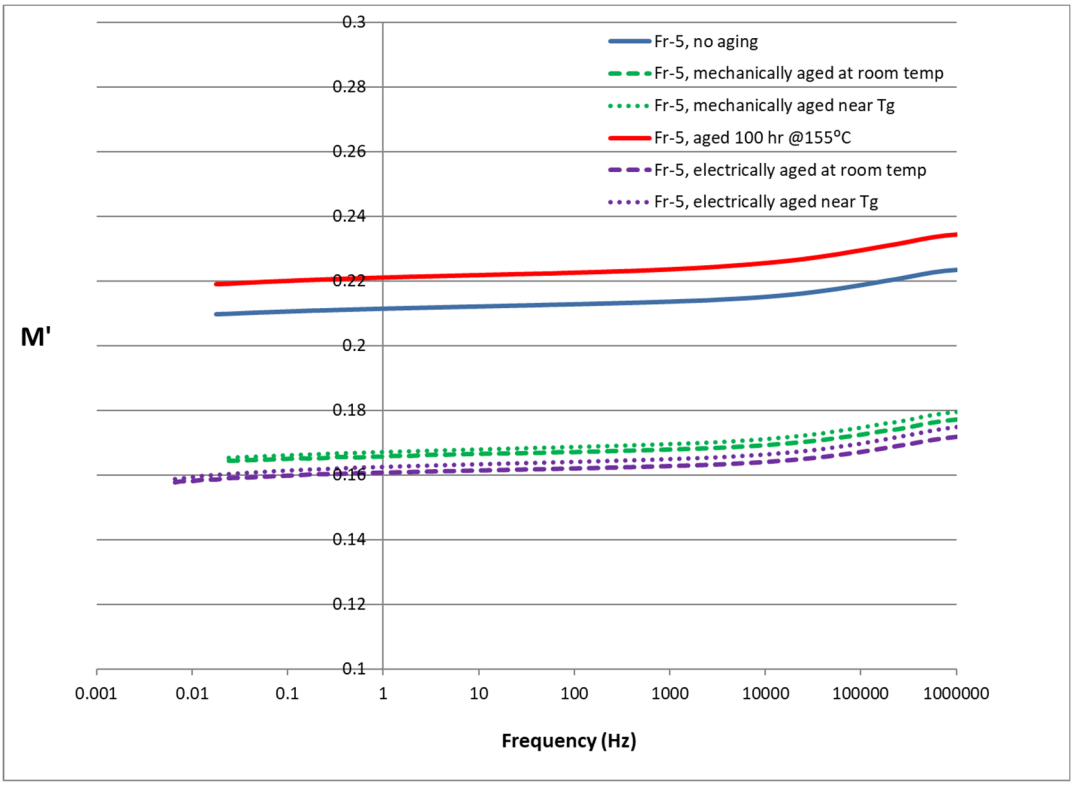


Figure 6.57. Dielectric storage modulus for Epoxy Laminate with aging treatment.

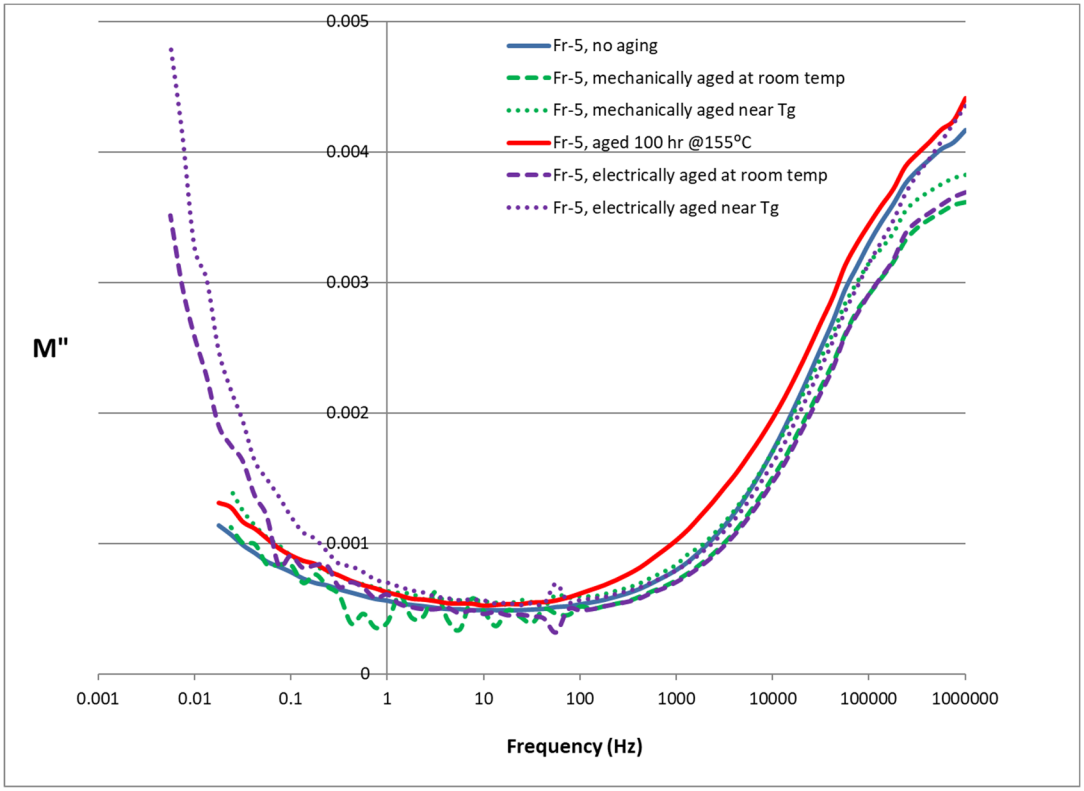


Figure 6.58. Dielectric loss modulus for Epoxy Laminate with aging treatment.

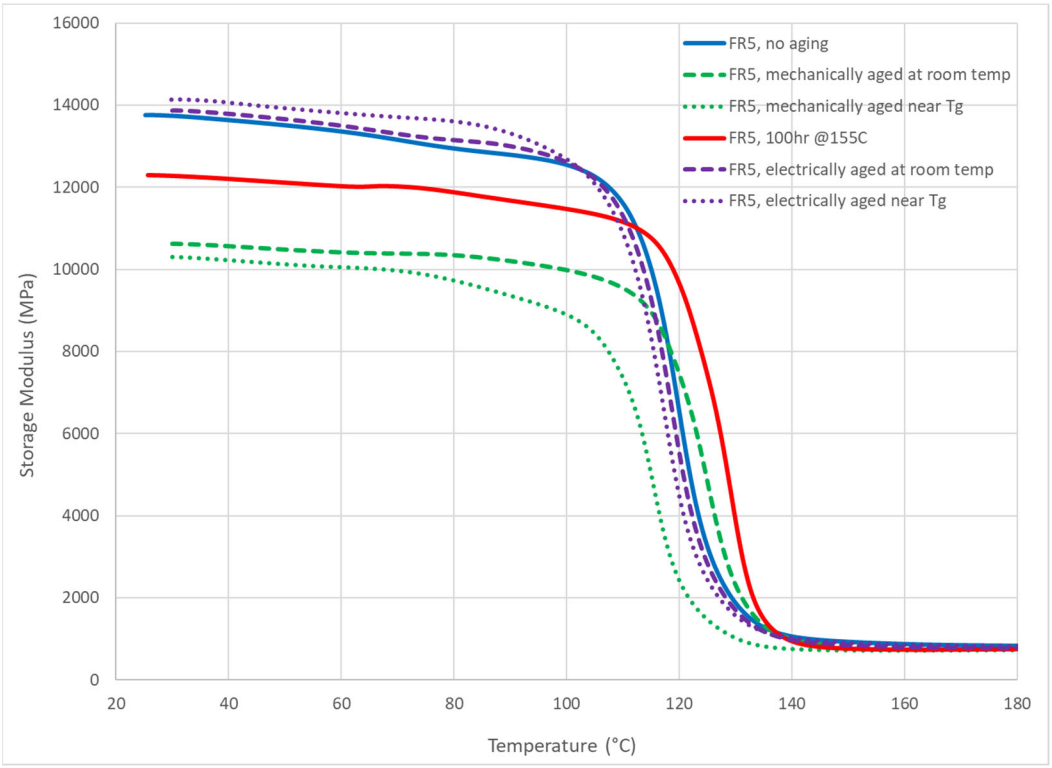


Figure 6.59. Mechanical storage modulus for Epoxy Laminate with aging treatment.

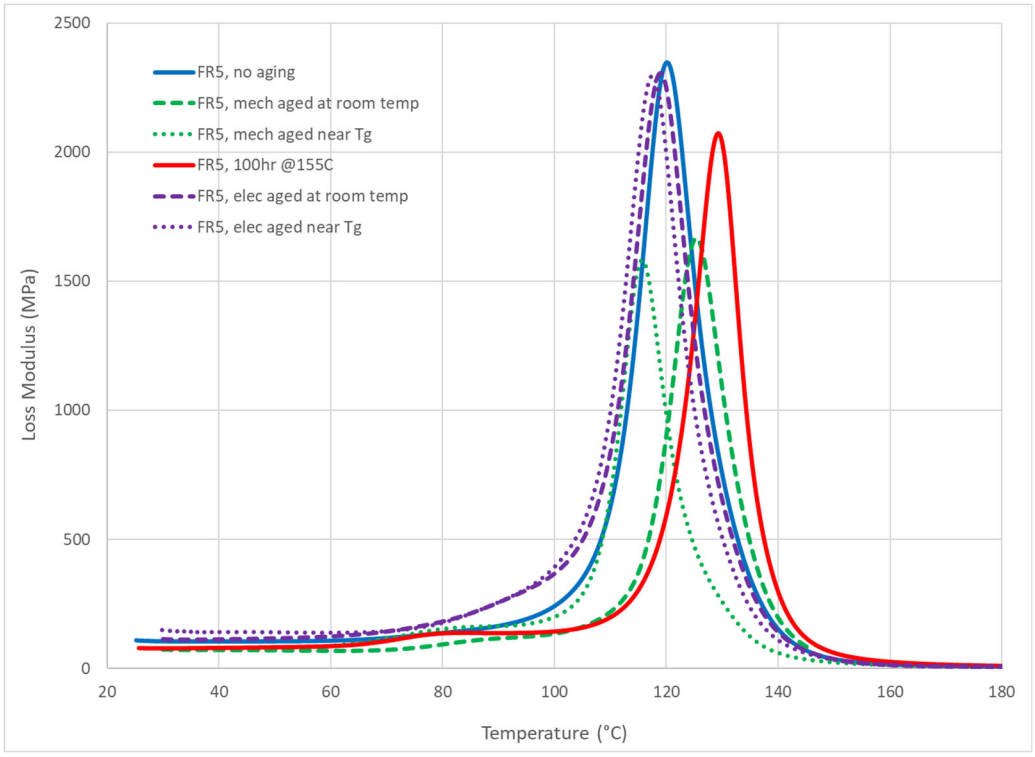


Figure 6.60. Mechanical loss modulus for Epoxy Laminate with aging treatment.

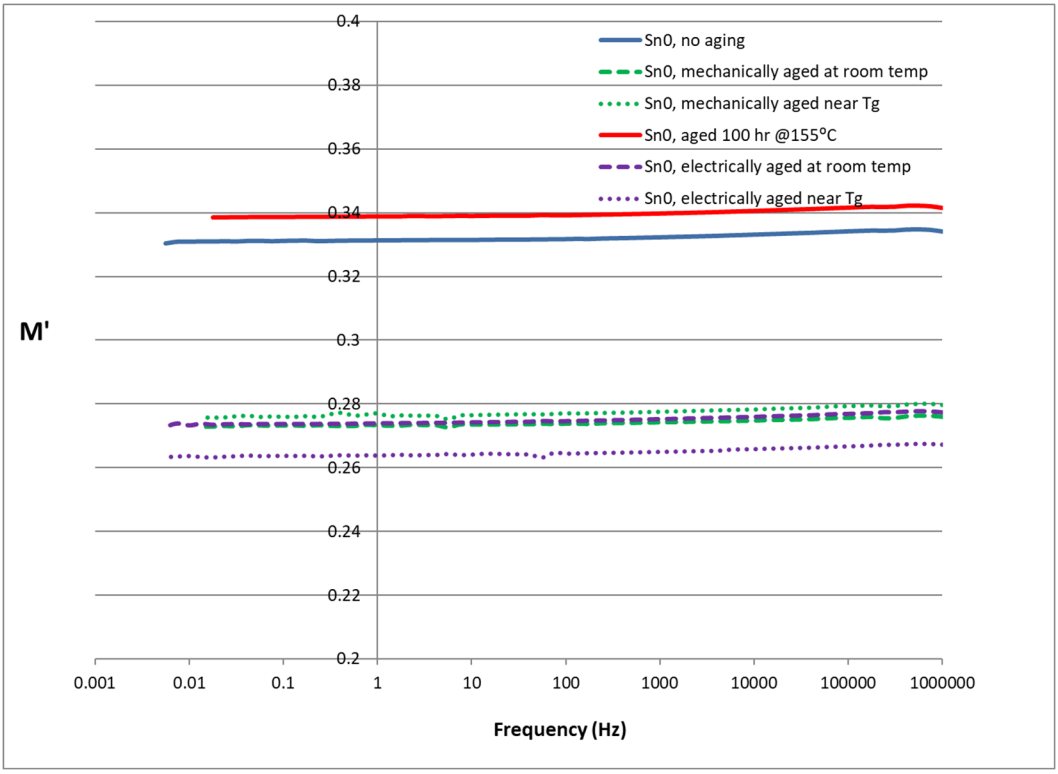


Figure 6.61. Dielectric storage modulus for Silicone with aging treatment.

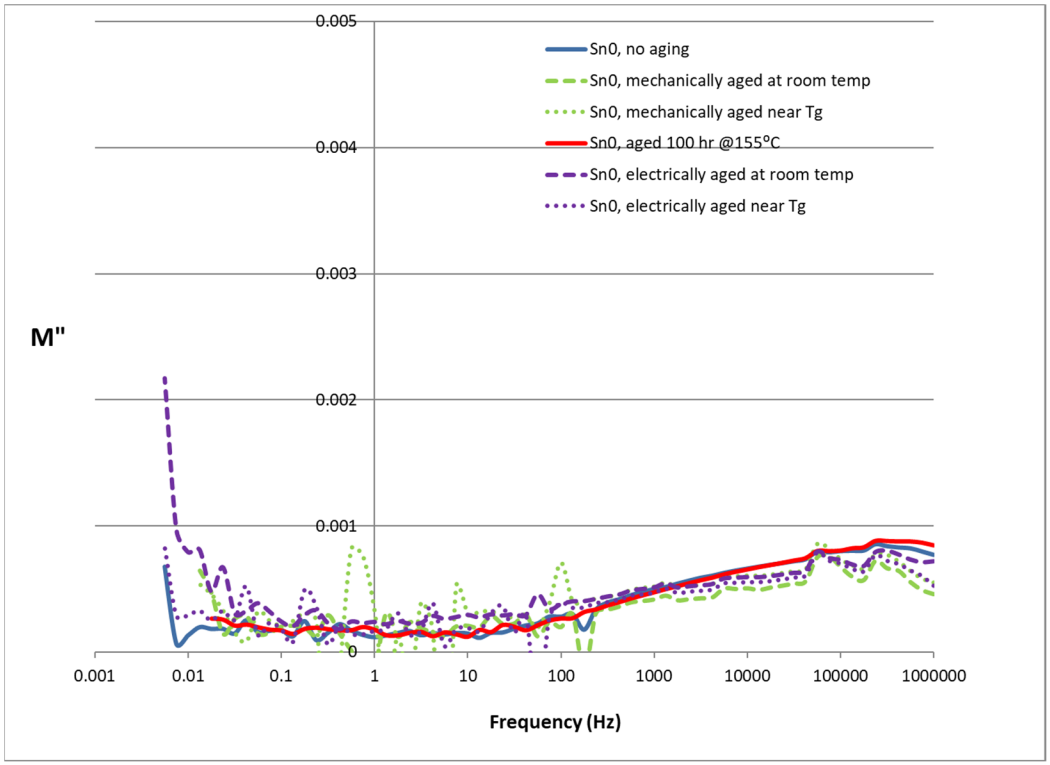


Figure 6.62. Dielectric loss modulus for Silicone with aging treatment.

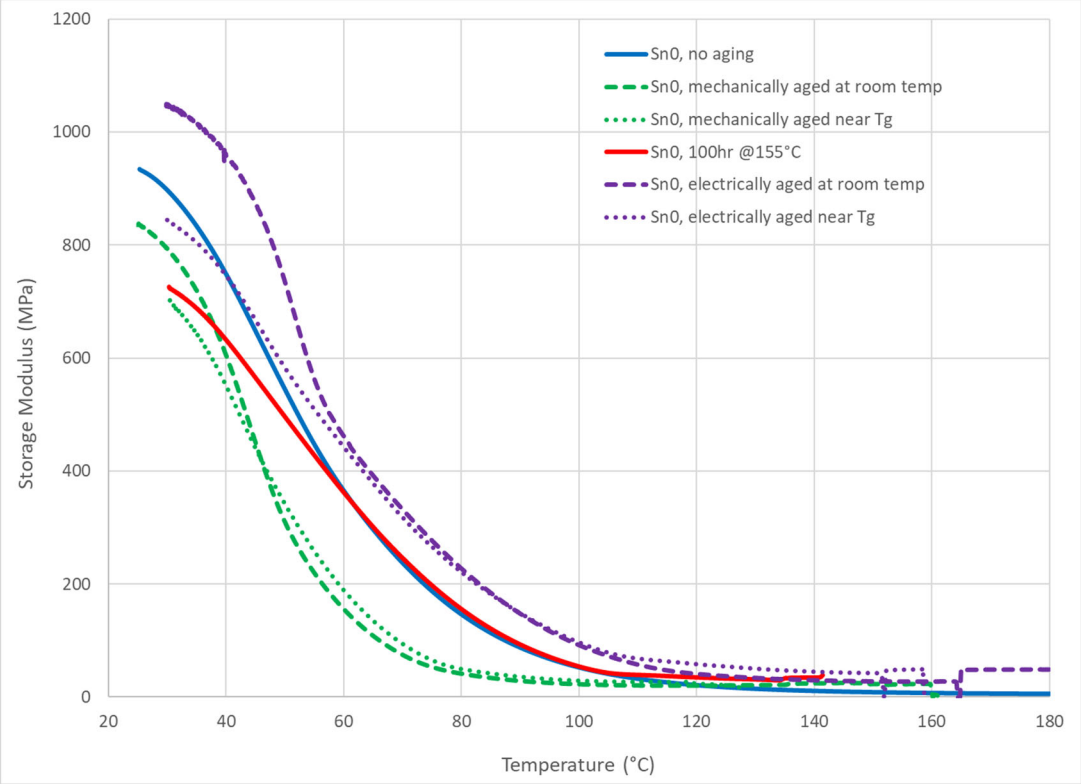


Figure 6.63. Mechanical storage modulus for Silicone with aging treatment.

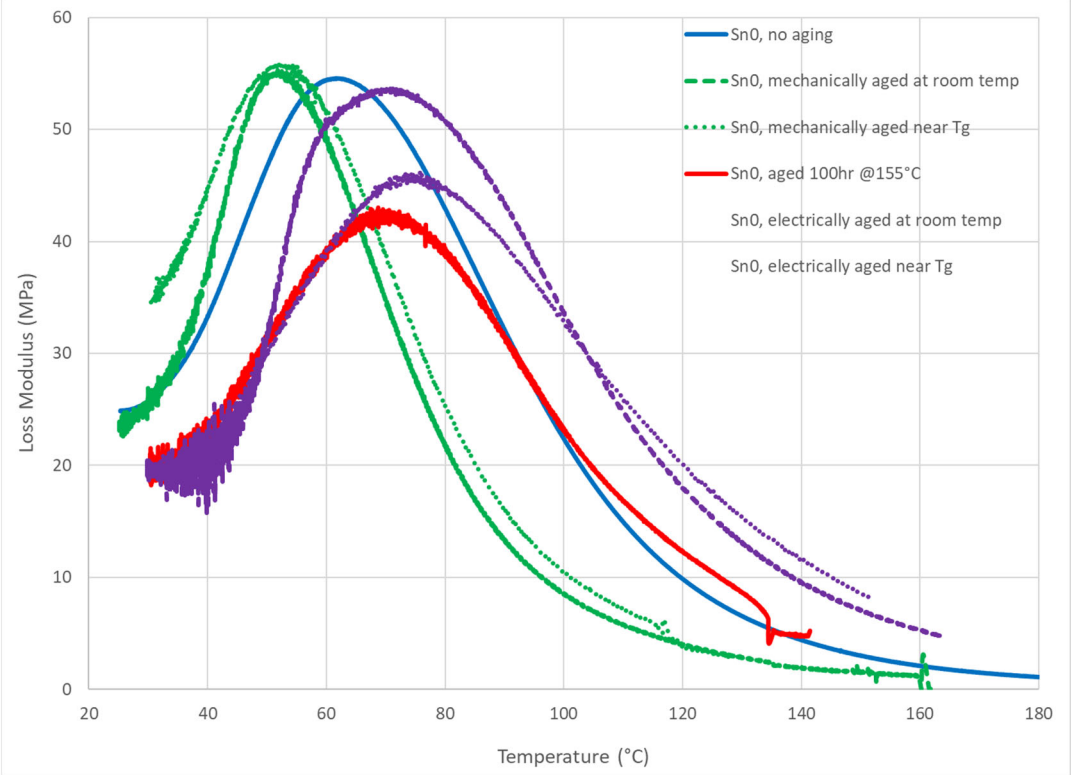


Figure 6.64. Mechanical loss modulus for Silicone with aging treatment.

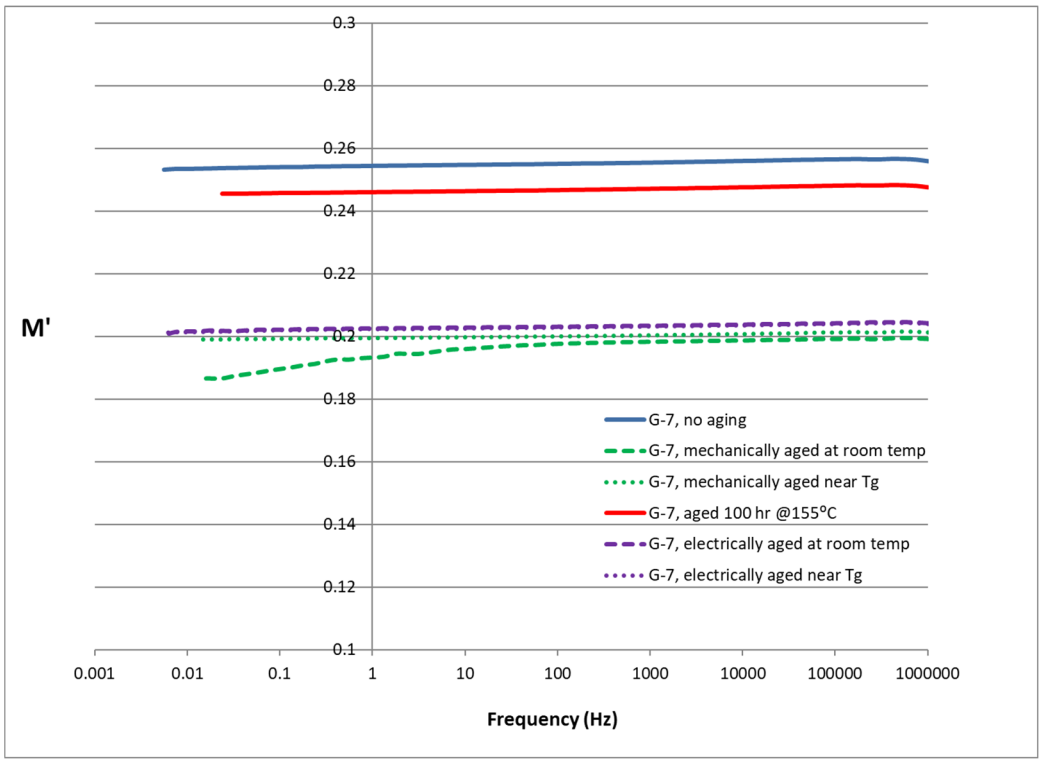


Figure 6.65. Dielectric storage modulus for Silicone Laminate with aging treatment.

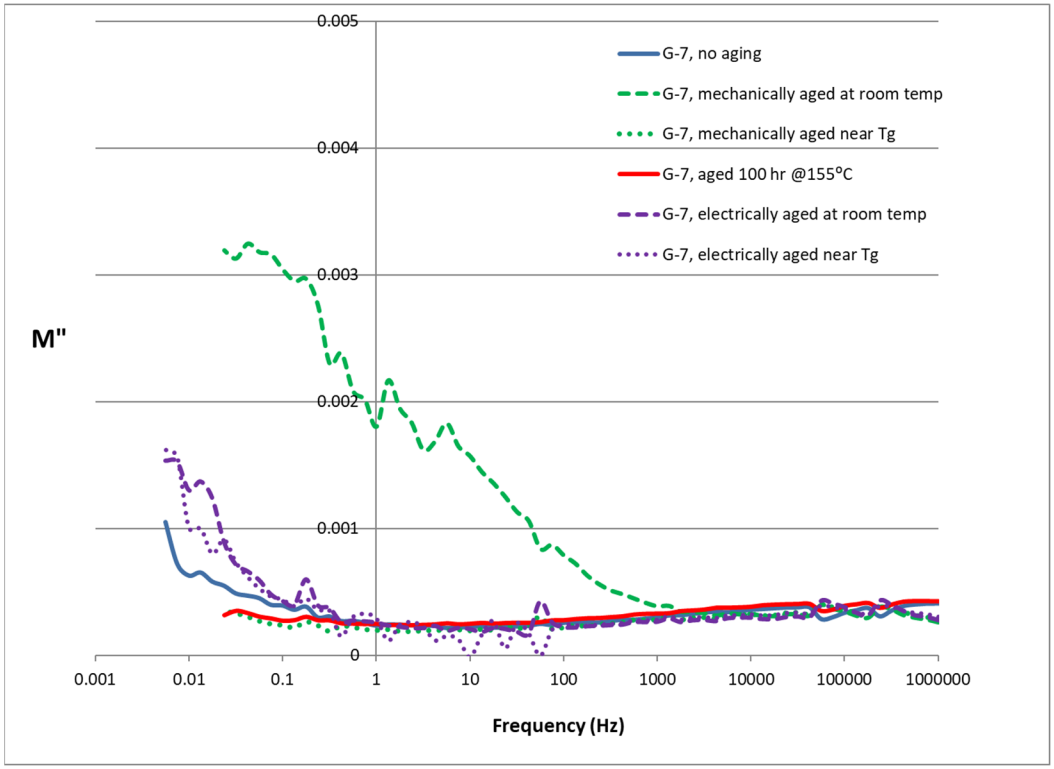


Figure 6.66. Dielectric loss modulus for Silicone Laminate with aging treatment.

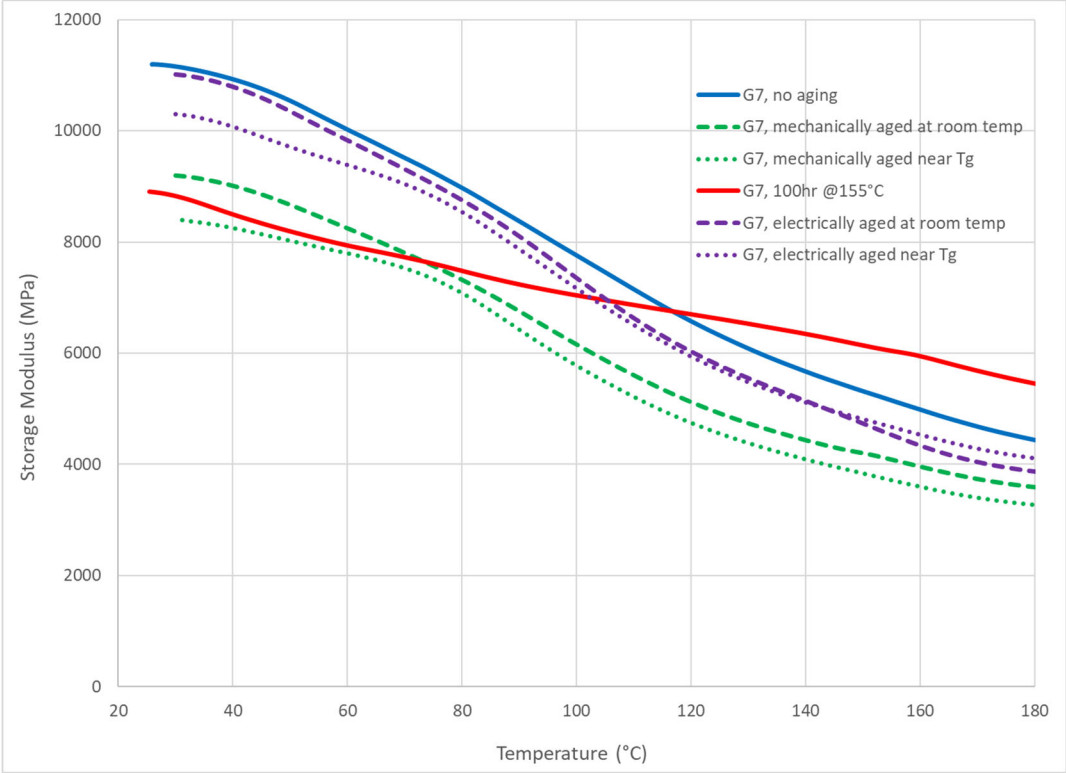


Figure 6.67. Mechanical storage modulus for Silicone Laminate with aging treatment.

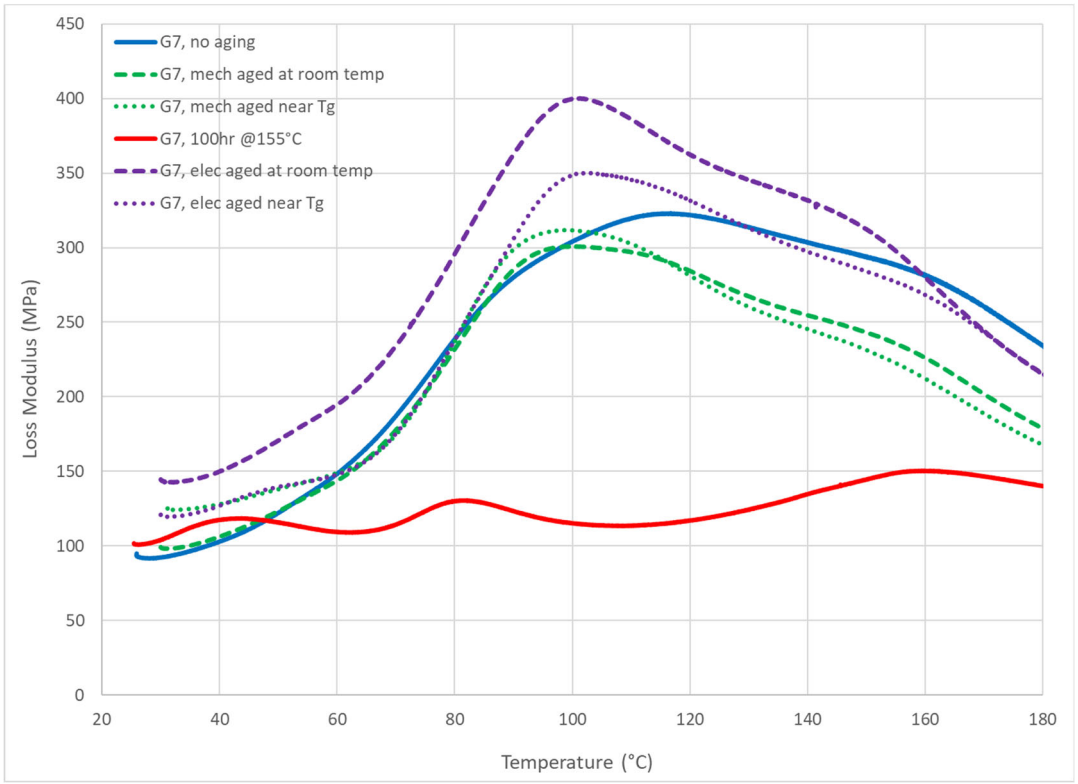


Figure 6.68. Mechanical loss modulus for Silicone Laminate with aging treatment.

6.5. Aging in Proximity to the Glass Transition

At active structural relaxations (e.g., near the glass transition), storage moduli undergo a rapid decrease with increasing temperature and loss moduli develop a peak with higher intensity. Aging treatments applied at temperatures of high loss (e.g., maxima in damping) could lead to an informative difference in behavior from aging at temperatures well above or below the maxima. The neat Epoxy glass transition is observed within the range of the reported characterizations. It is important to note that the neat Silicone exhibits a glass transition well below room temperature. The Silicone relaxations observed in the graphed data are for molecular dynamics changes occurring above that glass transition. The temperature of aging referred to here as T_g should be considered a second glass transition temperature. Differences in general moduli trends have been described for the Epoxy and Silicone (see section 3.4). Although the overall mechanical or electrical aging for Epoxy and Silicone was similar, there are a few notable exceptions.

The Epoxy dielectric storage and loss moduli are less sensitive to the temperature of aging than to the type of aging (i.e., electrical or mechanical). The mechanical storage and loss moduli, however, show more change after aging at room temperature than after aging at the glass transition. The changes in Epoxy Laminate dielectric storage and loss moduli (with mechanical and electrical aging) appear independent of the temperature of application. This is also observed for the elastic moduli. The Silicone electrically aged near the second (higher) glass transition temperature has the greatest change in dielectric storage modulus. The dielectric loss moduli are essentially unchanged with aging. The mechanical storage modulus only showed differences at low temperatures (<60°C) due to aging temperature. Here the mechanically aged and electrically aged Silicone were both more sensitive to aging near the second glass transition temperature. Aging of the Silicone Laminate was independent of temperature except for electrical aging near the transition temperature. This condition showed a marked decrease in dielectric storage modulus and increase in loss modulus at low frequencies. The mechanical storage and loss moduli also showed little effect on the temperature of mechanical or electrical aging. The exception is the loss moduli for the Silicone Laminate electrically aged at room temperature, which exhibited increased loss.

6.6. DETA & DMA Correlation

Based on the physical models for molecular dynamics that have been developed over the last three decades, our investigation of aging phenomena suggests a correlation between DETA and DMA for aging behaviors. The suggested correlation has not been previously described in the literature. The description here is intended to prepare to further explore the correlation in the future. The correlation, itself, could support an improved phenomenological understanding of the differences in thermal, mechanical, and dielectric aging behaviors. The discussion in this section is of a preliminary observation. A new approach to understanding aging behavior is suggested if molecular dynamics of these complex polymer structures is approached with the following seven tenants.

1.) At power frequencies (below 1 MHz) in dielectric materials having an amorphous thermoset "matrix" [10], external stimuli produce molecular dynamics that can be viewed as a combination of phonons and associated non-phonons.

2.) The non-phonons (due to phonon scattering by elastic or dielectric inhomogeneities) vary in intensity with frequency and temperature.

3.) Dynamic elastic moduli derived from DMA may be related to acoustic phonons and non-phonons. Acoustic phonons may represent collaborative motion of "locations" or "regions" that display distinct momentum.

4.) Dielectric moduli derived from DETA may be related to optical phonons and their non-phonons. Optical phonons represent opposing motion of dipolar "regions".

5.) DETA and DMA moduli may show that the "momentum regions" and the "dipolar regions" are not independent.

6.) Theoretical proof could be achieved by a density of states analysis for the "disordered extended modes".[21] Our phenomenological findings support pursuing such an analysis.

7.) Observations of "growing length scales" with aging [34] further support our findings and this approach.

Figure 6.69 is a graph of the dynamic elastic storage modulus and the real dielectric modulus as a function of temperature for Epoxy (cured Permafil 74050 resin). Figure 6.70 is a graph of the dynamic elastic loss modulus and the imaginary dielectric modulus as a function of temperature. The data includes dielectric moduli from DETA for the as-cured Epoxy, and elastic moduli from DMA for both the as-cured and the thermally aged Epoxy. Unlike the rest of the DETA data in this Report, here the data is shown at a constant frequency of 1 Hz as a function of temperature. A similar comparison could be made on a limited frequency scale.[11]

The changes in the real and imaginary elastic moduli for Epoxy with thermal aging were described in section 6.2 as suggesting a phase separation. A new relaxation after thermal aging near 145°C and a reduced intensity of the original relaxation at ~75°-82°C is observed. Prior to thermal aging, the dielectric moduli depict both relaxations. One possible explanation is that the optical phonon+non-phonon dynamics are active in two structural "regions" in the as-cured Epoxy. Only after significant time for structural relaxation above the glass transition temperature, the acoustic phonon+non-phonon dynamics also become active in the second structural region. Considering that the acoustic phonons require cooperative molecular dynamics, this explanation appears possible. The thermal aging produces structural changes (density fluctuations) that are more accommodating to a new acoustic phonon. Similar DETA as a function of temperature at 1 Hz for mechanically aged Epoxy is planned.

---

[10] The dielectric material is at least partially amorphous.

[11] A frequency domain comparison would require either a time-temperature-transposition of low frequency data (inadvisable if the spectra are anticipated to vary in number of bands) or availability of acoustic DMA apparatus. The DURIP instrumentation purchased in 2021 through ONR N00014-21-1-2457 permits measurement of shear moduli on these stiff materials, rather than extensional moduli (that include volume variations). Shear moduli are anticipated to show more precise correlation with dielectric moduli.

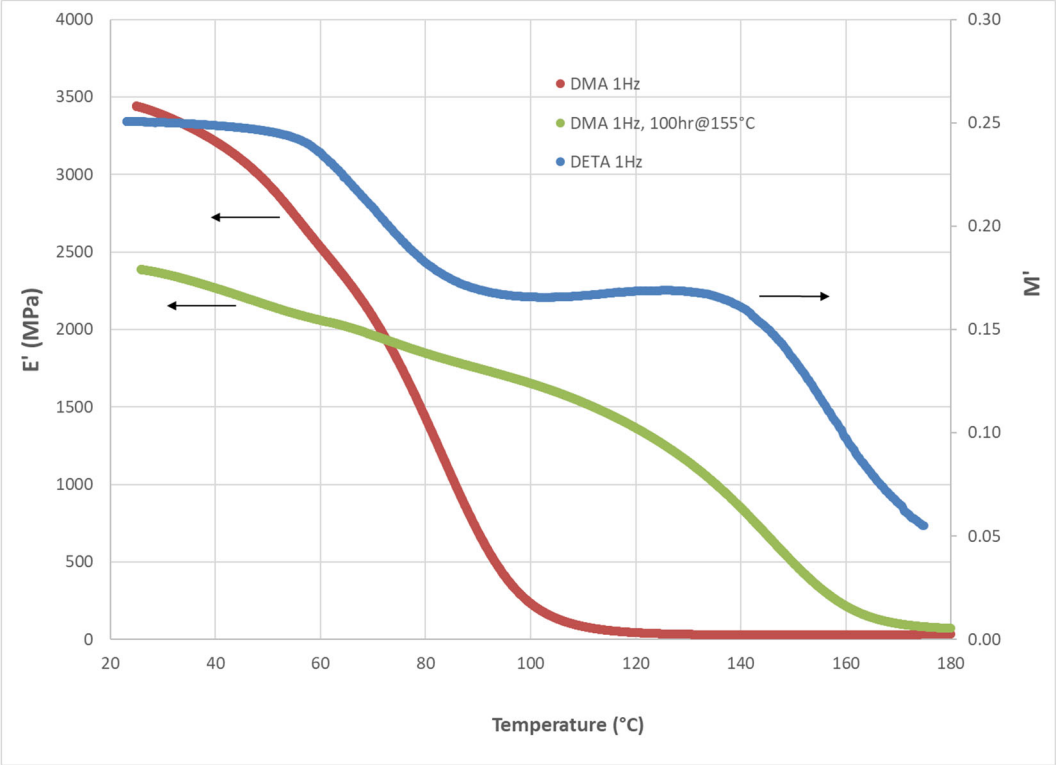


Figure 6.69. Mechanical and dielectric real moduli vs. temperature at 1 Hz for Epoxy.

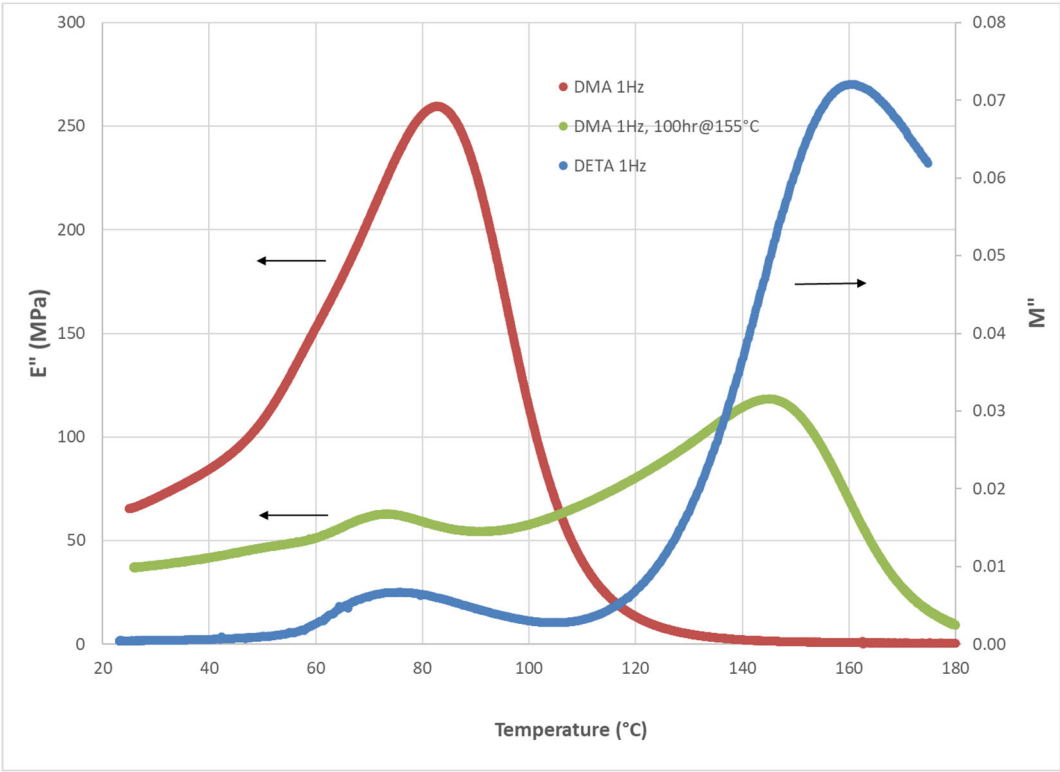


Figure 6.70. Mechanical and dielectric imaginary moduli vs. temperature at 1 Hz for Epoxy.

7. *Review:* DETA & AGING OF POLYMER MATRIX COMPOSITES

Efforts to engineer properties of polymer matrix composite (PMC) materials require scientific knowledge of the effects of design parameters. Much effort has been made over several decades to examine related properties. DETA has been used to gain insight into material behavior linked to a change in property. Because of the wide variety of materials, desired properties, and behavioral models, a literature survey was needed to establish what has been accomplished and what remains to be understood. Three summary points derived from the information contained in the survey follow.

(1.) Electrical insulation systems for power-dense applications utilize polymer matrix composite (PMC) materials that age under thermal, mechanical, and electrical stresses. The pertinent behaviors of PMCs and insulation systems remain empirical and must be measured. Few hard rules have been found for measured behaviors of nanodielectrics, in particular, even after decades of exploration. (This is problematic when the PMC is placed into an insulation system consisting of multiple layers.) The unpredictable variation in behaviors leads to the supposition that either the materials used are not well-controlled from lab to lab (i.e., there is a processing sensitivity that is not understood) or current characterization methods are inadequate for analysis.

(2.) Interphase behaviors in composites are accepted as responsible for behavioral deviations from neat polymers. Interface charge models, once used to explain such deviations, have been shown to be inadequate. (This is demonstrated by significant and reproducible improvement in voltage endurance using bimodal size distributions of particulate with high loadings of micro-particulate. Such reversals in understanding should be explored to move the science forward and minimize confusion.) As with most complex material systems, there are property & behavior trade-offs that need to be addressed for each application's requirements to effectively exploit PMC advantages in electrical insulation system design.

(3.) Variation in molecular dynamics of the polymer matrix *can* provide comparative information on aging behaviors. Characterization of molecular dynamics using DETA & DMA is widespread and of inconsistent technique. A more complete representation of the molecular dynamics behavior of the PMC is gleaned with a broader frequency range *and* temperature range using *both* techniques. Synthesis of this information is of particular urgency for layered insulation systems.

7.1. Introduction

The importance of composite dielectrics and the need to understand their behaviors is evidenced by the thousands of papers written about these materials. Composite design allows engineers to tailor material properties to improve performance over neat materials in targeted applications. Because of the high amount of activity in the field, this literature review is selective. We seek to clarify the field as related to our research by combining general understanding of composites with

specific publications that develop the science in detail. The topic is the use of Dielectric Thermal Analysis (DETA) to characterize polymer matrix composite (PMC) dielectric materials for high performance electric insulation.

Almost all electric machine insulation systems are composites. A general concept is that the nature, amount, and cohesion of interfaces drives many properties of a composite dielectric. This includes aging. The aging behavior of a composite dielectric may be different from the aging behavior of the matrix ("neat") polymer. Comparing the DETA of the composite with the neat polymer (matrix) under aging stresses can clarify behavior.

In section 7.2, this literature survey attempts to address the questions*:*

- *What discernable affects do multiple phases in a composite have on DETA spectra?* and
- *What discernable affects does the "size" of the second phase have on DETA spectra?*

Section 7.3 is written to attempt to address the following questions:

- *Where does DETA distinguish between the aging of dielectric composites and the matrix polymer?* and
- *How can this information be related to insulation behavior for electro-mechanical machinery?*

7.1.1. Overview

There are six major behavior/property categories that engineers seek to manipulate in composite insulation design:

1. Semiconduction or nonlinear impedance: a semiconductive particulate filler is added to a polymer matrix (e.g., graphite or SiC for stress-grading applications);
2. Permittivity or capacitance: a ferroelectric particulate filler is added to a polymer matrix (e.g., barium titanate in XLPE);
3. Viscosity control of the uncured resin (e.g., fumed silica added to enhance thixotropy);
4. Mechanical property enhancement to increase toughness and/or stiffness, reduce thermal expansion mismatch, etc. (e.g., embedded woven fiberglass tape, FR5 laminate board);
5. Thermal diffusivity by improving heat flow (e.g., addition of alumina fillers);
6. Partial discharge & surface corona endurance, and/or breakdown stress (e.g., some nanodielectric formulations).

This review will only consider dielectric composites of categories 3-6 that maintain good insulative properties. These materials are distinguished by a low permittivity of the composite dielectric- a direct indicator of electrical impedance (see Appendix 1 for more property relationships).

General Survey: There are many scientific models for each aging phenomenon observed in dielectric materials. No one model fully explains all observed dielectric behaviors so the model used often depends on the material. Over the last two decades, computer simulations have greatly augmented model development. Laboratory measurements, themselves, are not always entirely reproducible based on published information. A flow of typical procedure for laboratory measurements to develop scientific models is shown in Figure 7.1.

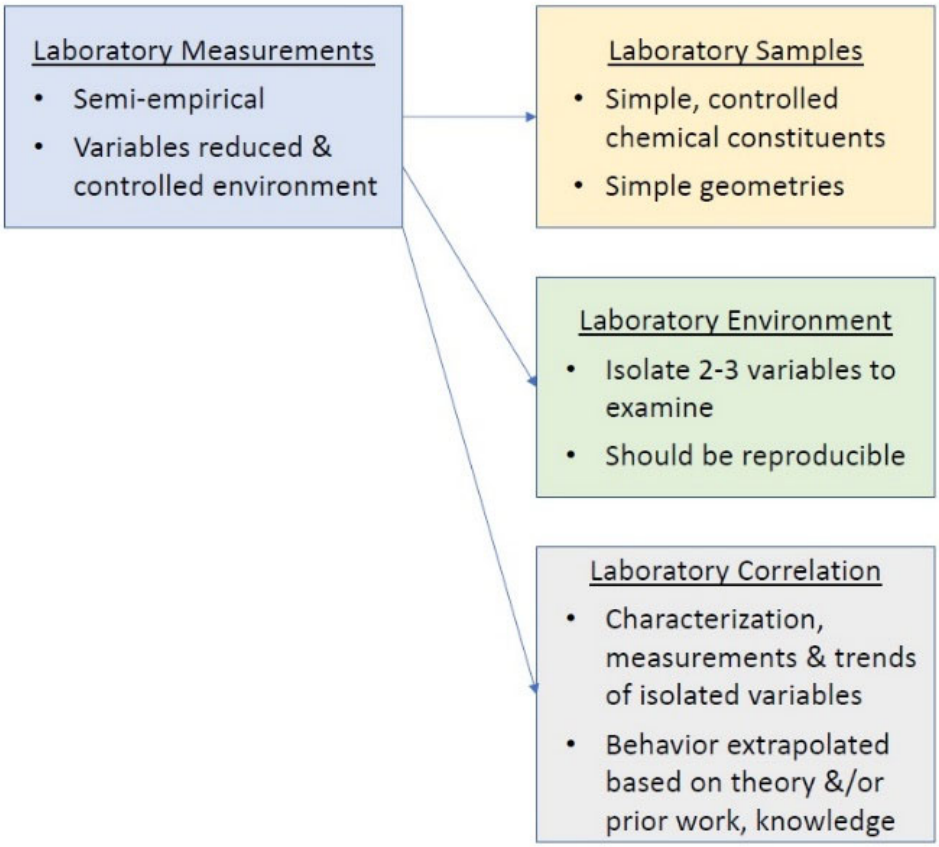


Figure 7.1. Schematic of considerations for laboratory measurements.

The extrapolation of semi-empirical models to commercially viable insulation systems requires materials engineering. The engineering for the field of dielectric composites is largely "experience based": complexity and performance requirements change as applications and knowledge evolve. The science supports this experience base. Improving information flow on health index monitoring and historical records during operation is critical for condition-informed maintenance. This path of information flow is indicated by dashed lines in Figure 7.2 (labeled "weak or non-existent"). Health index monitoring information is largely unavailable (perhaps proprietary) and would be enormously useful to the research community in promoting insulation longevity for all electromechanical applications. The caveat is that the monitoring and records need to be properly designed by utilizing known science.

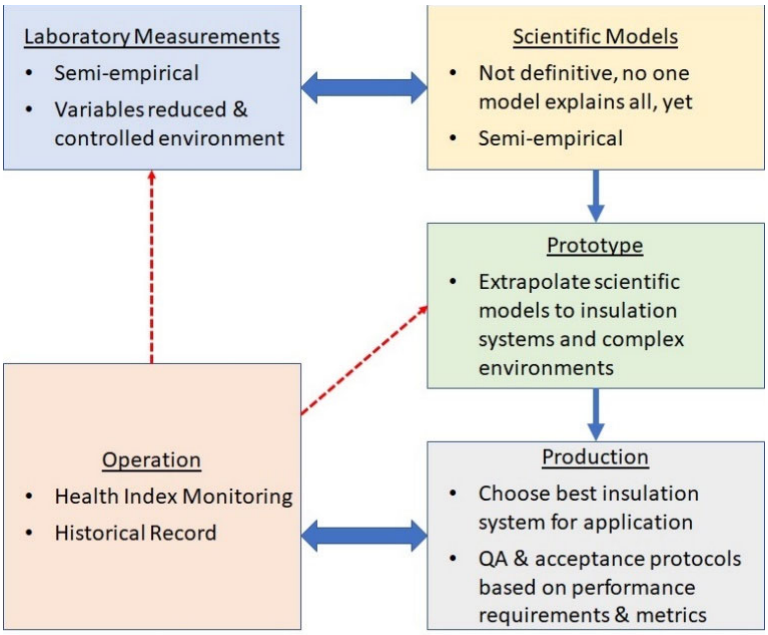


Figure 7.2. Schematic of information flow for improved insulation lifetime.

7.1.2. Selection of Literature

For insulative composites, the molecular dynamics of the polymer matrix dominates the dielectric spectra. For this reason, the literature described here will concentrate on composites with thermoset polymer matrices (e.g., epoxy) and avoid thermoplastic polymers (e.g., polyethylene). Modification of the local molecular dynamics of the polymer network near the second phase determines the difference from the neat response. Exceptions are noted. Additional relaxation modes are introduced in composites which greatly increase the complexity of fitting the data and models may be required. The choice of models is also an involved study. Unless the material relaxations are well-known, many researchers prefer to avoid curve fitting and instead report changes in spectral features.

7.1.3. Relaxation Processes

Five relaxation processes may be observed in dielectric spectra of composite materials:

- Conductivity relaxation (including electrical polarization, space charge mobility, and ohmic relaxation) or Quasi-DC relaxation;
- Glass to rubber transition of the polymer matrix (α-polarization);
- Re-orientation of polar side groups of the main polymer chain (β-relaxation);
- Possible secondary glass transition (γ-relaxation); and
- Interfacial polarization (also known as Maxwell-Wagner-Sillars (MWS) polarization).

Interfacial polarization specifically arises due to the presence of interfaces between regions of different materials in composites. The interface usually promotes "new" localized molecular dynamics.

7.2. DETA of Polymer Matrix Composites: Specific Interest Areas.

DETA is used to compare the effects of multiple phases: in particular, the size & shape factor (i.e., morphology) of a filler and the nature of the interphase. In DETA spectroscopy from ~10^{-3} to 10^{6} Hz, three general processes involving molecular dynamics are observed in polymer matrix composites having a thermoset matrix. These effects are observed in both ϵ' and ϵ" and depend on the process:

1. Electrode polarization, ionic conduction, and/or space charge motion at low frequencies, often observed as low frequency dispersion in ϵ'. These processes tend to be enhanced by humidity, free radicals, and temperature.
2. Coordinated polymer chain motions lead to α-relaxation and β-relaxation processes. (γ–relaxations may be observed in materials exhibiting relaxation due to side chains or polar groups within side chains having high mobility. The α-relaxation is also referred to as the normal, principle, or cooperative mode. This mode is related to the glass-to-rubber transition of the polymer matrix. These have been viewed as "micro-Brownian motions of chain segments".[46] The β-relaxation, also referred to as the secondary or local mode, arises from re-orientation of polar side groups. The latter mode tends to peak around 10^{6}–10^{8} Hz in thermoset polymers. Both processes are thermally activated.
3. Interfacial polarization may be observed when multiple phases of different conductivity are present. A popular mathematical model for this mode is the Maxwell-Wagner-Sillars (MWS) model. The model is based on polarization (charge accumulation) at the interface. The peak frequency is expected to change as the conductivities of either phase varies with temperature. Interfacial polarization for composites with insulative components is detected near 10^{3} Hz.

DETA of polymer matrix composites with low filler concentrations is anticipated to behave similarly to DETA of the matrix polymer. There are reports that filler additions can affect the density of the polymer matrix.[47] The addition of absorbed water with the filler is known to modify molecular dynamics (discussed in section 7.3). In general, the filler morphology is believed to impact an electric field within the polymer and the polarization scales with the field, so DETA may register a change in polarization as the field is applied.[48] Here we are interested in how this change can be interpreted. This section of the review seeks to answer: *What discernable affects do multiple phases in a composite have on DETA spectra?* It is important to understand interpretations that go beyond simple "weighting factors" of mixtures. Five discernable affects are discussed: interface behavior, charge distribution, water in solid polymers, mica, and layer/laminate stacks.

7.2.1. DETA of PMC: "Interphase Design"

The morphology choices for engineered polymer matrix composites (PMC) continue to expand. Traditionally, the polymer hosted particulate, fibers, or textiles as additional phases (all are found in a typical high voltage machine insulation system). Multiphase composite insulation has been used for over a century. Now layered, nano-patterned, and 3D nano-structured composites are being developed. These latter composites include patterned crystallization and precipitates from process solution with the polymer. Processing choices can develop highly variable nano-, meso-,

and micro-structures. This is a field of intense activity. Separation or agglomeration of additional components impact composite properties. A well-known schematic is shown in Figure 7.3, where a layered silicate (e.g., clay) is shown as incorporated in a polymer in three very different structures.

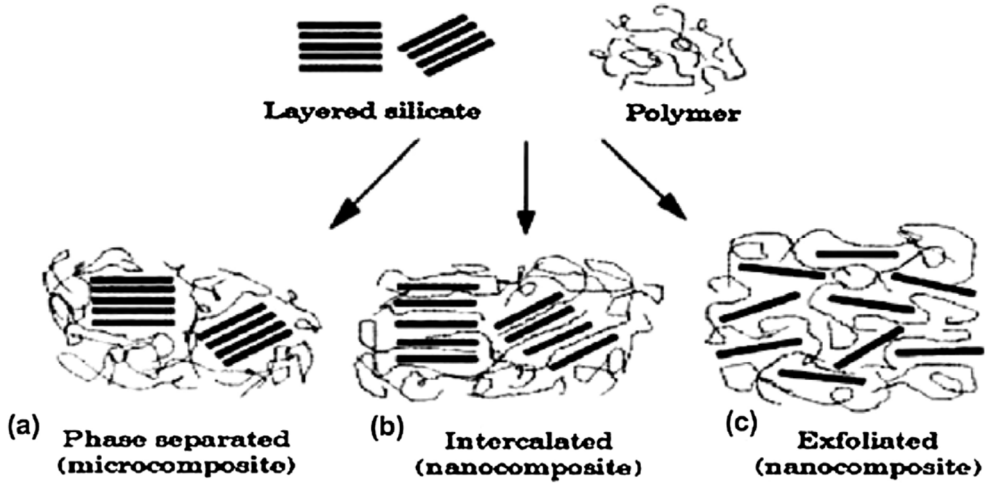


Figure 7.3. Schematic of different structures of layered silicates in a polymer matrix: (a) phase separated microcomposite, (b) intercalated nanocomposite, and (c) exfoliated nanocomposite.[49]

Choice of chemical compositions of available second phase materials ("fillers") for addition to a polymer matrix also continue to expand. Contaminants and chemicals remaining after surface treatments of particulate should be considered. Surface treatments are used to modify interface behavior. For example, filler surfaces are often chemically functionalized to improve dispersion in or adhesion with the polymer. The interfacial polarization can be decreased with treatment of the filler surface.[50]

Molecular mobilities change at the interface leading to a zone of modified behavior termed "the interphase". Polymer matrix composites are viewed as having three phases: the matrix, the filler, and the interphase (i.e., the interface considered as an additional phase). The interphase is thought to have significant impact on dielectric and aging behaviors. Many papers have used DETA to help investigate the following phenomena as related to the interphase:

- Conductivity and/or impedance
- Charge storage and traps
- Dipole mobility due to particle surfaces
- Dispersion of particulate within the composite
- Interfacial chain mobility

The listed phenomena are especially relevant in examining nanodielectrics where the extent of interphase is significant.

The permittivity in the broadband frequency range 10^{-4}-10^{8} Hz is a low frequency extension of the optical spectrum. A schematic of the real and imaginary permittivity spectra, with relaxation modes indicated, is shown in Figure 7.4. This is key information gained and interpreted with DETA.

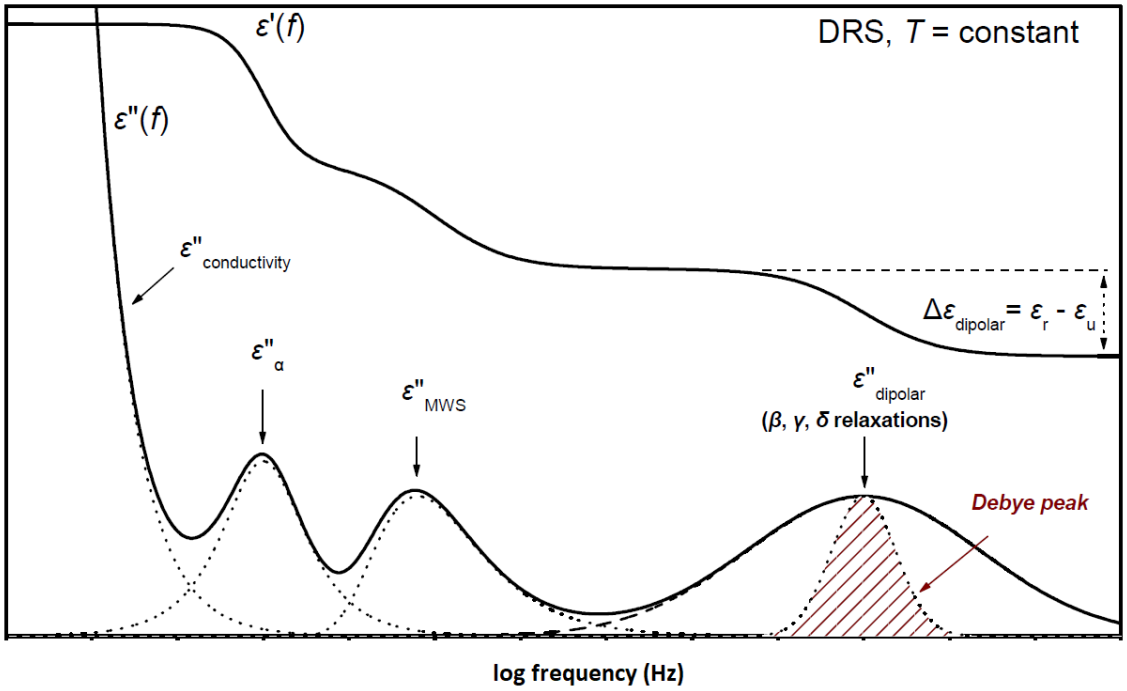


Figure 7.4. Schematic of the real and imaginary permittivity spectra.[after 51]

The relaxation[12] frequencies of PMC composites depend primarily on the polymer matrix. A well-designed interphase can result in restricted molecular dynamics of the lower elastic modulus phase (usually the polymer matrix). Restricted interphase molecular dynamics is also referred to as molecular "confinement", "tightly bound" molecules, and by the length of a "cooperativity scale". Restricted molecular dynamics leads to decreased interfacial polarization.[51] An analogy has been given of the orientation of water molecules next to an ion in solution: the coordinated and polarized water molecules effectively shield the ion's charge and reduce its mobility.[52] Several important properties are affected by this cooperativity, particularly viscosity [53] and adhesion [54].

Nanocomposites: The variability of the interphase molecular dynamics is considered a demonstration of the multiple parameters involved in forming the interphase.[51] The molecular dynamics of nanocomposites measured with DETA are not usually restricted or confined at the interphase and this can cause considerable confusion. The complexity potentially explains significant literature with seemingly conflicting results. At this time, properties are not generally predictable. Measurement of dielectric spectra is needed to examine each composite system and as a process control tool. Two categories of behavior have been assigned:

(i.) the α-relaxation shifts to lower frequency than that of the neat polymer (e.g., for 1.5-2.0 nm thick intercalated interphases with some nanoparticulate). This has been explained by the "potential formation of a layer of a modified polymer (bound polymer) around the nanoparticles leading to locally decreased molecular mobility…"[51]

[12] The modes observed in permittivity spectra are usually referred to as "relaxations", but correctly termed "retardations". The modes observed in electric moduli spectra are true relaxations.

(ii.) the α-relaxation shifts to higher frequency than that of the neat polymer (e.g., for some intercalated or exfoliated clay-polymer systems). This has been explained by the "loosened molecular packing of the polymer chains due to the presence of nanoparticles… leading to increased free space and enhanced molecular mobility…"[51]

Both categories were suggested to act *simultaneously* for a ZnO nanoparticle-epoxy system. The addition of ZnO nanoparticles decreased the cross-linking density of the polymer matrix, increasing the fractional free volume and the corresponding molecular mobility. Concurrently, strong interactions between the ZnO and the polymer matrix resulted in a reduction of the mobility of a fraction of the polymer chains at the ZnO interface.[55]

An increase in the α-relaxation frequency combined with an increase in the β-relaxation frequency is often observed as temperature increases. An investigation of a polyimide-nanosilica composite demonstrated a change in the dielectric strength of the polyimide's γ-relaxation, as well.[56]

Some investigations have avoided discussing the interphase by emphasizing a comparative size effect. Interfacial dynamics are suggested to cease when the particles are small enough to "act cooperatively with the host structure". This was demonstrated by the presence and absence of the MWS polarization for 1.5 μm TiO_2 and 23 nm TiO_2, respectively, in epoxy at low temperature.[57] In contrast, others have shown that the physical attraction between a polymer matrix material with nano-fillers or with micro-fillers are the same. The higher relative amount of interphase with strongly attracted nano-fillers is suggested to cause more restricted chain motion.[58]

The glass transition temperature, T_g, is strongly correlated with the α-relaxation mode in DETA. T_g has likewise been observed to decrease, increase, or remain constant with nanoparticulate additions to the polymer matrix.[58,59] A careful investigation showed an initial drop as nanoparticulate concentrations increased to 0.5%, than T_g increased as the concentration approached 20%.[60] At low nanoparticulate volumes, the real permittivity is also observed to decrease. Molecular confinement at the interphase is thought to reduce the overall polarizability of the matrix dipoles leading to this decrease. This explanation would require that polymer matrix composites have higher T_g than the corresponding neat polymers. Another study found that several nanoparticulate-epoxy composites had significantly lower T_g values than the corresponding microparticulate-epoxy composites. It was suggested that the lower T_g values were due to water located in the interphase.[61]

Thermal Activation: Permittivity spectra reported for different temperatures provide information in both frequency and temperature. A change in relaxation frequency is often observed with temperature and typically follows Arrhenius behavior as shown for polyurethane and two nano-titania composites in Figure 7.5. Very little change in the activation energies of the relaxations with particulate addition are observed suggesting that the local molecular dynamics are similar.[62] A plot of several epoxy composites with barium titanate (BT) and montmorillonite (oMMT) is shown in Figure 7.6. Here the low temperature (fast) relaxation process is independent of the filler type or quantity. A higher temperature relaxation is only observed in the composites, and the activation energy depends on the filler type and amount.[63] This provides a clear characterization of the change in the polymer molecular dynamics with added phases.

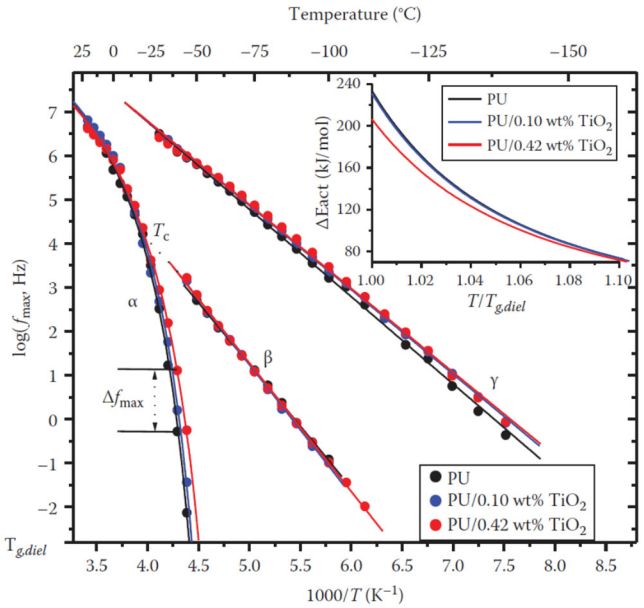


Figure 7.5. Arrhenius plots for polyurethane neat and with nano-titania, indicating no change in the polymer molecular dynamics with nanoparticulate addition for any relaxation mode.[62]

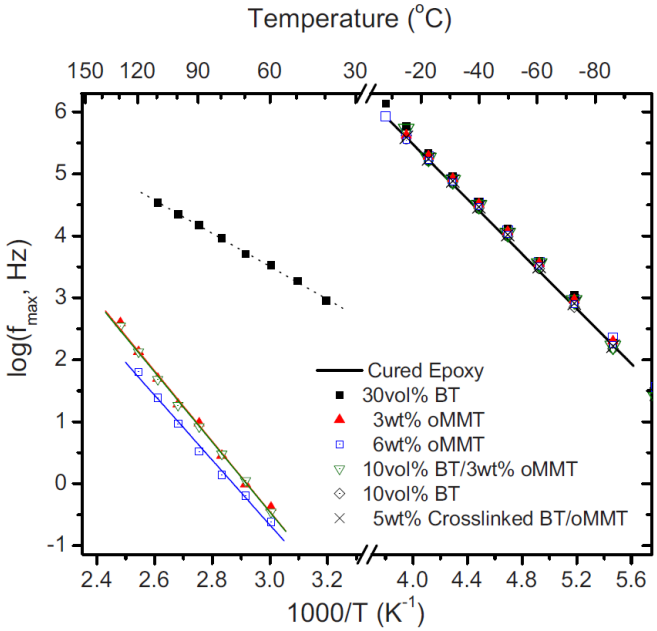


Figure 7.6. Arrhenius plots of an epoxy with barium titanate (BT) or montmorillonite (oMMT) particulate, depicting two relaxation processes.[63]

Figure 7.7 shows an essentially Arrhenius dependence of a sub-Hertz relaxation[13] of FR4, a commercial epoxy-fiberglass laminate used as a printed circuit board substrate.[64] The reported activation energy was 1.1 eV (10.6×10^4 J/mol). It was found that electrical aging could shift the process to higher frequencies, but the activation energy was constant until failure. Failure, suggested due to delamination of the fiberglass from the epoxy, caused the activation energy of this process to fall to ~0.7 eV below 50°C.

[13] The sub-Hertz relaxation or Q-DC process is discussed further in the section 7.2.2.

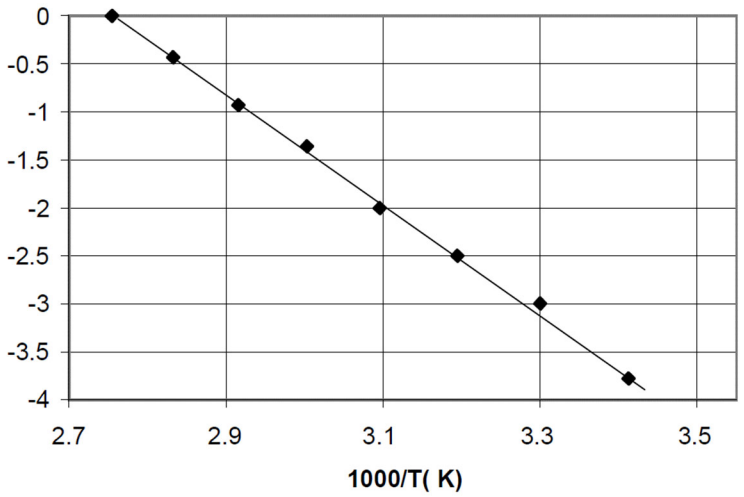


Figure 7.7. Temperature dependence of a "Q-DC process" in a FR4-fiberglass epoxy composite.[64]

In the future, computational simulations may help clarify interpretations. A recent effort was able to adapt viscoelastic relaxation theory to model dielectric permittivity using Finite Element Analysis (FEA) as a simulation tool. Interphase properties were then investigated with good correlations.[65]

7.2.2. DETA of PMC: "Charge Distribution"

Charge distribution is another way to conceptualize the effects of the interphase on composite behavior (i.e., interfacial polarization). Charge in dielectrics with low permittivity refers to some combination of dipole response of molecular moieties, mobile ionic species, and electrons/holes to an effective electric field. It is important that publications clearly differentiate these responses. The discussion of charge distribution has been of great interest in nanodielectrics. Some correlations made between charge distributions modified by nanofillers and electrical aging are reviewed in section 7.3.

The interest is in reducing localized field distortions within the insulation by controlling filler morphology and size. A goal in much recent effort in nanodielectrics is to try to separate out the dielectric behavior of the polymer-particulate interphase by examining how the combined behavior in the composite varies from mixing rules. It is claimed that "none of the existing mixing laws can fit the experimental data on a broad range of frequencies. Indeed, none of the numerous existing models can even come close to fitting the data…"[66] The conclusion is that the interphase does have a prominent role in the dielectric response and instantaneous charge distribution. A new model has been developed that shows some promise in predicting mixing behavior.[67]

A charge distribution (i.e., "charge accumulation") is visualized as formed by charge injection, transport, and trapping (following concepts for semiconductor technology). The decay of the charge distribution is often examined using time domain dielectric spectroscopy to assess the release of an "absorption current". Data interpretation can be aided by the popular Pulsed Electro-Acoustic Analysis (PEA), usually limited to DC fields. Books have been written on these subjects. Here a few important findings will be highlighted.

Charge Injection: Charge injection is a high voltage issue as more charge injection occurs as field strength increases. One study found no measurable difference in charge injection between XLPE composites with micro-silica, nano-silica, and the neat XLPE polymer. However, PEA revealed a "shielding" homocharge adjacent to the cathode for the nano-silica composite. No charge injection was observed at the anode, but the decay of an "image charge" was observed.[66]

Traps: Deep vs. shallow traps are a conceptual construct used to describe the ability of a material to retain polarization. Charge has been observed to remain trapped in epoxy for seconds after injection, much slower than the charge injection process.[68] Due to trapping, the charge distribution is not only dependent on the particulate size, but also on the quantity. For micro-alumina in epoxy, the particulate was shown to modify space charge trapping. Space charge accumulation increased with higher particle concentrations.[69] A study of nano-silica in crosslinked polyethylene is included here for clarity. It was found that the absorption current or "quasi-DC conductivity" is high in the nanocomposite and this was related to a *reduced* real permittivity (measured above 10^{-4} Hz). The nanoparticulate are thought to provide shallow traps at the interphase that permit efficient charge release.[70] The overall effect is to reduce polarization at frequencies near 10^{-4} Hz. Dubbed the "Q-DC process", this model has been suggested to explain anomalies in data from complementary sources.[70] Another study of clay dispersed in polyisoprene reported that the nanoparticulate increased the DC conductivity. The nanoparticulate simultaneously increased the β-relaxation frequency.[71] Charge trapping is also dependent on the difference in permittivities of the filler and the matrix.

Transport: A direct relationship has been shown between surface charge decay and absorption current. However, related very low frequency relaxations were observed for glass-filled epoxy but not neat epoxy.[72] In a classic study, the size of particulate in epoxy showed significant differences in charge accumulation. Micron-sized titania in epoxy exhibited charge accumulation at the anode suggesting that the charge was blocked from diffusing. The corresponding nano-sized titania-epoxy composite exhibited very rapid charge decay. Some injected charge was again observed at the cathode. The lower charge transport of the nanocomposite was thought a result of a larger density of shallower traps. With a larger trap density, the charge release rate can still be higher with more shallow traps, leading to lower charge accumulation. It was concluded that these nanoparticulate are able to reduce the interfacial polarization typically observed in composite materials if the concentration is greater than a few percent.[73] DETA was used to examine the transport properties of an alumina-epoxy micro-composite. By fitting the relaxation data, the investigators found correlation with the glass transition temperature. An increase in free volume was suggested to facilitate the molecular dynamics and charge transport as temperature increased.[74] A study of epoxy filled with micro-silica and nano-titania showed a marked increase in surface charge decay rate after surface corona was observed. This was related to changes in the surface potential.[75] Whether corona has occurred or not is important information for any surface charging study, particularly those with high working voltage levels.

7.2.3. DETA of PMC: Adsorbed Water

Adsorbed or semi-free water is observed in DETA as a relaxation mode near 10^3 Hz.[14] When this water is trapped in voids[15], the loss amplitude depends on the void morphology as shown in Figure 7.8.[76] Beyond serving as a host for clustered water, nanovoids are also thought to function as electron and/or hole traps. Trapping has been linked to electrostatic interactions of charge carriers with the clustered water.[77]

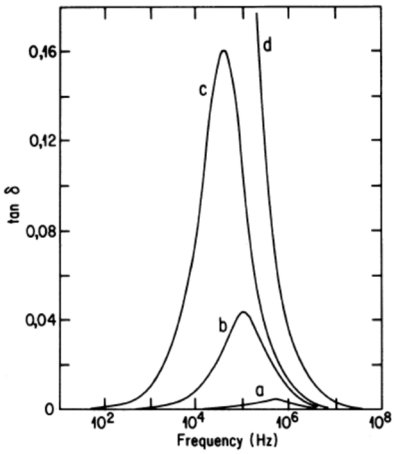


Figure 7.8. Calculated loss tangent for a dielectric (ϵ'=5) containing 0.2% water: curves a to c represent randomly distributed ellipsoids of water having axial ratios 5:1, 20:1, and 40:1, respectively. In d, filaments of water traverse the thickness of the dielectric.[76]

A similar loss mode has been observed due to high humidity in epoxy [78] and in fiberglass-epoxy composites [79]. In the epoxy, some water clustering was suggested, and ϵ' and tan δ were both observed to increase linearly with wt% (see Figure 7.9). For the fiberglass-epoxy composite, diffusion of water is believed to occur through voids rather than along the interphase.[79] Even so, regions where semi-free water is concentrated in the matrix are thought to connect with the interphase.[80]

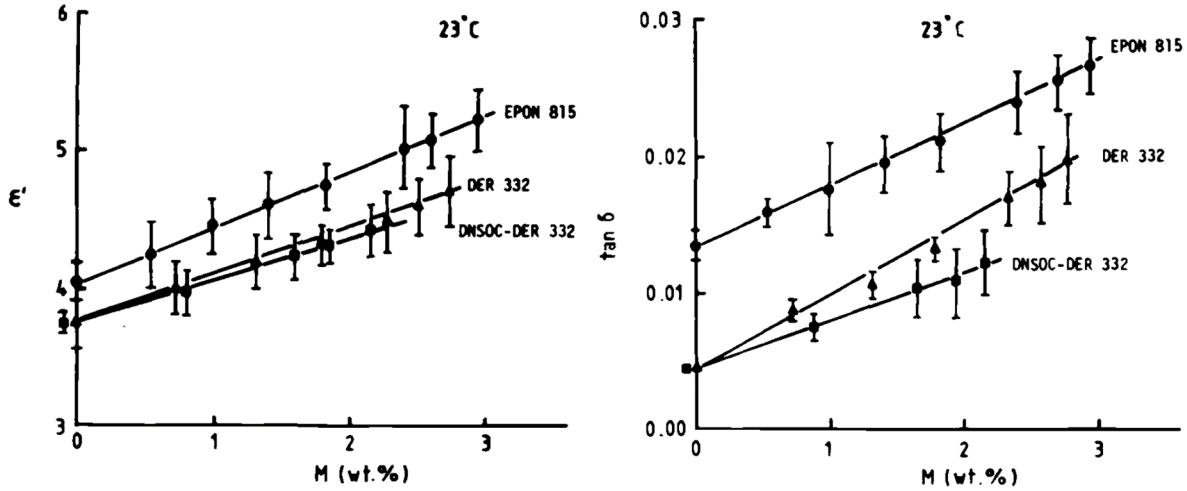


Figure 7.9. Dielectric behavior vs. water content of epoxy resin after immersion in water at 23°C: left is real permittivity and right is the loss tangent.[78]

[14] Although "clustering" and "void-filling" are discussed, here the 10^3 Hz relaxation is related to adsorption, not absorption of water.
[15] Voids can also be considered as nano- or meso-scale regions of lowered density.

A relaxation process in poly(propylene-graft-malic anhydride) has been assigned to polarizations of maleic anhydride groups. The unusual temperature dependence observed was attributed to a "redistribution" of water molecules in the polymer. When clay particulate were dispersed in this polymer, the relaxation frequency shifted higher by up to three orders of magnitude. The shift indicates a significantly enhanced molecular mobility of the maleic anhydride groups at the interphase. The diffusivity of water increased as the interphase mobility increased.[52]

Water in XLPE power cable insulation is associated with electrical aging and the formation of "water trees" or "electric trees". Figure 7.10 shows expected increases in loss tangent (ratio of ϵ"/ϵ') following the Wagner dispersion model. The exceptional behavior of sample 3 at low frequency was related to inclusions of foreign material in this isolated sample. The loss bands at 1.0 kHz for sample I and at 1.5 kHz for samples A and 5 are suggested as due to clustered adsorbed water.[81]

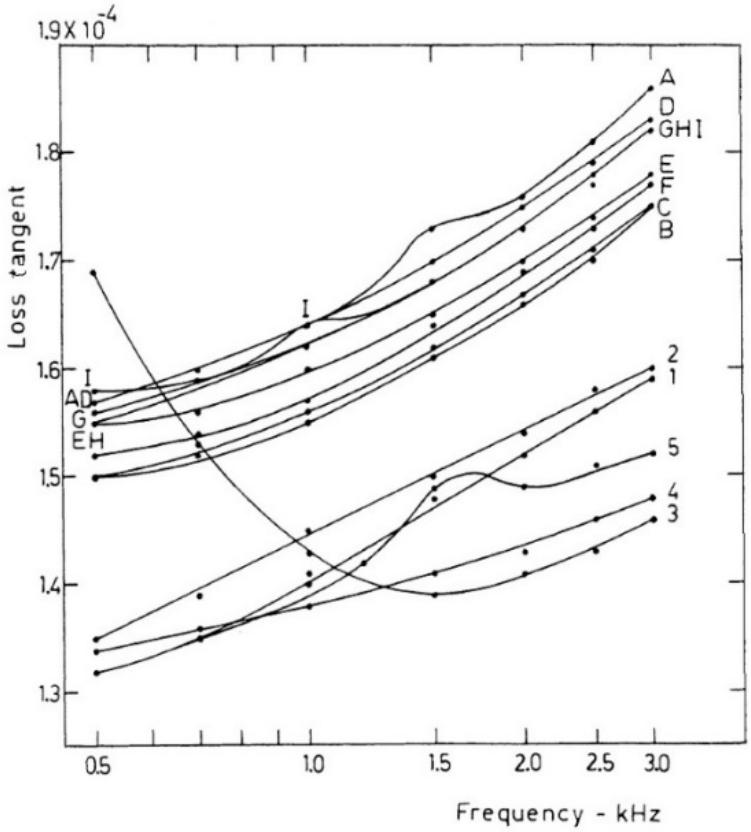


Fig. 7.10. Loss tangent vs. frequency for 5 new XLPE cable samples (numbered) and 9 cable samples that had experienced 2300 hours with 110 kV (15 kV/mm) at a conductor temperature of 90°C.[81]

An investigation of water sorption in three epoxy matrices with several clay additions found different results. The neat epoxies absorbed slightly higher amounts of water than the composites, but the water diffusion was the same. Not surprisingly, water sorption caused a reduction in glass transition temperature. The nanocomposites indicated slightly reduced thermal stability. This result is included here as the authors believed the water is dissolved in the network rather than located in free volume or voids. The peak temperatures of the α- and β-relaxations (from DMA) are observed to decrease with increasing clay concentration.[82]

7.2.4. DETA of Polymer Matrix Materials: Mica

Mica continues to be utilized in most high voltage insulation systems. Incorporating mica in a polymer matrix composite is known to improve voltage endurance, hardness, and resistance to thermo-oxidation. There is a long history of investigation of the behaviors of mica using DETA.[83] Functionalizing the mica surface to engineer the mica-epoxy interface and adhesion has proved successful. Improved thermal conductivity, lowered dielectric loss, and enhanced mechanical properties were achieved.[84]

DETA has been successfully used as a diagnostic tool for evaluating the interfacial adhesion of mica to epoxy.[54] Two main DETA features are monitored:

(i.) the intrinsic dispersion of mica causes ϵ' and ϵ" to both follow a power law with frequency (f^{n-1} where $0.64<n<0.83$) for all volume fractions of mica;[16] and

(ii.) ϵ" displays a broad MWS band at 1-10 kHz due to water.

There is a temperature dependence of the MWS band, linked to field-induced rotational motion associated with the epoxy network that follows Eyring's activated rate theory.[85] As temperature rises, electrical conduction (directly related to ϵ") is known to increase in the mica particle, in-plane. The effect on the composite's dielectric properties has been observed as a temperature-dependent dispersion of ϵ" that fits f^{-n}.[85] Another investigation found that the dispersion exponent changes with temperature, humidity, and frequency range.[86] The high sensitivity of the dielectric behavior underscores the importance of tightly controlling experimental conditions for meaningful data interpretation.

7.2.5. DETA of PMC: Layered or Laminated Composites

Insulation systems in power-dense electrical machinery are composed of multiple layers of different dielectric materials. The individual materials are often composites, themselves. The "weakest link" approach to failure would suggest that the interfaces (boundaries) between the layers would be most susceptible to void formation and delamination.

The main concern with layered systems is that the effective charge distribution at the interface may enhance the local electric field strength. The distribution is formed by charge injection, trapping, and transport. The layers may exhibit additive behaviors (i.e., follow simple scaling laws).[87,88] The interfaces formed between different materials depend on the processing. DETA, at a fixed frequency of 100 kHz, has been used to assess inter-diffusion at a boundary. As migration occurred across the boundary during processing, adhesion was shown to increase.[89] Concurrently, the α-relaxation band in the loss permittivity spectrum reduced in intensity and moved to higher temperatures.[90] Diffuse boundaries with good adhesion between insulation materials are highly desirable to improve mechanical properties. These macro-interfaces cause interfacial polarization whether any particulate encapsulated in a polymer matrix are involved or not.

The examination and design of layered dielectrics is a current intensive topic for energy storage devices and low frequency filters.[91,92] Design of thin layered dielectrics is also showing promise for reducing charge trapping times in MEMS capacitive switches.[93] Here the development goal is designing the layers for performance rather than designing a new composition by adding particulate. Unfortunately, in searching for publications on this topic, an in-depth study of the behavior of layered or stacked dielectrics for electrical insulation has not been found.

[16] This is surprising as the Kramer-Kronig relationship suggests that if $e" \sim f^{-n}$ than $e' \sim f^{1-n}$.

7.3. Polymer Matrix Composites: Insulation Aging & DETA

Insulation failure is known to have both a spatial scale and a time scale. The geometry often dictates localized stress magnitudes. Breakdown occurs when a threshold stress, characteristic of the insulation material's condition, is reached. Both breakdown and aging result from some combination of thermal, electrical, and mechanical conditions; both include a factor of time. The time scale can be viewed in terms of the failure modes as shown in Table 7.1. Aging occurs prior to insulation failure. Separating aging processes and failure modes can be difficult in practice.

Table 7.1. Time scale of electrical insulation failure modes.(after [94])

	Electric Breakdown	Thermal Breakdown	Electro-Mechanical Breakdown	Electrical Trees	Water Trees
Time to Breakdown (s)	$10^{-9} – 10^{-6}$	$10^{-7} – 10^{-3}$	$10^{-6} – 10^{-3}$	$10^{-2} – 10^{7}$	$10^{4} – 10^{10}$

The failure modes that lead to breakdown are difficult to separate. Here is an example: with the application of a DC threshold stress, a localized electron avalanche may occur (a number of mechanisms are possible and well-studied for different cases). With the avalanche, significant *localized heating* is predicted. Eventually the damage will become a defect that grows with *continued electrical activity*. The material defect that results in failure is *mechanical in nature*- usually observed as a pore, channel, or crack (a high conductivity path). The complexity has required separation to study each process. Researchers attempt to keep a few of the conditions or stresses constant while probing one or two stress variables. This must be looked at from the perspective of imperfect material samples from the start, so material processing becomes critically important in assessing material condition. Very simple thermoplastic polymers are used.

A goal of this section is to review insulation aging literature as close to use conditions as possible. For this reason, studies involving exaggerated temperatures are avoided. Aging at temperatures above the maximum use temperature ("over-temperature") are certain to cause severe degradation of the material. However, there is little control to validate what aging mechanisms occur below and above the maximum use temperature. Studies of ambient aging due to surface deposition of chemicals, dust, etc. are also avoided. In some studies, capacitance and tan δ are reported rather than ϵ' and ϵ". This is unfortunate as tan δ deptends inversely on the storage capacitance which is nonlinear in both temperature and frequency. This type of information is included if the results can be interpreted when both tan δ and capacitance are given. The three subsections are: 7.3.1 Thermal Aging, 7.3.2 Mechanical Aging, and 7.3.3 Electrical Aging.

7.3.1. Thermal Aging of PMC

Many studies have been published combining thermal aging with electrical aging of insulation materials. Perhaps it is not so surprising then that few papers have been published in the last three decades on just thermal aging and the examination of thermal aging effects using DETA. Three recent papers are reviewed that examine thermal aging of Roebel bars ("stator windings") with epoxy-mica-woven fiberglass. There is noteworthy information where excessive temperatures have not been employed. "Thermo-oxidation" is considered the dominant thermal aging mechanism of an epoxy (see Appendix 4). It is therefore considered the dominant thermal aging mechanism of insulation systems having an epoxy matrix.

Insulated Roebel bars were exposed for 7000 hours to dry air at <186°C. The before and after comparison of the insulation's capacitance and loss factor are shown in Figure 7.11. The capacitance decreased ~20% from 20 - 10^5 Hz with thermal aging. The loss factor does not vary at frequencies less than 10^5 Hz. In adjusting the variables to permittivities, this would correspond to a reduction in real permittivity, ϵ', of ~20% with treatment and a corresponding increase in loss permittivity, ϵ'' (as loss factor, $\tan \delta = \epsilon''/\epsilon'$). It was speculated that the decreasing capacitance is caused by delamination with the "formation of air capacitances in serial connection". No micrographic evidence of delamination was given.[95]

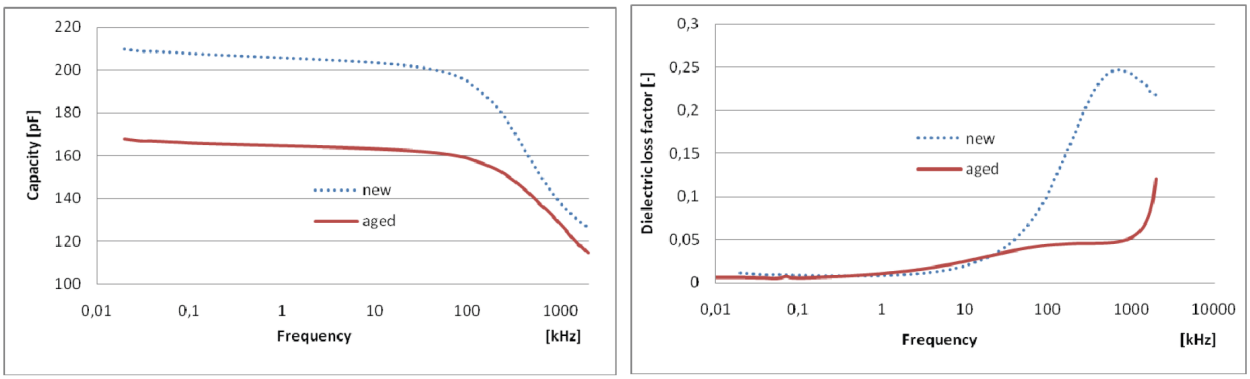


Figure 7.11. Dielectric response of new and aged epoxy-mica-fiberglass insulation: capacitance spectra and loss factor spectra.[95]

Mechanical properties are also known to change with thermal aging. Epoxy with relatively high filler loading of nano-silica was exposed to flowing air at 150°C for varying times. The samples were then examined using Dynamic Mechanical Analysis (DMA). The resulting storage moduli and loss tangents are shown in Figure 7.12 for a cycloaliphatic epoxy matrix.[96]

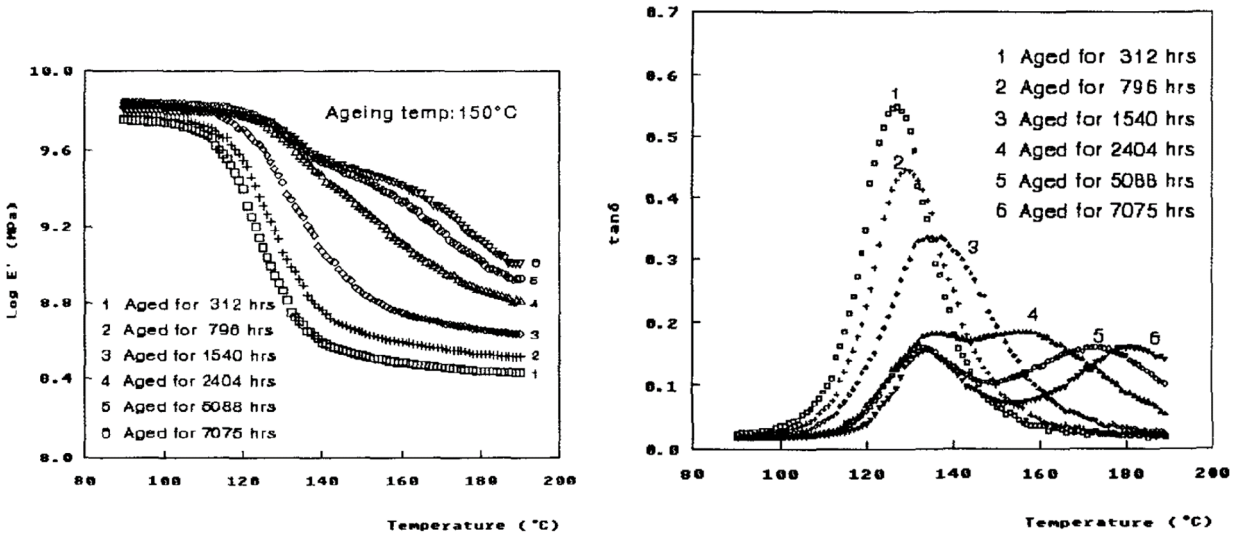


Figure 7.12. Dynamic mechanical response for an epoxy-nanosilica composite after aging at 150°C.[96]

The dynamic storage modulus, E', increased with thermal aging, particularly in and above the glass transition temperature range. The increased stiffness was thought to increase brittleness. It is attributed to higher crosslinking. The increase in glass transition temperature observed in the mechanical loss tangent (tan δ = E"/E') data supported this interpretation.[96] In a different study, an epoxy-mica-fiberglass composite insulation was thermally aged at 135°C (above the glass transition temperature). The DMA analysis showed a decreasing storage modulus with aging time. The glass transition (taken as the apex temperature of the loss tangent curve), was observed to increase with thermal aging time.[97]

Chemical change with oxidation is an alternative explanation to increased crosslinking (without accounting for chemical changes). Thermo-oxidation requires chemical change: the oxidation of epoxy molecules. In a well-controlled aging study, epoxy-mica-fiberglass composite insulation on stator windings was exposed to 2.3 bar oxygen pressure for multiple thermal cycles (varying from 50°-180°C).[98] The insulation was then examined using DETA and DMA. Water was produced by oxidation of the epoxy during the thermal cycling. Both the water presence and the oxidation were thought to be responsible for increases in dielectric loss. The glass transition temperature was observed to increase for short exposures. This was attributed to the formation of hydroperoxides and peroxides that increase crosslinking. For long exposures, the glass transition decreased, suggesting reduced cross-linking (or increased "chain scissions"). However, E' was observed to continue to increase. The Authors preferred the explanation that cross-linking increased with thermal aging, but "plasticization of the matrix" was caused by the formation of water. The insulation samples also experienced significant mass loss. (This suggests reduction of side groups.) The dielectric loss tangent increased above and below 10^3 Hz, as shown in Figure 7.14. With no change in capacitance, this can be interpreted as significant increase in the imaginary permittivity, ϵ".

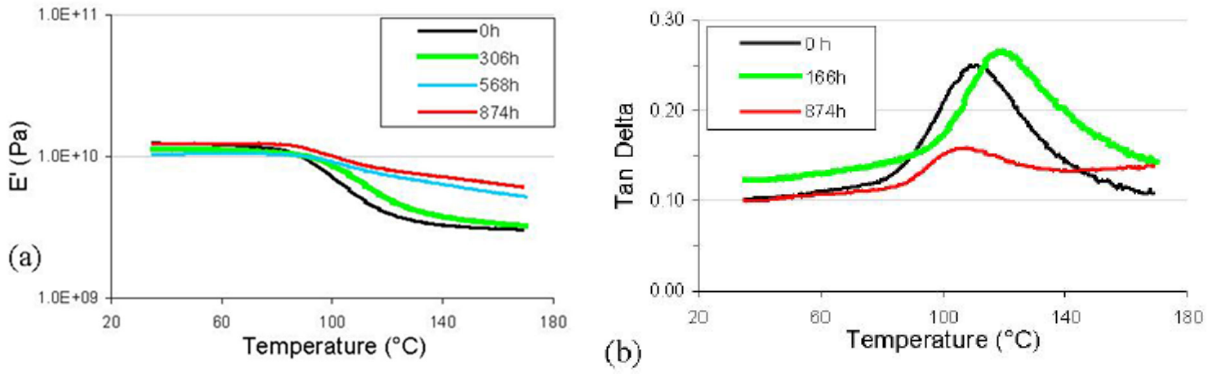


Figure 7.13. Dynamic mechanical temperature scans for an epoxy-mica-fiberglass insulation after aging at 135°C.[97].

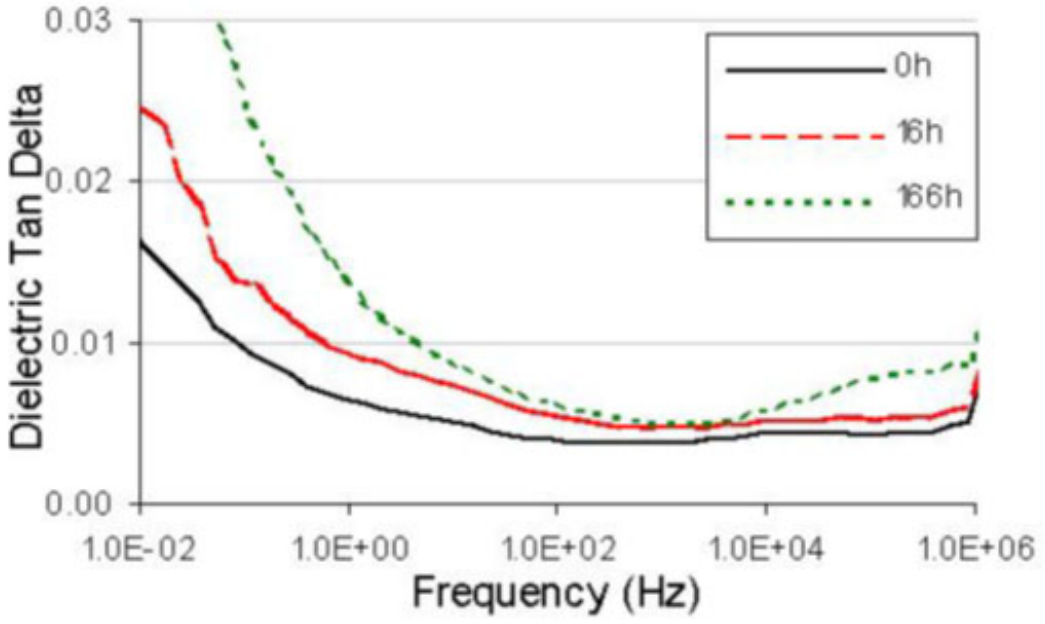


Figure 7.14. Dielectric loss tangent spectra for epoxy-mica-fiberglass composite thermally aged to 180°C.[98]

7.3.2. Mechanical Aging of PMC

Limited DETA information has been published where the mechanical aging of neat and composite insulation materials have been compared, particularly with aging frequencies above 200 Hz. Rotating and linear electromagnetic machinery experience a different mechanical and acoustic environment than semiconductors/power electronic building blocks (PEBBs) or power cables making mechanical aging specialized information. Successful insulation systems for machines have been specifically designed for the mechanical stress environment. An overview of insulation quality [99] stated that:

> "Performance under mechanical stress is one of the most important aspects in deciding the materials for rotating machine insulation… Thermal aging… will lead not only to an increase of internal gas pressure and decrease of adhesive strength of epoxy to mica surface, but also results in delamination at the interface between mica and epoxy. Delamination further aggravates under thermo-mechanical force. Small cracks are likely to be generated in epoxy rich areas due to thermal aging which could trigger electrical trees." (Note here the mechanical defect is initiated and electro-mechanical aging ensues.)

However multifactor stress models often diminish the importance of mechanical aging:

> "The assumption that the electric stress is the main cause of failure and the mechanical and thermal stresses only promote the degradation indirectly is vindicated by the experimental results."[100]

There are several noteworthy foundational studies that do not include DETA. Christensen[101] recently published a landmark model that predicts ductile-brittle transitions in a wide variety of materials from first principles. Guedes[102] reviewed the treatment of viscoelasticity in fracture mechanics for polymer matrix composites. Lewis et al.[103] found displacements at the metal-dielectric interface that varied with the fundamental frequency of the applied electric field. They propose an electrokinetic model to calculate the resulting interfacial stresses. Griffiths et al.[104] proposed a revision to Lewis' model using the polymer's yield stress as the dominant mechanical property. They further suggest that the main aging mechanism is one involving polymer yield.[104] (Note that static yield stress is related to dynamic shear stress and mechanical fatigue endurance.)

Careful attention to experimental details can help clarify the complexity of this topic. For example, mechanical property studies of carbon fiber-epoxy matrix composites with "nano-modifiers" found improved toughness and a "modest decrease" in tensile strength compared to the "unmodified" composite. A key problem was that the fiber tows prevented even dispersion of clay particulate in the epoxy as the composite was processed. This was thought to promote crack propagation rather than the intent to inhibit crack growth in specific stress orientations.[105] There may be the same issue with woven fiberglass in epoxy-mica-fiberglass systems. Another example is an optimal filler loading. In a nano-silica modified polyimide film, mechanical properties were observed to improve for up to 3% silica and then decline with additional particulate filler. This included tensile strength and elongation to failure.[106] A study that compared epoxy filled with either ~1 um TiO_2 or ~20 nm TiO_2 found that fracture toughness increased with the amount of filler added. The micron-sized particulate had more effect on increasing toughness than the nano-sized particulate.[107] Much attention has been given to modifying the filler surface to engineer

the particulate-matrix interface.[108] Researchers have found that thermal conductivity and low dielectric loss in epoxy matrix composites improve with "quality of the interface".[63] Surface modification of mica was also claimed to exert a "strong influence" on the mechanical fatigue of mica-filled epoxy.[109]

Another recent study examined both bending and torsional fatigue of an epoxy-mica-fiberglass composite. The Authors sought to identify the weak interfaces most likely to result in the initiation and propagation of defects. The testing "clearly identify the cleavage between the mica flakes as the dominating failure mechanism in the insulation composite. This finding is in agreement with previous research work in this field. Very low magnitudes of fracture toughness highlighted the weakness of the interface externally loaded, and more specifically in the opening mode. The fracture toughness could be increased with an increase in the resin content."[110] The "previous research work" mentioned above found a linear relationship between shear strength and bending modulus. The shear strength can be improved by using an epoxy with a higher bending modulus. The recommendation was to limit the use of the insulation to temperatures below the glass transition to maintain the shear strength of the composite.[111]

A landmark study showed that the effect of thermal aging and mechanical fatigue on breakdown strength is not additive in a mica-epoxy composite. The thermal aging was observed to have a profound effect on the subsequent mechanical fatigue as shown in Figure 7.14b. The study included images of micro-cracks developing with both thermal aging and mechanical fatigue.[112]

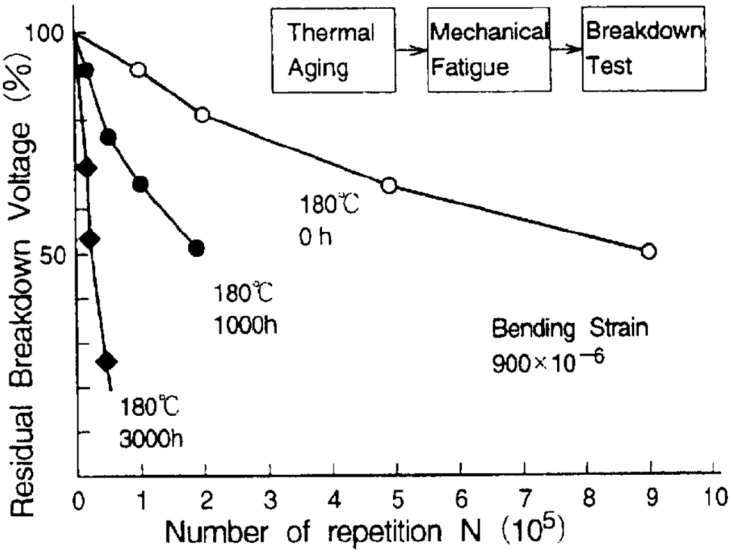


Figure 7.14b. Effect of mechanical fatigue on residual breakdown characteristics with prior thermal aging.[112]

One study used the dielectric loss tangent to assess mechanical aging with bending at 100 Hz or with torsion at 100 Hz. The loss tangent as a function of applied voltage is shown in Figure 7.15. The samples were 2 mm thick composites of mica paper and fiberglass tape in a cured epoxy resin. Two different mica products were compared. The loss tangent is shown to increase over a wide voltage range. Mechanical fatigue aging by both bending and torsion caused increases in the loss tangent with the largest increase measured after torsion. [113]

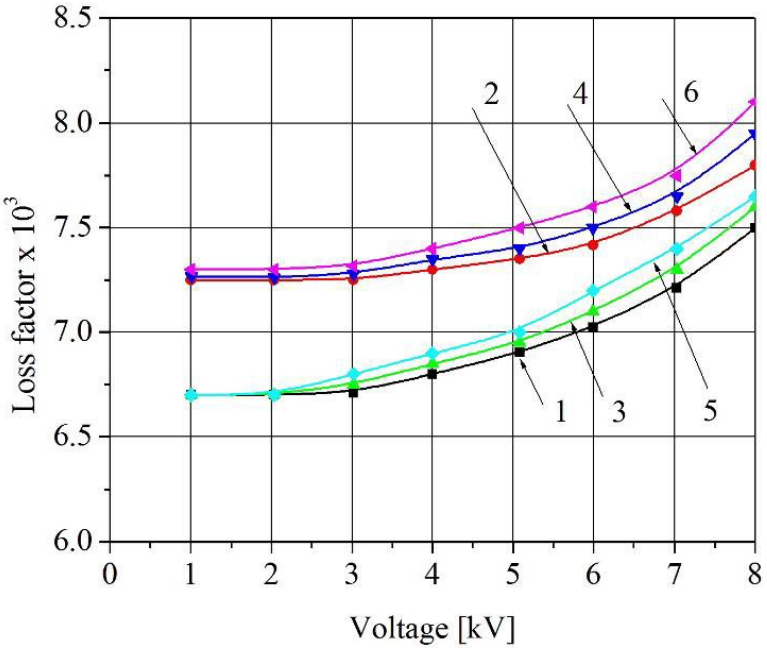


Figure 7.15. Dielectric loss tangent with the test voltage for two different composites after mechanical aging: unaged (1, 2), stressed in bending (3, 4) and in torsion (5, 6).[113]

Two thermoset polymers, an epoxy and a silicone, were mechanically aged at ultrasound frequencies. Using Dynamic Mechanical Analysis (DMA), the epoxy was shown to become less compliant after mechanical aging. The silicone became more compliant after mechanical aging.[114] The DETA of the mechanically aged silicone exhibited a decrease in dielectric loss factor, tan δ, at sub-Hertz frequencies at temperatures above 50°C (see Figure 7.16).

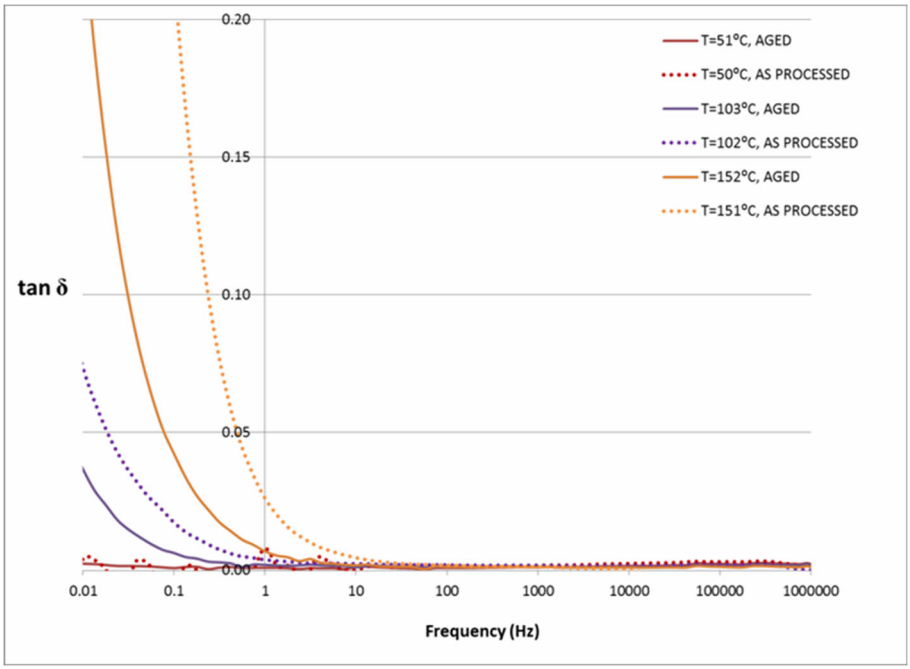


Figure 7.16. Comparison of loss factor for mechanically aged vs. as-processed silicone.[114]

7.3.3. Electrical Aging of PMC

Aging of insulation under electrical stress has received tremendous attention over the last several decades as power density requirements increased in many engineering sectors. Even so, empirical studies are required as behavior is difficult to predict. Some generalizations can be made. Short-term performance (e.g., breakdown behavior) has a strong dependence on the voltage waveform and the geometry. Some researchers found that addition of nanoparticulate improve short-term performance [115,116,117] and others found a comparative deterioration [118]. Long-term performance (e.g., voltage endurance) has a strong dependence on the choice of thermoset polymer matrix. The addition of nanoparticulate generally improves performance under electric stress compared with microparticulate additions or the neat polymer. Best performance is achieved when the PMC components can be "tuned" to the specific requirements of the application. Due to the wealth of information in this area, this section will be presented in three parts: Breakdown behaviors; Voltage endurance, bulk; and Voltage endurance, surface.

Breakdown Stress Behaviors: Addition of particulate to a polymer matrix affects the breakdown stress to widely varying degrees. A thorough review of this subject is presented in [119]. Others have used a parameter, k_2 = breakdown stress of composite / breakdown stress of neat polymer, to summarize published trends.[94] In Figure 7.17, k_2 is plotted as a function of the dielectric constant (~ϵ') of the polymer matrix. The variation is large, indicating that a finding for one polymer should not be expected in another. Epoxy has an average k_2 ~1.06, but with a range of 0.83-1.32.

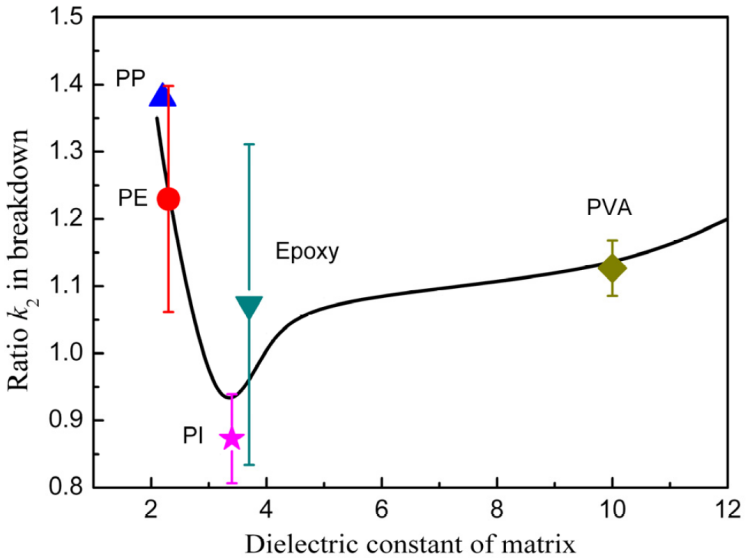


Figure 7.17. Ratio of breakdown stresses of filled to neat polymer matrix composite, k_2, vs. dielectric constant.[94]

DC breakdown stress is considered important for power cable applications whereas AC breakdown stress is more important for machine applications. The wide experimental variations should not be ignored. However, some generalizations can be made as follows. DC breakdown and AC breakdown show different trends with the percentage of filler added. Figure 7.18 compares k_2 for

DC breakdown with percentage of filler for nano-composites and micro-composites. The micro-composites show a dramatic reduction in DC breakdown stress as the filler increases above 1%. However, the DC breakdown stress improves with ≤10 wt% of nanoparticulate. This is a generally accepted trend.

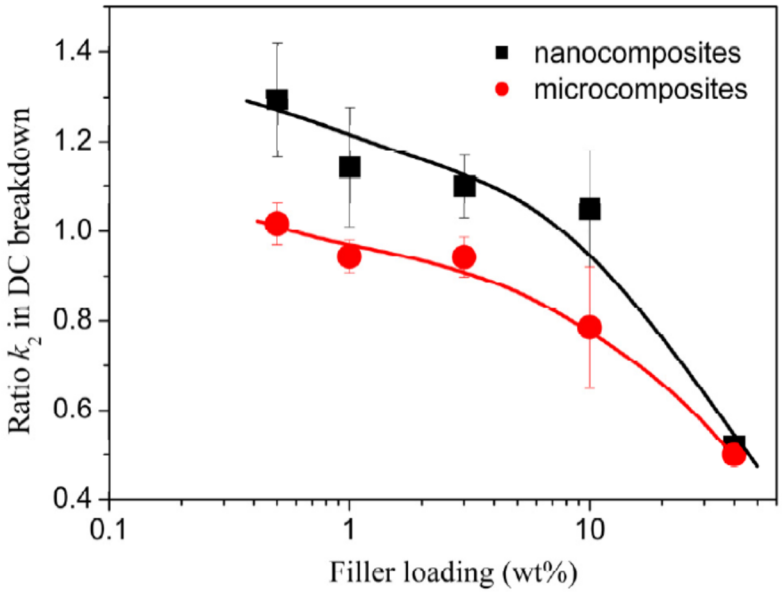


Figure 7.18. Ratio of DC breakdown stresses of filled to neat polymer matrix composite, k_2, vs. percentage of filler.[94]

A thorough comparison of epoxy, epoxy with "ex-situ" nano-titania (mixed into the resin) and epoxy with "in-situ" nano-titania (nucleated in the resin) showed different results (see Figure 7.19). The "ex-situ" composite failed at lower electric stress than the epoxy. However, the "in-situ" composite showed improved performance. By analyzing the dielectric spectroscopy, dynamic elastic moduli, and the DC breakdown behaviors, the conclusion was made that the improvement in breakdown stress for the in-situ nano-titania composite was due to improved dispersion and reduced size. The segmental motion of the epoxy molecular dynamics was restricted by the in-situ nano-titania.[120]

With AC breakdown, a smaller improvement is found for nano-composites at <2 wt% of nanoparticulate. The summary data is shown in Figure 7.19b. An important round-robin study also showed an improvement with addition of 5 wt% nanoparticulate (sample 0M5N). However, the *addition of both nanoparticulate and microparticulate* (samples 60M5N and 62.5M2.5N) showed a dramatic improvement (see Figure 7.20).[121] This data trend has led to refutation of some prior hypotheses based on charge distribution that attempted to explain the improvement in breakdown stress with nanocomposites (improvement not observed in Figure 7.20). Due to the significantly improved properties on laboratory samples, more investigations are including bimodal size distributions of particulate (see for examples [75,122]).

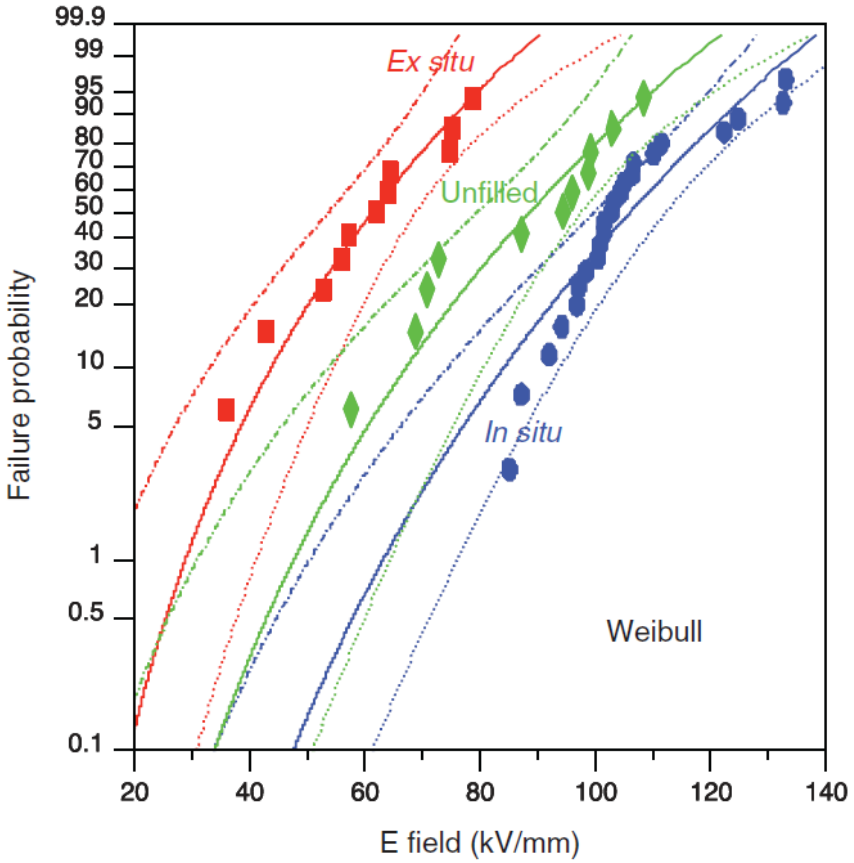


Figure 7.19. Comparison of DC breakdown at 77°C of epoxy, and epoxy containing either ex-situ or in-situ titania.[120]

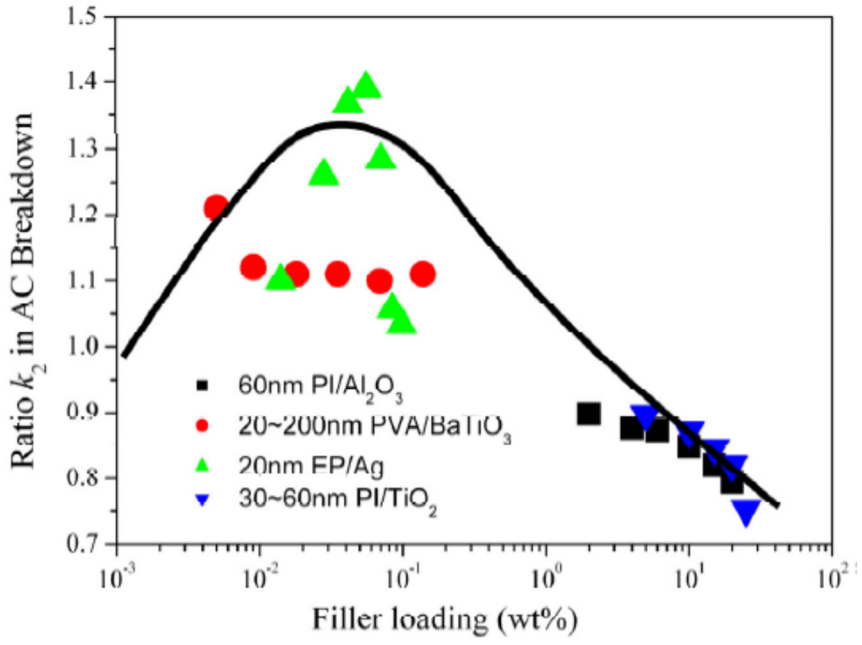


Figure 7.19b. Ratio of AC breakdown stresses of filled to neat polymer matrix composite, k_2, vs. percentage of filler.[94]

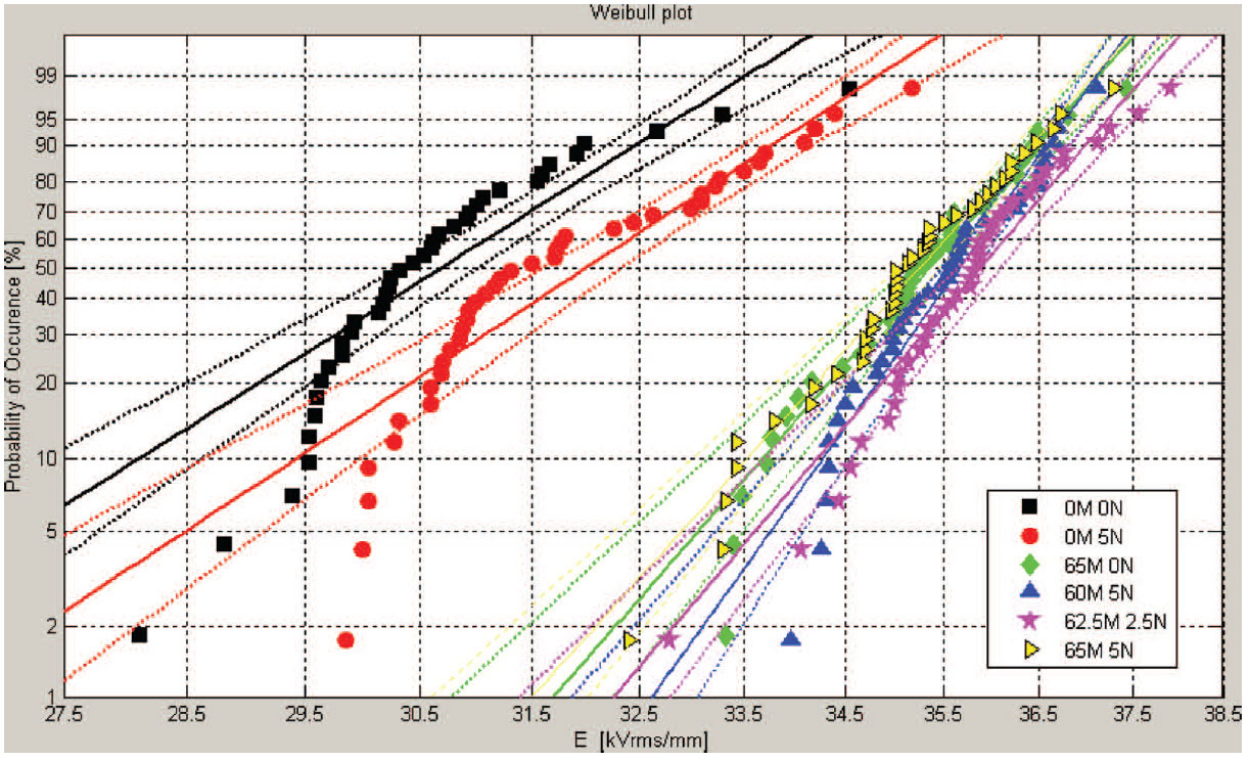


Figure 7.20. Weibull plot with 80% confidence intervals for AC breakdown stress as a function of particulate size and amount added to an epoxy matrix (wt% given in legend where M designates microparticulate and N designates nanoparticulate).[121]

The dependence of AC breakdown stress and DC breakdown stress on composite formulation are different, and the sizes and percentages of particulate can greatly affect the values. (This will be important to consider with voltage endurance, where the material ages to the condition at which the breakdown stress is reached by the electric field.)

Cross-linked polyethylene (XLPE) is a preferred polymer for power cables. The loss tangent (tan $\delta = \epsilon''/\epsilon'$) may increase with DC voltage aging (see Figure 7.7). In another study, XLPE samples were aged at one electric field, U_o, within a range of voltages. The samples were then tested to breakdown at 0.1 Hz in either a pulsed breakdown test or a step breakdown test (giving U_{bd}). The normalized breakdown stress, U_{bd}/U_o, was found to decrease with increasing loss tangent for both testing regimes.[123] This method may provide more insight into electrical aging than the time-to-failure ("endurance") method.

In contrast to XLPE, one study showed that an aging treatment (that caused a significant increase in tan δ) had very little effect on the AC breakdown stress of epoxy composite.[124] Two different epoxy resins were examined, both filled with 1 wt% nano-silica. Samples were aged at 155°C and with 4 kV at 50 Hz for varying time periods. Loss tangents and AC breakdown stress were then measured. The Authors claim that whereas the loss tangent was a sensitive indication of thermal aging, the breakdown stress was not sensitive to thermal aging.

Another study employed low frequency dielectric analysis to examine multistress aging of generator bars ("coils") prior to breakdown testing.[35] The straight bar sections were insulated with an epoxy-mica-fiberglass layer and covered with a stress grading coating. The bars were aged with either 1049 thermal cycles (40°C-155°C) or 1500 thermal cycles (40°C-155°C) plus a voltage of 16 kV_{rms}. The dielectric response remained flat between 10^{-4}-10^{-1} Hz. The Authors concluded that differences in the breakdown stress were due to aging damage to the stress grading coating and not the epoxy-mica-fiberglass layer.

In attempting to improve thermal conductivity, boron nitride (BN) was added to an epoxy resin in a mica tape.[125] Roebel bars were then prepared with an epoxy-mica+BN-fiberglass insulation. The limited amount of BN involved was found to double the thermal conductivity. No difference in breakdown stress, voltage endurance, and tan δ was measured with the presence of BN.

Voltage Endurance, Bulk: Voltage endurance, or the time required for a material to degrade to a breakdown level under an applied voltage, is a complicated phenomenon. Temperature and mechanical stresses do affect the endurance time. When a polymer responds to the applied stress environment by forming nano-voids, partial discharge may initiate. Once initiated by a nano-void of sufficient size, the partial discharge irreversibly ages the polymer. The breakdown stress decreases over time as the total accumulation of damage with partial discharge increases. Single breakdown channels, delamination, or electric trees may develop. The temporal behavior of aging with partial discharge resembles classic mechanical fatigue. A relationship between partial discharge initiation voltage (the effective lower limit of voltage endurance) and real permittivity, ϵ', was described by Dakin et al. in 1955.[126] Here the "corona threshold voltage" is the initial voltage at which partial discharge was observed at the dielectric, where the voltage was applied between two 0.5 inch diameter electrodes (in a parallel plate configuration). The partial discharge initiation voltage for many types of dielectrics follow the same trend with thickness divided by real permittivity, t/ϵ', as shown in Figure 7.21. Any relationship between voltage endurance and dielectric parameters is much more complex.

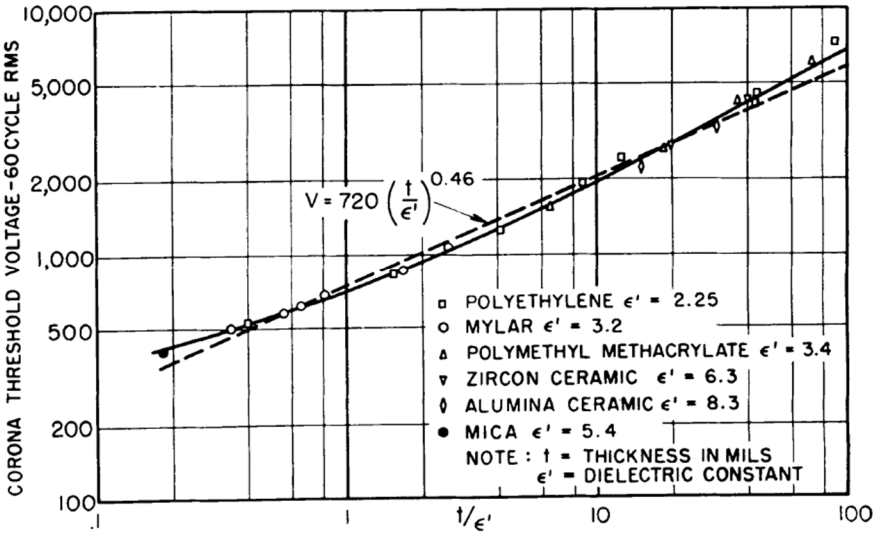


Figure 7.21. Partial Discharge threshold voltage vs. the ratio of dielectric thickness/real permittivity.[126]

A ratio, k_3 = voltage endurance with particulate / voltage endurance of neat polymer, is useful in summarizing data for general trends. Figure 7.22 shows that fillers improve the voltage endurance of epoxy. At long aging times (>100 hours), nanocomposites are shown to have significant advantage.[94]

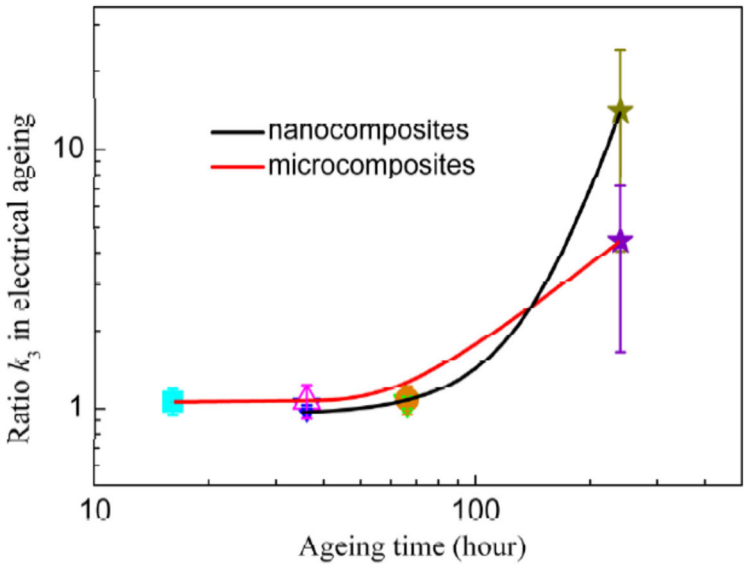


Figure 7.22. Ratio of the voltage endurance of filled to neat epoxy matrix composite, k_3, vs. aging time.[94]

The nanoparticle filler loading should be ~1% or more to achieve this advantage in voltage endurance. A schematic is given in Figure 7.23 that combines the breakdown dependence (given in Figure 7.19) and voltage endurance with filler loading.

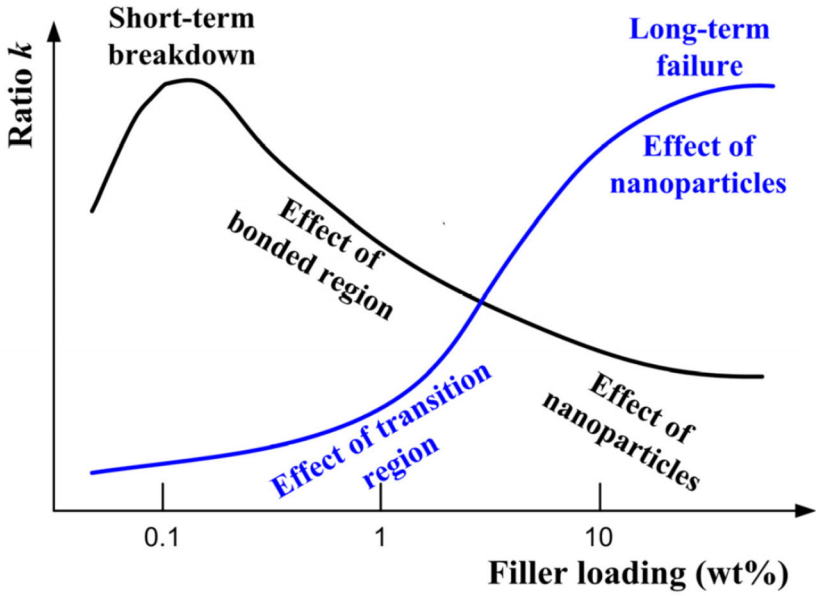


Figure 7.23. Schematic of effect of nanoparticulate concentration on breakdown stress and voltage endurance compared with the neat epoxy.[94]

The dependence of partial discharge aging on temperature has been studied in an epoxy resin. Voltage endurance increased with increasing temperature. The temperature of lowest PD activity was T = 0.75 T_g.[127]

Power factor "tip-up" has been used as a diagnostic test on stator bars for many decades. The measured dielectric tan δ (dissipation factor) increases with applied voltage. The tip-up curve is expected to increase in slope as insulation aging progresses. The measured tan δ is considered a combination of losses due to conduction, polarization, and partial discharge ("ionization"). Dakin recommended that the change in capacitance at test voltage should also be monitored as a total measure of partial discharge activity.[128]

Although no study was found comparing the power factor "tip-up" for a filled and unfilled polymer, two studies reported both capacitance and tan δ during aging of a VPI epoxy-mica-fiberglass stator bar insulation.[129,130] A multi-stress aging regime consisted of repeated cycles of (i.) mechanical vibration at 60 Hz for 1 hour; (ii.) humidity exposure for 48 hours; (iii.) nondestructive measurements; (iv.) 50 Hz test voltage for 1 min.; and (v.) exposure to multiple days at select temperatures. Figure 7.24 gives the capacitance and tan δ plotted as a function of the increasing test voltage applied each aging cycle. The number of aging cycles is shown to the right. The capacitance is observed to decrease with number of cycles while tan δ increases (but only above a threshold test voltage).[130]

Another study by this group examined the effect of adding void volume to epoxy samples (essentially a second phase). A controlled number of channels were drilled through epoxy disks. The resulting capacitance and tan δ are shown as a function of test voltage in Figure 7.25.[131] The tan δ behavior observed in Figure 7.25 correlates with that in Figure 7.24, supporting the Authors' assertion that the latter behavior is due to delamination and increased total void volume in the VPI epoxy-mica-fiberglass insulation.

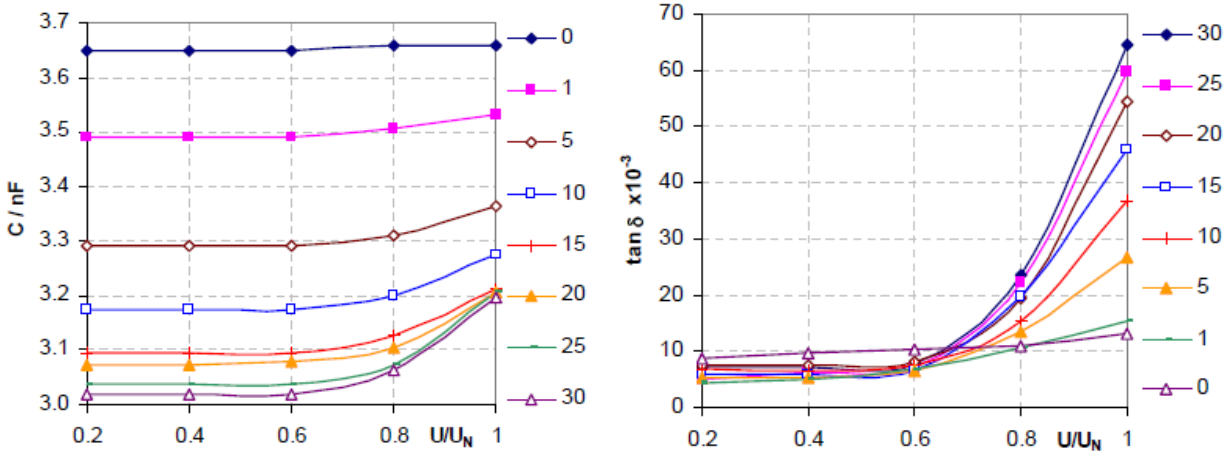


Figure 7.24. Capacitance and tan δ as a function of normalized test voltage for aged insulation; key to number of aging cycles to the right.[130]

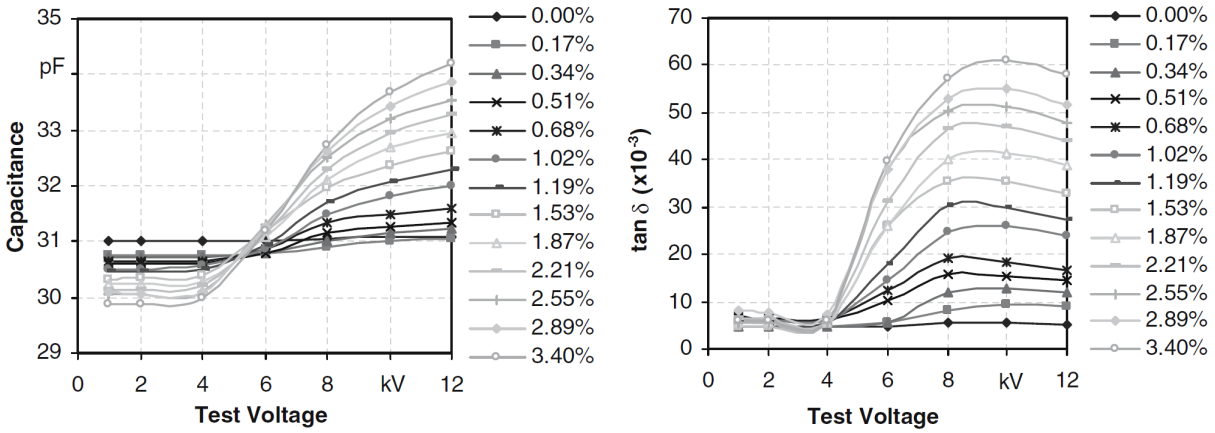


Figure 7.25. Capacitance and tan δ as a function of test voltage for epoxy disks; key to void volume shown to the right.[131]

Voltage Endurance, Surface: Precise speed and frequency control of electric machinery can be achieved with modulated voltage source converters. The energy efficiency with this paradigm for low horsepower applications is outstanding. The inherent high frequency switching and harmonics of the modulated power waveform may accelerate aging of the dielectric insulation. This has been linked to partial discharge, electroluminescence, and charge trapping/injection phenomena. "Corona resistant" wire enamels have been commercially available for two decades to alleviate this aging. These enamels contain inorganic nano-particulate in a polymer matrix. When the wire enamel remains exposed to air, as in many random-wound coil designs, the exposed surface becomes active. There is concern that corona resistant enamels are actually less effective than neat enamels as temperature increases. The partial discharge initiation voltage was found to be less for neat enamels than corona resistant enamels. In one test, the voltage endurance of the neat enamel was dramatically longer than that of the corona resistant enamel.[132] The following discussion is limited to high-resistance dielectric composites, excluding stress-grading coatings. Along with voltage endurance of the nanocomposite surface in air, surface flashover and surface erosion are useful metrics.

As with partial discharge interior to dielectric materials, surface flashover may occur at electric fields well below breakdown stress. Surface flashover is highly dependent on the gas pressure and ambient environment (e.g., humidity). To summarize literature studies, a parameter k_1 = surface flashover voltage with filler / surface flashover to neat polymer was defined. This parameter is plotted in Figure 7.26 versus voltage rise time. The results indicate essentially the same improvement in surface flashover with both nano-particulate and micro-particulate fillers.[94] Loadings above a few percent may further improve surface flashover but the coatings become brittle. Surprisingly, addition of nano-silica gave a low k_1 value. A mixed fill of nano- and micro-particulate in epoxy gave superior surface flashover properties.[121]

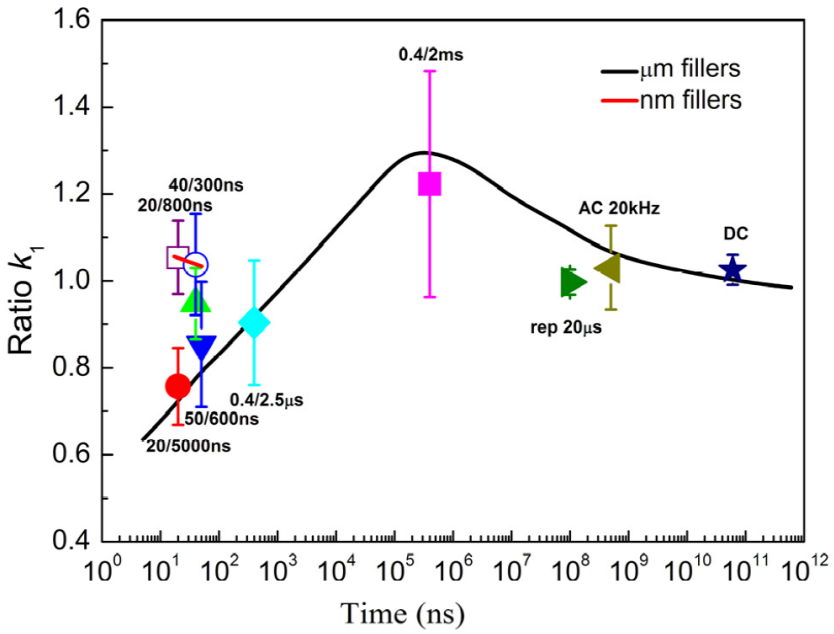


Figure 7.26. The ratio of surface flashover voltage of filled epoxy to neat epoxy, k_1, vs. voltage rise time.[94]

Surface voltage endurance is measured as the time to form a conductive breakdown path on the surface, usually dominated by corona. Studies of surface voltage endurance may use a metal needle electrode with an air gap to a flat, coated electrode, thus producing a divergent field. For wire coatings, discharge between wires forming a twisted pair is monitored. Although surface flashover voltage diminished with the addition of nano-silica, other authors found an increase in surface voltage resistance with the presence of nano-silica ("POSS") in epoxy.[133] Further study of the surface after corona using FTIR showed high levels of silica.[133] Another study with 72-74 wt% micro-silica filler found mixed results compared with the neat epoxy. The short-time endurance was lower (breakdown stress at lower voltage) but the long-term endurance was higher (see Figure 7.27). Although the Authors concluded that the filled epoxy composite had a "superior discharge resistance at lower stresses", an alternative explanation is that it took some time ("corona activity") for a protective surface to form.[134] This behavior with microparticulate also follows the schematic shown in Figure 7.23. These results have been corroborated.[135] Another study recommended 1% nano-silica addition to wire coatings based on interfacial charge accumulation between coating layers examined using time domain dielectric spectroscopy.[136]

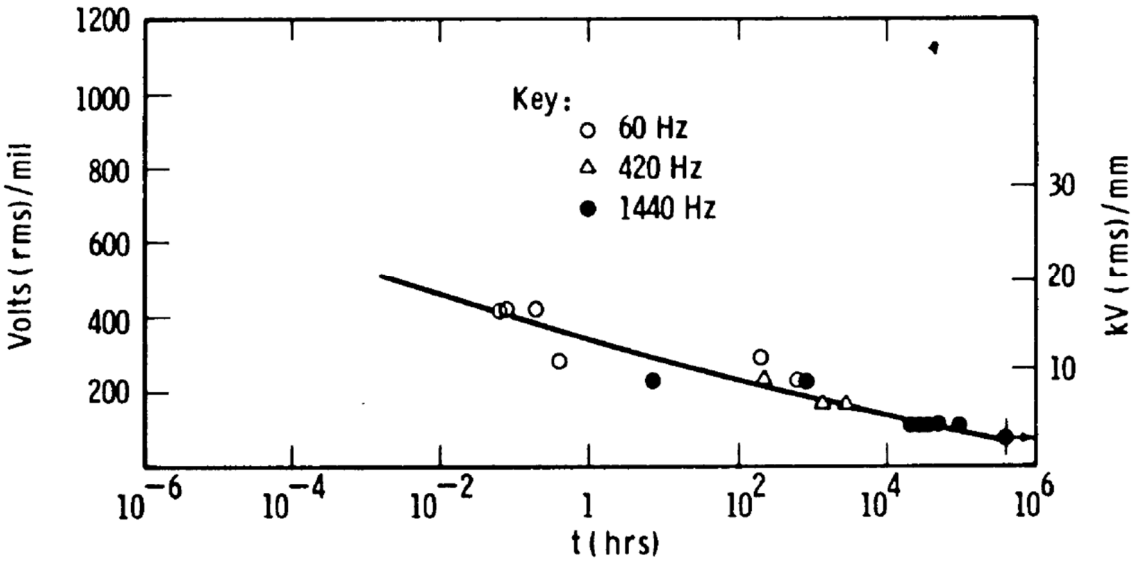


Figure 7.27. Surface voltage endurance of micro-silica filled epoxy.[134]

The ability of the composite to form a protective surface may be the explanation for the rather large difference in surface voltage endurance with filler type (see Figure 7.28).[137]

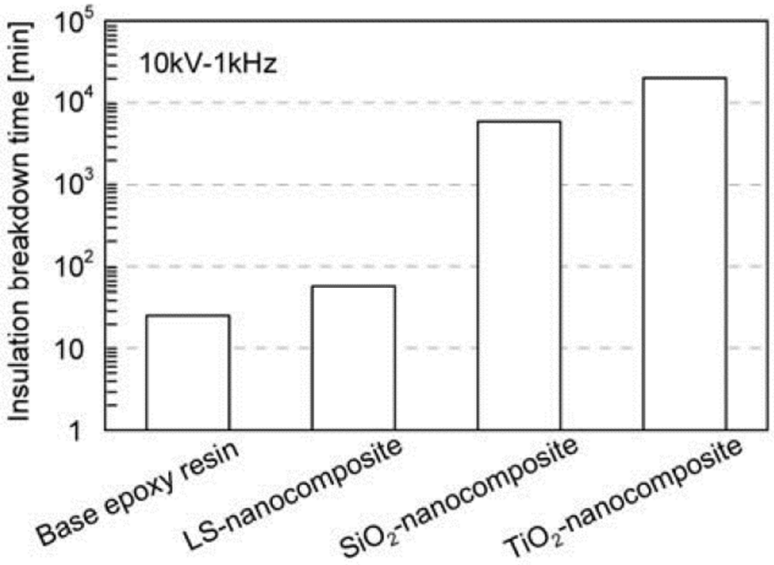


Figure 7.28. Comparison of surface voltage endurance for neat and filled epoxy nanocomposites (10 kV at 1 kHz): note "LS" is layered silicate.[137]

Surface erosion is usually measured as a maximum depth in a surface profile after electric aging. The surface erosion is higher for the neat polymer than for the filled polymer. A comparative example of erosion depth with test time is shown in Figure 7.29. The erosion depth is greatly reduced as the filler loading increases. Furthermore, surface charge accumulation has been reduced by the presence of nano-particulate at very high DC stress levels. Even so, the electric stress threshold for space charge accumulation is lower for the filled composite.[47]

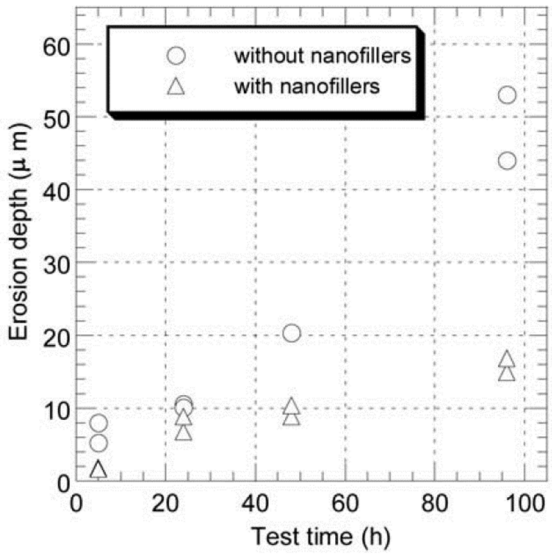


Figure 7.29. Erosion depth vs. time for a nano-titania filled epoxy and the neat epoxy (6 kV at 60 Hz).[137]

Clay-filled polymer composites may also exhibit a large reduction in surface erosion. The behavior is highly dependent on the chemical composition of the clay and any surface modifiers. Figure 7.30 shows the results of a thorough study with two clay filler loadings. A needle electrode to a flat, coated electrode with air gap was used with voltage application of 5 kV at 500 Hz (coating 0.2 mm thick).[138]

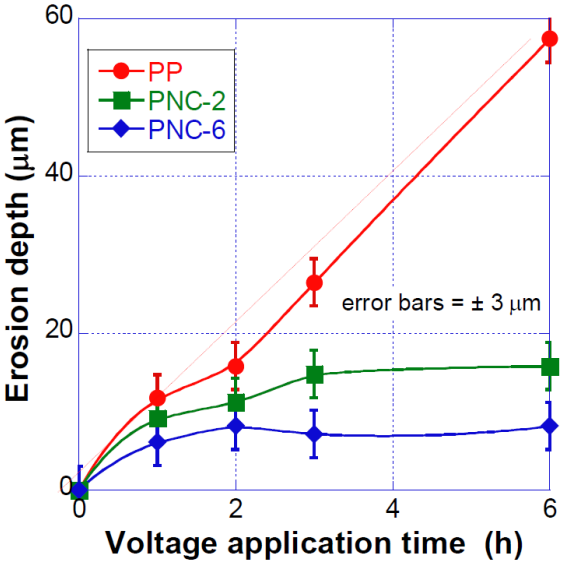


Figure 7.30. Erosion depth vs. time for two clay-filled composites compared to the neat polypropylene (5 kV at 500 Hz).[138]

The dielectric spectra for these three materials are shown in Figure 7.31. Both clay-filled composites had higher real permittivity and imaginary permittivity than the neat polypropylene. The total surface charge developed during the erosion time was calculated. The erosion depth is

shown versus this surface charge in Figure 7.32. Although neat polypropylene showed less surface charge accumulation, the erosion depth was much more pronounced. The Authors conclude that erosion depth is independent of surface charge and the dielectric properties.[138]

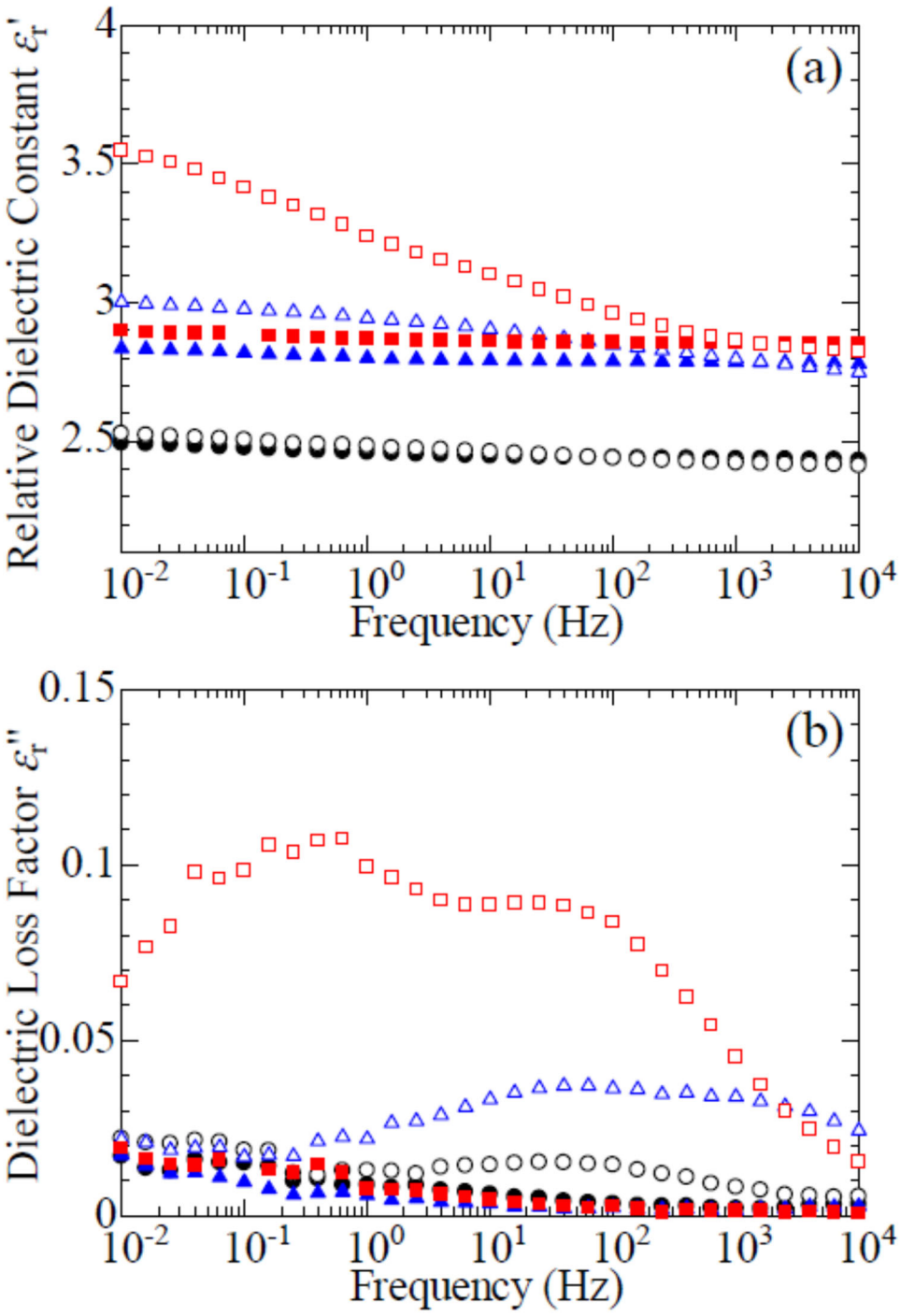


Figure 7.31. Real permittivity (a) and imaginary permittivity (b) spectra for PP-0 (circles), PP-2 (triangles) and PP-6 (squares) at -20°C (solid symbols) and at 80°C (open symbols).[138]

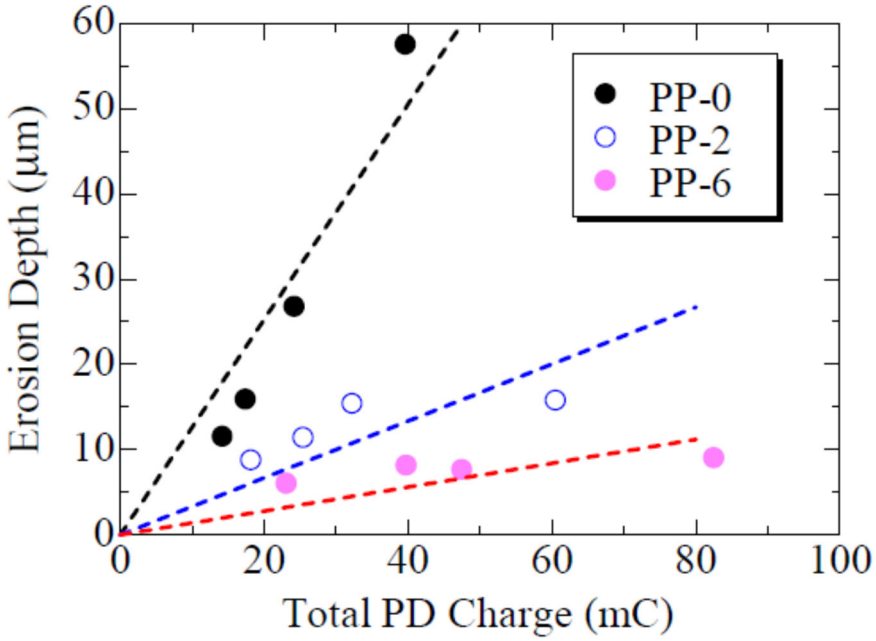


Figure 7.32. Erosion depth vs. total surface charge.[138]

7.4. Recommendations From Literature Survey

Five recommendations are listed. The recommendations are considered the most important based on the information contained in this Literature Survey.

(1.) Health Index Monitoring records of in-service insulation system case studies would be valuable to the research community. These environments cannot be easily duplicated and monitored in most research laboratories. Examples are:

- Insulation response with power-dense EMA with ~60,000 rpm, permanent magnet motor system (nominal 1 MHz PEBB drive);
- Insulation response with form-wound, medium voltage generator using SiC PEBB drive; and
- Insulation response in high density GaN and SiC PEBB packaging.

(2.) Leadership in promoting an insulation Working Group/Workshop community to review and promote excellence in dielectric characterization techniques and reported information. The Working Group could be tasked to encourage the R&D community to use resources to resolve targeted issues. This is particularly of interest as insulation suppliers are largely headquartered off-shore and hold much product information proprietary.

(3.) Characterization of the molecular dynamics of layered electrical insulation needs attention. Macro-interfaces of layers (not well investigated) are significantly different than those of particulate fillers (already investigated as shown here). This is a key science issue for power-dense electrical insulation of medium to high voltages that has not been addressed to date.

(4.) Improved characterization tools that extend the available and sensitive DETA frequency range would be beneficial. The relaxation modes of stiff, thermoset polymers appear in different frequency than model thermoplastic polymers. Thermoplastic polymers are more readily examined by DETA. When the principle relaxation modes are identified, the literature agrees with the schematic in Figure 7.4. The α-relaxation is centered at lower frequencies for thermosets as the glass transition temperature is usually higher. The α-relaxation is located at ~10^{-5}-10^{-3} Hz. The β–relaxation is located at ~10^{6}-10^{8} Hz. Both relaxations progress to higher frequencies as the measurement temperature increases. (These progressions are observed in the spectra plotted for a series of temperatures in the Appendices.) The majority of the dielectric spectrum measured between 10^{-3} – 10^{6} is influenced by the leading edge of the α-relaxation and the trailing edge of the β–relaxation. Extending the accessible DETA frequency range would improve analyses.

(5.) A quantitative connection between DETA and voltage endurance data and/or breakdown needs to be established for lifetime prediction. This is the fourth "proof" or knowledge piece that is needed. The three accomplished are:

- Computational mechanics can predict macroscopic stress states (at frequency) in thermoset polymers given aged material characteristics.
- DETA and DMA can monitor the molecular dynamics of thermoset polymers. Changed molecular dynamics are observable at low levels of thermal and dynamic field aging (i.e., accelerated aging is not required).
- PMC aging is principally dependent on the matrix polymer and its interaction with the other phases. Thermal aging, mechanical fatigue, and voltage endurance studies already have established relationships with lifetime.

8. *Characterization:* DETA & AGING OF PMC DIELECTRICS

Both sequential aging treatments and aging of polymer matrix composites (PMC) are described in this section. Sequential aging is studied and documented to determine if the dynamic field aging treatments persist. The polymer matrix composite sample materials were designed to explore components of a complex insulation system typically applied to form-wound coils for high power density electromagnetic machines. These are nano-silica modified polymer, mica-filled polymer, and fiberglass-polymer laminate. Nano-silica is routinely used to modify the rheology of commercial polymer resins for improved flow characteristics during processing. Mica is used as a filler in higher power-density insulation to improve voltage endurance. As a filler, mica also increases thermal conductivity. Fiberglass is routinely used to improve mechanical properties of the coil, particularly by wrapping the wire turn bundle with a fiberglass-polymer tape prior to VPI processing. The fiberglass laminates, themselves, may be machined to use as insulative spacers and other fixtures within the machine. A multicomponent insulation based on mica, fiberglass, and epoxy tape was also examined. By first investigating simpler PMC, the dielectric response of the multicomponent insulation system after aging will be more easily analyzed. This is important as the layered nature of the insulation will add additional complexities to the DETA.

The five sections that follow are: 8.1. Sequential Aging; 8.2. DETA of PMC: Nano-silica Modified PMC; 8.3. DETA of PMC: Mica-filled; 8.4. DETA of PMC: Fiberglass Laminate; and 8.5. DETA of PMC: Epoxy-Mica-Fiberglass Tape.

8.1. Sequential Aging

Serial aging treatments were carried out for cured silicone resin (Sn0) and cured epoxy resin (Pn0). Thermal Aging (100 hrs @ 155°C) after Electrical Aging did not remove the effect of Electrical Aging but there is a small reduction in its effect. For Sn0, additional Electrical Aging caused a slightly greater effect. The real and imaginary permittivities for four Sn0 samples are shown in Figure 1. With Pn0, additional Electrical Aging caused a slightly reduced effect. Changes in dielectric response due to phase separation are suggested to be complicating the aging behavior observed for Pn0. The real permittivity (ϵ') and imaginary permittivity (ϵ") for three Pn0 samples are shown in Figure 2. More specific observations are the following:

Real permittivity of aged silicone: The ϵ' for Electrically Aged silicone (Sn0-ERT) was 22% higher at 50°C and 20% higher at 150°C as compared with that of the heat-treated silicone (Sn0-HT). Sn0 samples heat-treated after Electrical Aging maintained ~20% increase in ϵ' at both temperatures (Sn0-ERT-HT). The percentages are listed in Table 8.1.

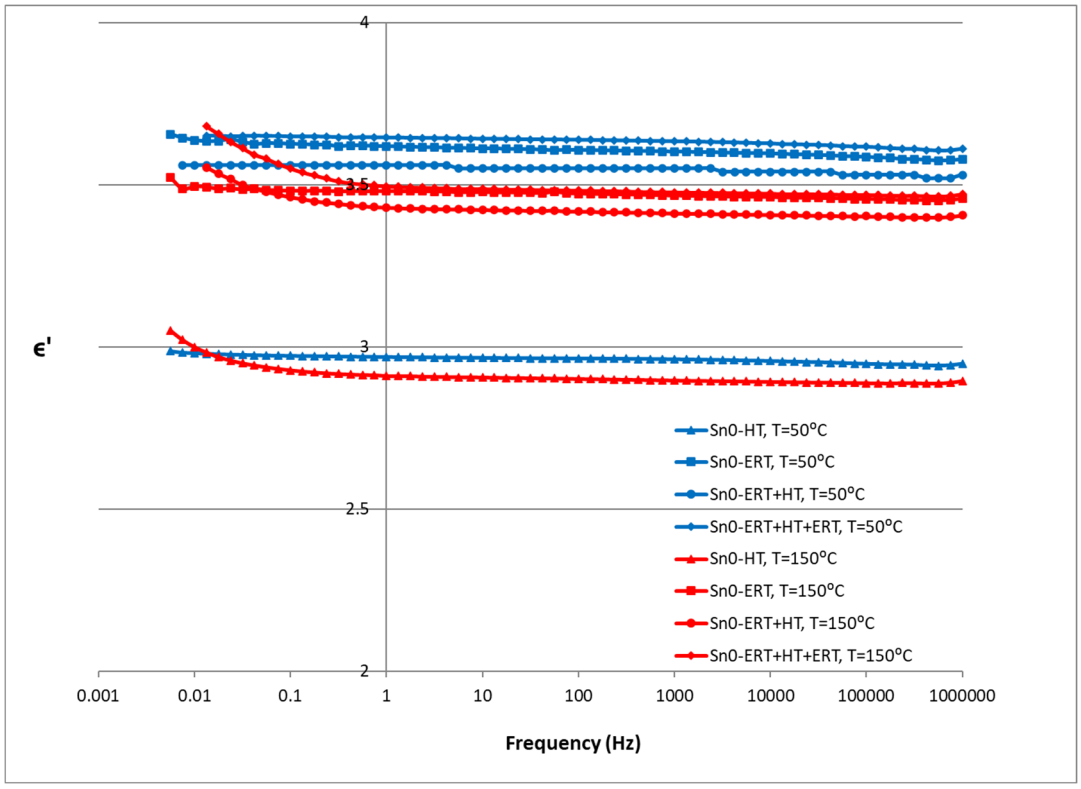
Imaginary permittivity of aged silicone: At 50°C, ϵ" was lowest for the heat-treated sample. At 150°C, samples that received both Electrical Aging and heat-treatment had significantly higher imaginary permittivity at frequencies below 10 Hz. All Sn0 samples exhibited the same low frequency behavior dependent on temperature attributed to conductivity loss.

Real permittivity of aged epoxy: The ϵ' at 50°C after Electrical Aging (Pn0-ERT) was 5% higher than that of the heat-treated epoxy (Pn0-HT). After the second Electrical Aging, Pn0-ERT2 had a small reduction in real permittivity across the frequency range. At 150°C, the real permittivities of the Electrically Aged samples showed similar behavior. The broad band at 10^2 – 10^3 Hz suggests phase separation. This band was not observed in the heat-treated sample. The difference in real permittivity at 150°C with both Electrical Aging treatments is larger at ~12%.

Imaginary permittivity of aged epoxy: The outstanding features of the imaginary permittivity are the appearance of a relaxation peak at 10^3 Hz with Electrical Aging (thought to be related to a secondary γ-relaxation related to newly active, lower temperature T_g); and the large increase at 150°C in ϵ" at frequencies below 1 Hz.

Table 8.1. Percentage change in real permittivity at 1 Hz, compared with heat-treatment, only.

Sample	**Temperature (°C)**	**ϵ'**	**%**
Sn0-HT	50	2.97	-
Sn0-ERT	50	3.62	22
Sn0-ERT+HT	50	3.56	20
Sn0-ERT+HT+ERT	50	3.65	23
Sn0-HT	150	2.91	-
Sn0-ERT	150	3.48	20
Sn0-ERT+HT	150	3.43	18
Sn0-ERT+HT+ERT	150	3.5	20
Pn0-HT	50	4.24	-
Pn0-ERT	50	4.45	5
Pn0-ERT2	50	4.36	3
Pn0-HT	150	4.9	-
Pn0-ERT	150	5.43	11
Pn0-ERT2	150	5.52	13



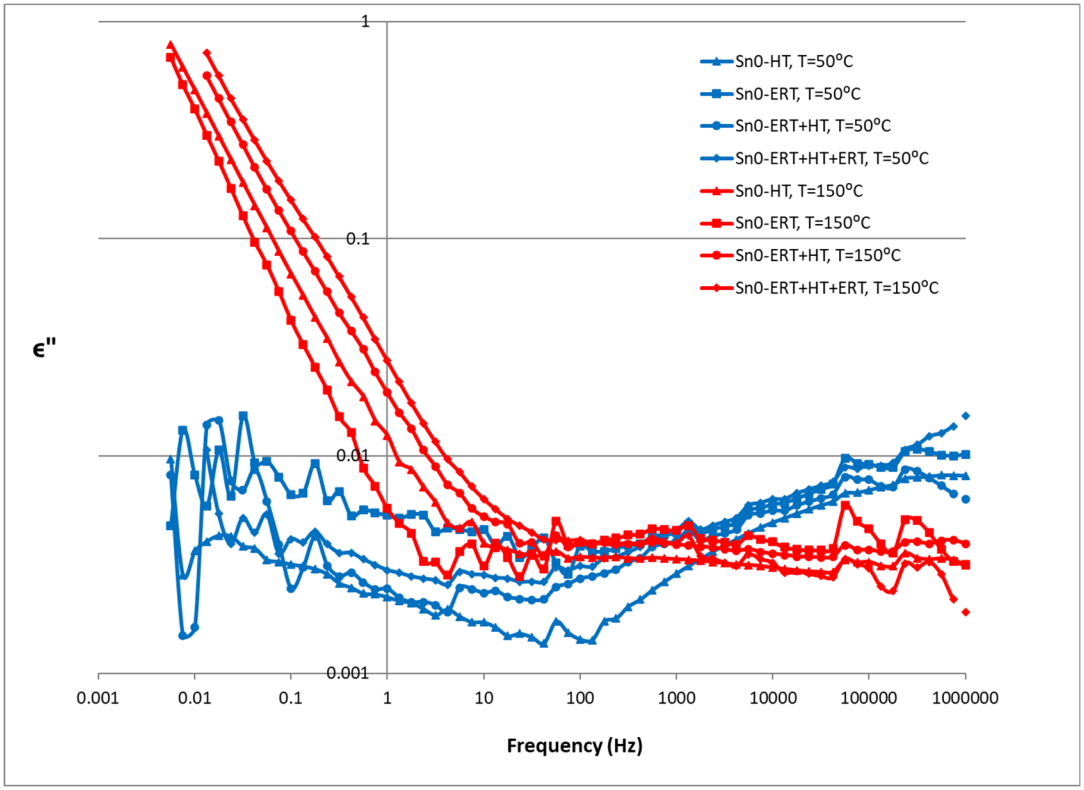


Figure 8.1. Real permittivity (top) and imaginary permittivity (bottom) vs. frequency for Sn0 aged by heat-treating (Sn0-HT), Electrically Aging (Sn0-ERT), Electrically Aging & subsequent heat-treating (Sn0-ERT+HT), and Electrical Aging, subsequent heat-treating, & second Electrical Aging (Sn0-ERT+HT+ERT).

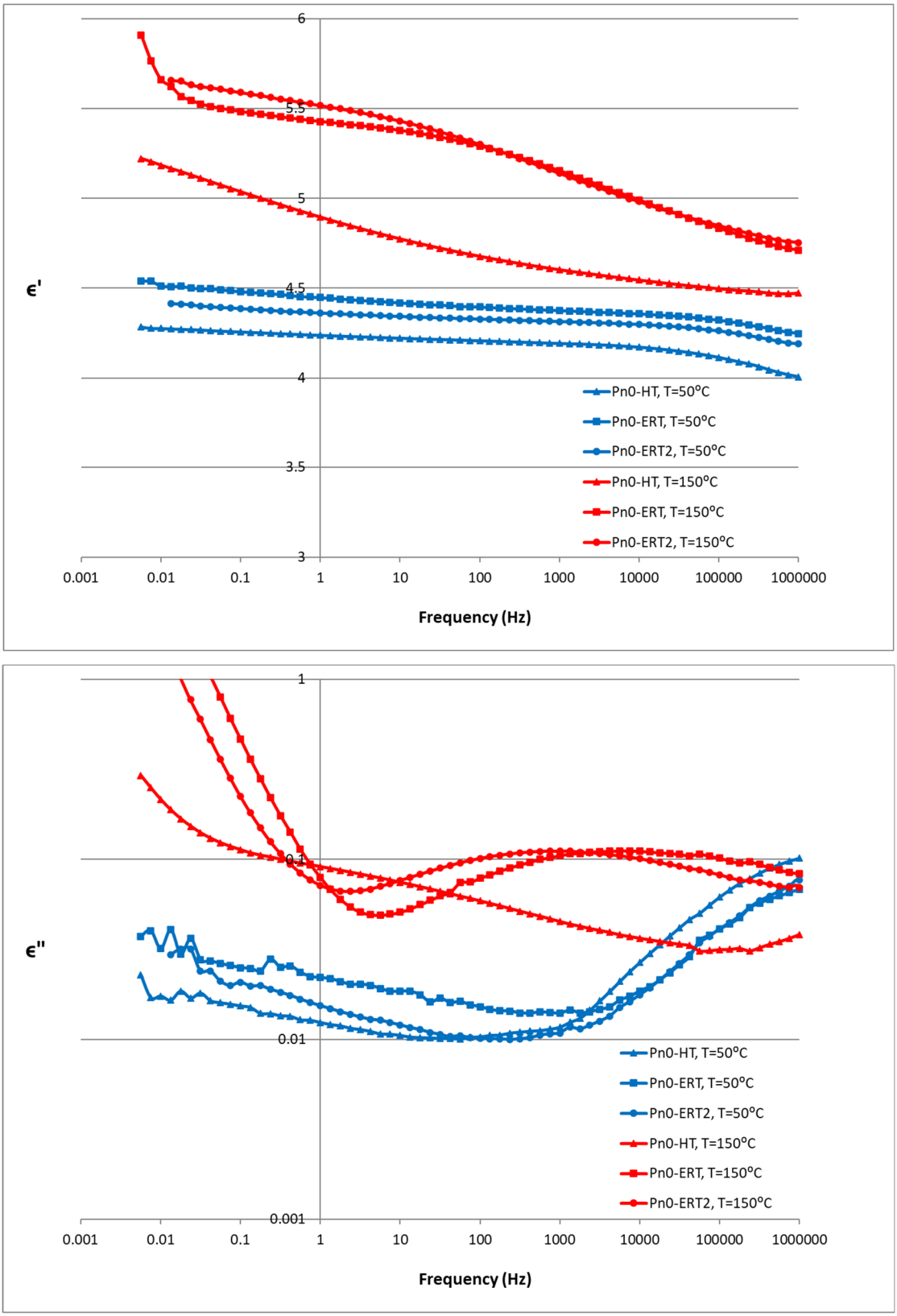


Figure 8.2. Real permittivity (top) and imaginary permittivity (bottom) vs. frequency for Pn0 aged by heat-treating (Pn0-HT), Electrically Aging (Pn0-ERT), and an added second Electrical Aging (Pn0-ERT2).

8.2. DETA of Polymer Matrix Composites: Nano-silica Modified

Modification of an epoxy thermoset and a silicone thermoset by the addition of nano-silica caused small changes in the dielectric behaviors. Larger property changes were observed for the dynamic elastic moduli. The dielectric behavior of the modified and aged epoxy is similar to that of the neat epoxy. DETA at temperatures below room temperature allowed exploration of the β-relaxation.

8.2.1. Nano-silica Modified PMC compared with Neat Polymer

Pn0 is the neat thermoset epoxy polymer cured from commercial resin Permafil 74050 from Von Roll. Pt0 is Permafil 74050T, the same resin as 74050 and modified by the addition of nano-silica to provide thixotropy prior to cure. The real and imaginary permittivity spectra for Pn0 and Pt0 in as-cured condition are compared in Figure 8.3. The real and imaginary permittivities are similar across the frequency spectrum at both temperatures. At 150°C, a low intensity and broad γ-relaxation between 1-10^4 Hz is readily observed for Pt0, but more difficult to detect for Pn0. This mode is not indicated at 50°C and is believed related to a second T_g. The dynamic storage modulus of the epoxy was reduced 11% at room temperature with the addition of the nano-silica. The same modification lowered the glass transition temperature from 84°C to 52°C (see Figure 8.4).

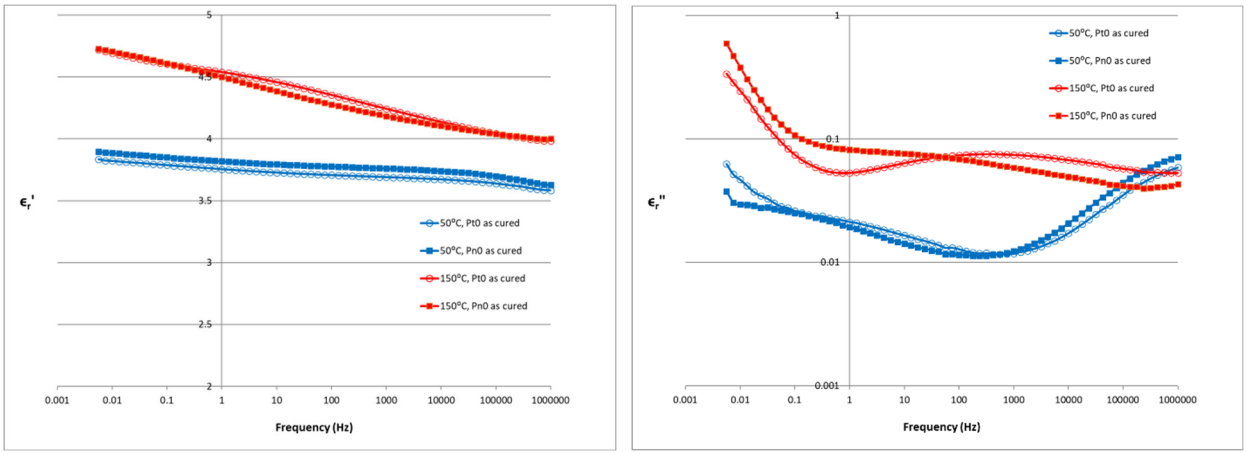


Figure 8.3. Real permittivity (left) and imaginary permittivity (right) spectra for Pt0 (nano-silica modified epoxy) and Pn0 (neat epoxy).

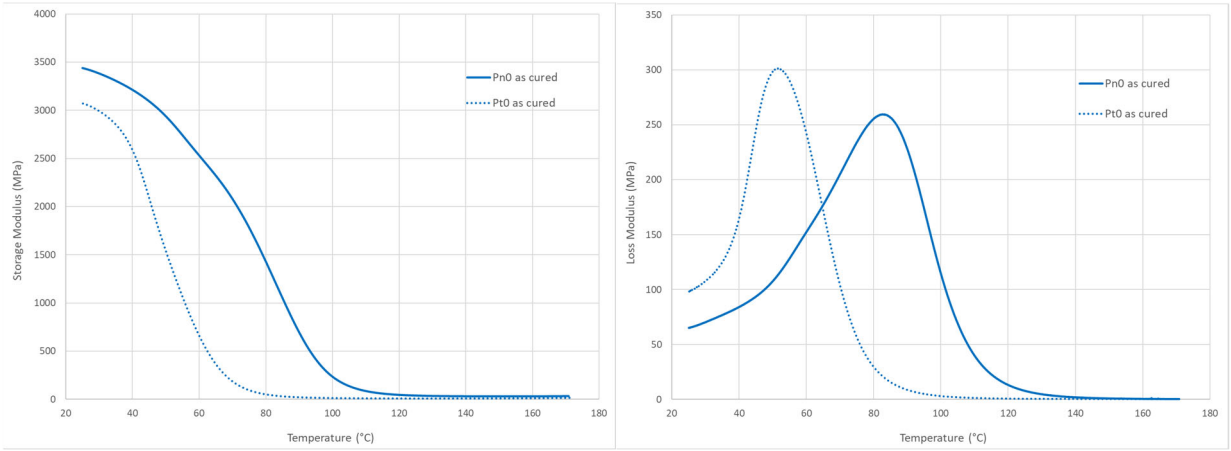


Figure 8.4. Dynamic storage modulus (left) and loss modulus (right) for Pt0 (nano-silica modified epoxy) and Pn0 (neat epoxy) as a function of temperature.

A similar comparison was made for Sn0 and St0.[17] Sn0 is the neat thermoset polymer cured from commercial resin H62c from Wacker Chemicals Co. St0 is a nano-silica composite produced by addition of 1 wt% TM-710 Cabosil to the H62c resin prior to curing. St0 may be less dense than Sn0, leading to a lower real permittivity across the frequency spectrum at 30°C (see Figure 8.5). A stiffer molecular structure was indicated by Dynamic Mechanical Analysis (DMA), where the dynamic elastic storage modulus for St0 was 12% higher than that of Sn0 at room temperature and the glass transition temperature increased from 55°C to 60°C (see Figure 8.6). Both as-cured silicone materials are brittle. The real permittivity response is essentially flat between 10^1–10^6 Hz, decreasing by less than 2%. At 150°C, a low frequency increase in real permittivity indicates an increase in conductivity, possibly due to the edge of the α-relaxation. The imaginary permittivity of St0 shows no evidence of a MWS-relaxation around 10^3 Hz. The imaginary permittivities for St0 and Sn0 are similar across the frequency spectrum. For Sn0 at 150°C, a small increase in imaginary permittivity between 10^{-2} and 10^2 Hz may indicate a γ-relaxation active above the T_g.

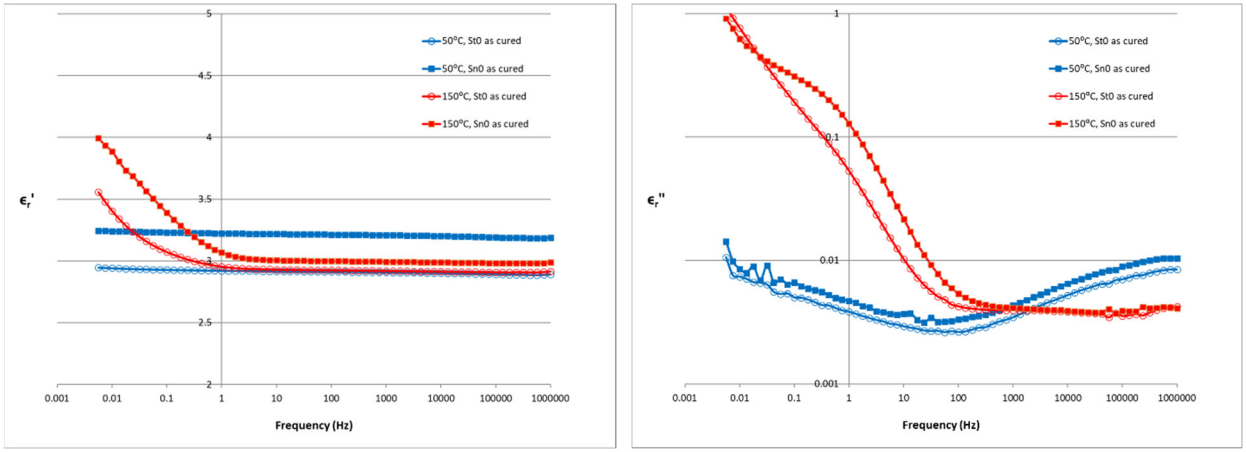


Figure 8.5. Real permittivity (left) and imaginary permittivity (right)spectra for St0 (nano-silica modified silicone) and Sn0 (neat silicone).

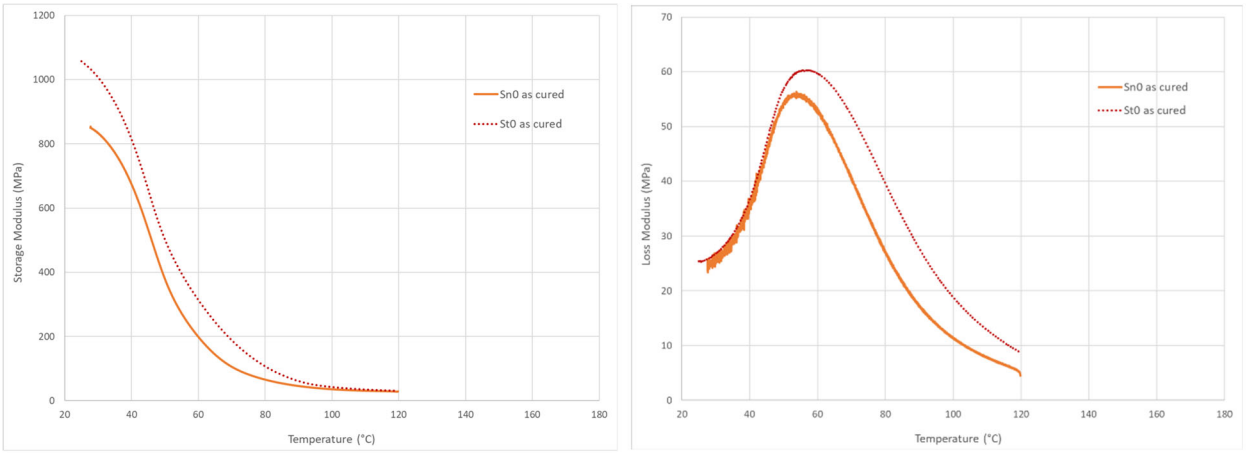


Figure 8.6. Dynamic storage modulus (left) and loss modulus (right) for St0 (nano-silica modified silicone) and Sn0 (neat silicone) as a function of temperature.

[17] The DETA of Sn0 and St0 after dynamic field aging treatment is not available at this time.

8.2.2. Mechanical Aging of Nano-silica Modified Epoxy

Samples of Pt0 and Pn0 were mechanically aged at room temperature. DETA spectra were then produced. The spectra shown in Figure 8.7 were measured at 30°C. The electric moduli of Permafil epoxy show evidence of mechanical aging both with and without nano-silica modification. Pn0 and Pt0 respond to mechanical aging in the same manner: the real moduli decrease. The imaginary moduli also indicate a small decrease across the spectrum.

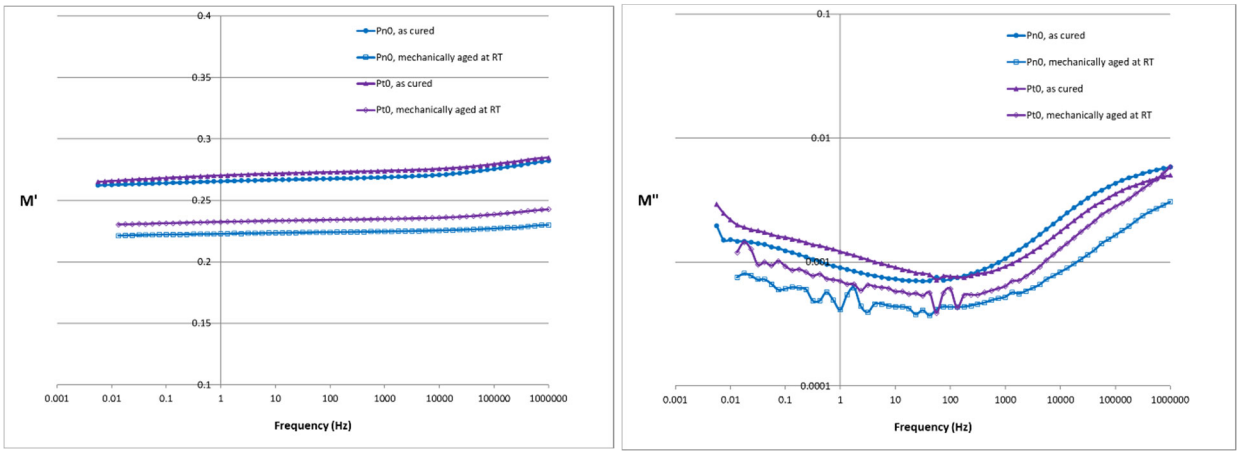


Figure 8.7. Real electric modulus (left) and imaginary electric modulus (right) at 30°C for Pt0 (nano-silica modified epoxy) and Pn0 (neat epoxy), with mechanical aging as noted.

Phase separation was suggested for unfilled Pn0 as cured (described in section 6.8.1). A similar relaxation mode is observed above 77°C in both M' and M". Termed a γ-relaxation, the mode moves to higher frequencies as temperature increases. Figure 8.8 shows data measured at 150°C. The γ-relaxation is centered around ~50 Hz at 100°C and 10^4 Hz at 150°C for the mechanically aged epoxy; and around ~50 Hz at 100°C and 10^3 Hz at 150°C for as-cured epoxy. Mechanical Aging appears to encourage the γ-relaxation behavior. The presence of nano-silica does not seem to impact the relaxation behavior of the matrix. The γ-relaxation attributed to a newly active glass transition appears at high temperatures in the same frequency range as expected for a γ -relaxation.

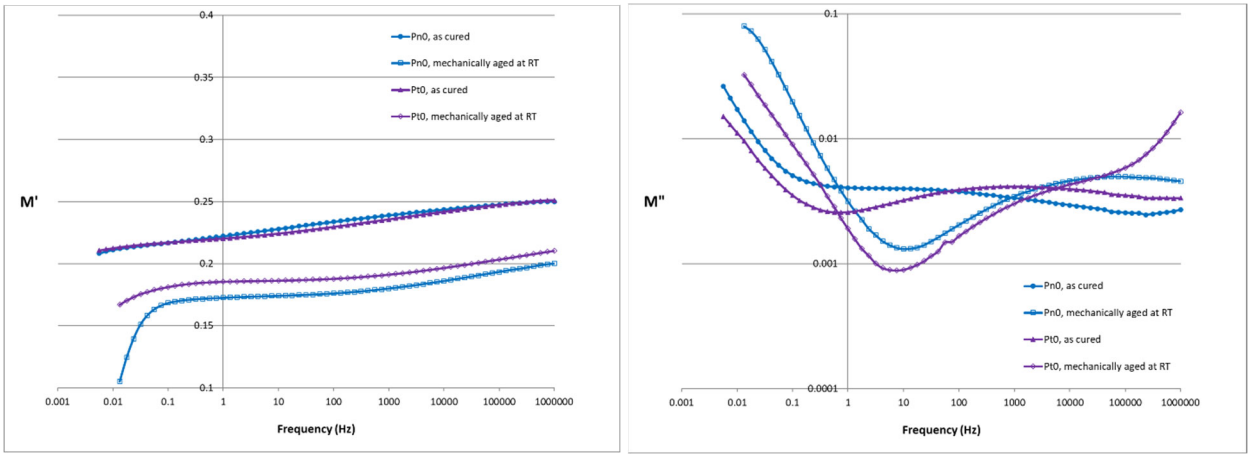


Figure 8.8. Real electric modulus (left) and imaginary electric modulus (right) at 150°C for Pt0 (nano-silica modified epoxy) and Pn0 (neat epoxy), with mechanical aging as noted.

8.2.3. β-relaxation

For the 1 wt% nano-silica modified PMC with epoxy or silicone thermoset matrix, the β-relaxation mode is centered at or above 10^6 Hz at temperatures above room temperature. To examine this relaxation mode, DETA was carried out at lower temperatures. The progress of the relaxation towards lower frequency is shown in Figure 8.9 for Pt0 as an example. The slight reduction in slope past the apex of the relaxation (towards higher frequency) was observed for all thermoset materials studied. The edge of the α-relaxation at low frequency is observed to shift lower in frequency as the temperature is reduced.

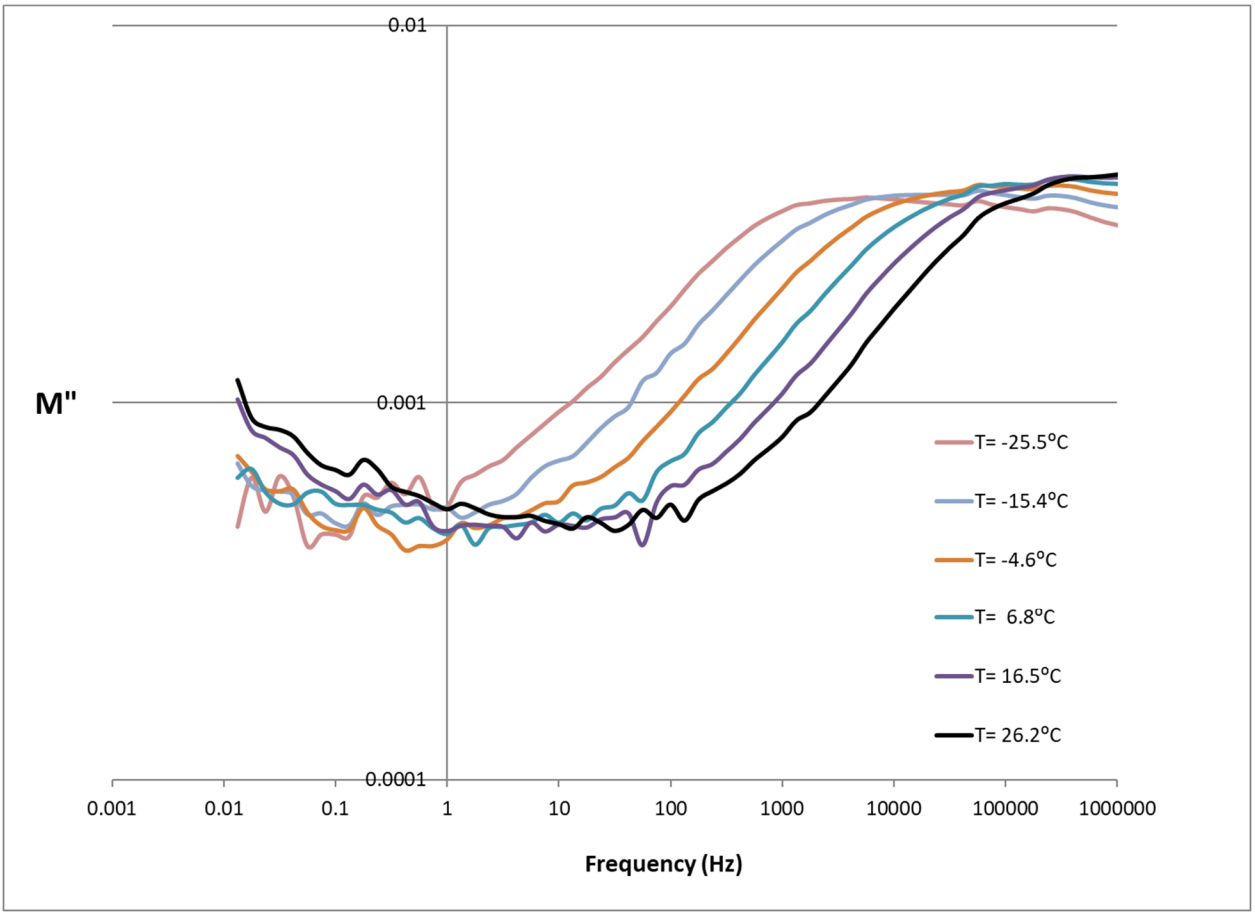


Figure 8.9. Imaginary electric modulus of Pt0 at reduced temperatures.

8.3. DETA of PMC: Mica-Filled

Mica continues to be used in most power-dense insulation systems as its presence provides improved voltage endurance when fully encapsulated by a polymer matrix. The mechanism of this improvement is not fully understood. By its very nature, mica contains a considerable quantity of potassium, fluorine, and hydroxyl ions. The presence of these ions should increase the low frequency polarizability of the polymer matrix composite, particularly as temperature rises. The PMC with mica reported here are:

- Pm0: Permafil 74050 epoxy (Pn0) with 1 wt% synthetic muscovite
- Sm0: H62c silicone (Sn0) with 1 wt% synthetic muscovite
- ME: commercial mica board consisting of ~90 wt% muscovite and 10 wt% epoxy
- MS: commercial mica board consisting of ~90 wt% muscovite and 10 wt% silicone

8.3.1. Mica-Filled PMC compared with Neat Polymer

The real permittivity of Pm0 (1 wt% mica in epoxy) precisely matches that of Pn0-HT (neat epoxy after heat treatment) at 50°C (see Figure 8.10.). At 150°C, the real permittivity of Pm0 has increased above that of Pn0-HT. The imaginary permittivity of Pm0 again mirrors that of Pn0-HT with a pronounced increase at <1 Hz at both 50°C and 150°C. At 150°C, a broad relaxation is visible around 10^3 Hz.

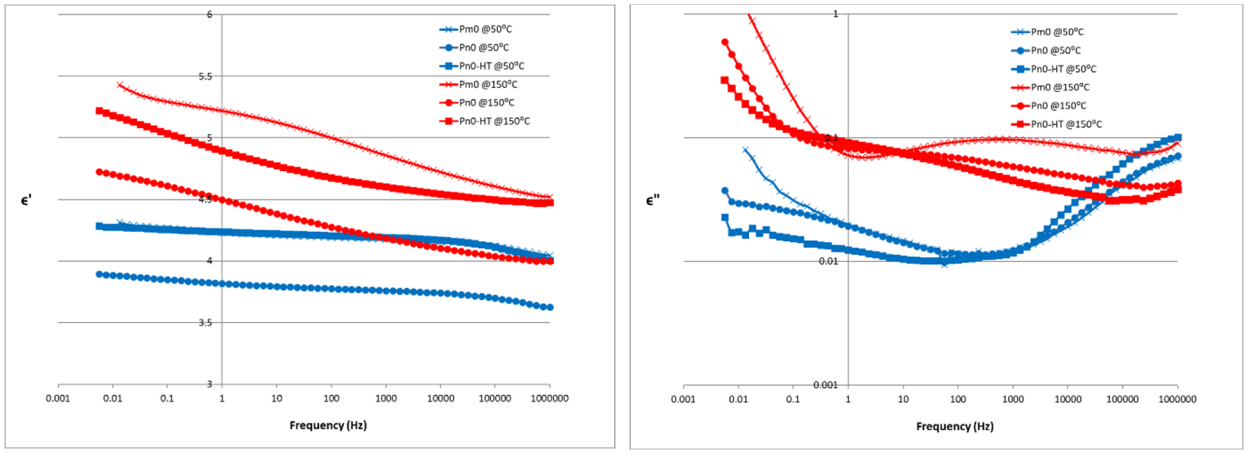


Figure 8.10. Real permittivity (left) and imaginary permittivity (right) for Pm0 (mica-filled epoxy), Pn0 (neat epoxy), and Pn0-HT (heat treated neat epoxy) at 50°C and 150°C.

The permittivities of Sm0 (1 wt% mica in silicone) show similar trends (see Figure 8.11). The real permittivities are higher at both 50°C and 150°C as compared with the neat silicone materials; but maintain the low slope of the heat-treated silicone, Sn0-HT. The imaginary permittivities again mirror those of Sn0-HT for both temperatures. There is indication of an γ–relaxation around 1 Hz for Sn0 only at 150°C. The addition of 1 wt% mica improves the impedance behavior of the neat silicone resin, particularly at high temperatures.

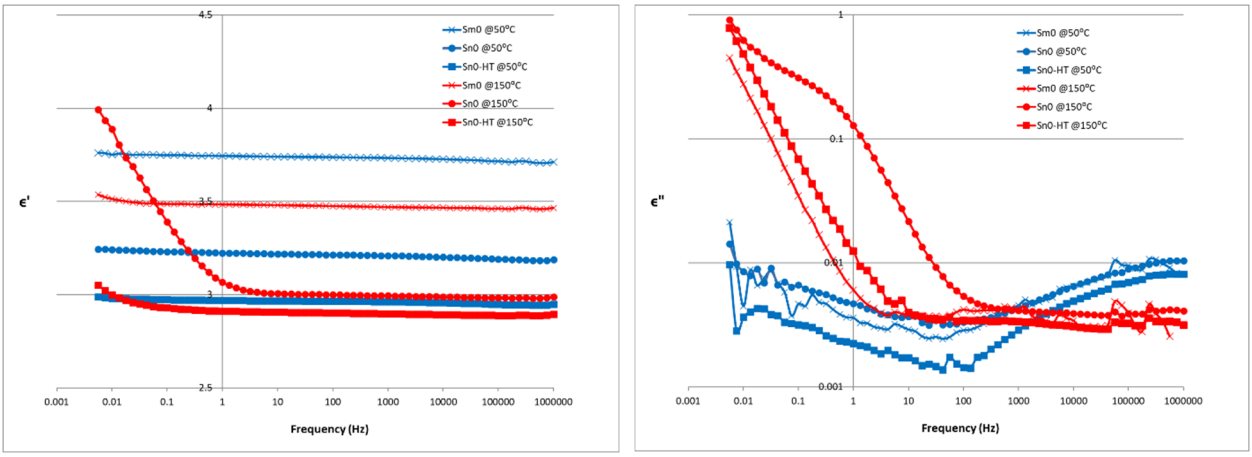


Figure 8.11. Real permittivity (left) and imaginary permittivity (right) for Sm0 (mica-filled silicone), Sn0 (neat silicone), and Sn0-HT (heat treated neat silicone).

8.3.2. Aging of Mica-Filled PMC

Figures 8.12 and 8.13 show the real and imaginary permittivity spectra for Pm0 with various treatments. Pm0-HT was thermally aged, Pm0-ERT was electrically aged, and Pm0-MRT was mechanically aged. DETA was then conducted on the prepared samples. The real permittivities indicate the same general trends with frequency at both temperatures shown. However, the thermal aging appears to have minimal impact, whereas the real permittivities after electrical aging and mechanical aging both show the same pronounced increase in permittivity across the spectrum. The increase in real permittivity with thermal aging was also observed in the neat epoxy, Pn0-HT (see Figure 8.10), but the values here are slightly higher. It is suggested that these uniform differences represent changes in density due to the treatments.

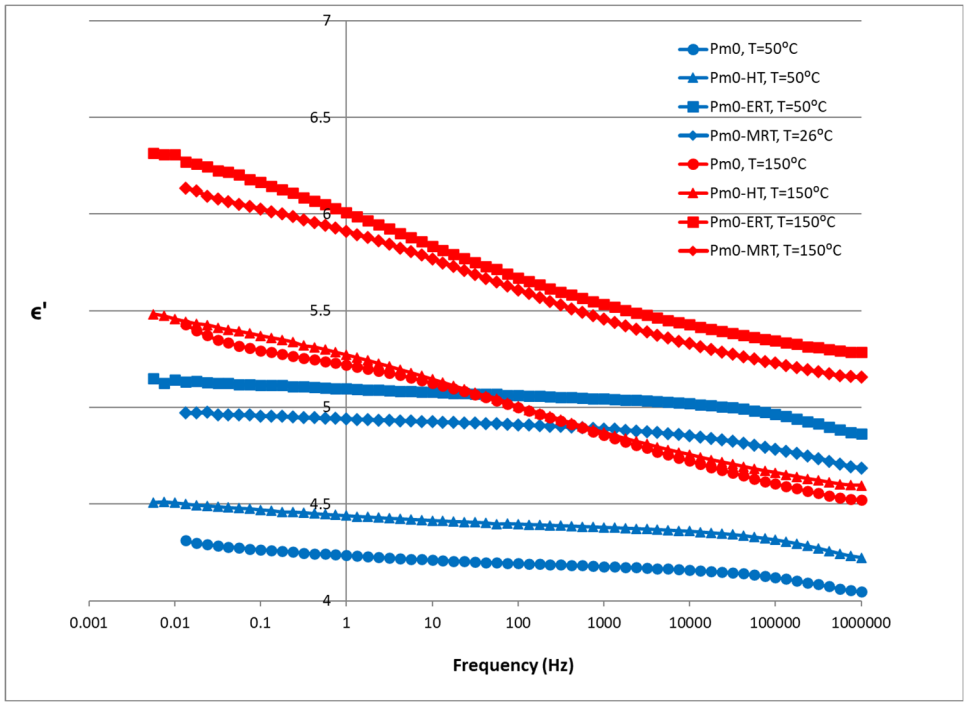


Figure 8.12. Real permittivity for Pm0 (mica-filled epoxy) after treatments, measured at 50°C or 150°C.

The imaginary permittivites show the typical behavior of thermoset polymers for this frequency range. The imaginary permittivities increase at frequencies below 1 Hz and this increase is accentuated at 150°C. This is progression of the α-relaxation edge. At 10^6 Hz, the imaginary permittivities are on the same order of magnitude for both 50°C and 150°C. At 150°C, all indicate an additional broad relaxation around 10^3 Hz, suggested to be a secondary γ-relaxation.

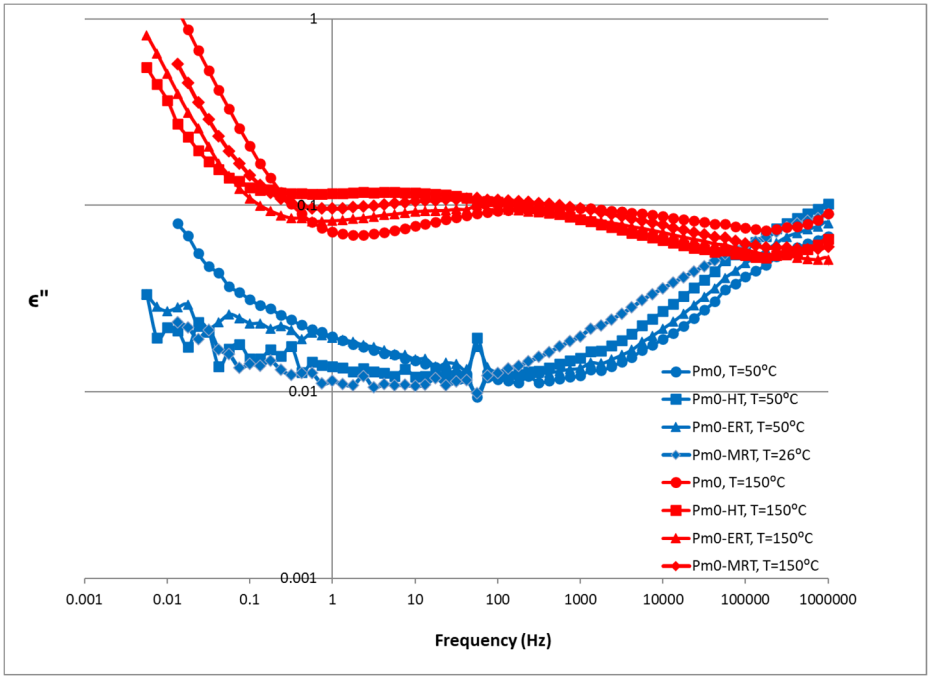


Figure 8.13. Imaginary permittivity for Pm0 (1 wt% mica-filled epoxy) after treatments, measured at 50°C or 150°C.

The permittivities for 90% mica PMC after thermal aging and thermal aging+dynamic electric aging are shown in Figures 8.14 and 8.15. The values are significantly higher than for PMC with low mica concentrations. Both ME and MS present high slopes decreasing towards 10^6 Hz. The slopes are more pronounced at 150°C then 50°C. This low frequency activity is suggested to be due to the high concentration of ions present in the mica.

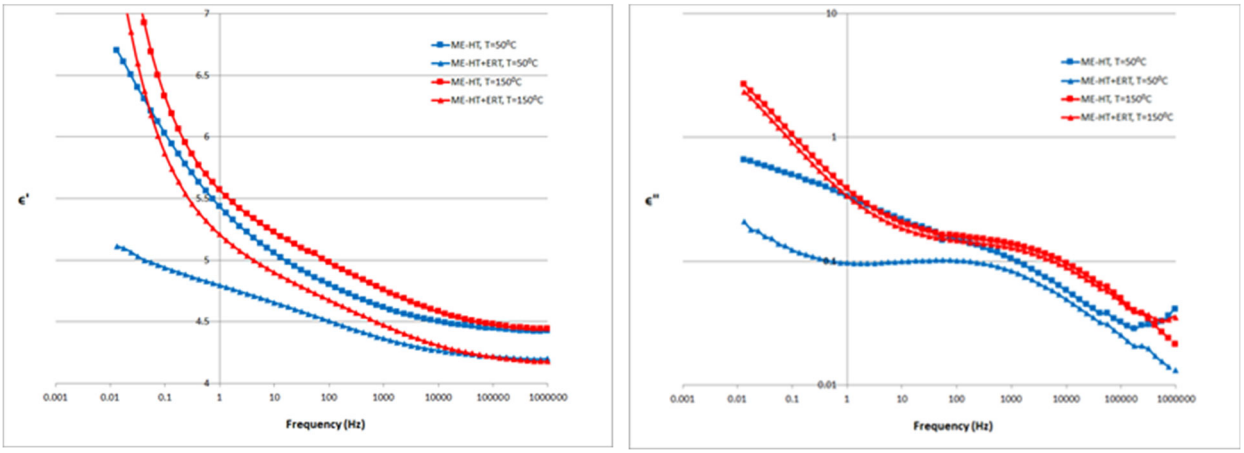


Figure 8.14. Real permittivity (left) and imaginary permittivity (right) for ME-HT (high mica-epoxy after heat treatment), and ME-HT+ERT (after heat treatment and electrical aging).

The heat-treated and subsequently electrically aged ME-HT+ERT material shows a pronounced reduction in real permittivity. Interestingly, the loss permittivity is lower for ME-HT+ERT at low temperature, but the values are almost identical at high temperature. A broad relaxation is again observed around 10^3 Hz at both temperatures. The effect of electrical aging on the MS material after heat treatment had less impact on permittivities within this frequency range. A slight increase in real permittivity tapering to 10^6 Hz was observed for MS-HT+ERT at 50°C.

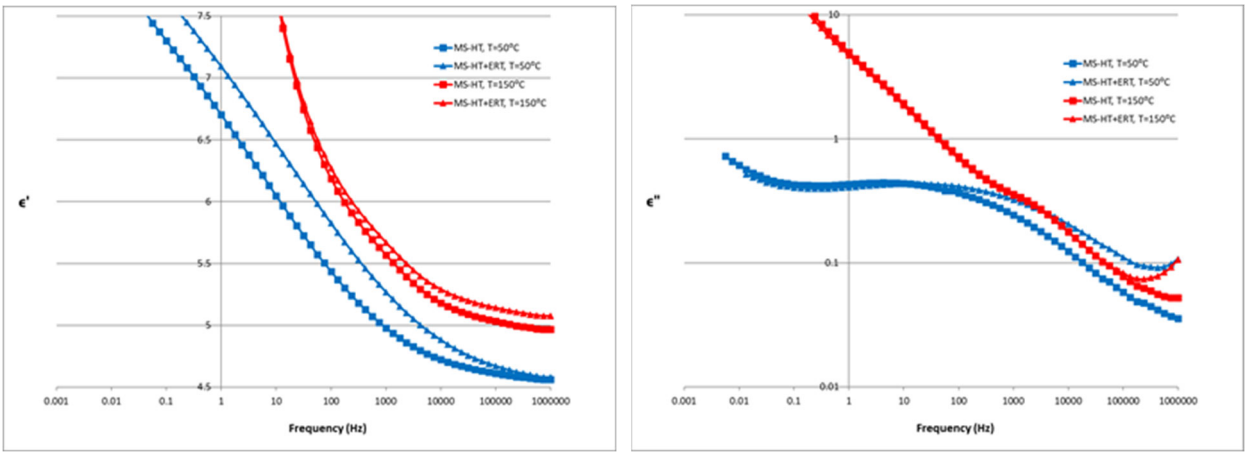


Figure 8.15. Real permittivity (left) and imaginary permittivity (right) for MS-HT (high mica-silicone after heat treatment), and MS-HT+ERT (after heat treatment and electrical aging).

8.3.3. MWS-relaxation

The 90% mica PMC exhibit a broad relaxation around 10^3 Hz in the imaginary permittivity spectra. All indications are that this is the Maxwell-Wagner-Sillars (MWS) relaxation expected of dielectric composites where there is a difference in the permittivities of the phases. It appears in the same frequency regime as observed α-relaxations (corresponding to a low T_g, lower than the T_g corresponding to the primary α-relaxations for these polymers). This relaxation was observed in the neat polymers at 150°C. With both thermoset polymer matrices, the 1 wt% mica-filled composites presented a γ-relaxation around 10^3 Hz at 150°C (see Figure 8.13). With aging treatments, this relaxation appears to shift to lower frequencies. The γ-relaxation was not observed at 50°C for 1 wt% mica-filled composites. The MWS-relaxation was present for all temperatures in the imaginary permittivity spectra of 90% mica PMC. The MWS-relaxations were also more intense at the high mica concentration. Curve fitting algorithms may help to determine if the MWS-relaxation shifts in frequency with temperature and concentration (see section 9). However, any such shifts present are relatively small compared with those of α-relaxations and β-relaxations.

8.4. DETA of PMC: Fiberglass Laminate

The two commercial fiberglass laminate PMC materials described in this section contain woven fiberglass textile and qualify for MIL-1-24768/17 (NEMA G7) and MIL-1-24678 (NEMA FR5). These commercial laminate materials are fully processed unlike resin-impregnated fiberglass tapes used as coil windings. The dielectric behaviors of the fiberglass laminates and fiberglass tapes after cure should be similar. A full set of six aging treatments with subsequent DETA and DMA were completed.

8.4.1. Aging Behaviors of Laminate Composites

The real permittivity and imaginary permittivity for both FR5 (epoxy matrix) and G7 (silicone matrix) laminate PMC materials are compared. Spectra are depicted for both as cured and aged conditions at 50°C and 150°C. (Dielectric response at intervening temperatures were also measured. Spectra for these two temperatures are used to illustrate main points.)

For FR5, a significant relaxation is operational at low frequencies when 150°C is reached (see Figure 8.16). The difference with temperature for both real and imaginary permittivity was more pronounced at lower frequencies gradually tapering by 10^6 Hz. Thermal aging produced a small shift in this relaxation towards higher frequencies. In general, no difference is detected between FR5 when electrically or mechanically aged at room temperature or at the glass transition temperature (see Figures 8.17 and 8.18). Unlike the thermally aged FR5, the real permittivity of the dynamically aged FR5 is observed to increase at both low frequency and high frequency by ~15% as compared with the "as cured" condition. Based on studies with neat epoxy and silicone, an increased density is suggested to be responsible for this increase in real permittivity. The highly nonlinear real and imaginary permittivities of all FR5 samples measured at 150°C are large in magnitude. This indicates a lowered impedance. The nonlinearity observed is assumed due to multiple processes. The electric moduli spectra clearly show the α-relaxation mode. Thermally activated mobility of ionic groups (a Q-DC process) or contribution from a MWS-relaxation is also likely as a contribution of the glass fiber-epoxy interphase.

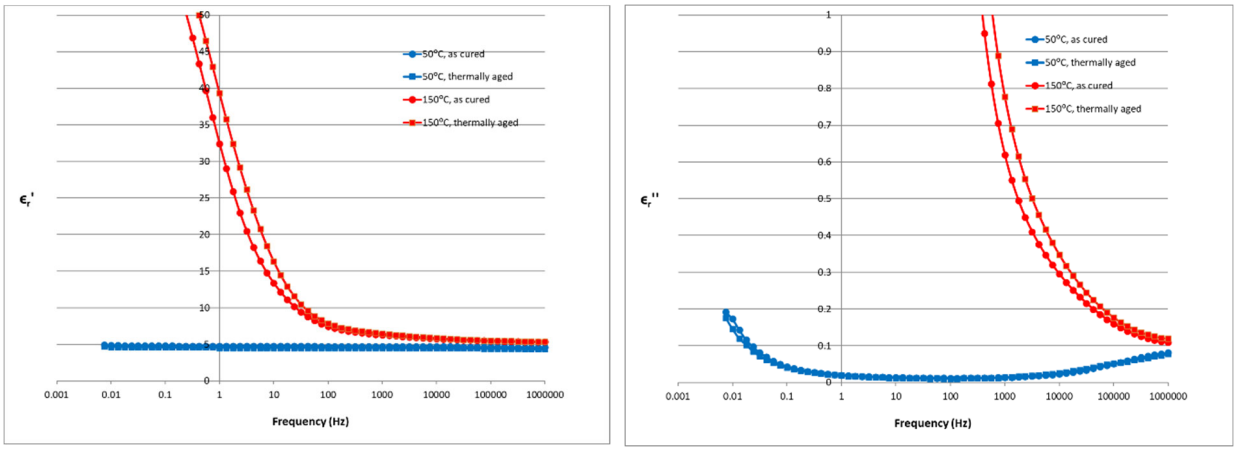


Figure 8.16. Real permittivity (left) and imaginary permittivity (right) for FR5 laminate before and after thermal aging.

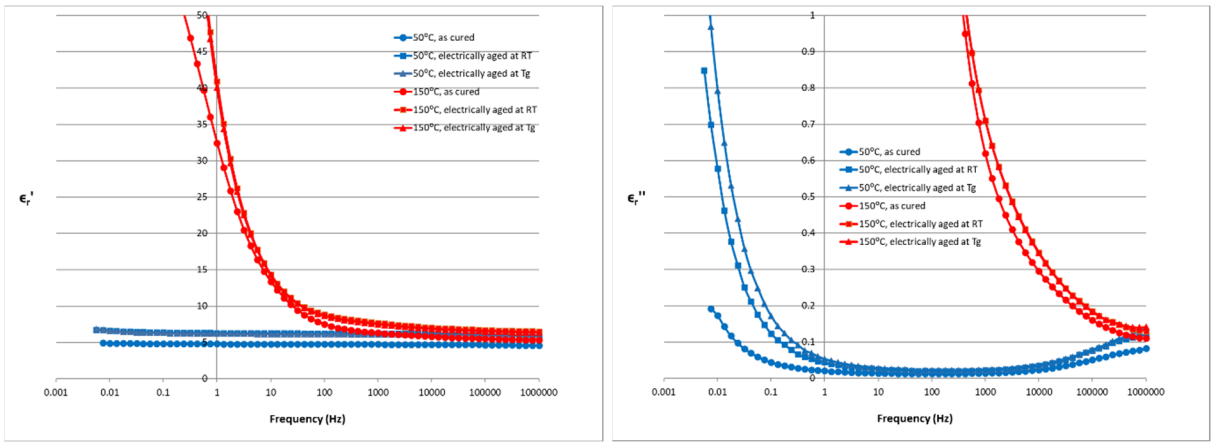


Figure 8.17. Real permittivity (left) and imaginary permittivity (right) for FR5 laminate before and after electrical aging.

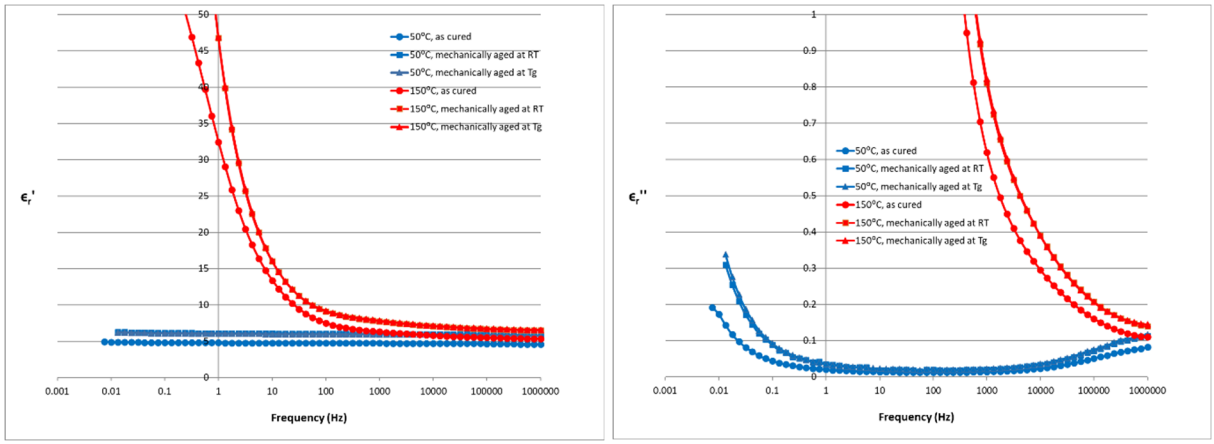


Figure 8.18. Real permittivity (left) and imaginary permittivity (right) for FR5 laminate before and after mechanical aging.

For G7, a pronounced relaxation is again observed at the elevated temperature for all sample conditions. Although similar changes in the spectral form of the real and imaginary permittivities are observed for G7 with temperature, a reduced vertical scale is used in Figures 8.19-8.21. Another general difference is the absence of a high frequency increase (relaxation) in imaginary permittivity at 50°C within this spectral range. The real permittivity of G7 increased slightly (2%) across the frequency range at 50°C after thermal aging. The real permittivity of G7 increased across the frequency range by ~20% for both electrical aging and mechanical aging as compared with "as cured" condition. For electrical aging, no difference was observed when electrically aged at room temperature or at the glass transition temperature. For mechanical aging, however, the room temperature treatment produced enhanced real and imaginary permittivities at low frequencies, a definite difference in dielectric response. The increase in loss was pronounced at low frequencies at both 50°C and 150°C. The behavior mirrors the increase in real permittivity under the same conditions.

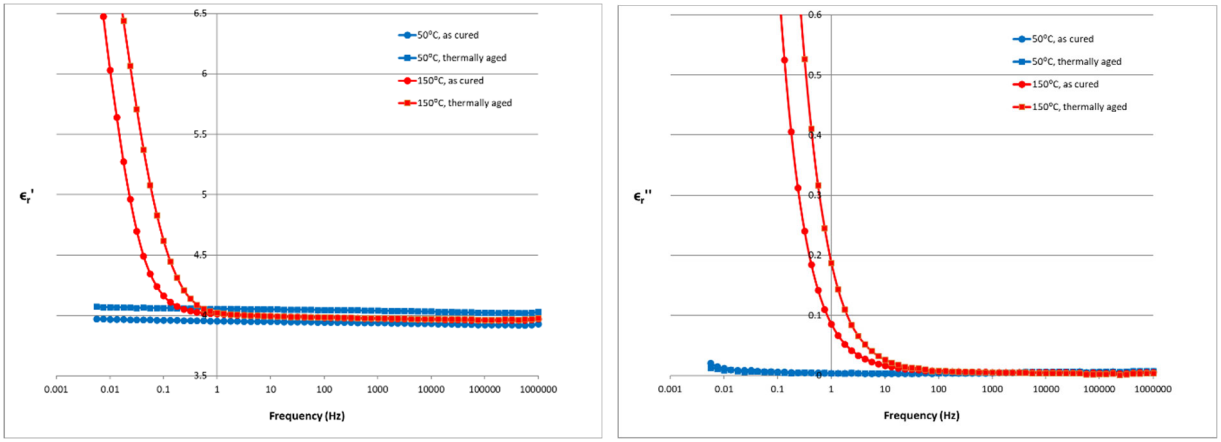


Figure 8.19. Real permittivity (left) and imaginary permittivity (right) for G7 laminate before and after thermal aging.

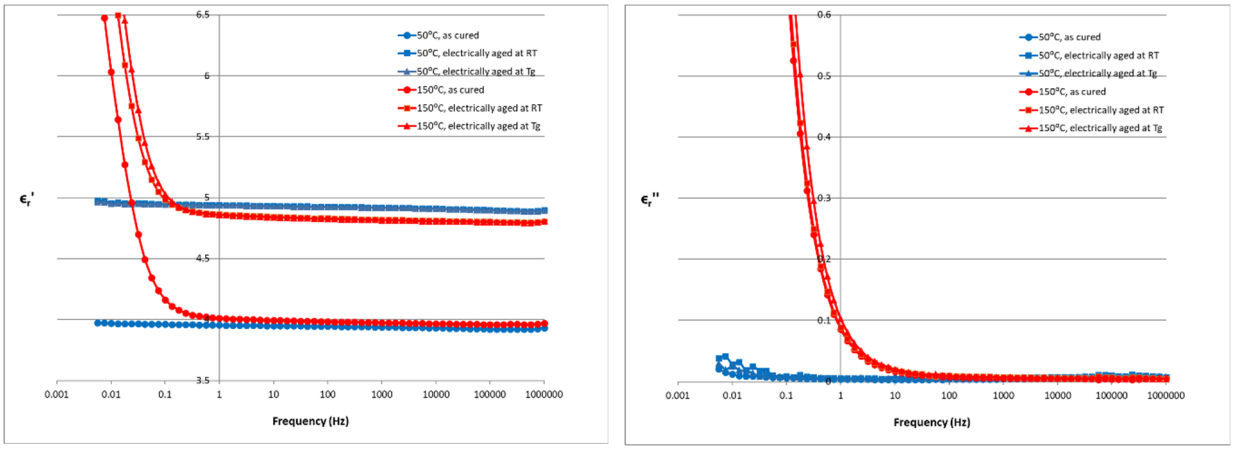


Figure 8.20. Real permittivity (left) and imaginary permittivity (right) for G7 laminate before and after electrical aging.

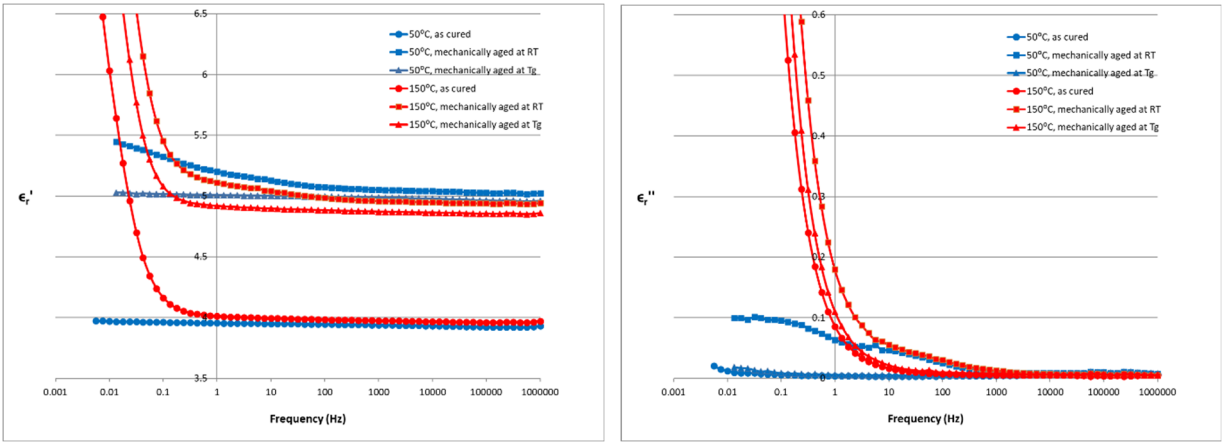


Figure 8.21. Real permittivity (left) and imaginary permittivity (right) for G7 laminate before and after mechanical aging.

As this behavior is unusual in comparison with the other G7 sample conditions, it is high-lighted in Figure 8.22 by green shading. The available data suggests that mechanical aging of the G7 laminate at room temperature actually caused mechanical damage (de-bonding at the glass fiber-silicone matrix interface). The mechanism for the spectral change would be a MWS mechanism, although appearing at frequencies three orders of magnitude less than anticipated (perhaps due to low impedance of the interphase at 50°C).

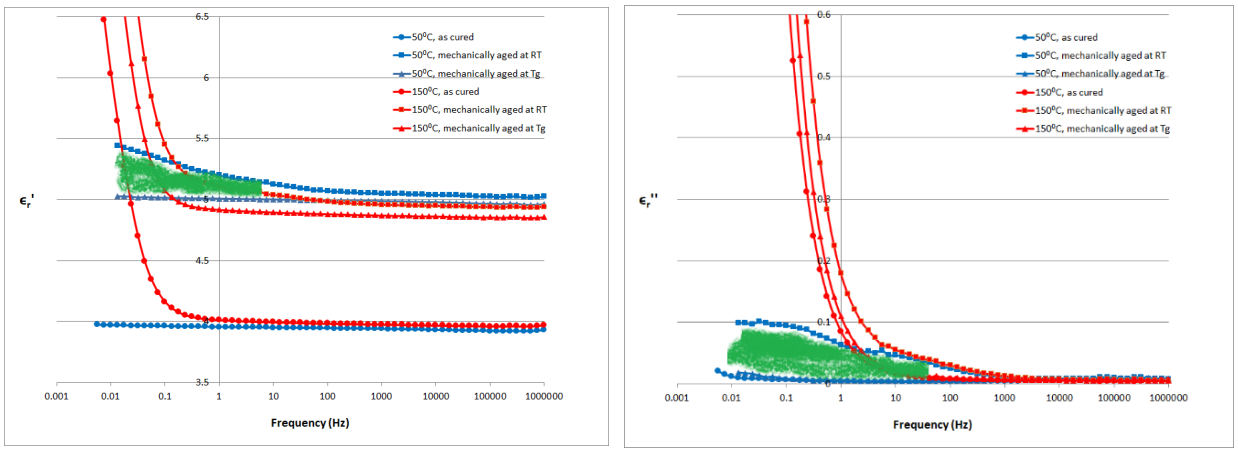


Figure 8.22. Real permittivity (left) and imaginary permittivity (right) for G7 laminate before and after mechanical aging at room temperature with shading added.

8.4.2. Comparison with Neat Resins

The DETA of FR5 laminate is compared with Pn0 and the DETA of G7 is compared with Sn0. All the data in this section are measured at 30°C and depicted as electric moduli.

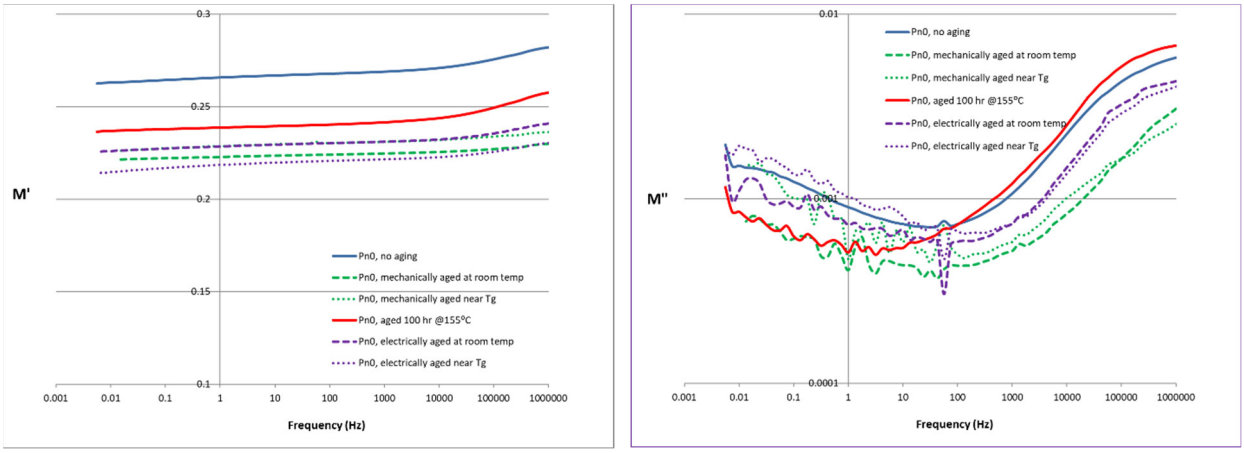


Figure 8.23. Real modulus (left) and imaginary modulus (right) for neat epoxy Pn0 at 30°C before and after aging treatments.

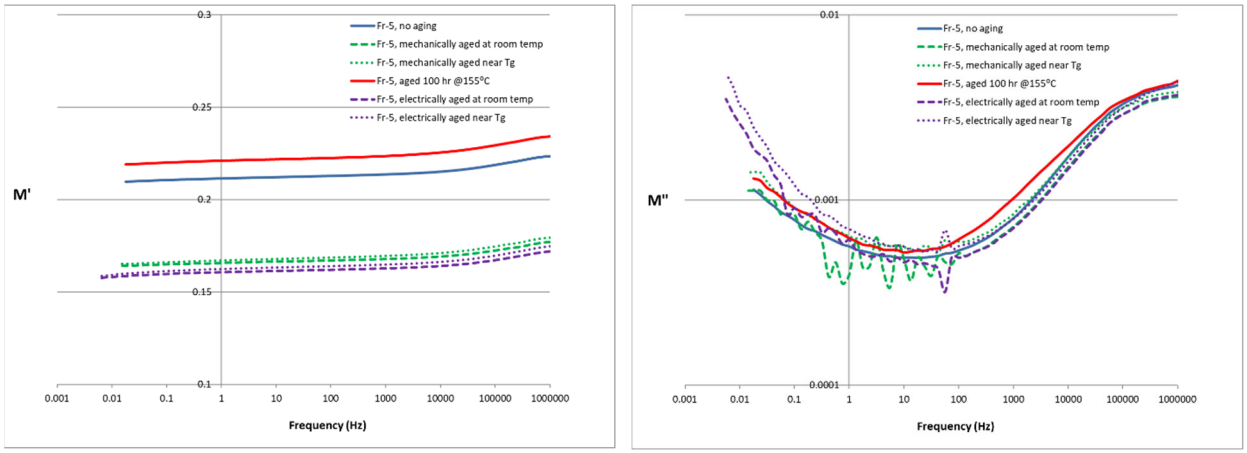


Figure 8.24. Real modulus (left) and imaginary modulus (right) for FR5 laminate at 30°C before and after aging treatments.

The above spectra of electric storage moduli indicate that the aging behaviors of the cured epoxy resin, Pn0, and the fiberglass laminate with epoxy matrix, FR5, are similar near room temperature. Note that at room temperature both polymers are below their glass transition, thus the spectra are essentially dominated by secondary relaxations associated with localized motions of permanent dipoles in the network. The storage moduli are approximately linear with frequency until 10^4 Hz where the slope increases slightly. The real electric moduli for dynamic field aged FR5 are less than 80% of the "no aging" or heat-treated laminate. Although the FR5 real moduli indicate differences with aging treatment, this was not the case with the imaginary moduli. The imaginary loss moduli spectra show the following:

- Pn0 at 30°C is characterized by α-relaxation peaking at $\leq 1x10^{-3}$ Hz and a high intensity β-relaxation peaking at 10^6 - 10^7 Hz. The β-relaxation peak intensity changed very little with aging treatment. FR5 is characterized by α-relaxation peaking at ~$1x10^{-3}$ Hz (higher than pure epoxy) and a high intensity β-relaxation peaking at 10^6 - 10^7 Hz. Only minor differences in β-relaxation peak intensity with aging treatment are observed.
- No MWS-relaxation was identified for FR5 laminate at 30°C, with or without aging treatment.

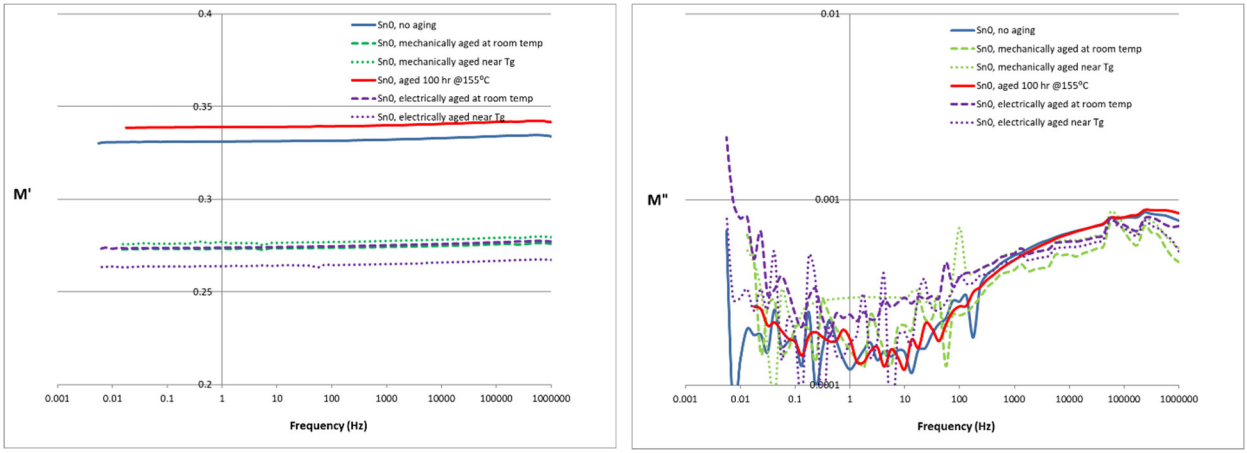


Figure 8.25. Real modulus (left) and imaginary modulus (right) for neat silicone Sn0 before and after aging treatments.

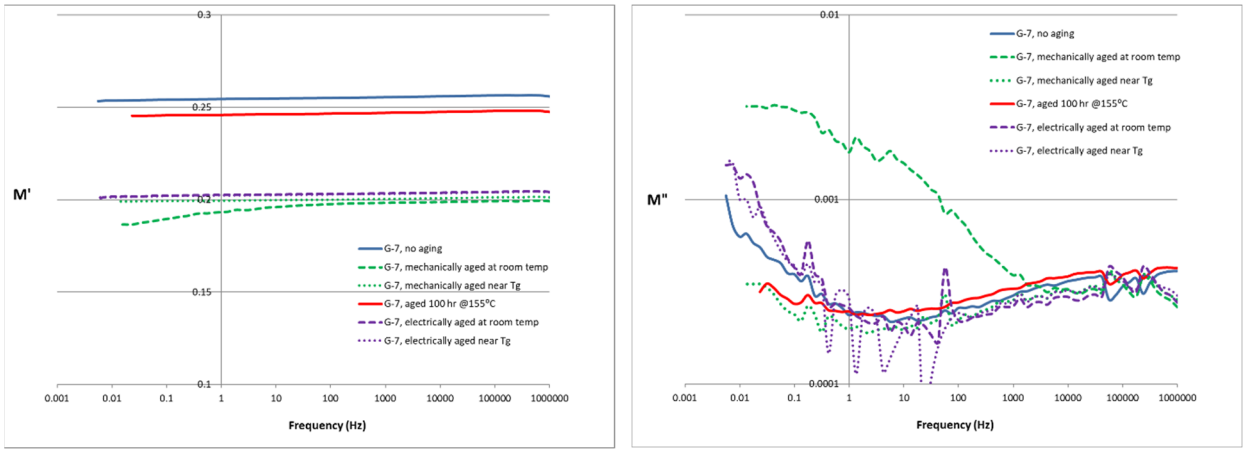


Figure 8.26. Real modulus (left) and imaginary modulus (right) for G7 laminate at 30°C before and after aging treatments.

The spectra of real electric moduli in Figures 8.25 and 8.26 indicate that the aging behaviors of the cured silicone resin, Sn0, and the fiberglass laminate with silicone matrix, G7, are similar. The real electric moduli of the dynamic field aged G7 is ~80% of the "no aged" or heat-treated laminate. All real electric moduli are linear with frequency and have a very low slope. The exception is G7-MRT (mechanically aged at room temperature) that exhibits a reduced modulus at low frequencies. The imaginary electric loss moduli spectra show the following:

- Sn0 at 30°C is characterized by α-relaxation peaking at $\leq 1x10^{-3}$ Hz and a low intensity β-relaxation peaking at $\sim 10^{7}$ Hz, both peaks beyond the range of these spectra. G7 is characterized by α-relaxation peaking at $<2x10^{-2}$ Hz (higher than neat silicone) and a very low intensity relaxation peaking at $\sim 10^{7}$ Hz. This relaxation behavior suggests excellent dielectric response for a highly filled, insulating PMC near room temperature.
- Mechanical aging may be an issue. DETA of G7-MRT indicates a broad MWS-relaxation at $\sim 10^{1}$ Hz, not observed with other aging treatments. The presence of this relaxation is interpreted as due to the initiation of de-adhesion of the fiberglass surfaces to the silicone matrix with the application of 9 kHz vibrations at room temperature. The "relaxation" was not observed with application of 9 kHz at the glass transition temperature. Viscoelastic damping during mechanical aging at the glass transition (G7-MTG) may have protected against de-adhesion at the fiber surfaces.

8.5. DETA of PMC: Multilayer Epoxy-Mica-Fiberglass Tape

Epoxy-mica-fiberglass tapes are used to wrap form-wound coils prior to resin impregnation. This wrapped layer usually forms the ground-wall insulation and is important in mechanically stiffening the coil. As these tapes consist of a minimum of three material components, the structure and properties are complicated. The aging for one tape was assessed to compare with aging of related binary composites. A commercial epoxy-mica-fiberglass tape, Calmicaglas® 4800, was stacked in several layers and cured under pressure. After curing, all samples were heat-treated for 100 hours at 155°C as a thermal aging treatment. Some samples then received additional aging in dynamic fields at room temperature. The tape layers could be peeled apart, suggesting that the epoxy matrix did not fully fill cavities in and between the layers (no epoxy impregnation step was involved). The related binary composites are epoxy-fiberglass laminate (FR5) and epoxy-90%mica (ME).

Figure 8.27 shows the real permittivity and loss permittivity for the thermally aged tape stack (C0-HT), the stack receiving additional electric aging (C0-HT+ERT), and the stack receiving additional mechanical aging (C0-HT+MRT). The real permittivity was reduced at both 50°C and 150°C after dynamic aging treatments. (The exception is a slightly higher permittivity at 50°C and below 1 Hz.) The imaginary permittivities were similar at 150°C for all three conditions. At 50°C, however, the loss permittivity of the dynamically aged samples exhibits a very broad relaxation from <1 Hz – 10^3 Hz. In Figure 8.28, this broad loss band is shown to move towards lower frequencies as temperature increases, beginning to overlap with the α-relaxation. This broad loss band was also observed in C0-HT+MRT, but not for the C0-HT sample (shown in Figure 8.29).

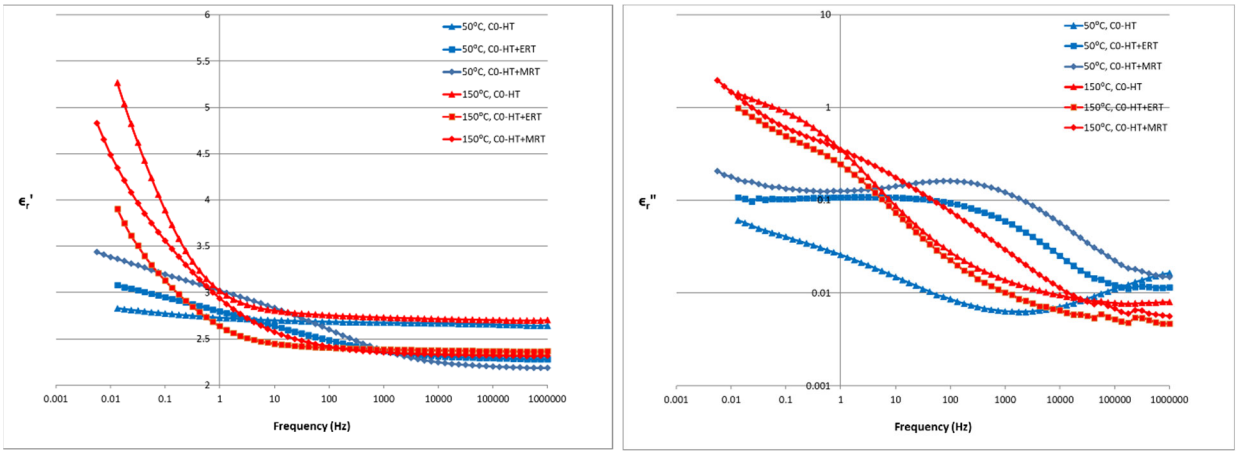


Figure 8.27. Real permittiity (left) and imaginary permittivity (right) for heat-treated Calmicaglas (C0-HT), and after dynamic electric or mechanical aging treatment at room temperature (C0-HT+ERT, C0-HT+MRT).

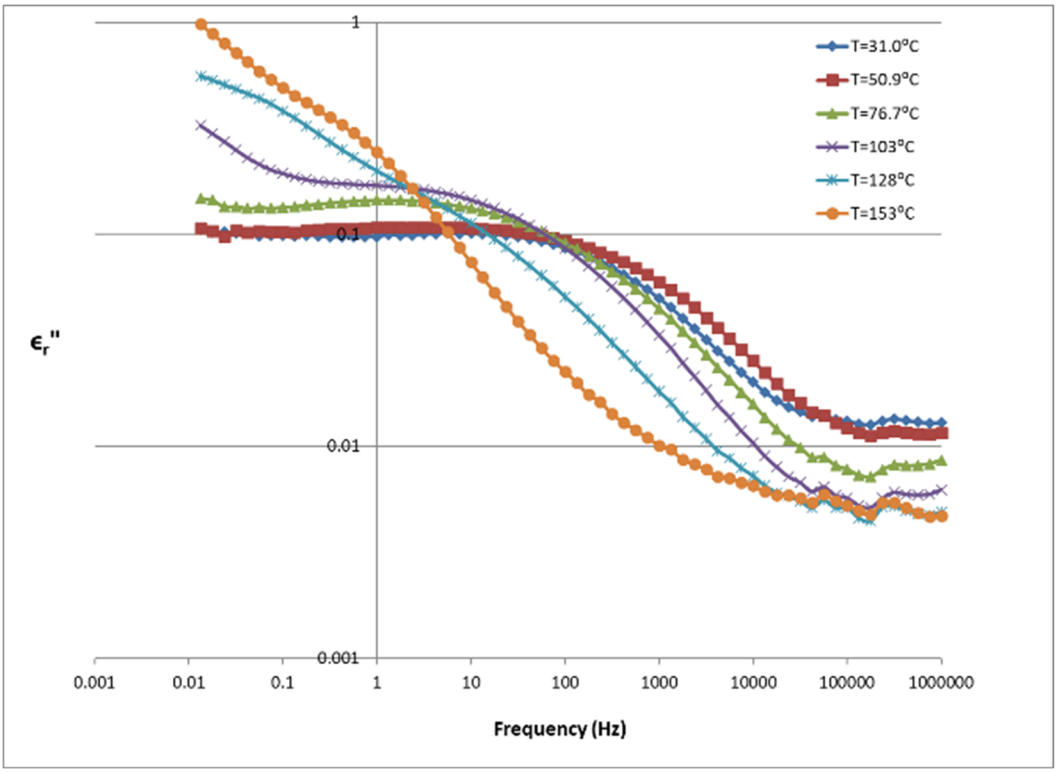


Figure 8.28. Imaginary permittivity at a series of temperatures for heat-treated Calmicaglas (C0-HT+ERT) after dynamic electrical aging treatment .

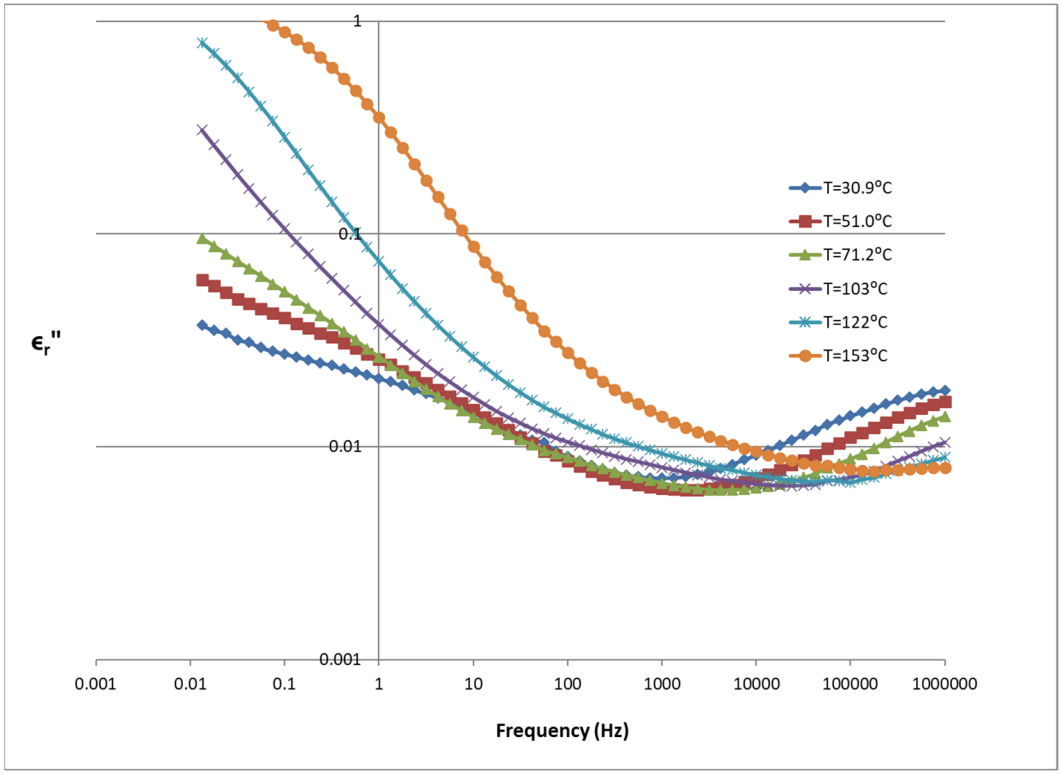


Figure 8.29. Imaginary permittivity at a series of temperatures for heat-treated Calmicaglas (C0-HT).

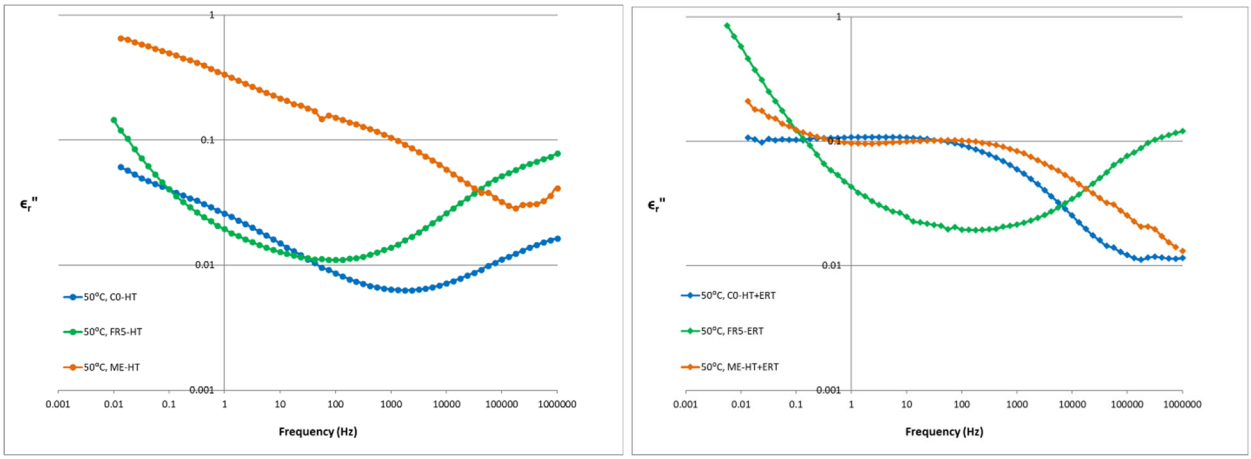


Figure 8.30. Imaginary permittivity at 50°C for Calmicaglas (C0-HT), epoxy-fiberglass (FR5-HT), and epoxy-90%mica (ME-HT) after heat treatment, only (left) and after thermal treatment and/or dynamic electrical aging treatment (right).

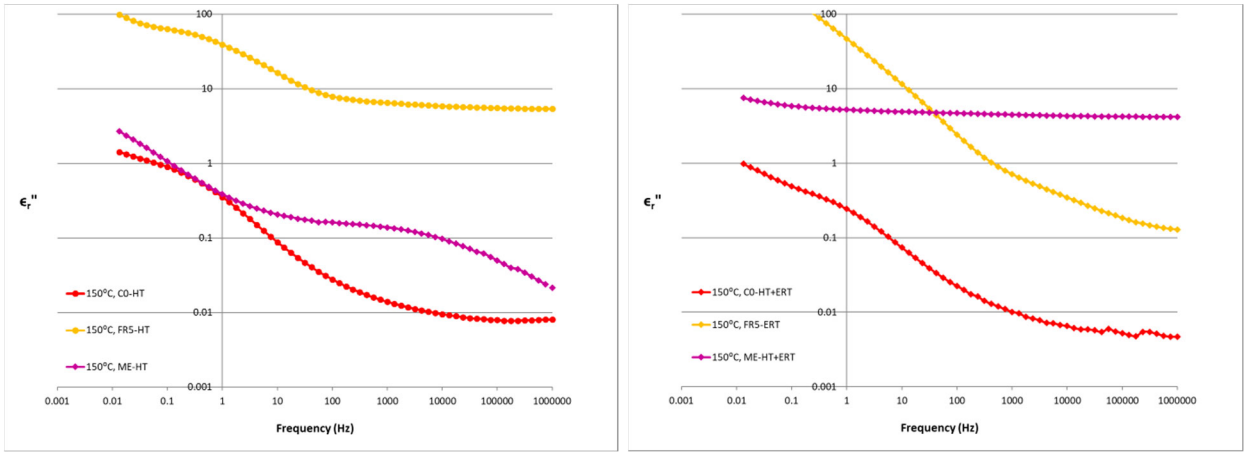


Figure 8.31. Imaginary permittivity at 150°C for Calmicaglas (C0-HT), epoxy-fiberglass (FR5-HT), and epoxy-90%mica (ME-HT) after heat treatment, only (left) and after thermal treatment and/or dynamic electrical aging treatment (right).

Examining the spectral profiles of the three composites, some interesting observations can be made. At 50°C, the Calmicaglas' loss mimics the behavior of the epoxy-90%mica composite. At 150°C, the Calmicaglas' loss mimics the behavior of the epoxy-fiberglass composite. The dominant loss mechanism in the binary composites appears to dominate in the complex composite, as well. This, of course, is surmised as the compositions and dimensions of the components (e.g., the epoxy, the mica, and the glass) were not the same.

Here again it is shown that thermal aging and dynamic field aging produce different effects in dielectrics, yet insulation often is subjected to the stresses that cause varied aging simultaneously and/or intermittently. The change in aging mechanisms with temperature and with aging treatment precludes the accurate use of kinetic models based solely on a simple Arrhenius relationship. A new approach to kinetic modeling is warranted. Furthermore, accelerated aging regimes based on simple Arrhenius models are unlikely to give accurate predictions of aging lifetimes.

Dynamic extensional moduli characterized with DMA are shown graphically in Figure 8.32. The dynamic storage modulus of the layered epoxy-mica-fiberglass sample decreased when dynamic mechanical aging was applied after thermal aging (C0-HT+MRT) and increased with dynamic electrical aging after thermal aging (C0-HT+ERT). Surprisingly, the combination of both electrical aging and mechanical aging after thermal aging further increased the dynamic storage modulus. The dynamic storage moduli at room temperature ranged from 16,000-20,000 MPa (16-20 GPa), above that measured for the epoxy laminate FR5 (~14 GPa, see Figure 6.59). The dynamic loss moduli indicate a glass transition for the epoxy near 100°C and a glass transition for the fiberglass at ~185°C. The large spread in the response may be an indication of less than full encapsulation by the epoxy matrix.

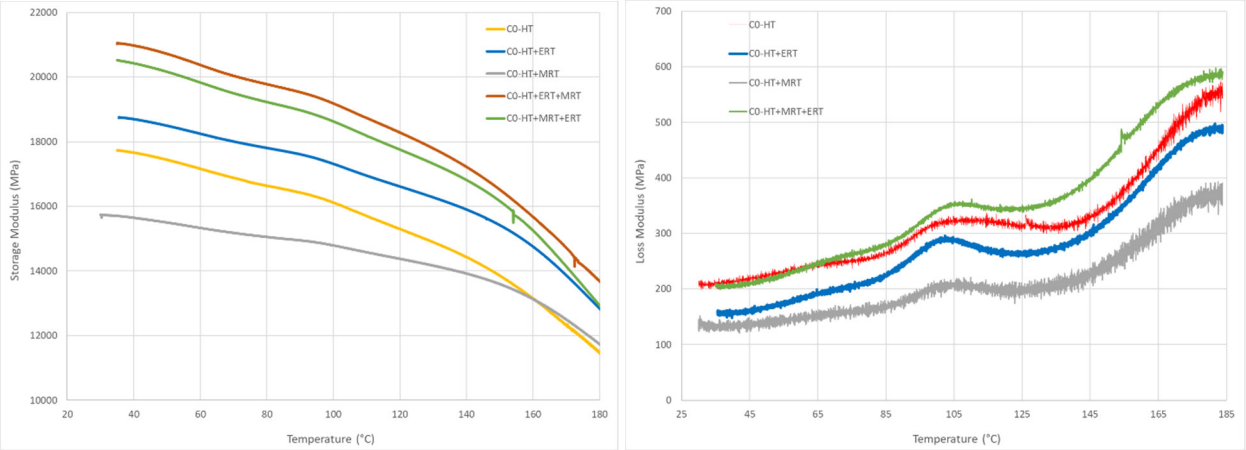


Figure 8.32. Dynamic elastic real modulus (left) and dynamic elastic loss modulus (right) for Calmicaglas after aging treatments.

Large differences between dynamic elastic moduli of samples with identical treatments were measured. This is thought to be due to the incomplete penetration of the epoxy matrix, probably resulting in a low level of residual porosity.

9. Characterization: RELAXATION MODES & ACTIVATION ENERGIES

Dielectric spectra can be represented as a sum of relaxation processes or molecular dynamic modes centered at peak frequencies. The peak frequency is inversely related to the mode's relaxation time, $\tau = 1/(2\pi f_{pk})$. In section 9.1, the spectra are interpreted model-free by using the frequency at peak imaginary electric modulus. Curve fitting of spectra are discussed in section 9.2.

9.1. Activation Energies from Imaginary Electric Moduli

Addressing the thermal energy of a mode is important information. Where N is Avogadro's number, an Arrhenius form of equation typically used is:

$$f_{pk} = f_o \exp \frac{-E}{NkT}$$

Data are fit to this equation to extract a characteristic activation energy, *E*. Another option is based on the Eyring equation, best suited for phase transitions:

$$f_{pk}/T = f_e \exp \frac{-E_e}{NkT}$$

The following compares the derived activation energies for various material conditions. Figure 9.1 shows an example of the α-relaxation mode peaking at frequencies below 10^3 Hz at six temperatures for FR5-ERT, an electrically aged, fiberglass-epoxy laminate. The peak or apex of the relaxation increases in frequency (increases energy) as the temperature is raised. A plot of the $\ln(f_{pk}/T)$ as a function of reciprocal temperature is shown in Figure 9.2, following the Eyring equation.

Linear fits to this data were made at the two highest temperatures (both above the glass transition temperature for each material) and for three temperatures below the glass transition temperature. Both activation energies for the α-relaxation for six FR5 conditions are listed in Table 9.1. (For the lowest temperatures, only the edge of the relaxation was recorded and the peak frequency was extrapolated based on the time-temperature-transposition principle. As the peak frequency of the α-relaxation at the highest reciprocal temperature (lowest temperature) was extrapolated with high uncertainty, this datapoint was not included.) The low temperature activation energy was approximately half of the activation energy above the glass transition temperature. The activation energies of the aged laminates decreased at temperatures below the glass transition temperatures. At temperatures above the glass transition temperatures, the activation energies were higher than for the as received material. This indicates that the aging treatments improved the ability of the polymer network to perform coordinated molecular motion in response to electric fields. (Similar activation energies were calculated using the Arrhenius relationship.)

At 127°C, close to glass transition temperature for four aging conditions of FR5, the full α-relaxation is recorded within the available spectral range. Figure 9.3 shows a Cole-Cole plot of the complex electric moduli. This plot most clearly indicates differences in dielectric response after aging.

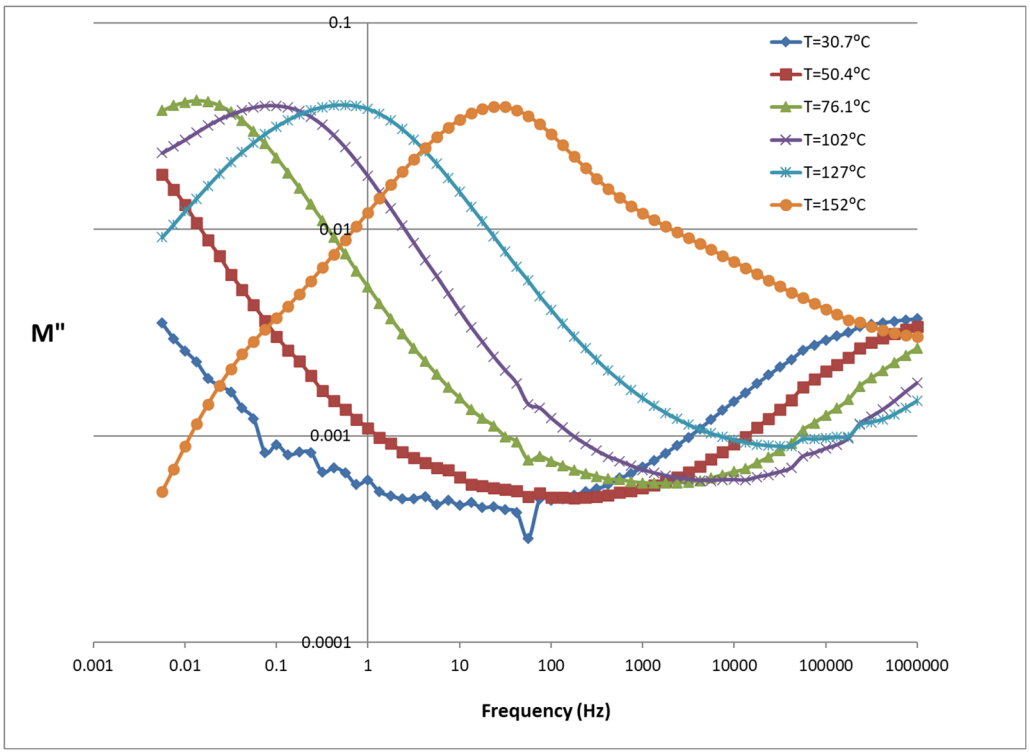


Figure 9.1. Imaginary electric moduli vs. frequency for FR5-ERT (electrically aged at room temperature) shown for six temperatures.

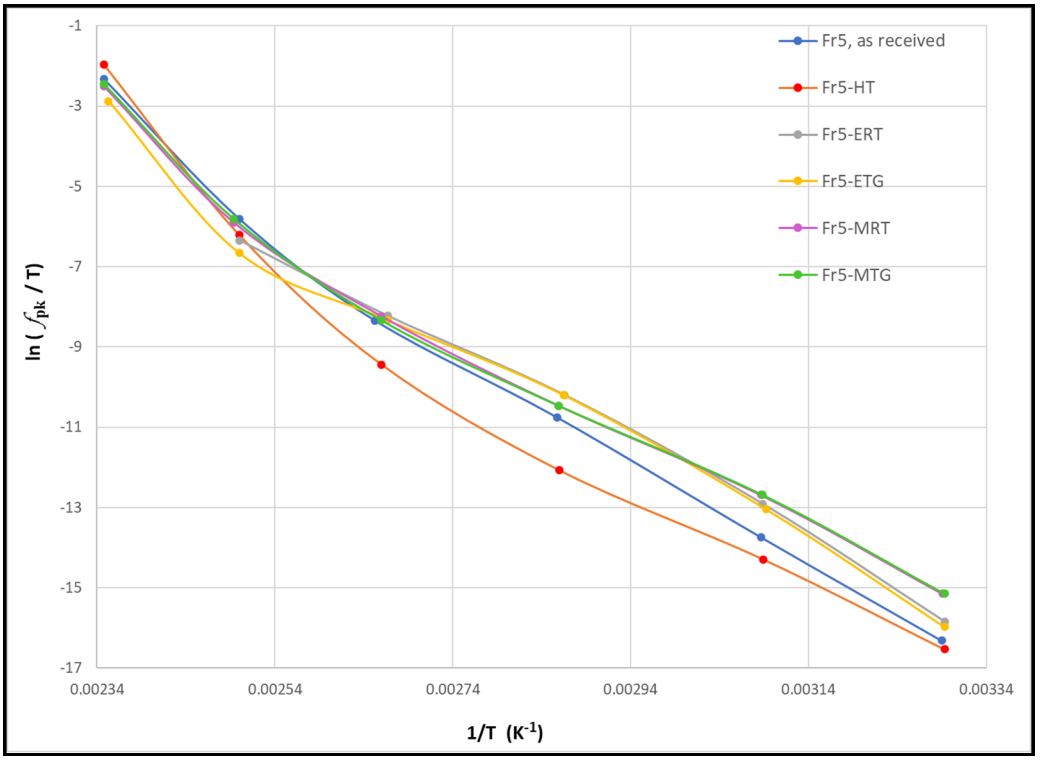


Figure 9.2. Frequency of peak imaginary electric modulus, M", divided by temperature vs. reciprocal temperature for FR5 shown for six aging conditions (as listed in Table 9.1).

Table 9.1. Activation energies for the α-relaxation of FR5 for each aging condition.

Condition	Activation Energy at T>Tg (J/mol)	Activation Energy at T<Tg (J/mol)
FR5 (as received)	1.90×10^5	1.04×10^5
FR5-HT (heat-treated)	2.32×10^5	0.94×10^5
FR5-ERT (electrically aged at RT)	2.09×10^5	0.93×10^5
FR5-ETG (electrically aged at Tg)	2.14×10^5	0.92×10^5
FR5-MRT (mechanically aged at RT)	1.93×10^5	0.87×10^5
FR5-MTG (mechanically aged at Tg)	1.91×10^5	0.84×10^5

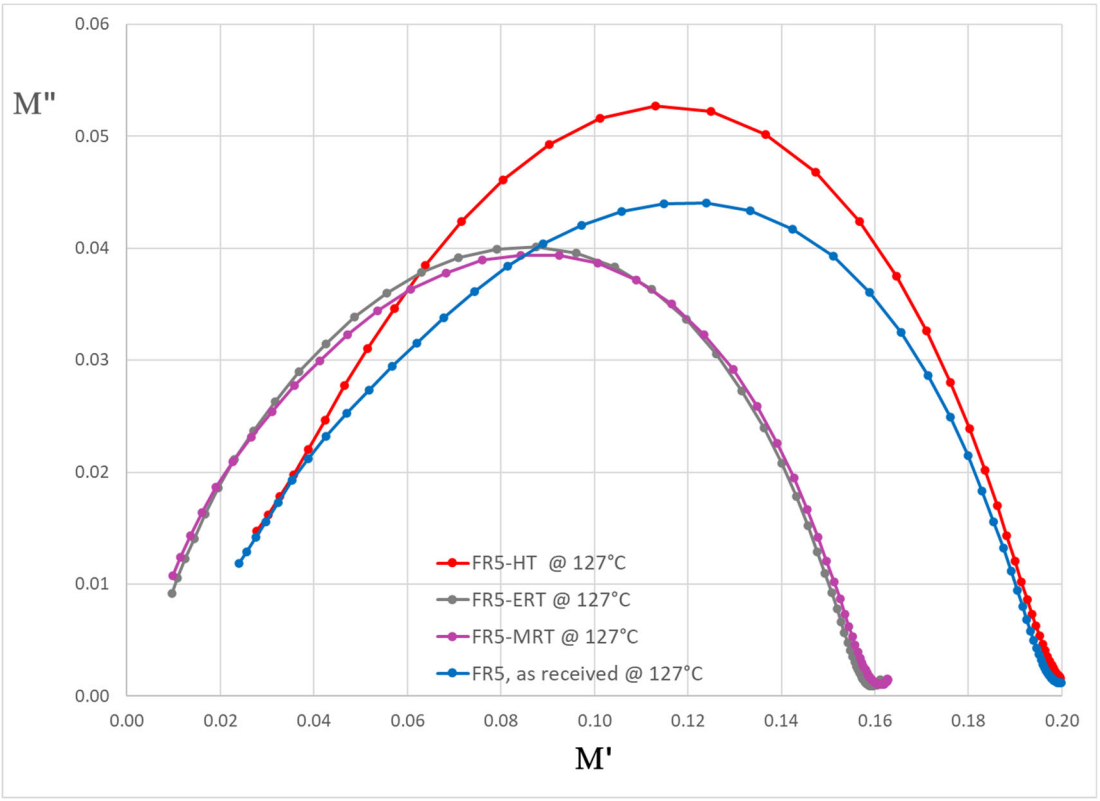


Figure 9.3. Cole-Cole plot of the imaginary electric modulus, M" vs. the real electric modulus, M' for four aging conditions as measured at 127°C.

The MWS-relaxation is not expected to exhibit thermal dependence.[46] The frequency of maximum imaginary loss modulus for this relaxation appears to be somewhat constant for a composite material. As described in section 6, the breath and dielectric strength of the MWS-relaxation does appear to be related to the temperature and amount of second phase. In the case of phase separation or a second glass transition, the γ-relaxation appears to shift in frequency with the changing temperature. These observations require further exploration.

All nano-silica modified and mica-filled PMC exhibited possible γ-relaxation (believed related to a newly active second glass transition at high temperature. At low temperature, the relaxation was not observed. The 90 wt% mica-epoxy composite, ME-HT+ERT, exhibited a uniform progression of the MWS-relaxation mode through the temperature range explored. This commercial PMC had been subjected to heat-treatment followed by electrical aging at room temperature. The MWS-relaxation can be observed as a broad band in the imaginary electric modulus around 10^3 Hz (see Figure 9.3). A slight progression to higher frequency as temperature increased followed an Arrhenius-type behavior with a low activation energy of 1.2×10^4 J/mol. There is a possibility that this shift results from thermal expansion and frequency shifts of the α-relaxation and β-relaxation with temperature. Without significant curve-fitting, weak Arrhenius behavior can only be suggested.

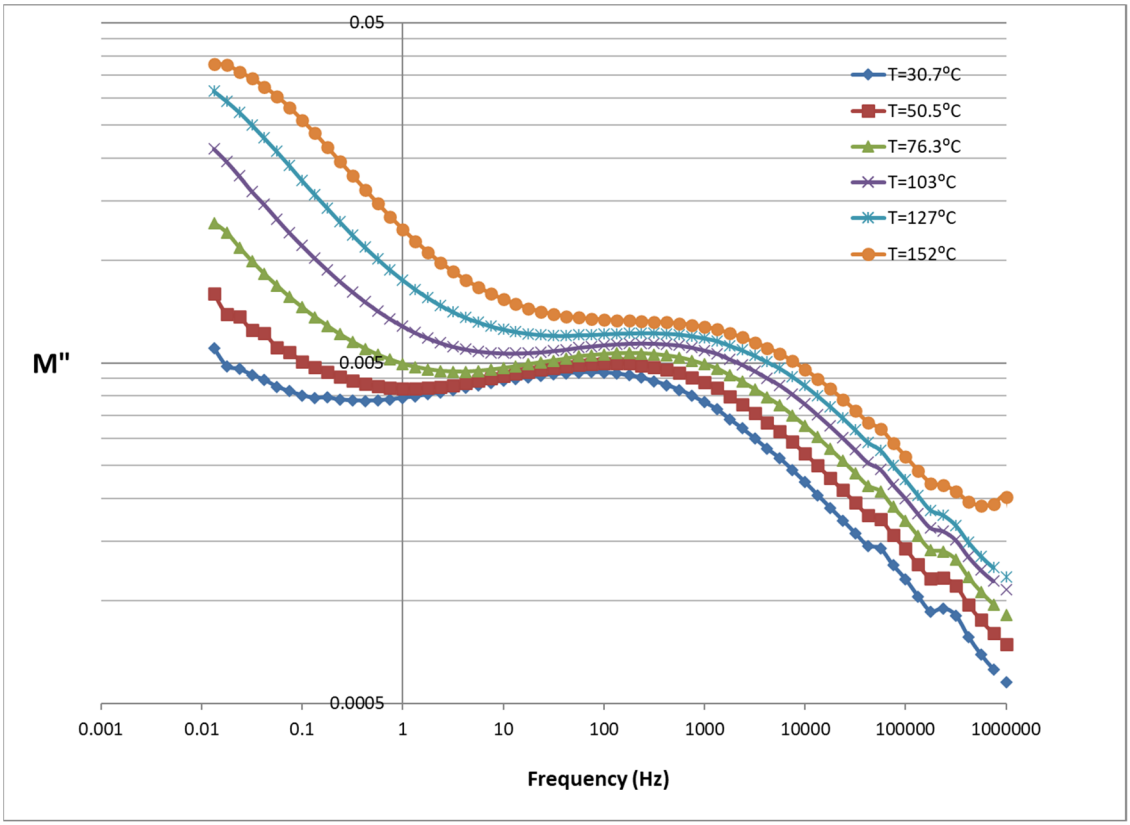


Figure 9.3. MWS-relaxation of 90% mica-epoxy PMC, ME-HT+ERT.

DETA spectra were measured for four epoxy PMC at temperatures below room temperature (an example of epoxy with 1 wt% nanosilica, Pt0, is shown in Figure 8.9). The peak frequency values are considered reliable as the maxima were observed within the spectral range (extrapolations were unnecessary). To access the β-relaxation activation energies, the peak frequencies are plotted vs. the reciprocal temperature as in Figure 9.4. The β-relaxation mode follows Arrhenius behavior. Table 9.3 lists the derived activation energies. Aging treatment and particulate addition appear to have essentially no effect on the activation energies for the β-relaxation mode.

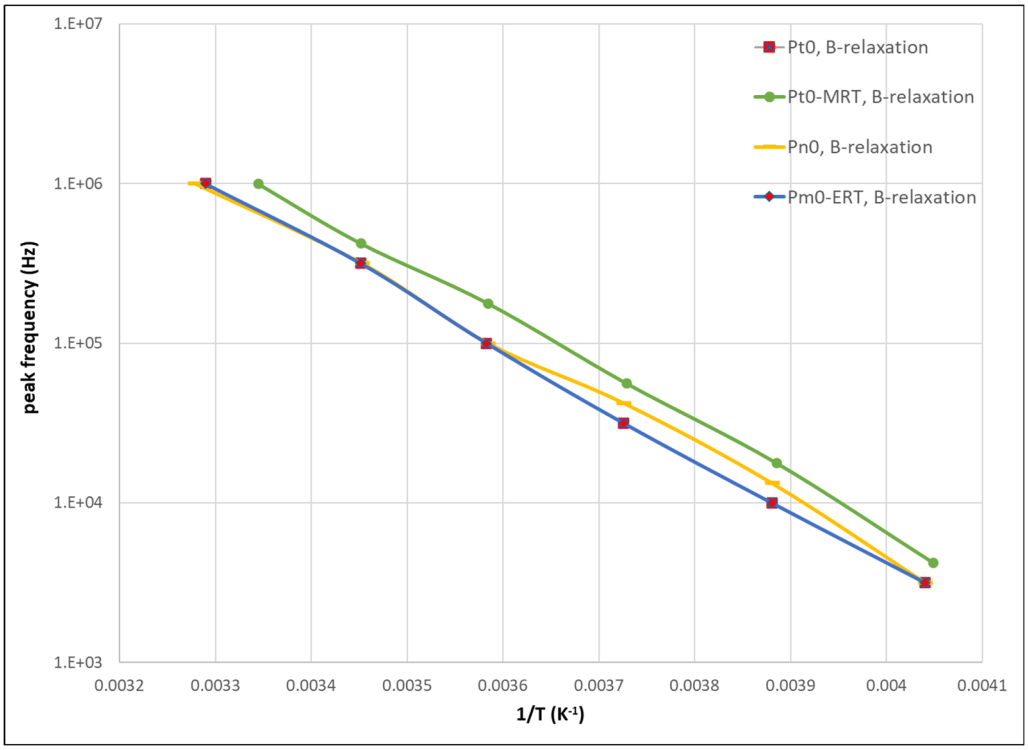


Figure 9.4. Peak frequency of the β-relaxation mode for four epoxy materials as a function of reciprocal temperature.

Table 9.2. Activation energies for the β-relaxation of filled epoxy for each condition.

Condition	Fit to M" spectra	Activation Energy (J/mol)
Pn0 (neat, no aging)	$f_{pk} = 1.26 \times 10^{17} e^{-7770/T}$	6.5×10^4
Pt0 (nano-silica modified, no aging)	$f_{pk} = 1.26 \times 10^{17} e^{-7770/T}$	6.5×10^4
Pt0-MRT (nano-silica modified, mechanically aged at RT)	$f_{pk} = 1.40 \times 10^{17} e^{-7670/T}$	6.4×10^4
Pm0-ERT (mica-filled, electrically aged at RT)	$f_{pk} = 1.26 \times 10^{17} e^{-7770/T}$	6.5×10^4

The dielectric strength of the β-relaxation (i.e., mode intensity) is known to be dependent on the nature of the dipole moments exhibited by ligands attached to the main network structure (e.g., "chain" or "backbone").[51] Higher rigidity side groups generate weak β-relaxations as observed for the silicone thermoset, Sn0. More flexible and polarizable side groups generate strong β-relaxations as observed for epoxy, Pn0. For these thermoset polymers, the β-relaxation is observed around 1 MHz, close to the frequency target of new high switching speed PEBBs and within the third harmonic range of lower switching PEBBs.

In summary, the above PMC with an epoxy matrix demonstrated average activation energies of $6.5x10^4$ J/mol for a β-relaxation and $1.2x10^4$ J/mol for a MWS-relaxation in epoxy-fiberglass laminate. The $6.5x10^4$ J/mol for the β-relaxation found here is close to the $6.7x10^4$ J/mol (0.69 eV) published for a cured neat epoxy.[139] The α-relaxation was found to vary with aging treatment and did not follow Arrhenius behavior. However, estimates of two activation energies were made: one above the glass transition temperature and one below the glass transition temperature. The lower temperature activation energy (~$1x10^5$ J/mol) was about half that of the high temperature activation energy (~$2x10^5$ J/mol). Of the three modes, the coordinated primary α-relaxation has the highest activation energy. A Cole-Cole plot of the electric modulus was the clearest indicator of aging differences.

9.2. Activation Energies from Curve Fitting of Spectral Data

To determine the peak frequency when there is a superposition of multiple processes it is necessary to find the best fit to the spectra of a superposition of relaxation function. The analysis of the spectra also helps to determine the presence of relaxation processes that may be hidden by larger losses (e.g.. conductivity).

To analyze the spectra of Sn0, Pn0, Pm0 and Sm0, we used a linear superposition of a Kohlrausch-Williams-Watts (KWW) two Cole-Cole (CC) functions and an additional term to describe the conductivity [21].

$$\varepsilon^*(\omega) = \frac{\sigma_{DC}}{\varepsilon_0 (i\omega)^n} + \Delta\varepsilon_\alpha L_{i\omega}\left[-\frac{d\varphi_\alpha(t,\tau_\alpha)}{dt}\right] + \frac{\Delta\varepsilon_\beta}{1+(i\omega\tau_\beta)^{1-\alpha_{cc}^\beta}} + \frac{\Delta\varepsilon_\gamma}{1+(i\omega\tau_\gamma)^{1-\alpha_{cc}^\gamma}} + \varepsilon_\infty$$

where $\Delta\varepsilon$ is the dielectric strength, τ the relaxation time (=$(2\pi f_{peak})^{-1}$) , α_{cc} is the shape parameter of the CC function, ε_∞ is the relaxed dielectric constant. $\varphi(t)$ is the KWW function:

$$\varphi(t) = \exp\left[-(t/\tau)^{\beta_{KWW}}\right]$$

where β_{KWW} is the stretching parameter ($0 < \beta_{KWW} \leq 1$).

For the results below the best fit was done simultaneously to both the real and imaginary part of the permittivity. The KWW function was used to describe the α process, while the CC function to describe the secondary processes (i.e. β and γ).

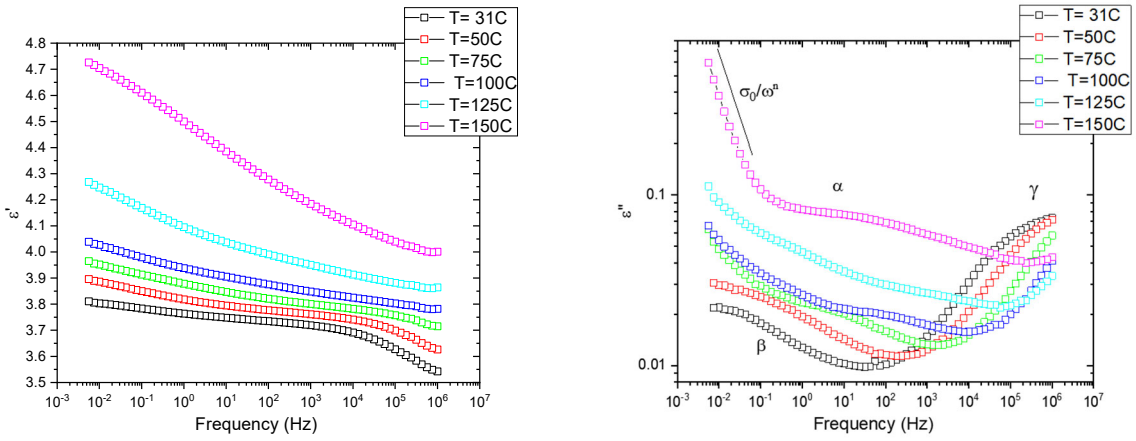


Figure 9.5.1. Real (left) and Imaginary (right) part of the permittivity of Pn0 at several temperatures. Below the glass transition are evident two secondary processes (β and γ), while above T_g the spectra are dominated but the α process and the conductivity.

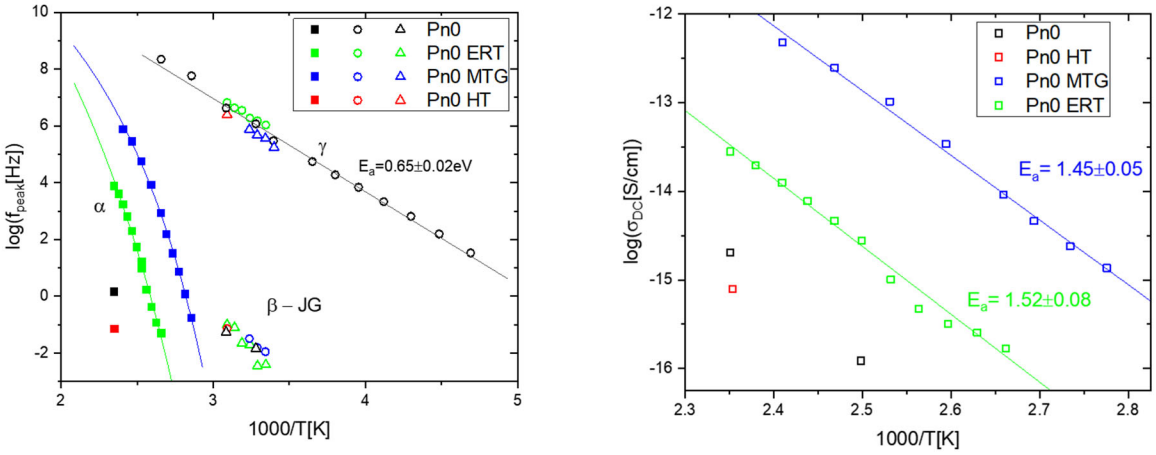


Figure 9.5.2 (left) Arrhenius plot for the relaxations in Pn0 before aging and after electrical (Pn0-ERT), mechanical (Pn0-MTG) and high temperature (Pn0-HT) aging. (right) conductivity vs inverse temperature for the same materials.

From the analysis of the spectra of Pn0 it is evident the presence of three relaxation processes (α, β, and γ) and a low frequency losses due to the DC conductivity due to impurities present in the sample. The secondary processes show an Arrhenius temperature dependence

$$\tau_{\beta,\gamma}(T) = \tau^{\infty}_{\beta,\gamma} \exp\left(\frac{E_{\beta,\gamma}}{kT}\right)$$

With a constant activation energy $E_{\beta,\gamma}$, where k is the Boltzmann constant and $\tau^{\infty}_{\beta,\gamma}$ is the high temperature limit of $\tau_{\beta,\gamma}$. The best fit to the Arrhenius equation are shown as solid lines in fig.9.5.2 and the activation energies reported in the figure.

The main result of this analysis is that there is no appreciable difference between the secondary dynamics of Pn0 before aging and after any type of aging.

The temperature behavior of τ_{α} is characterized by an activation energy increasing with decreasing temperature that is well described by a Vogel-Fulcher-Tamman (VFT) function

$$\tau_{\alpha}(T) = \tau^{\infty}_{\alpha} \exp\left(\frac{B}{T - T_0}\right)$$

Where τ^{∞}_{α} is the high temperature limit of τ_{α}, B is the fragility parameter and T_0 is the Vogel temperature. The best fits for τ_{α} of Pn0 MRT and Pn ERT are shown as solid lines in figure 9.5.2, for the other two materials there were not enough data above T_g to attempt a best fit. The glass temperature is usually determined from dielectric spectra as $\tau_{\alpha}(T_g) = 100s$, using this definition we

determined the T_g for the four materials reported in table 9.5.1. For the cases of Pn0 and Pn0-HT since it is available only one single data for τ_α, T_g was determined from the temperature shift necessary to superimpose to the other two data sets.

The conductivity was found to have an Arrhenius behavior with similar activation energy for the different materials. However, it was larger for the samples having a smaller T_g, this is an expected correlation (unless there is a change of impurity density) since a slowed segmental dynamics will slow down the diffusion of impurities in the samples.

Table 9.5.1. Glass transition temperatures determined from $\tau_\alpha(T_g)=100s$.

Material	**T_g (ºC)**
Pn0	130.5
Pn0-HT	141.5
Pn0-MTG	67.0
Pn0-ERT	94.5

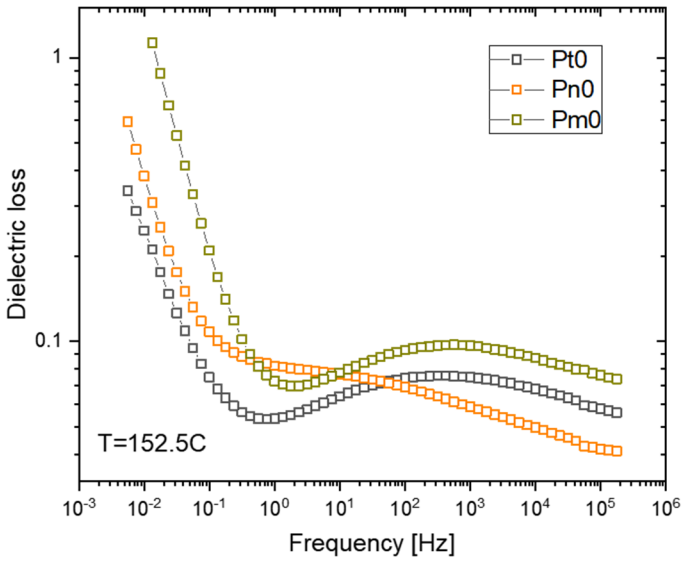


Figure 9.5.3. Comparison of spectra of Pn0 neat crosslinked epoxy Permafil 74050 with that of the same materials with added 1% silica (Pt0) and mica (Pm0) nanofillers.

The high temperature spectra of Pn0 crosslinked epoxy Permafil 74050 with that of the same materials with added 1% silica (Pt0) and mica (Pm0) nanofillers is showed in figure 9.5.3. The addition of nanofillers to Pn0 was found to speed up the segmental relaxation (α process) and consequently decrease the glass temperature by more than 15 degrees (P_n0 T_g= 130.5ºC, P_m0 T_g= 115.5ºC, P_n0 T_g= 113.5ºC). However, no additional relaxation were observed in the spectra.

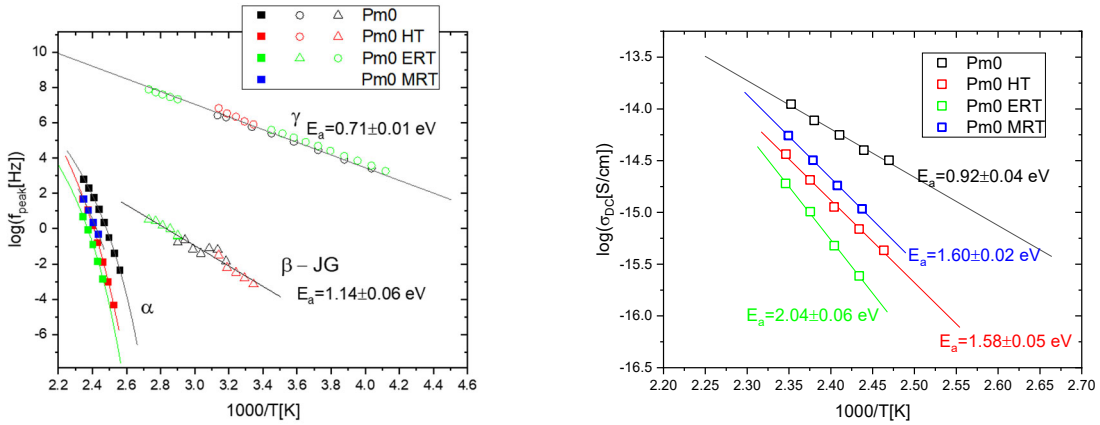


Figure 9.5.4. (left) Arrhenius plot for the relaxations in Pm0 before aging and after electrical (Pm0-ERT), mechanical (Pm0-MRT) and high temperature (Pm0-HT) aging. (right) conductivity vs inverse temperature for the same materials.

Like in the case of the neat Pn0, for the nanocomposite Pm0 the secondary dynamics was found not be affected by aging. As shown from in Figure 9.5.4, both β and γ process had the same dynamics after aging with the same activation energy.

The main effect of the different aging was to slow the segmental dynamics, although the overall change of dynamics appears smaller than in the case of the neat Pn0. All aging in this case increased the sample glass transition as showed in Table 9.5.2.

In the investigated temperature range the temperature behavior of the conductivity can be described by an Arrhenius behavior. After aging the activation energy was found to increase, and the absolute value to decrease with increasing the T_g of the sample.

Table 9.5.2. Glass transition temperatures of Pm0 before and after aging determined from $\tau_\alpha\left(T_g\right)=100s$.

Material	**T_g (°C)**
Pm0	115.5
Pm0-HT	128.5
Pm0-MRT	129.8
Pm0-ERT	133.8

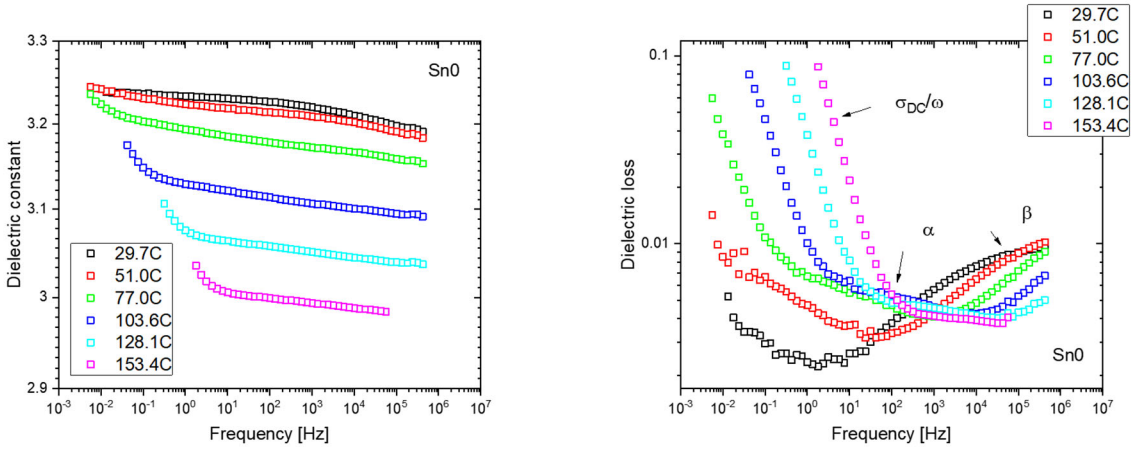


Figure 9.5.5. Real (left) and Imaginary (right) part of the permittivity of Sn0 at several temperatures. Below the glass transition are evident one secondary processes (β), while above Tg the spectra are dominated but the α process and the conductivity.

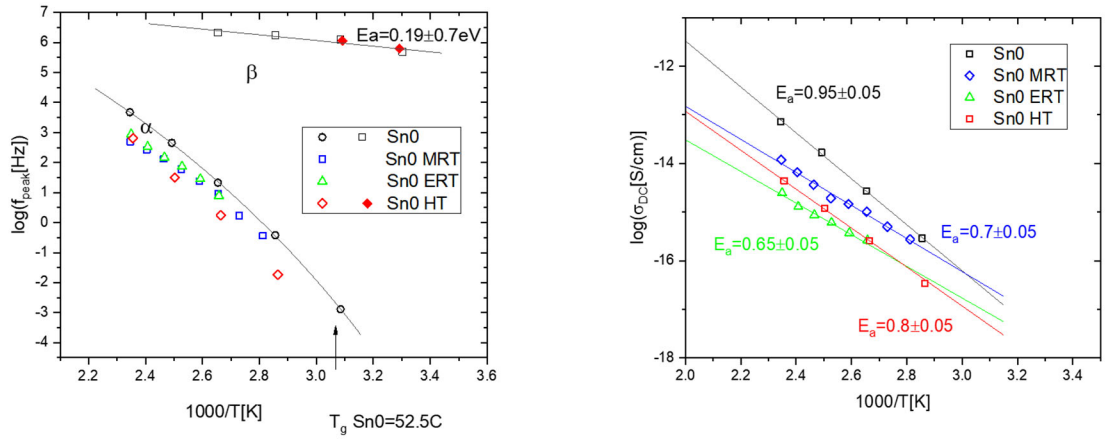


Figure 9.5.6. (left) Arrhenius plot for the relaxations in Sn0 before aging and after electrical (Sn0-ERT), mechanical (Sn0-MRT) and high temperature (Sn0-HT) aging. (right) conductivity vs inverse temperature for the same materials.

In the case of the material Sn0 (H62c silicone) in the dielectric spectra (figure 9.5.5) is present only one secondary process (β process) and the α process and conductivity losses above T_g (=52.5ºC). It is worth noticing that for this material the dielectric losses are about one order of magnitude smaller than for Pn0.

The temperature behavior of the peak frequencies obtained from the best fit of the equation describe above (with a single CC function since there is only one secondary process) are shown in Figure 9.5.6. Also, in this case the aging has a not appreciable effect on the secondary dynamics,

while there is an observed change in the segmental dynamics and conductivity. The change of the segmental dynamics is reflected in an increase of the glass transition as showed in Table 9.5.3.

The temperature behavior of the DC conductivity is described by an Arrhenius behavior, after aging the activation energy is found to decrease as well as the absolute value is found to decrease with the increase of Tg.

Table 9.5.3. Glass transition temperatures of Sn0 before and after aging determined from $\tau_\alpha\left(T_g\right)=100s$.

Material	**T_g (°C)**
Sn0	52.5
Sn0-HT	68.5
Sn0-MRT	62.5
Sn0-ERT	63.5

From the analysis of the dielectric spectra reported above, we found that the main effect of the different aging was on the segmental dynamics while the secondary processes were not appreciably affected. The change of the segmental dynamics was reflected in a change of T_g. Consequently, a large change of the losses at high temperatures was observed, since the intensity of the conductivity losses is larger for materials with lower T_g. The change of glass temperature is expected to have a large effect on the mechanical properties with a difference of orders of magnitude between the glassy and rubber elastic moduli.

REFERENCES

[1] A. T. Wilder, *Characterization of power losses in soft magnetic materials*. IEEE Electric Ship Tech. Symp., Philadelphia, PA, 27 July 2005.

[2] Saeed Ul Haq, *A Study on Insulation Problems in Drive Fed Medium Voltage Induction Motors.* Dissertation, University of Waterloo, Ontario, Canada (2007).

[3] A. K. Jonscher, *Dielectric loss under transient excitation.* J. Phys. C: Solid State Phys., Vol.11 (1978): L601-L606.

[4] T. Guillod et al., *Computation and analysis of dielectric losses in MC power electronic converter insulation.* IEEE Proc. Energy Conversion Congress & Expo., Milwaukee, WI, 18-22 September 2016.

[5] K. Niayesh and E. Gockenbach, *On the aging mechanism of solid insulating materials exposed to repetitive high voltage pulses*. IEEE Trans. Diel. Elec. Insulation, Vol. 21(1) (2014): 304-310.

[6] A. T. Wilder and J. Pearce, *Heat Flow Simulations of Epoxy-based Stator Insulation at 100 kHz*. IEEE Electrical Insulation Conference (2021): accepted for publication.

[7] J. Horwath, D. Schweickart, G. Garcia, D. Klosterman, and M. Galaska, *Improved performance of polyhedral oligomeric silsesquioxane epoxies.* IEEE Conf. Elect. Insul. Diel. Phen. (CEIDP), Nashville, TN, 16-19 October 2005: 155-157.

[8] Federico Fuentes, Leszek Demkowicz, and Aleta Wilder, *Using a DPG method to validate DMA experimental calibration of viscoelastic materials.* Computer Methods in Applied Mechanics and Engineering. Vol. 325, 1 Oct 2017: 748-765.

[9] A. S. Merenga, C. M. Papadakis, F. Kremer, J. Liu, A. F. Yee, *Broadband dielectric spectroscopy of the inter- and intramolecular dynamics of a series of random polyester copolymers.* Colloid Polym. Sci., 279 (2001): 1064-1072.

[10] A. S. Maxwell, W. R. Broughton, G. Dean, and G. D. Sims, *Review of accelerated ageing methods and lifetime prediction techniques for polymeric materials.* DEPC MPR 016, National Physical Laboratory, Middlesex, UK (2005).

[11] Mike J. Richardson, *The glass transition region, Chapter 6*, in Comprehensive Polymer Science, Vol. 1, ed. G. Allen, Pergamon Press, Oxford (1989).

[12] E. David and L. Lamarre, *Low-frequency dielectric response of epoxy-mica insulated generator bars during multi-stress aging.* IEEE Trans. Diel. Elect. Insul., 14 (2007): 212-226.

[13] R. Casalini and C. M. Roland, *Aging of the secondary relaxation to probe structural relaxation in the glassy state.* Phys. Rev. Lett., Vol. 102 (2009): 035701.

[14] B. Wunderlich, *Thermodynamics and kinetics of crystallization of flexible molecules.* J. Polymer Sci.: Part B: Polymer Physics, Vol. 46 (2008): 2647-2659.

[15] A. T. Wilder and R. Casalini, *Dielectric Heating of Commercial Insulation Materials*. IEEE Electrical Insulation Conference (2020): 521-524.

[16] D. Tommasini, *Dielectric insulation and high-voltage issues*. CERN Accelerator School CAS, (2009): 335-355.

[17] Dynamical Heterogeneities in Glasses, Colloids, and Granular Media. eds. L. Berthier et al., Series Monographs on Physics, no. 150, Oxford Univ. Press (2011).

[18] A. S. Maxwell, W. R. Broughton, G. Dean, and G. D. Sims, *Review of accelerated ageing methods and lifetime prediction techniques for polymeric materials.* NPL Report DEPC MPR 016, National Physical Laboratory, UK (2005).

[19] E. A. Feilat, *Lifetime assessment of electrical insulation*. Chpt. 11, Intech Open (2018): 231-253.

[20] G. W. Ehrenstein and S. Pongratz, Resistance and Stability of Polymers. Hanser Publications (2013).

[21] Broadband Dielectric Spectroscopy. eds. F. Kremer and A. Schonhals, Springer (2003).

[22] T. J. Lewis, *Nano-composite dielectrics: the dielectric nature of the nano-particle environment.* IEEF Trans. FM, 126 (2006): 1020-1030.

[23] A. Schonhals, *Dielectric spectroscopy on the dynamics of amorphous polymeric systems.* Novocontrol Appl. Note, 1 (1998), Novocontrol Technologies, Montabaur Germany.

[24] S. Javadi et al., *Interfacial effects on dielectric properties of ethylene propylene rubber-titania nano- and micro-composites.* J. Polym. Res., 22 (2015): 162.

[25] E. Kubyshkina and M. Unge, *Impact of interfacial structure on the charge dynamics in nanocomposite dielectrics.* J. Appl. Phys., 125 (2019): 045109.

[26] B. J. Anderson and C. F. Zukoski, *Rheology and microstructure of polymer nanocomposite melts: Variation of polymer segment-surface interaction*. Langmuir, 26 (2010): 8709-8720.

[27] N. A. Othman, M. A. M. Piah, Z. Adzis, N. A Ahmad, *Comparative study on space charge distribution measurements using PEA and PWP methods on high voltage insulation*. Jurnal Teknologi, 64 (2013): 43-47.

[28] J. H. Geng and B. Y. Jia., *Research on the influence of surface accumulation charge on flashover voltage of ceramic insulator.* Intl. Conf. Energy and Environ. Tech. (2009): 244–246.

[29] P. Conner, J. P. Jones, J. P. Llewellyn, and T. J. Lewis*, An exploration of physical ageing in electrically-stressed polymeric insulating films using the quartz crystal shear wave sensor technique*. IEEE Intl. Conf. Solid Diel., Eindhoven the Netherlands (2001): 39-42.

[29b] H. Kim, Y. Cang, E. Kang, B. Graczykowski, M. Secchi, M. Montagna, R. D. Priestley, E. M. Furst, and G. Fytas, *Direct observation of polymer surface mobility via nanoparticle vibrations.* Nature Comm., 9 (2018): 2918.

[30] M. Baggioli and A. Zaccone, *Low-energy optical phonons induce glassy-like vibrational and thermal anomalies in ordered crystals*. J. Phys.: Materials, 3 (2019): 015004.

[31] A. Marruzzo, W. Schirmacher, A. Fratalocchi, and G. Ruocco, *Heterogeneous shear elasticity of glasses: the origin of the boson peak*. Sci. Rep., 3 (2013): 1407.

[32] C. Ganter and W. Schirmacher, *Rayleigh scattering, long-time tails, and the harmonic spectrum of topologically disordered systems*. Phys Rev B, 82 (2010): 094205.

[33] H. Mizuno, H. Shiba, and A. Ikeda, *Vibrational properties and phonon transport of amorphous solids.* Phys. Rev. E, 98 (2018): 062612.

[34] F. Corberi, L. F. Cubliandolo, and H. Yoshino, *Growing length scales in aging systems*. Chpt. 11, Dynamical Heterogeneities in Glasses, Colloids and Granular Media, eds. L. Berthier et al., (2011) Oxford University Press.

[35] R. W. Dakin, *Electrical insulation deterioration treated as a chemical rate phenomenon.* AIEE Trans., 67 (1948): 113-118.

[36] J. H. Flynn, *Degradation kinetics applied to lifetime predictions of polymers*. Polym. Eng. Sci., 20 (1980): 674-676.

[37] J. K. Nelson, S. Azizi-Ghannad, and H. Li, *Theory and application of dynamic aging for lifetime estimation in machine insulation*. IEEE Trans. Diel. Elect. Insul., 7 (2000): 773-782.

[38] Y. Guo, N. Wang, R. D. Bradshaw, and L. C. Brinson, *Modeling mechanical aging shift factors in glassy polymers during nonisothermal physical aging*. J. Polym. Sci. Part B: Polym. Phys., 47 (2009): 340-352.

[39] G. Mazzanti, G. C. Montanari, and L. A. Dissado, *A space-charge life model for ac electrical aging of polymers*. IEEE Trans. DEI, 6 (1999): 864-875.

[40] J. P. Crine, *An electrical aging model including Kramers friction, phonon vibrations and electrostriction.* IEEE Intl. Conf. Solid Diel, pp. 283-286, Bologna Italy, 30 June 2013.

[41] C. M. Roland, K. J. McGrath, and R. Casalini, *Dynamic heterogeneity in poly(vinyl methyl ether)/poly(2-chlorostyrene) blends.* Macromolecules, 39 (2006): 3581-3587.

[42] H. Mizuno, H. Shiba, and A. Ikeda, *Continuum limit of the vibrational properties of amorphous solids.* PNAS, 31 October 2017, E9767-E9774.

[43] C. Riedel, A. Alegria, J. Colmenero, and P. Tordjeman, *Polymer rheology by Dielectric Spectroscopy*. in Rheology, Chpt. 1, ed. J. de Vicente (2012): www.intechopen.com

[44] *Insulation integrity for power dense, medium voltage, electric machinery.* Final Technical Report, submitted 17 August 2018: Office of Naval Research N00014-15-1-2496.

[45] *Insulation aging behaviors characterized with Dielectric Thermal Analysis (DETA).* Technical Report 1, submitted 7 June 2019: Office of Naval Research N00014-18-1-2586.

[46] F. Kremer and A. Schonhals, *Broadband dielectric measurement techniques*. Chpt. 2 (pg. 80) in Broadband Dielectric Spectroscopy, (2002), Springer-Verlag: ISBN: 3-540-43407-0

[47] Intl. Collective of Scientists, *Nanodielectrics.* Intl. Conf. Solid Diel., (2010) Potsdam, Germany.

[48] Y. Huang and L. S. Schadler, *Understanding the strain-dependent dielectric behavior of carbon black reinforced natural rubber- an interfacial or bulk phenomenon?* Comp. Sci. Tech., 142 (2016): 91-97.

[49] N. M. Renukappa, B. Suresha, R. M. Devarajaiah, and K.N. Shivakumar. *Dry sliding wear behavior of organo-modified montmorillonite filled epoxy nanocomposites using Taguchi's Techniques*. Mater. Design, 32 (2011): 4528-4536.

[50] J. P. Adohi, C. Guillermin, P. Rain, and S. W. Rowe, *Filler treatment effects on the dielectric properties of a filled epoxy resin*. IEEE Conf. Elect. Insul. Diel. Phenomena (2004): 158-161.

[51] I. M. Kalogeras, *Contributions of dielectric analysis in the study of nanoscale properties and phenomena in polymers.* Prog. Polym. Nanocomp. Res., Chpt. 10, eds. S. Thomas and G. E. Zaikov, (2008): ISBN:978-1-60456-484-6.

[52] M. Bohning, H. Goering, A. Fritz, K.-W. Brzezinka, G. Turky, A. Schonhals, and B. Schartel, *Dielectric study of molecular mobility in poly(propylene-graft-maleic anhydride)/clay nanocomposites.* Macromolecules, 38 (2005): 2764-2774.

[53] R. Kotsilkova, D. Fragiadakis, and P. Pissis, *Reinforcement effect of carbon nanofillers in an epoxy resin system: Rheology, molecular dynamics, and mechanical studies*. J. Polym. Sci., Part B: Polym. Phys., 43 (2005): 522-533.

[54] L. Paquin, H. St-Onge, and M. R. Wertheimer, *The complex permittivity of polyethylene/mica composites.* IEEE Trans. Elect. Insul., EI-17 (1982): 399-404.

[55] C. Tsonos, A. Kanapitsas, G. C. Psarras, and Th. Speliotis, *Effect of ZnO nanoparticles on the dielectric/electrical and thermal properties of epoxy-based nanocomposites*. Sci. Adv. Mater., 7 (2015): 588-597.

[56] V. A. Bershtein, L. M. Egorova, P. N. Yakushev, P. Pissis, P. Sysel, L. J. Brozova, *Molecular dynamics in nanostructured polyimide-silica hybrid materials and their thermal stability*. J. Polym. Sci., Part B: Polym. Phys., 40 (2002): 1056-1069.

[57] J. K. Nelson and J. C. Fothergill, *Internal charge behavior of nanocomposites*. Nanotechnology, 15 (2004): 586-595.

[58] S. Javdi, M. Sadroddini, M.; Razzaghi-Kashani, P. N. B. Reis, and A. A. Balado, *Interfacial effects on dielectric properties of ethylene propylene rubber-titania nano- and micro-composites.* J. Polym. Res., 22 (2015): paper 162.

[59] J. K. Nelson and Y. Hu, *Nanocomposite dielectrics- properties and implications*. J. Phys. D: Appl. Phys., 38 (2005): 213-222.

[60] S. Singha and M. J. Thomas, *Influence of filler loading on dielectric properties of ZnO-epoxy nanocomposites.* IEEE Trans. DEI, 16 (2009): 531-542.

[61] Y. Sun, Z. Zhang, K.-S. Moon, C. P. Wong, *Glass transition and relaxation behavior of epoxy nanocomposites.* J. Polym. Sci.: Part B: Polym. Phys., 42 (2004): 3849-3858.

[62] G. Polizos et al., *Effect of polymer-nanoparticle interactions on the glass transition dynamics and the conductivity mechanism in polyurethane titanium dioxide nanocomposites.* Polymer, 53 (2012): 595-603.

[63] V. Tomer, G. Polizos, E. Manias, and C. A. Randall, *Epoxy-based nanocomposites for electrical energy storage. I: Effects of montmorillonite and barium titanate nanofillers*. J. Appl. Phys., 108 (2010): 074116.

[64] M. N. Ajour, J. C. Fothergill, K. B. A. See, and L. A. Dissado, *"Sub-Hertz" dielectric spectroscopy*. IEEE Intl. Multi-Conf. Systems, Signals and Devices (2009): 1-4.

[65] H. Zhao, Y. Li, L. C. Brinson, Y. Huang, T. M. Krentz, L. S. Schadler, M. Bell, and B. Beniicewicz, *Dielectric spectroscopy analysis using viscoelasticity inspired relaxation theory with Finite Element Analysis.* IEEE Trans. Diel. Elect. Insul., 24 (2017): 3776-3785.

[66] S. Siddabattuni and T. P. Schuman, *Dielectric spectroscopy and stimulated current analyses of polymer-ceramic nanocomposites*. Chpt. 10 in Spectroscopy of Polymer Nanocomposites, (2016): 276-311.

[67] M. Rahaman, T. K. Chaki, D. Khastgir, *Consideration of interface polarization in the modeling of dielectric property for ethylene vinyl acetate (EVA)/polyaniline conductive composites*. Euro. Poly., 48 (2012): 1241-1248.

[68] T. Hibna and H. R. Zeller, *Direct measurement of space-charge injection from a needle electrode into dielectrics.* J. Appl. Phys., 59 (1986): 1614-1620.

[69] H. Chakroborty and A. Sinha, *Effect of space charge density and high voltage breakdown of surface modified alumina reinforced epoxy composites*. Trans. Elect. Elec. Mater., 14 (2013): 121-124.

[70] R. C. Smith, L. Hui, J. K. Nelson, and L. S. Schadler, *Interfacial charge behavior in nanodielectrics*. IEEE Conf. Elect. Insul. Diel. Phenomena (2009): 650-653.

[71] J. Mijovic, H. K. Lee, J. Kenny, and J. Mays, *Dynamics in polymer-silicate nanocomposites as studied by dielectric relaxation spectroscopy and dynamic mechanical spectroscopy*. Macromolecules, 39 (2006): 2172-2182.

[72] V. Pouilles, T. Lebey, and P. Castelan, *Determination of the very low-frequency characteristics of dielectric materials: A surface potential approach*. J. Appl. Phys., 79 (1996): 8620-8628.

[73] J. K. Nelson, J. C. Fothergill, L. A. Dissado, W. Peasgood, *Towards an understanding of nanometric dielectrics*. IEEE Conf. Elect. Insul. Diel. Phen., (2002): 295-298.

[74] S. Lin, Y. Huang, D. Xie, Z. Li, D. Min, S. Yu, and S. Li, *Dielectric relaxation and carrier transport in epoxy resin*. IEEE Intl. Conf. Diel. (2016): 1167-1170.

[75] S. Babu, R. Sarathi, N. J. Vasa, and T. Imai, *Understanding the influence of nano micro filler on electrical and mechanical behavior of epoxy nanocomposites.* IEEE Trans. Diel. Elect. Insul, 26 (2019): 1098-1106.

[76] R. W. Sillars, *Electrical Insulating Materials and their Application*. Peter Peregrinus Ltd., London (1973).

[77] D. J. Yaron and T. Kowalewski, *Beware the nanovoids*. Nature Mater., 18 (2019): 1146-1155.

[78] M. Woo and M. R. Piggott, *Water absorption of resins and composites: I. Epoxy homopolymers and copolymers.* J. Comp. Tech. Res., 9 (1987): 101-107.

[79] M. Woo and M. R. Piggott, *Water absorption of resins and composites: IV. Water transport in fiber reinforced plastics.* J. Comp. Tech. Res., 10 (1988): 20-24.

[80] J. J. Chrusciel and E. Lesniak, *Modification of epoxy resins with functional silanes, polysiloxanes, silsequioxanes, silica and silicates.* Prog. Polymer Sci. 41 (2015): 67-121.

[81] Th. Kwaaitaal and W. M. M. van den Eijnden, *Dielectric loss measurement as a tool to determine electrical aging of extruded polymeric insulated power cables.* IEEE Trans. Elect. Insul., EI-22 (1), (1987): 101-105.

[82] O. Becker, R. J. Varley, G. P. Simon, *Thermal stability and water uptake of high performance epoxy layered silicate nanocomposites*. Eur. Polym. J. 40 (2004): 187-195.

[83] K. S. Cole and R. H. Cole, *Dispersion and absorption in dielectrics: I. Alternating current characteristics.* J. Chem. Phys., 9 (1941): 341-351.

[84] H. Mo, G. Wang, F. Liu, and P. Jiang, *The influence of the interface between mica and epoxy matrix on properties of epoxy-based dielectric materials with high thermal conductivity and low dielectric loss.* RSC Adv., 6 (2016): 83163-83174.

[85] D. E. Gavrila and H. C. Gavrila, *Dielectric properties of the composite insulator mica epoxy-Novolac*. Adv. Mater. Res., 701 (2013): 47-52.

[86] M. A. Chaudhry and A. K. Jonscher, *The dielectric properties of mica paper in variable temperature and humidity.* J. Mater. Sci., 20 (1985): 3581-3589.

[87] S. Samet, V. Levchenko, G. Bolteux, G. Seytre, A. Kallel, and A. Serghei, *Electrode polarization vs. Maxwell-Wagner-Sillars interfacial polarization in dielectric spectra of materials: Characteristic frequencies and scaling laws.* J. Chem. Phys., 142 (2015): 194703.

[88] M. G. Todd and F. G. Shi, *Complex permittivity of composite systems: A comprehensive interphase approach.* IEEE Trans. Diel. Elec. Insul., 12 (2005): 601-611.

[89] P. Bartolomeo, J. F. Chailan, J. L. Vernet, *Dielectric investigation of interphase formation in composite materials. I. Ionic Conductivity and permittivity exploration*. J. Poly. Sci., 38 (2000): 2154-2161.

[90] P. Bartolomeo, J. F. Chailan, J. L. Vernet, *Dielectric investigation of interphase formation in composite materials. II. Relaxation Process*. J. Poly. Sci., 38 (2000): 2162-2169.

[91] Y. Wang, UJ. Cui, Q. Yuan, Y. Niu, Y. Bai, and H. Wang, *Significantly enhanced breakdown strength and energy density in sandwich structured barium titanate/ poly(vinylidene fluoride) nanocomposites.* Adv. Matls., 27 (2015): 6658-6663.

[92] Z. Shi, J. Wang, F. Mao, C. Yang, C. Zhang, and R. Fan, *Significantly improved dielectric performances of sandwich-structured polymer composites induced by alternating positive-k and negative-k layers*. J. Matls. Chem. A, 28 (2018): 14575-14582.

[93] K. Makasheva et al., *Dielectric engineering of nanostructured layers to control the transport of injected charges in thin dielectrics.* IEEE Trans. Nanotech., 15 (2016): 839-848.

[94] S. Li, G. Yin, G. Chen, J. Li,, S. Bai, L. Zhong, Y. Zhang, and Q. Lei, *Short-term breakdown and long-term failure in nanodielectrics: A review.* IEEE Trans. Diel. Elect. Insul, 17 (2010): 1523-1535.

[95] R. Cimbala, J. Kurimshy, and I. Kolcunova, *Determination of thermal ageing influence on rotating machine insulation system using dielectric spectroscopy*. Electrical Rev., 87 (2011): 176-179.

[96] Y. Li and J. Unsworth, *Dynamic mechanical behaviors of epoxy insulating composites*. Proc. Elect. Electronics Insul. Conf. (1993): 7-11.

[97] Y. Hao, Z. Jia, X. Jiang, N. Gao, and H. Xie, *The changes of mechanical properties of epoxy/mica insulation materials in aging process*. IEEE Intl. Conf. Prop. Appl. Diel. Matl., (2000): 185–188.

[98] V. Boucher, P. Rain, G. Teissedre, P. Schlupp, *Mechanical and dielectric properties of glass-mica-epoxy composites along accelerated thermo-oxidative aging.* IEEE Intl. Conf. Solid Diel., (2007): 162-165.

[99] R. B. Nageshwar, K. Mallikarjunappa, R. J. Sundara, B. Ramachandra and A. Sudhindra, *Assessment of stator winding insulation*. Power Res., 6 (2010): 61-76.

[100] M. B. Srinivas and T. S. Ramu, *Multifactor aging of HV generator stator insulation including mechanical vibrations*. IEEE Trans. Elect. Insul., 27 (1992): 1009-1021.

[101] R. M. Christensen, *Evaluation of ductile/brittle failure theory and derivation of the ductile/brittle transition temperature.* J. Appl. Mech., 83 (2016): 021001.

[102] R. M. Guedes, *Time-dependent failure criteria for polymer matrix composites: a review.* J. Reinforced Plastics and Comp., 29 (2010): 3041-3047.

[103] T. J. Lewis, J. P. Llewellyn and M. J. van der Sluijs, *Electrokinetic properties of metal-dielectric interfaces*. IEE Proceedings-A, 140 (1993): 385-392.

[104] C. L. Griffiths, S. Betteridge, J. P. Llewellyn, and T. J. Lewis, *The importance of mechanical properties for increasing the electrical endurance of polymeric insulation*. IEE Diel. Matl. Meas. Appl., 473 (2000): 408-412.

[105] M. Quaresimin and R. J. Varley, *Understanding the effect of nano-modifier addition upon the properties of fibre reinforced laminates.* Comp. Sci. Tech., 68 (2008): 718-726.

[106] Y. Li, S.Y. Fu, D.J. Lin, Y.H. Zhang, and Q.Y. Pan, *Mechanical properties of polyimide composites filled with SiO_2 nano-particles at room and cryogenic temperature*. Acta Mater. Compos. Sin., 22 (2005): 11–15.

[107] M. Hussain, A. Nakahira, S. Nishijama, and K. Niihara, *Fracture behavior and fracture toughness of particulate filled epoxy composites*. Mater. Lett., 27 (1996): 21–25.

[108] S. Fu, A. Sun, P. Hang, Y. Li, and N. Hu*, Some basic aspects of polymer nanocomposites: A critical review*. Nano Matl. Sci., 1 (2019): 2-30.

[109] H. Mo, G. Wang, F. Liu, and P. Jiang, *The influence of the interface between mica and epoxy matrix on properties of epoxy-based dielectric materials with high thermal conductivity and low dielectric loss.* (Royal Society of Chemistry) RSC Advances, 6 (2016): 83163-83174.

[110] H. K. R. Pothukuchi, P. Fuchs, G. Pinter, and S. Stelzer, *Fracture mechanical characterization of mica-filled epoxy glass composites under monotonic and cyclic loading*. J. Comp. Matl., 53 (2019): 741-751.

[111] M. Akatsuka, Y. Takezawa, and H. Kamiya, *Delamination mechanism of high-voltage coil insulators made from mica flakes and thermosetting epoxy resin*. J. Appl. Polym. Sci., 79 (2001): 2164–2169.

[112] K. Kimura and Y. Kaneda, The role of microscopic defects in multistress aging of micaceous insulation. IEEE Trans. Dielec. Elect. Insul., 2 (1995): 426-432.

[113] C. Rusu-Zagar, P. V. Notingher, and C. Stancu, *Ageing and degradation of electrical machines insulation.* J. Intl. Sci. Publ.: Matl, Methods, & Testing, 8 (2014): 526-546.

[114] A. Wilder, *Characterization of insulation aging with power-dense environments*. IEEE Elect. Insul. Conf. (2018): 280-285; and *Insulation integrity for power dense, medium voltage, electric machinery.* N00014-15-1-2496, 15 July 2018.

[115] T. Tanaka, *Dielectric Nanocomposites with Insulating Properties*. IEEE Trans. Diel. Elect. Insul., 12 (2005): 914-928.

[116] T. Imai, F. Sawa, T. Nakano, T. Ozaki, T. Shimizu, S. Kuge, M. Kozako and T. Tanaka, *Insulation properties of nano- and micro- filler mixture composite*. IEEE Conf. Elect. Insul. Diel. Phenomena (2005): 171-174.

[117] S. Masuda, S. Okuzumi, R. Kurniant, Y.Murakami, M. Nagao, Y. Murata, and Y. Sekiguchi, *DC conduction and electrical breakdown of MgO and LDPE nanocomposite*. IEEE Conf. Elect. Insul. Diel. Phenomena (2007): 290-293.

[118] J. K. Nelson, Y. Hu and J. Thiticharoenpong. *Electrical properties of TiO2 nanocomposites*. IEEE Conf. Elect. Insul. Diel. Phenomena (2003): 719-722.

[119] D. Q. Tan, *The search for enhanced dielectric strength of polymer-based dielectrics: a focused review on polymer nanocomposites*. Appl. Poly. Sci., 137 (2020): 1-32.

[120] E. Tuncer, G. Polizos, I. Sauers, D. R. James, A. R. Ellis, and K. L. More, *Epoxy nanodielectrics fabricated with in situ and ex situ techniques*. J. Exp. Nanoscience, 7 (2010): 274-281.

[121] A. Krivda et al., *Characterization of epoxy microcomposite and nanocomposite materials for power engineering applications*. IEEE Elec. Insul. Mag., 28 (2012): 38-51.

[122] A. Tsekmes, P. H. F. Morshius, J. J. Smit, and R. Kochetov, *Enhancing the thermal and electrical performance of epoxy microcomposites with the addition of nanofillers*. IEEE Elect. Insul. Mag, 31 (2015): 32-42.

[123] P. Werelius, P. Tharning, R. Eriksson, B. Holmgren, and U. Gafvert, *Dielectric spectroscopy for diagnosis of water tree deterioration in XLPE cables*. IEEE Trans. Diel. Elect. Insul., 8 (2001): 27-42.

[124] L. Harvanek, V. Mentlik, P. Trnka, and J. Hornak, *Effect of electrical/thermal aging on dielectric properties of polymer/SiO_2 nanocomposites.* IEEE Intl. Conf. Diel. (2016): 92-95.

[125] M. Tari,, K. Yoshida, S. Sekito, J. Allison, R. Brutsch, and A. Lutz, *A high voltage insulating system with increased thermal conductivity for turbo generators*. Coil Winding, Insul. Elect. Manuf. Conf., Berlin (2001): 1-5.

[126] T. W. Dakin, H. M. Philofsky, and W. C. Divens, Effect of electric discharges on the breakdown of solid insulation. Trans. Amer. Inst. Elect. Eng., 73 (1954): 155-162.

[127] A. Campoccia and R. Schifani, *On Testing Methodology of Thermosetting Dielectrics Subjected to Partial Discharges: Effect of Temperature*. IEEE Trans. Elect. Insul., 23 (1988): 419-426.

[128] T. W. Dakin, *The relation of capacitance increase with high voltages to internal electric discharges and discharging void volume*. Trans. Amer. Inst. Elect. Eng., 78 (1959): 13-16.

[129] L. C. Castro, J. L. Oslinger, N. Taylor and M. Wahlander, *Dielectric and physico-chemical properties of epoxy-mica insulation during thermoelectric aging*. IEEE Trans. Diel. Elect. Insul, 22 (2015): 3107-3117.

[130] M. Farahani, E. Gackenbach, H. Borsi, K. Schafer, and M. Kaufhold, *Behavior of machine insulation systems subjected to accelerated thermal aging test.* IEEE Trans. Diel. Elect. Insul., 17 (2010): 1364-1372.

[131] M. Farahani, H. Borsi, and E. Gockenbach, *Study of capacitance and dissipation factor tip-up to evaluate the condition of insulating systems for high voltage rotating machines*. Elect. Eng., 89 (2007): 263-270.

[132] C. Hudon, N. Amyot, and D. Jean, *Long-term behavior of corona resistant insulation compared to standard insulation of magnet wire.* IEEE Intl. Symp. Elect. Insul., (2000): 13-16.

[133] J. Horwath, D. Schweickart, G. Garcia, D. Klosterman, and M. Galaska, *Improved Performance of Polyhedral Oligomeric Silsesquioxane Epoxies.* Conf. Elect. Insul. Diel. Phenomena, (2005): 155-157.

[134] S. A. Studniarz and R. W. Dakin, *The voltage endurance of cast epoxy resin-II*. IEEE Intl. Conf. Elect. Insul., (1982): 19-25.

[135] M. Kozako, R. Kido, N. Fuse, Y. Ohki, T. Okamoto and T. Tanaka, *Differences in Surface Degradation due to Partial Discharges Between Polyamide Nanocomposites and Microcomposites.* IEEE Conf. Elect. Insul. Diel. Phenomena, (2004): 398-401.

[136] S. U. Haq, *A study on insulation problems in drive fed medium voltage induction motors.* Dissertation, The University of Waterloo, Waterloo Ontario, Canada (2007).

[137] T. Imai, F. Sawa, T. Ozaki, Y. Inoue, T. Shimizu, and T. Tanaka, *Comparison of insulation breakdown properties of epoxy nanocomposites under homogeneous and divergent electric fields.* Conf. Elect. Insul. Diel. Phenomena (2006): 306-309.

[138] N. Fuse, T. Tanaka and Y. Ohki, *Evaluation of dielectric properties in polypropylene/clay nanocomposites.* IEEE Conf. Elect. Insul. Diel. Phenomena (2009): 507-510.

[139] R. Kotsilkova, D. Fragiadakis, and P. Pissis, *Reinforcement effect of carbon nanofillers in an epoxy resin system: rheology, molecular dynamics, and mechanical studies*. Poly. Sci. Part B, Polym. Phys., 43 (2005): 522-533.